



**Assessment of the efficacy and safety of a novel  
pharmacological strategy designed to enhance liver  
regeneration following tumour resection**

Thesis submitted in accordance with the requirements of  
the University of Liverpool for the degree of  
Doctor in Philosophy

By  
**Tobias Bunday**

**May 2023**

## **Declaration**

This thesis is the result of my own work. The material contained within this thesis has not been presented, nor is currently being presented, either wholly or in part for any other degree or qualification.

Tobias Bunday

This research was conducted in the Department of Pharmacology and Therapeutics, The University of Liverpool, UK.

## Contents

<b>Acknowledgements</b> .....	3
<b>Publications</b> .....	4
<b>Abbreviations</b> .....	5
<b>Abstract</b> .....	9
<b>Chapter 1: General introduction</b> .....	11
<b>Chapter 2: Pharmacological activation of Nrf2 enhances post-operative liver regeneration</b> .....	51
<b>Chapter 3: Pharmacological activation of Nrf2 does not promote <i>in vitro</i> proliferation of liver cancer cell lines</b> .....	98
<b>Chapter 4: Pharmacological activation of Nrf2 does not promote the proliferation of tumours forming from an orthotopic xenograft of human HCC and CRC cells in an <i>in vivo</i> model</b> .....	130
<b>Chapter 5: General discussion</b> .....	202
<b>References</b> .....	215

## Acknowledgments

This thesis would simply not have been possible without the support and encouragement of several people. Above all, I would like to express my sincere gratitude to my primary supervisor Prof. Ian Copple. Thank you for your continued support, expert guidance and inquisitive questions which have helped me to become a better and more thorough researcher. I would also like to thank Prof. Chris Goldring for the additional supervision and insightful discussions.

I have the deepest appreciation for Dr. Shiva Foorotan, Ben Chan and Adeeb Rehman for their endless support, friendship, and encouragement throughout the course of my PhD. The incredibly long days of surgery and MRI were made significantly easier and funnier with the conversations we shared.

I am incredibly grateful to the entire BSU technical team, specifically Esther, Katharine and Edita and the team within CPI. Thank you to Ema, Julie, and the rest of the Leahurst team for all the histopathological support. I would also like to thank Prof. Michael Schmid and Dr. Yuliana Astuti for their assistance in planning, optimising, and running the initial tumour xenograft work. Many thanks to Dr. Giusy Russomanno and Dr. Rowena Sison-Young for all their help with the human hep and transcriptomics work, and Dr. Michael Cross for his guidance surrounding in vitro assays.

Special thanks to everyone in the lab for making the whole PhD so much more enjoyable and for helping me stay sane throughout the highs and lows of the past several years. Thank you to the PhD elite for the many happy days and one too many pints in the AJ on sunny Friday afternoons. I will sincerely miss our conversations, Bongo's bingo trips and spontaneous evenings filled with laughter. It has been a pleasure working with you all and I hope to have the pleasure of doing so again at some point in the future.

Geo, thank you for your ever-lasting patience, support, love, and continuous supply of delicious baked goods throughout. Thank you for being there through the rollercoaster of emotions and for simply listening when I needed a good old moan, it has been a journey I couldn't have completed without you.

Finally, I can't thank my family enough for everything. Dad, Mum, and Hattie, thank you for putting up with me and for providing constant love and support.

## **Publications**

Chan, B.K.Y., Elmasry, M., Forootan, S.S., Russomanno, G., **Bunday, T.M.**, Zhang, F., Brilliant, N., Starkey Lewis, P.J., Aird, R., Ricci, E., Andrews, T.D., Sison-Young, R.L., Schofield, A.L., Fang, Y., Lister, A., Sharkey, J.W., Poptani, H., Kitteringham, N.R., Forbes, S.J., Malik, H.Z., Fenwick, S.W., Park, B.K., Goldring, C.E. and Copple, I.M. (2021), Pharmacological Activation of Nrf2 Enhances Functional Liver Regeneration. *Hepatology*, 74: 973-986. <https://doi.org/10.1002/hep.31859>

## Abbreviations

5-FU	5-fluorouracil
ABL2	ABL Proto-Oncogene 2
ActR	Antibody coupled T-cell receptor
ADRs	Adverse drug reactions
AFP	Alpha-fetoprotein
ALR	Augmenter of liver regeneration
AOM/DSS	Azoxymethane/Dextran sodium sulphate
AP1	Activating-protein 1
APC	Adenomatous polyposis coli
ARID1A	AT-rich interaction domain-containing protein 1A
ATP	Adenosine triphosphate
BCA	Bicinchoninic acid
BCLC	Barcelona Clinic Liver Cancer
BRAF	V-raf murine sarcoma viral oncogene homolog B1
BSA	Bovine serum albumin
BSL	Biosafety level
BTB	Broad-complex, Tramtrack and Bric a brac
BWR	Bodyweight ratio
bZIP	Basic Leucine zipper
CALI	Chemotherapy associated liver injury
CASH	Chemotherapy-associated steatohepatitis
CDDO-Me	2-Cyano-3,12-dioxooleana-1,9(11)-dien-28-oic acid methyl ester
cDNA	Copy deoxyribonucleic acid
CEA	Carcinoembryonic antigen
c-Met	c-Mesenchymal-epithelial transition factor
CRC	Colorectal cancer
CRLM	Colrectal liver metastases
Ct	Cycle threshold
CTR	C-terminal region
Cul 3	Cullin-dependent E3
DEGs	Differentially expressed genes
DEN	Diethylnitrosamine
DGR	Double-glycine repeat
dH <sub>2</sub> O	Distilled water
DILI	Drug induced liver injury
DMEM	Dulbecco's Modified Eagle's Medium
DMF	Dimethyl fumarate
DMSO	Dimethyl sulfoxide
DNA	Deoxyribonucleic acid
DTNB	5-5'-Dithiobis(2-nitrobenzoic acid)
ECL	Enhanced chemiluminescence
EDTA	Ethylenediaminetetraacetic acid
EdU	5-ethynyl-2'-deoxyuridine
EGF	Epidermal growth factor
EGFR	Epidermal growth factor receptor
ELISA	Enzyme-linked immunosorbent assay

FBS	Fetal bovine serum
FGFR1OP	Fibroblast Growth Factor Receptor 1 Oncogene Partner
FLI1	Friend leukemia integration 1 transcription factor
FLR	Future liver remnant
FOS	C-Fos proto-oncogene
GalNAc	N-acetylgalactosamine
Gapdh	Glyceraldehyde 3-phosphate dehydrogenase
GI	Gastrointestinal
GO	Gene ontology
GSEA	Gene set enrichment analysis
GSH	Glutathione
GST	Glutathione S-transferases
HCC	Hepatocellular carcinoma
HE	Haematoxylin-eosin
HEPES	N-2-hydroxyethylpiperazine-N-2-ethane sulfonic acid
HGF	Hepatocyte growth factor
HPF	High-power fields
HRP	Horseradish peroxidase
ICCA	Intrahepatic cholangiocarcinoma
IHC	Immunohistochemistry
IL-6	Interleukin-6
INR	International normalised ratio
IP	Intraperitoneal
ISGLS	International Study Group of Liver Surgeries
IVIS	In vivo imaging system
IVR	Intervening region
Keap1	Kelch-like ECH-associated protein 1
KRAS	Ki-ras2 Kirsten rat sarcoma viral oncogene homolog
LATS2	Large Tumor Suppressor Kinase 2
LCK	Lymphocyte-specific protein tyrosine kinase
LDS	Lithium dodecyl sulfate
LRP1B	Low density lipoprotein Receptor Related Protein 1B
MAF	Musculoaponeurotic fibrosarcoma
MAPK	Mitogen-activated protein kinase
MET	C-Met proto-oncogene
miRNA	Micro RNA
MMF	Monomethyl fumarate
MOPS	3-(N-morpholino)propanesulfonic acid
MRI	Magnetic Resonance Imaging
MTT	3-(4,5-dimethylthiazol2-yl)-2,5-diphenyl tetrazolium bromide
MYB	V-myb avian myeloblastosis viral oncogene homolog
NAD	Nicotinamide adenine dinucleotide
NADP	Nicotinamide adenine dinucleotide phosphate
NAFLD	Non-alcoholic fatty liver disease
NES	Normalised enrichment score
NF-E2	Nuclear factor erythroid 2
NFE2L2	Nuclear factor erythroid 2-related factor 2
NMP	Normothermic machine perfusion

NO	Nitric oxide
Notch1	Neurogenic locus notch homolog protein 1
NQO1	NAD(P)H quinone oxidoreductase 1
NRAS	Neuroblastoma RAS viral oncogene homolog
Nrf2	Nuclear factor erythroid 2-related factor 2
NTR	N-terminal region
OCT	Optimal cutting temperature
PARP	Poly-ADP ribose polymerase
PBS	Phosphate buffered saline
PCNA	Proliferating cell nuclear antigen
PD-1	Programmed Cell Death Protein 1
PEI	Purcutaneous ethanol injection
pES	Permutation enrichment scores
PFA	Paraformaldehyde
Pgd	Phosphogluconate Dehydrogenase
PHH	Primary human hepatocytes
PHLF	Post-hepatectomy liver failure
PHx	Partial hepatectomy
PI3K	Phosphoinositide 3-kinase
PPI	Protein-protein interaction
PTEN	Phosphatase and tensin homolog
PVE	Portal vein embolisation
PYDDT	2-(Pro-1-ynyl)-5-(5,6-dihydroxypenta-1,3-diynyl) thiophene
qPCR	Quantitative polymerase chain reaction
RARE	Rapid acquisition with refocused echoes
Ras	Rat sarcoma
REL	C-Rel proto-oncogene
RET	Ret Proto-Oncogene
REVIGO	Reduce and visualise gene ontology
RFA	Radiofrequency ablation
RIPA	Radioimmunoprecipitation assay
RLV	Remnant liver volume
RNA	Ribonucleic acid
ROI	Region of interest
ROS	Reactive oxygen species
ROS1	C-ros oncogene 1
RPM	Revolutions per minute
RPMI	Roswell Park Memorial Institute
RRMS	Relapse-remitting multiple sclerosis
saRNA	Small activating RNA
Scd1	Stearoyl-CoA desaturase 1
SDS	Sodium dodecyl-sulfate
SFSS	Small for size syndrome
SFX-01	Sulforadex
siRNA	Small interfering RNA
SMAD2/3	Mothers against decapentaplegic homolog 2/3
sMAF	Small maf
SSA	Sulfosalicylic acid



STAT3	Signal transducer and activator of transcription 3
TACE	Transarterial chemoembolization
TBS	Tris-buffered saline
TBS-T	Tris buffered saline tween
TGF-a	Transforming growth factor alpha
TGF-b	Transforming growth factor beta
TNF-a	Tumour necrosis factor alpha
TNFR1	TNF receptor 1
TP53	Tumour protein 53
UK	United Kingdom
vst	Variance stabilising transformation

## Abstract

Liver cancer, encompassing both primary cancers such as hepatocellular carcinoma (HCC), and secondary cancers such as colorectal liver metastasis (CRLM), is becoming increasingly prevalent worldwide. Despite significant advances in treatment strategies, liver cancer remains incredibly challenging to treat. These challenges can be attributed in part to post-operative complications, such as post-hepatectomy liver failure (PHLF), that can occur following surgical resection of liver tumours and subsequent inadequate regeneration of liver tissue. Current PHLF management and preventative strategies are insufficient in reducing its incidence and can lead to further complications, thus illustrating the need for novel therapeutics aimed at promoting post-surgical liver regeneration, in turn reducing the clinical burden of PHLF. Owing to the implication of antioxidant, inflammatory and metabolic pathways in these post-operative complications, and the somewhat recent progression of nuclear factor erythroid 2-related factor 2 (Nrf2) activators into late-stage clinical trials and even routine clinical use, such small molecule compounds have the potential to rectify this currently unmet need for novel therapeutics. However, due to the vastly conflicting reported findings associated with the role of Nrf2 in liver cancer, and the nature in which surgical liver resection occurs, it is essential to ensure that any Nrf2 stimulating therapeutic strategy is safe in the context of liver tumour surgery and does not worsen the burden of liver cancer by promoting the growth of pre-existing liver tumours.

In chapter 2, I hypothesised that pharmacological activation of Nrf2 would enhance liver regeneration following a two-thirds partial hepatectomy (PHx) in wild-type mice. In order to test this hypothesis, I utilised a well-tolerated and reproducible two-thirds PHx rodent model (Mitchell & Willenbring, 2008) in combination with non-invasive Magnetic Resonance Imaging (MRI), to investigate the effect of the Nrf2 activator, bardoxolone methyl (CDDO-Me), on the functional restoration of liver volume in wild-type C57BL/6 mice. The findings of this chapter show that CDDO-Me, and subsequent activation of the Nrf2 pathway, significantly enhances liver regeneration following two-thirds PHx. Furthermore, through the use of *in vitro* functional assays, the molecular mechanisms underpinning Nrf2 driven liver regeneration were determined. The findings confirmed the importance of hepatic cell proliferation in liver regeneration and that proliferation is enhanced following treatment with CDDO-Me. Additionally, the biochemical analyses conducted in chapter 2 provide evidence for the enhancement of metabolic remodelling and adaptation in the livers of mice treated with CDDO-Me. Finally, the clinical translatability of such a rodent PHx model was illustrated through the exposure of primary human hepatocytes to CDDO-Me, in which pharmacological Nrf2 activation was shown to modulate many of the biochemical and transcriptional processes associated with enhanced liver regeneration in the livers of mice treated with CDDO-Me.

In chapter 3, I hypothesised that pharmacological Nrf2 activation would not promote *in vitro* proliferation in liver cancer and colorectal cancer cell lines. In order to test this hypothesis, an *in vitro* cell ATP proliferation assay was utilised to investigate the proliferative ability of the hepatocellular carcinoma (HCC) cell lines, HepG2 and Huh7, as well as the colorectal cancer (CRC) cell lines, HCT116 and SW480, treated or not with CDDO-Me. The findings of this chapter highlighted the potential of CDDO-Me to elicit an anti-tumour effect in both human HCC and CRC cell lines *in vitro*, thus supporting previously published findings (Gee et al., 2018; Hao et al., 2020) and providing promise for the use of CDDO-Me to enhance liver regeneration without adversely affecting HCC or CRC cell proliferation. It is however essential that such methods are translatable, and the role of Nrf2 in liver cancer investigated using relevant *in vivo* liver tumour models.

In chapter 4, I utilised an *in vivo* subcapsular intrahepatic orthotopic xenograft model in which human HCC and CRC cells, stably expressing luciferase, were implanted into immunocompromised mice. Non-invasive bioluminescence IVIS imaging was then used to monitor the burden of resulting liver tumours in mice treated or not with CDDO-Me. The findings of such non-invasive bioluminescence imaging demonstrate that CDDO-Me does not promote the growth of tumours formed from the orthotopic xenograft of HCC or CRC cells. This was further confirmed with histological examination, aimed at investigating how the tumours grew in the presence of CDDO-Me, in which treatment with CDDO-Me was shown to elicit no effect on the mitotic index, tumour fibrosis and necrosis, or overall tumour burden. Such findings, coupled to the previously demonstrated enhancement of liver regeneration, illustrate the potential of CDDO-Me and pharmacological Nrf2 activation to improve treatment strategies for liver cancer with the confidence that such acute stimulation of Nrf2 will not cause further development of cancer.

The overall findings of this thesis, obtained from the development and utilisation of reproducible *in vivo* and *in vitro* approaches, coupled with the discussed further work and future directions, provides key insight into how Nrf2 activating therapies can play a novel and safe role in enhancing liver regeneration in patients following tumour resection. The refinement of such a therapeutic approach, in which the risk of PHLF is reduced following an enhancement of liver regeneration, would drastically improve liver cancer treatment options by reducing the current burden of complications and expanding the eligibility of existing curative liver cancer treatments.

## **Chapter 1**

### **General introduction**

## Contents

<b>1.1 Introduction</b> .....	13
<b>1.2 Liver physiology</b> .....	14
<b>1.3 Liver cancer</b> .....	18
1.3.1 Causes and risk factors.....	19
1.3.2 Current treatments.....	21
<b>1.4 Liver regeneration</b> .....	25
1.4.1 Mechanisms of liver regeneration.....	26
1.4.2 Surgical complications and PHLF.....	31
<b>1.5 Nuclear factor erythroid 2-related factor 2 (Nrf2)</b> .....	35
1.5.1 Basal response of Nrf2 and regulation by Keap1.....	36
1.5.2 Activation of Nrf2.....	39
1.5.3 Pharmacological Nrf2 activators – past and present.....	41
<b>1.6 Nrf2 in the liver</b> .....	45
1.6.1 Nrf2 in liver regeneration.....	45
1.6.2 Nrf2 in liver cancer.....	47
<b>1.7 Thesis aims</b> .....	49

## 1.1 Introduction

The incidence of liver cancer has continually increased worldwide over the last few decades (Bosch et al., 2004; Akinyemiju et al., 2017), resulting in an escalating clinical burden (Are et al., 2017). Despite there being an abundance of well-established standards of care (Liu et al., 2015), and significant advancements in treatment strategies (Gosalia et al., 2017), liver cancer remains incredibly challenging to treat (Colagrande et al., 2016; Erstad and Tanabe, 2017).

Whilst the standard of care is considered inadequate in many cases, there are therapeutic approaches regarded as curative, which are often labelled as superior options (Pecorelli et al., 2017). Such curative approaches, which include, transplant (Abreu et al., 2019), surgical resection (Orcutt and Anaya, 2018) and percutaneous treatment via both cryoablation (Ma et al., 2019) and radiofrequency ablation (Izzo et al., 2019), are recommended following early detection of liver cancer (Sacco et al., 2016). However, although regarded as curative, surgical resection carries further risk and complication, specifically post-operatively due to the sheer insult inflicted on the liver. Post-hepatectomy liver failure (PHLF) is one of the most serious complications (Stoffels et al., 2016) and is a key factor in mortality following surgical resection (Narita et al., 2015) despite advances in its management and prevention (Rahnemai-Azar et al., 2018).

By targeting antioxidant pathways, there is a potential to alleviate the clinical difficulties that PHLF creates. As a result of its ability to upregulate a battery of cytoprotective and metabolic genes, allowing maintenance of cellular redox homeostasis (Tebay et al., 2015), Nuclear factor erythroid 2-related factor 2 (Nrf2) has been shown to provide protection against numerous chronic diseases encompassing oxidative stress and metabolic disorders (Cuadrado et al., 2018; Robledinos-Antón et

al., 2019). Pharmacological activation of Nrf2 may therefore be a promising therapeutic strategy in aiding surgical resection, subsequently reducing the associated risk of PHLF.

However, it is crucial to remember the oncological nature in which surgical resection occurs, with the potential for patients to still possess cancerous masses within the remnant liver, especially as the hyperactivation of Nrf2 is being increasingly documented in liver cancer (Levings et al., 2018; Rogers et al., 2021). It is therefore of key importance that any therapeutic approach aimed at aiding surgical resection, and reducing the risk of PHLF, does not promote cancer growth. This thesis therefore seeks to investigate if pharmacological activation of Nrf2 can aid liver regeneration, whilst ensuring such treatment does not worsen the burden of liver cancer by promoting the growth of tumours.

## **1.2 Liver physiology**

The liver is an essential organ responsible for performing a large number of differing functions, such as the detoxification and metabolism of drugs and other toxic compounds (Rui, 2014), thus aiding with the maintenance of homeostasis and general health (van den Berghe, 1991). The liver is located predominantly in the right hypochondrium, extending into the left hypochondrium above the stomach. Macroscopically, the liver comprises of a larger right lobe and a smaller left lobe, separated by the falciform ligament. This sickle-shaped ligament, consisting of two layers of peritoneum, also anchors the anterior surface of the liver to the diaphragm. In addition, there are two further, much smaller, accessory lobes known as the caudate and quadrate lobes, that originate from the larger right lobe (Abdel-Misih and Bloomston, 2010). The outside of the liver is then covered by a layer of fibrous tissue called the Glisson's capsule, helping to hold the liver in place whilst providing protection from physical damage (Ger, 1989) (Figure 1.1).

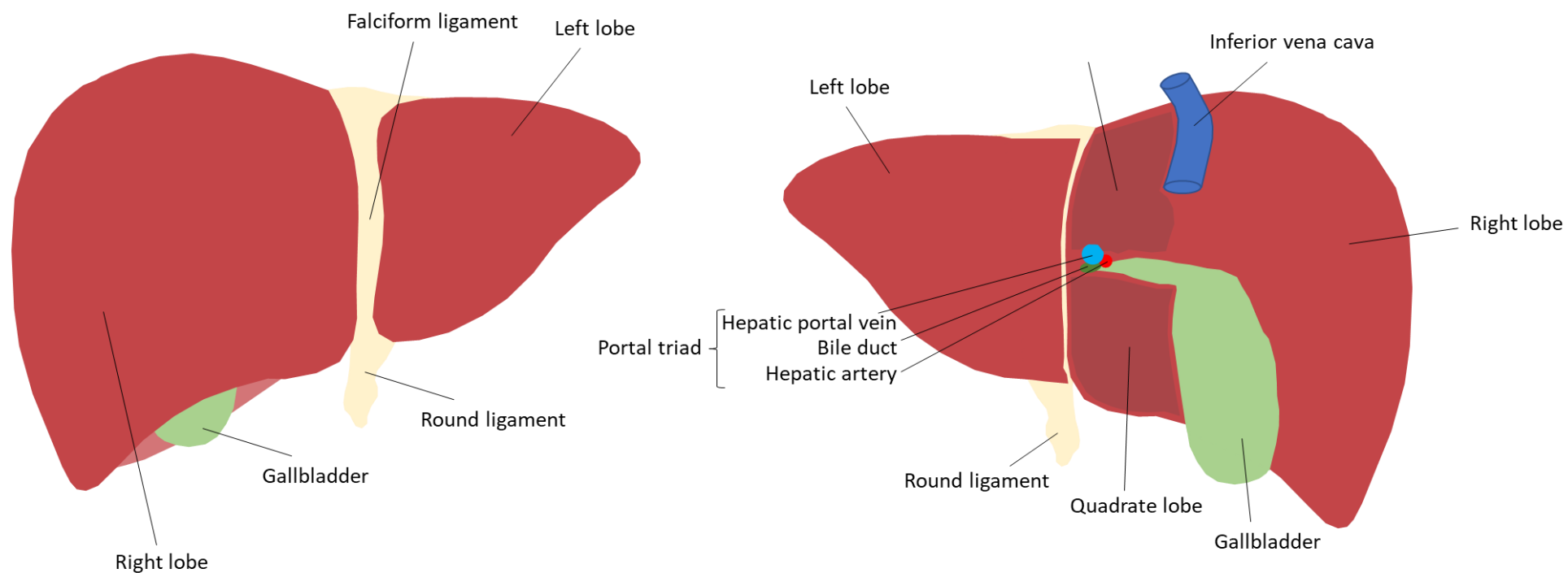


**Figure 1.1 Macroscopic anatomy of the human liver**

Macroscopically, the liver comprises of a larger right lobe and a smaller left lobe, separated by the falciform ligament. In addition, there are two further, much smaller, accessory lobes known as the caudate and quadrate lobes, that originate from the larger right lobe. Adapted from (Guido et al., 2019).



Microscopically, the liver comprises of numerous structural units known as hepatic lobules. Making up the majority of these hexagonal lobules are parenchymal hepatocytes. Hepatic lobules can be separated into three different metabolic zones, with each zone performing a distinct function (Krishna, 2013). Zone 1, otherwise known as the periportal zone, specialised for oxidative liver functions, therefore predominantly playing a huge role in oxidative metabolisms such as gluconeogenesis (Ekberg et al., 1995),  $\beta$ -oxidation of fatty acids (Jungermann, 1983) and cholesterol formation (Krueger et al., 2013). Zone 2, otherwise referred to as the intermediary zone, contains hepatocytes located between zones 1 and 3. Hepatocytes in this region receive partially oxygenated blood with moderate exposure to toxic substances (Kietzmann, 2017). Zone 3, or the perivenous zone, contains hepatocytes specialised for detoxification, due to the abundance of cytochrome P450 enzymes, and therefore play a huge role in: biotransformation of drugs (Dionne et al., 2008); ketogenesis (Jungermann, 1986); glycolysis and lipogenesis (Jungermann and Katz, 1989), amongst other detoxifying reactions (Comar et al., 2010) (Figure 1.2).

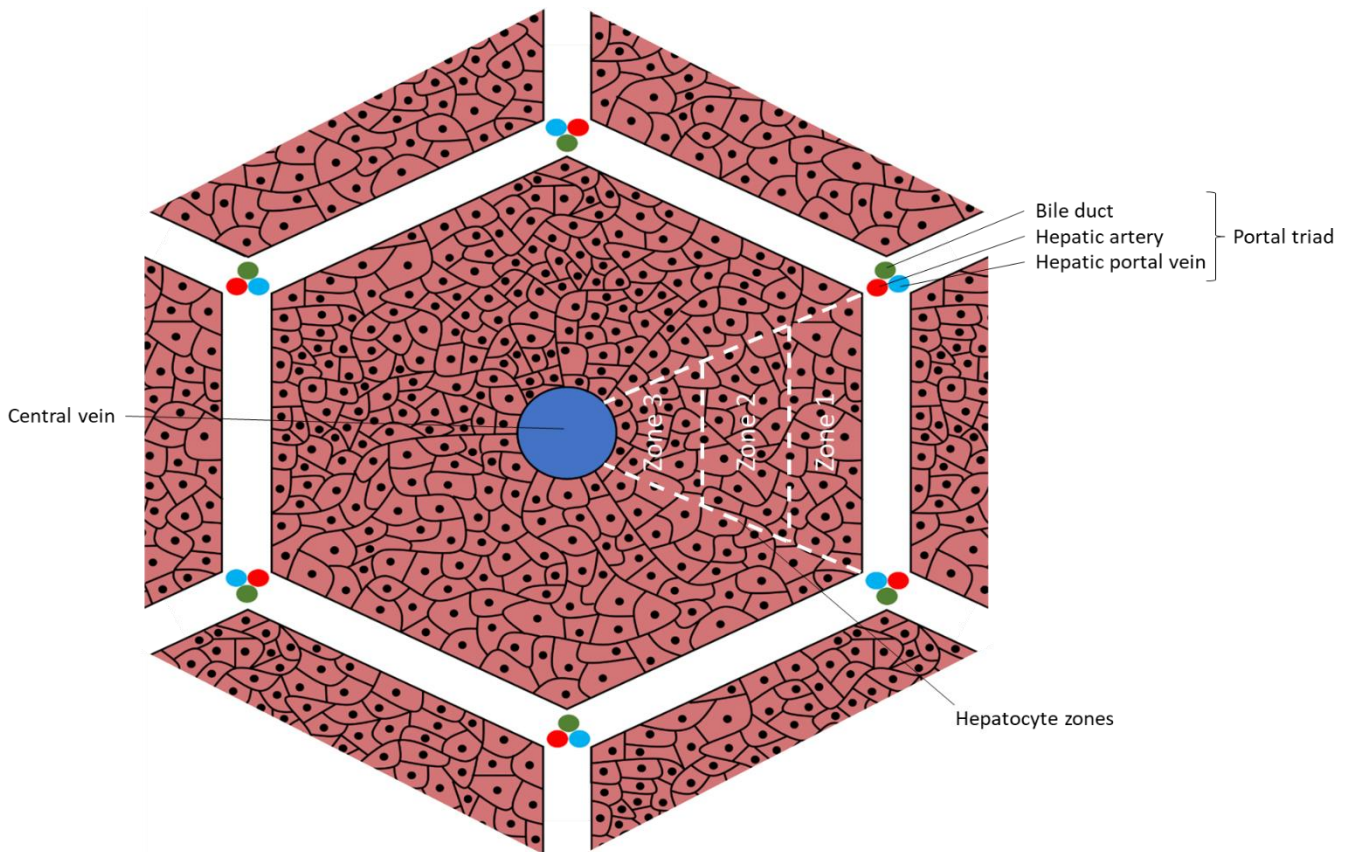


**Figure 1.2 Microscopic anatomy of the human liver – hepatic lobule**

Microscopically, the liver comprises of numerous structural units known as hepatic lobules. Making up the majority of these hexagonal lobules are parenchymal hepatocytes. Hepatic lobules can be separated into three different metabolic zones, 1-3, each one performing a distinct function.

### 1.3 Liver Cancer

Liver cancer is the term used to describe a diverse family of malignancies, encompassing both primary and secondary cancers. Liver cancer, including both primary and secondary, has a recurrently rising incidence (Liu et al., 2019) and is within the six most deadly cancers in the UK and worldwide (Siegel et al., 2021; Sung et al., 2021), with estimates predicting a continuation of this trend (Smittenaar et al., 2016).

Primary liver cancers are defined as a tumour(s) originating within the liver itself. The most common subtype of primary liver cancer, accounting for 80-90 % of all cases (Llovet et al., 2016; Yang et al., 2019) is hepatocellular carcinoma (HCC), an epithelial tumour which presents hepatocytic differentiation (Burton et al., 2021). Intrahepatic cholangiocarcinoma (ICCA), an epithelial tumour presenting biliary differentiation (Rizvi et al., 2018) is the second most common subtype, accounting for 10-20 % of all cases (Kirstein and Vogel, 2016). There are also rare subtypes of primary liver cancer, including hepatoblastoma and other sarcomas, however these only typically account for 1-2 % of all primary liver cancer cases (Mitra et al., 2017).

On the other hand, secondary liver cancers are defined as a tumour(s) originating in another region of the body which then metastasises to the liver. Such cancers are more frequent than primary liver cancer (Watson et al., 2016). Typically, secondary liver cancers originate from primary tumours in the breast, lung, and colon (Ayoub et al., 1998; Ananthkrishnan et al., 2006), with almost 15 % of primary colorectal cancer patients presenting liver metastases (Manfredi et al., 2006). Colorectal liver metastases (CRLM) account for roughly 20 % of all secondary liver cancers (Wang et al., 2021).

### 1.3.1 Causes and risk factors

Liver cancer, both primary and secondary, has numerous differing causes and risk factors associated with its development, such as: hepatitis infection (Trépo et al., 2014); high-fat diet (Marengo et al., 2016); long-term alcohol abuse (Chuang et al., 2009); and chemical insult from chemotherapeutic compounds used to treat cancers in other regions of the body (Maor and Malnick, 2013).

Viral hepatitis infection, mainly hepatitis B and C, can promote hepatocarcinogenesis in a variety of ways, with inflammation and subsequent cirrhosis accounting for only a small percentage of these (Ringehan et al., 2017). In the majority of cases, viral hepatitis genomes are able to integrate into the host genome, thus inducing alteration of chromosomes and insertional mutagenesis of cancer genes (Buendia and Neuveut, 2015). This in turn promotes hepatocarcinogenesis. Chemotherapeutic compounds can similarly cause DNA damage within hepatocytes due to the drug metabolising role of the liver. Unlike viral hepatitis infections however, this DNA damage is commonly caused by the off-target adverse drug reactions (ADRs) of these cytotoxic agents (Sharma et al., 2014), or as a result of the production of reactive oxygen species (ROS) originally intended to induce tumour cell apoptosis (Lim et al., 2009). In both cases, drug-induced liver injury (DILI) occurs, subsequently leading to extensive cirrhosis and eventually the development of liver cancer (Bahirwani and Reddy, 2014; Ricart, 2017).

Occurring in 10-40 % of patients either currently undergoing, or recently finishing a chemotherapy regimen (White et al., 2016; Meunier and Larrey, 2020), chemotherapy-associated steatohepatitis (CASH) is amongst the most common abnormality observed with chemotherapy associated liver injury (CALI), especially in patients receiving chemotherapy regimens which include irinotecan or oxaliplatin (Fernandez et al., 2005). Steatohepatitis and subsequent inflammation of the liver tissue

can then lead to fibrosis, cirrhosis and eventually the development of cancer (Robinson et al., 2012; Reddy et al., 2014; Paternostro et al., 2021). In contrast and unlike viral hepatitis infection and chemical insult, high-fat diets, leading to non-alcoholic fatty liver disease (NAFLD), and long-term alcohol abuse, directly cause chronic inflammation of the liver (Pocha and Xie, 2019). This again then results in fibrosis, cirrhosis, and the development of cancer (Singal and El-Serag, 2015; Brar and Tsukamoto, 2019).

Despite the differences in each respective mechanism, all of the associated causes and risk factors share the common outcome of inducing widespread hepatic damage, subsequently leading to the development and maturation of liver cancer. Although there is an abundance of evidence and knowledge surrounding the underlying aetiology (Ghoury et al., 2017), liver cancer has a drastically increasing prevalence within the United Kingdom (UK) and other Western countries (Burton et al., 2021). This continually rising prevalence in both primary and secondary malignancies is a result of significant alterations to routine diet and worsening lifestyle factors. More specifically, an increase in high-fat diets, and associated obesity, as well as an increase in long-term alcohol abuse (Huang et al., 2022). However, this rising prevalence and in turn growing mortality rate could also be attributed to an increase in the rates of other cancers. If the routine use of cytotoxic chemotherapeutic compounds continues for other malignancies, greater rates of CASH may be observed in the clinic, further adding to the liver cancer burden. Reducing the number of chemotherapy cycles, or increasing the intervals between each cycle has been shown to reduce the risk associated with CASH (Karoui et al., 2006), and alterations to current standards of care to include novel therapies could help significantly reduce the current incidence (Maor and Malnick, 2013).

### 1.3.2 Current treatments

Most commonly, the treatment offered depends not only the type of cancer present, but also on the location of the tumour(s), how advanced the malignancy is, and the overall health of the patient (Volk and Marrero, 2008; Bruix and Sherman, 2011; Lin et al., 2012). In the UK, the Barcelona Clinic Liver Cancer (BCLC) staging system is used to determine how advanced HCC is. This system has five different stages, these being: stage 0; A; B; C and D (Reig et al., 2014; Díaz-González et al., 2016) (Figure 1.3). Stage 0, or very-early HCC, is defined as a single tumour nodule measuring less than 2 cm, with normal liver function and good patient health (Bruix et al., 2016). These patients present optimal conditions for treatment strategies that are often labelled as curative, such as transplantation (Hackl, 2014), ablation (Ryan, 2016) and surgical resection (Tsim, 2010), with resection frequently being the most common option due to the wide availability of surgery and reproducible success (Kow, 2019) and the considerable difficulties associated with transplant such as organ shortage (Jadlowiec, 2016). Immediate surgical resection, made possible due to the liver's remarkable ability to regenerate itself and restore normal liver function following surgical insult, reduces the risk of metastasis and recurrence, whilst boosting the chances of patient survival, with 5-year survival rates ranging from 60-80 % (Livraghi et al., 2007; Roayaie et al., 2013).

Stage A, or early HCC, is defined as less than three tumour nodules measuring no greater than 3 cm each, with good patient health and normal liver function (Tellapuri et al., 2018). Patients presenting HCC at this stage are again eligible for surgical resection, providing their bilirubin levels are normal and they do not present portal hypertension (Manzini et al., 2017). Patients with stage A HCC and increased levels of bilirubin normally undergo one of either: liver transplantation; percutaneous ethanol injection (PEI) in which ethanol is injected into the tumour nodule(s), causing dehydration, denaturing of cellular proteins and subsequently death of the nodule(s) (Weis et al., 2015); or radiofrequency ablation (RFA) in which high-energy radio waves are passed through the tumour

nodule(s), thus killing the cancerous cells (Minami, 2010). As with stage 0, the treatment options for stage A HCC are considered curative with 5-year survival rates ranging from 50-80 % (Lee et al., 2014; Bruix et al., 2016).

Stage B, or intermediate HCC, is defined as multinodular with reasonably good patient health and liver function (Jianyong et al., 2014). Despite good patient health, it is often deemed that a curative treatment such as resection is not immediately possible. This is commonly due to the numerous tumour nodules occupying a large region of the hepatic parenchyma, thus preventing effective and safe surgical resection of affected liver tissue. Instead, patients typically undergo the only recommended treatment strategy for intermediate HCC, this being transarterial chemoembolization (TACE) (Piscaglia and Ogasawara, 2018). During this, the cytotoxic agents: doxorubicin; cisplatin and mitomycin are administered, either alone or in combination, directly into the hepatic artery, thus allowing for localised high doses of chemotherapy (Lencioni et al., 2013). If the patient responds well and the tumour nodules decrease in size and number, then future curative strategies such as surgical resection may be possible (Chen et al., 2017). In cases where TACE does not succeed in shrinking the size or number of tumour nodules, or does not prevent metastatic growth, patients are categorised as TACE non-responders and treatment strategies are re-evaluated (Georgiades et al., 2012). Following this, and after assessing whether patients are presenting any of the adverse effects associated with TACE, treatment involves either repeating TACE up to an additional two times, or the commencement of sorafenib as a stage C, or advanced stage HCC, targeted therapy (Bruix et al., 2012; Raoul et al., 2014).

Stage C, or advanced HCC, is defined as multinodular in which portal invasion and extrahepatic spread have occurred, with patients also presenting poor liver health and cancer-related symptoms (Maida, 2014). Due to the widespread liver damage and aggressive behaviour of the cancer,

conventional chemotherapy and curative strategies are ineffective in patients possessing advanced HCC, leaving oral administration of sorafenib as the only conventional first line treatment option. However, outcomes remain suboptimal with sorafenib reducing patients' risk of death by approximately 30 %, providing only a further 3 months survival in most cases (Sinn et al., 2015; Jun et al., 2017). As a result of the poor prognosis and lack of effective treatment, there is a crucial need for novel approaches and thus some patients are advised to trial new therapeutic strategies for advanced HCC as part of a randomised controlled trial (Lee and Abou-Alfa, 2013). Such clinical trials commonly include the use, and repurposing of, existing therapies used to treat other forms of cancer. Recent trials have highlighted some efficacy with targeted therapies such as the multi-targeted tyrosine kinase inhibitor lenvatinib, and immunotherapies such as the PD-1 inhibitor pembrolizumab (Desai et al., 2017; Raoul et al., 2018).

Stage D, or terminal HCC, is defined as multinodular, with multiple metastases, severe dysfunction of the liver and poor patient health with symptoms related to chronic liver failure (Lin et al., 2012).

Patients presenting stage D HCC will only receive end of life symptomatic treatment and appropriate palliative care, with median survival being less than 3 months (Cabibbo et al., 2010).



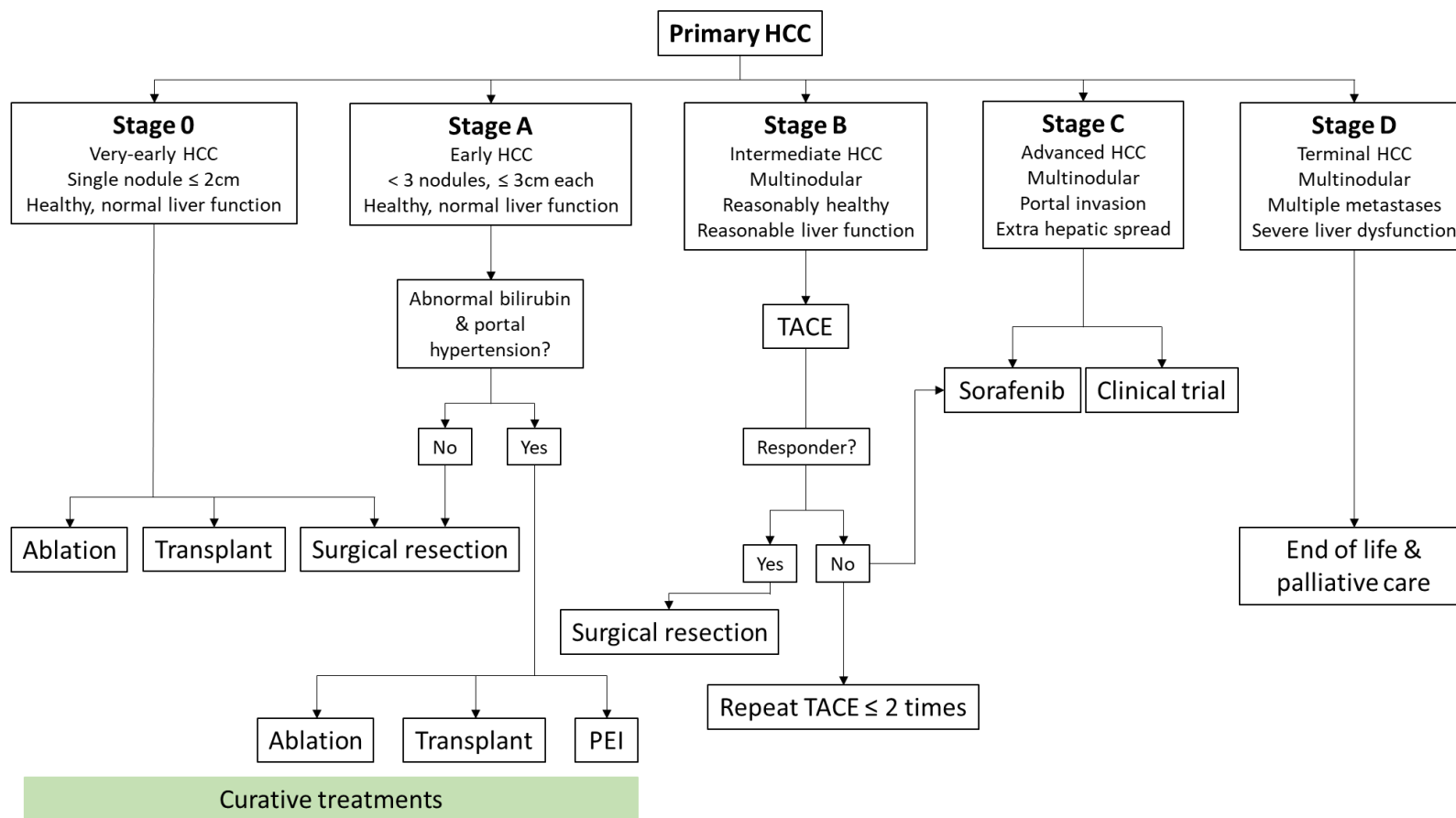


**Figure 1.3 Treatment options for primary HCC according to the BCLC staging system**

Patients presenting primary HCC are staged according to the Barcelona Clinic Liver Cancer (BCLC) staging system. The treatment options available then vary depending on the stage of HCC presented. Adapted from (Bruix et al., 2016).

Unlike primary HCC, there is no generic scoring system for secondary liver cancer arising from colorectal metastasis. Instead, CRLM is scored based on the prognostic factors proposed by Ueno et al. in 2000. (Ueno et al., 2000), these being: stage A, none or either liver metastasis at <1 year or three or more liver metastases; stage B, primary tumour aggressiveness or both liver metastasis at <1 year and three or more liver metastases; stage C, all three risk factors (Gomez and Cameron, 2010). As with primary HCC, treatment for secondary colorectal metastasis primarily starts with surgical resection in an attempt to completely remove all tumours. However, this is entirely dependent on the extent of metastases present and is commonly only available to patients in stage A (Chakedis and Schmidt, 2018). Patients possessing extensive colorectal metastasis are initially ineligible for surgery and hence undergo preliminary radiotherapy ablation (Ryan, 2016) or chemotherapy treatment with regimens including oxaliplatin, irinotecan and 5-fluorouracil (5-FU) to shrink and prevent further metastasis, before surgical resection is reconsidered (Misiakos, 2011).

#### **1.4 Liver regeneration**

The liver is the only organ within the human body that is able to regenerate itself. Liver regeneration is a phenomenon in which normal hepatic mass and function is restored following the loss of liver tissue, commonly a result of surgical resection in liver cancer patients. This highly complex and well-orchestrated process involves cross-talk between numerous signalling cascades and can be defined by three crucial, distinct phases: priming; proliferation and termination (Tao et al., 2017).

Immediately following the loss of hepatic tissue, the liver enters the priming phase. An increase in liver shear stress leads to the production and release of augments of liver regeneration (ALR), in turn upregulating the mitogen-activated protein kinase signalling cascade, and inducing hepatocyte proliferation and survival (Fausto, 2000). Following this, the liver enters the proliferation phase.

Aided by various mitogens, hepatocytes are able to enter mitosis allowing for the induction of hepatocyte DNA synthesis, thus promoting hepatocyte proliferation (Jia, 2011). The liver then enters the termination phase to allow regeneration to be efficiently halted. Though not fully understood, the most accepted mechanism involves the utilisation of well-known antiproliferative factors which cause inhibition of hepatocyte proliferation and termination of liver growth (Derynck and Zhang, 2003).

However, in some cases liver regeneration following surgical resection does not occur efficiently or successfully, leading to a variety of post-operative complications. The most severe of these, having numerous patient, liver, and surgery related risk factors associated with initiation and maturation, is post-hepatectomy liver failure (PHLF) (Stoffels et al., 2016). PHLF presents a significant clinical burden, with its limited treatment strategies often proving ineffective in reversing the extensive hepatic damage observed.

#### **1.4.1 Mechanisms of liver regeneration**

As mentioned previously, surgical resection is made possible due to the liver's ability to regenerate and restore both mass and function. The process of liver regeneration comprises of three distinct phases: priming; proliferation and termination, with each phase involving the utilisation of multiple complex pathways, as well as the production and release of numerous signalling molecules and growth factors (Tao et al., 2017). Immediately after surgical resection, in which blood flow is routinely restricted, the surgical team reinstates the blood supply, allowing blood to enter through the hepatic inflow system and pass through the diverse vascular network of the remnant liver section. This blood flow causes an immediate increase in shear stress within the liver, increasing the production and release of augments of liver regeneration (ALR). This crucial protein activates the mitogen-activated

protein kinase pathway, thus upregulating the production of tumour necrosis factor alpha (TNF- $\alpha$ ), interleukin-6 (IL-6) and nitric oxide (NO) from Kupffer cells (Nalesnik et al., 2017), allowing the liver to enter the priming phase of regeneration (Fausto, 2000). TNF- $\alpha$  then further enhances the expression of IL-6 through the activation of TNF receptor 1 (TNFR1), eventually resulting in the activation of signal transducer and activator of transcription 3 (STAT3), which then induces hepatocyte proliferation and survival following resection (Li et al., 2002).

Partial hepatectomy (PHx) is the name given to the well-established surgical procedure in which resection of part of the liver takes place. In humans, this is conducted via open laparoscopic or robotic-assisted surgery (Aragon and Solomon, 2012) to remove cancerous tissue. This procedure is often modelled in rodents, as first described in 1931 by Higgins et al. (Higgins et al., 1931), and involves the ligation and excision of the left lateral and median lobes, encompassing approximately 2/3 of the total liver mass, through a small midline abdominal incision (Boyce and Harrison, 2008; Mitchell and Willenbring, 2008).

It has been demonstrated that blocking TNF- $\alpha$  signalling in rats prior to PHx, through the use of TNF- $\alpha$  neutralising antibodies, drastically reduces the proliferative ability of both hepatocytes and non-parenchymal liver cells (Akerman et al., 1992). In addition, mice lacking TNFR1, a crucial receptor involved in the modulation of immune homeostasis, displayed severely impaired DNA synthesis following PHx, thus preventing efficient liver regeneration, and increasing mortality rate (Yamada et al., 1998). Nitric oxide (NO) has also been shown to play an essential role during the early stages of liver regeneration in rodents, following observed impairment of liver regeneration in nitric oxide synthase deficient mice (Rai et al., 1998). This role of NO in liver regeneration is achieved through the cytoprotective, anti-apoptotic, and pro-angiogenic, effects exerted on Kupffer cells within the liver, in

turn allowing normally quiescent hepatocytes to progress through a mitogen driven cell cycle, promoting proliferation. (Carnovale and Ronco, 2012).

Following priming, the liver progresses to the proliferation phase, allowing hepatocytes to enter mitosis. This process is aided by various mitogens including, but not limited to, hepatocyte growth factor (HGF), epidermal growth factor (EGF) family and transforming growth factor alpha (TGF- $\alpha$ ) (Tao et al., 2017). HGF binds to the receptor tyrosine kinase c-Met, which in turn activates the PI3K and Ras/MAPK pathways, inducing hepatocyte DNA synthesis. Subsequently, hepatocyte proliferation is promoted (Organ and Tsao, 2011), increasing the levels of proliferative markers such as proliferating cell nuclear antigen (PCNA). The crucial need for both HGF and c-Met has been demonstrated as hepatocyte proliferation is suppressed following the knock-down of HGF (Paranjpe et al., 2007) or c-Met (Huh et al., 2004) in rodents. EGF and TGF- $\alpha$  promote hepatocyte proliferation through the Ras/MAPK pathway following the binding of either mitogen to their identical receptor, epidermal growth factor receptor (EGFR) (Michalopoulos and Khan, 2005). Interestingly, knocking down EGF (Mitchell et al., 2005) or TGF- $\alpha$  (Russell et al., 1996) in rodents, independently of each other, has little to no effect on liver regeneration, highlighting a potential compensatory mechanism between the two mitogens (Natarajan et al., 2007). The combinatorial effect of HGF, EGF family and TGF- $\alpha$ , amongst others, provides the necessary conditions for cellular proliferation to occur, in turn allowing for the restoration of the hepatic architecture. However, it is crucial that this proliferation, and regeneration of hepatic tissue, is halted once the normal liver mass/body mass ratio has been restored.

In order to efficiently halt regeneration, the liver must carry out the termination phase. Although the exact mechanisms involved within the termination phase are not fully understood, it is commonly proposed that transforming growth factor beta (TGF- $\beta$ ) and activins aid this process of termination

(Tao et al., 2017). TGF- $\beta$  existing in three isoforms (TGF- $\beta$ 1-3) is a potent inhibitor of cellular growth. In addition, included within the TGF- $\beta$  superfamily are activins, which are also able to exert an anti-proliferative function. Following binding to their respective receptors, TGF- $\beta$ R or ActR, induction of SMAD2/3 occurs, which subsequently causes inhibition of hepatocyte proliferation and the termination of liver growth (Böhm et al., 2010). However, interestingly, the termination of cellular proliferation, and in turn liver regeneration, appears to require the presence of both TGF- $\beta$  and activin in rodent models, with upregulation or overexpression of either TGF- $\beta$  or activin failing to further inhibit hepatocyte proliferation and in turn liver regeneration beyond what is normally observed in wild-type, untreated rodents (Russell et al., 1988; Oe et al., 2004). It is therefore highly likely that TGF- $\beta$  and activin work together, with a compensatory mechanism. It is also probable that, in addition to TGF- $\beta$  and activin, other proteins are involved in the termination phase of liver regeneration (Figure 1.4).

Although rodent PHx models provide crucial insight into the molecular processes and signalling mechanisms underpinning liver regeneration, such models can lack translatability to the clinical observations of patients undergoing surgical resection. This is mainly due to the considerable differences in the approaches of such studies and the availability of tissue and blood samples, the latter of which being significantly lower in patients when compared to rodent models, in which there is uncompromised access (Forbes and Newsome, 2016). Despite this however, the underlying mechanisms of liver regeneration are widely accepted and further advances in clinical practices will undoubtedly better the understanding of the translatability of such mechanisms.

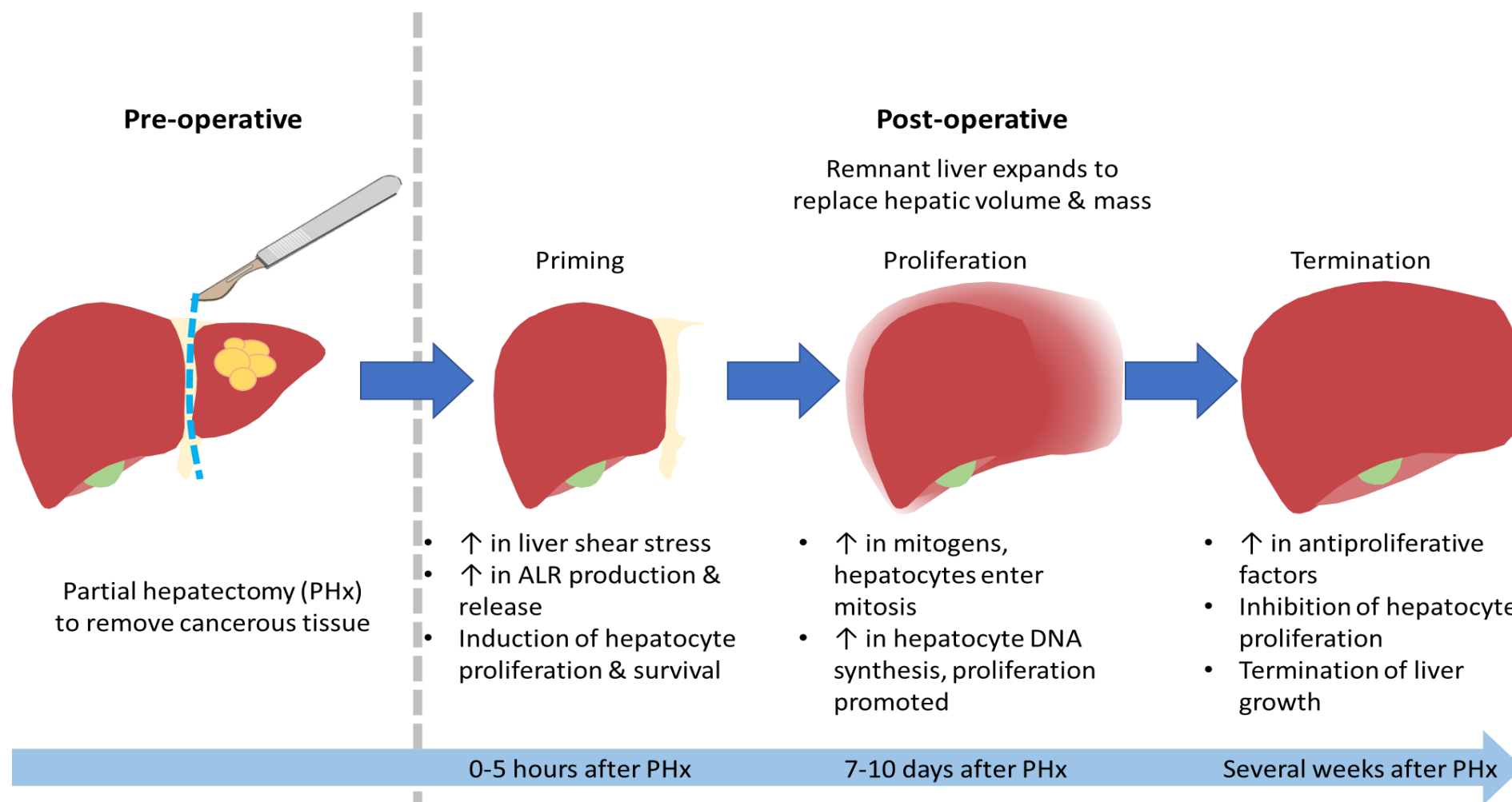


Figure 1.4 Overview of the mechanisms of liver regeneration

### 1.4.2 Surgical complications and PHLF

Despite surgical resection of cancerous liver tissue being a well-established procedure, and the abundance of knowledge surrounding the restoration of the hepatic architecture, liver regeneration does not always occur efficiently. As a result, a number of postoperative issues, associated with poor hepatic function, can arise. The most severe of these issues, occurring in up to 10 % of patients undergoing liver resection, and causing the highest number of postoperative mortalities, is post hepatectomy liver failure (PHLF) (van Mierlo et al., 2016). The severity of PHLF is graded according to the International Study Group of Liver Surgeries (ISGLS), who in 2011, defined PHLF as an increase in the international normalized ratio (INR) and hyperbilirubinemia on or after post-operative day five. The ISGLS scoring system includes three grades, with grade A requiring no change of clinical PHLF management with a mortality rate of 0 %, and grades B and C requiring a change in the patients clinical PHLF management with mortality rates of 13 % and 54 % respectively (Rahbari et al., 2011). PHLF has numerous different risk factors related to its initiation and maturation. These can be patient, liver or surgery related (Van Den Broek et al., 2008; Ray et al., 2018).

Patient related risk factors include, but are not limited to, age and poor metabolic function. Although the true effect of ageing on liver function is unclear, it is understood that the volume and blood flow of the liver can decrease by 20-40 % with age (Iber et al., 1994), and further proposed that an aging liver can exhibit a decrease in the mass of functional liver cells (Wakabayashi et al., 2002). Combined, it is likely that an ageing liver is less able to produce the necessary reactants for liver regeneration to occur efficiently, increasing the risk of PHLF occurring. A large-scale study, conducted on 775 patients, revealed that age >65 years was a valuable predictor of PHLF and post hepatectomy mortality (Balzan et al., 2005). Poor metabolic function has been reported as a risk factor for PHLF, with animals possessing an insulin depletion displaying a higher incidence of hepatic atrophy and PHLF (Bucher, 1977).



Liver related risk factors are associated with the injury inflicted by chemotherapeutic agents in the treatment of CRLM, as well as the extent of cirrhosis present in the patient's liver. Chemotherapeutic regimens containing irinotecan or oxaliplatin can cause steatohepatitis, and subsequent inflammation of the liver. Inflammation and related hepatic damage reduce liver function and prevent efficient regeneration from occurring, in turn increasing the risk of PHLF (Mehta et al., 2008). Similarly, the presence of widespread hepatic cirrhosis, labelled using the Child-Pugh scoring system (Cancer Research UK, 2021), drastically reduces liver function and impedes regeneration. It has been shown that patients presenting Child's B/C cirrhosis prior to undergoing a partial hepatectomy, have significantly higher mortality rates when compared to patients undergoing the same procedure with Child's A, or mild, cirrhosis (Capussotti et al., 2005).

Surgery related risk factors mainly comprise of intraoperative blood loss, and poor remnant liver volume. Excessive blood loss during surgery may induce bacterial translocation, resulting in inflammation of liver tissue, predisposing the patient to PHLF (Imamura, 2003). Initially described in 1996, by Emond et al. (Emond et al., 1996), small for size syndrome (SFSS) demonstrates how poor remnant liver volume can act as a risk factor for PHLF. SFSS causes an increase in portal pressure within the remnant liver, leading to widespread hepatocyte damage and inefficient liver regeneration. As a result of SFSS, there are two crucial determining factors assessed prior to surgical resection taking place which have been found to be highly predictive of PHLF. The first of these is remnant liver volume (RLV) which is defined as the percentage of remaining functional liver volume compared with the pre-operative liver volume. In otherwise healthy patients, an RLV  $\geq$  25-30 % generally delivers a good post-resectional outcome, with an RLV below 25 % predicting PHLF with a 90 % positive predictive value (Shoup, 2003; Schindl, 2005). In patients with already restricted liver function, RLV should be as high as 40 % to reduce the risk of PHLF (Fan, 2002). As RLV is part of the criteria for assessing the eligibility of curative surgery, a therapy that could increase liver

regeneration and enable patients with a lower RLV to become eligible for surgery, would enhance the clinical management of liver cancer. The second determining factor is the remnant liver volume to bodyweight ratio (RLV-BWR), with an RLV-BWR  $\geq 0.5$  % providing a good post-resectional outcome (Truant et al., 2007; Li et al., 2012).

In addition, PHLF has various direct causes, including abnormally high levels of bacteria within the liver, and excess bile salt accumulation. Post hepatectomy liver regeneration involves the use of the innate immune system, to fight potential bacterial infection. However, patients with hepatic dysfunction commonly experience considerable impairment of the innate immune system following surgical resection. As a result, bacteria is able to accumulate, significantly increasing the risk of infection and subsequently PHLF (Schindl, 2005). This has been demonstrated in rats possessing depleted Kupffer cells, in which higher levels of endotoxins were observed and the degree of hepatic damage observed was increased (Prins et al., 2004). Furthermore, excess bile salt accumulation can lead to greater levels of hepatic necrosis, in turn increasing the risk of PHLF. Mice possessing deranged bile salt homeostasis, and subsequent bile salt accumulation, exhibited greater levels of hepatic necrosis, and early mortality, following partial hepatectomy, when compared to mice possessing normal bile salt levels (Uriarte et al., 2013).

Despite their differing mechanisms, all PHLF contributing factors share the underlying aetiology that post hepatectomy liver regeneration occurs inefficiently and too slowly. Currently, the clinical treatment of PHLF utilises various support systems such as bio-artificial livers and modified fractionated plasma separation and adsorption (Prometheus<sup>®</sup>) (Van Den Broek et al., 2008). Bio-artificial livers consist of hepatocytes embedded within an artificial matrix. In addition to detoxification, bio-artificial livers are able to support the metabolic functions of the patient's liver, providing an advantage over conventional liver dialysis systems (Demetriou et al., 2004).

Prometheus® utilises an albumin bound permeable membrane in order to remove albumin-bound toxins before returning clean, detoxified albumin to the patient (Sen et al., 2005; Krisper and Stauber, 2007). However, there is a considerable lack of studies on the application of both systems, and the large majority of hospitals are unable to access such systems routinely, if at all.

It is therefore more common to attempt to prevent PHLF from occurring in the first place. Most strategies aim at augmenting the volume of the remnant liver, prior to surgery, in order to provide a better post-resectional outcome and reduce PHLF. The most common of these is known as portal vein embolization (PVE). This procedure involves infusing microspheres into the portal vein supplying the area of liver containing the tumour, thus embolizing that section of tissue by cutting off the blood supply. This then induces hypertrophy in the other, non-embolized, section of liver as blood flow is redirected specifically to this area. After several weeks, the non-embolized section of liver will reach a size in which surgical resection can successfully take place, ensuring adequate RLV is achieved. Surgical resection involves removing the embolized section of liver containing the tumour (May and Madoff, 2012).

PVE is advised in otherwise healthy patients when their estimated RLV is below 25 %, and in patients possessing impaired liver function when their estimated RLV is below 40 % (Madoff et al., 2005). The effectiveness of PVE depends entirely on the extent of liver damage, and the degree of cancer presented, but is believed to increase RLV between 28-46 % after 2-4 weeks (Imamura et al., 1999) and it is reported that PVE increased patients' eligibility for surgical resection by 19 % (Azoulay et al., 2000). It has been suggested that, due to increasing the arterial flow in the embolized segments, PVE could also increase the size of tumours (Ray et al., 2018). A study conducted by Kokudo et al. demonstrated such increase in the tumour volume of intrahepatic colorectal metastases following

PVE as well as a significantly poorer disease-free patient survival (Kokudo, 2001). Therefore, despite being effective, it is essential to exercise caution when selecting patients for PVE.

Although these treatments, or management strategies, provide some relief for PHLF, they have limited success and often fail to revert the extensive hepatic damage. Moreover, there is a lack of conclusive evidence to support the use of such support systems in the management of PHLF. This is mainly due to the inability to prevent the underlying issue of inefficient and slow liver regeneration following surgical resection. As a result of this, coupled to the increasing incidence and mortality of PHLF, it is essential that a safe and effective solution is found in order to enhance post-resectional liver regeneration, in turn reducing or even eliminating the risk of PLF within the clinic. As well as the potential to reduce the burden of post-resectional complications, it may also be possible to improve the treatment options of patients who are currently only eligible for experimental treatment or palliative care. If patients need large resections, there is a choice between not operating or risking PHLF, which can result in the only curative option being denied. As previously mentioned, there are some surgical approaches to improving RLV prior to hepatectomy, but these also carry risk of morbidity, mortality, and cancer growth or recurrence. This therefore highlights the need for a pharmacological approach to improve access of patients to curative surgery.

### **1.5 Nuclear factor erythroid 2-related factor 2 (Nrf2)**

The basic Leucine zipper (bZIP) transcription factor, Nrf2, was first identified in 1994 by Moi et al. following the screening of a cDNA library from a hemin-induced myelogenous leukaemia cell line (Moi et al., 1994). Nrf2, possessing a cap'n'collar structure, was found to bind to the AP1 (activating-protein 1)-nuclear factor erythroid 2 (NF-E2) promoter sequence, indicating its similarity to NF-E2. This similarity resulted in the inclusion of Nrf2 in the NF-E2 transcription factor family, consisting of

P45-NFE2, Nrf1 and Nrf3 (Ohtsubo et al., 1999). Nrf2, encoded by the NFE2L2 gene, has low tissue specificity and is expressed throughout the entire human body, with higher levels presented in certain organs, such as those exposed to external environmental stimuli, and those involved in metabolism and detoxification, including but not limited to, the liver (Uhlén et al., 2015). The importance of Nrf2 and the reduction of oxidative and chemical stress was shown by Chan et al in 1996. (Chan et al., 1996). Through the novel use of a replacement vector targeting segments of DNA containing specific exons of Nrf2, the first mice possessing an Nrf2 knockout were produced. The replacement vector deleted the carboxyl 457 amino acid of the Nrf2 molecule, thus effectively silencing the Nrf2 gene function. The utilisation of this model illustrated that mice lacking Nrf2 are viable and have a normal phenotype with only minimal phenotypic differences being detected or exhibited. However, despite the viability, analysis of these animals showed a susceptibility to stresses. These innovative findings indicated that the absence of Nrf2 may have wider consequences, thus suggesting a crucial need for Nrf2. Following this, a landmark study conducted by Itoh et al. demonstrated that the inducible expression of phase II detoxifying enzymes, including GSTs and NQO1, was lost following the silencing, or knocking out, of Nrf2 (Itoh et al., 1997). These findings revealed that Nrf2 regulates drug metabolising enzymes in vivo and developed a better understanding of what effects Nrf2 causes downstream of its initial activation. As a result, the transcription factor has since been referred to as the master regulator of the response to both oxidative and chemical stress within the body.

### **1.5.1 Basal response of Nrf2 and regulation by Keap1**

Under basal conditions, Nrf2 is repressed within the cytoplasm by Kelch-like ECH-associated protein 1 (Keap1). Keap1, and its ability to form a strong interaction with the Neh2 domain of Nrf2, was initially discovered in 1999 through the use of a yeast two-hybrid screening assay (Itoh et al., 1999). Following this, the structure of Keap1, consisting of five distinct regions, was determined, with these

regions being the: N-terminal region (NTR); Broad-Complex, Tramtrack and Bric a brac (BTB) domain; intervening region (IVR); double-glycine repeat (DGR) domain and C-terminal region (CTR) (Namani et al., 2014). The deletion of the DGR region completely abolished the ability of Keap1 to bind to Nrf2, illustrating that the DGR domain is responsible for forming this strong interaction with the Neh2 domain of Nrf2 (Kobayashi et al., 2004). The cullin-dependent E3 ubiquitin ligase complex binds to a Keap1 homodimer, following an interaction with the BTB region of Keap1. This subsequent heterodimer then facilitates ubiquitination and subsequent proteasomal degradation of Nrf2 (McMahon et al., 2003) (Figure 1.5). Interestingly, it was discovered that inhibition of the proteasome leads to a marked increase in the accumulation of Nrf2 within the cytoplasm and nucleus, thus promoting induction of Nrf2-related genes (Kwak et al., 2003). It has also been shown that mice possessing a knock-out of Keap1 possess constitutively accumulated Nrf2 and in turn, constitutively activated Nrf2-related genes. Despite this however, mice possessing a knock-out of Keap1 fail to survive adulthood due to fatal malnutrition caused by hyperkeratosis of the upper digestive tract (Wakabayashi et al., 2003).

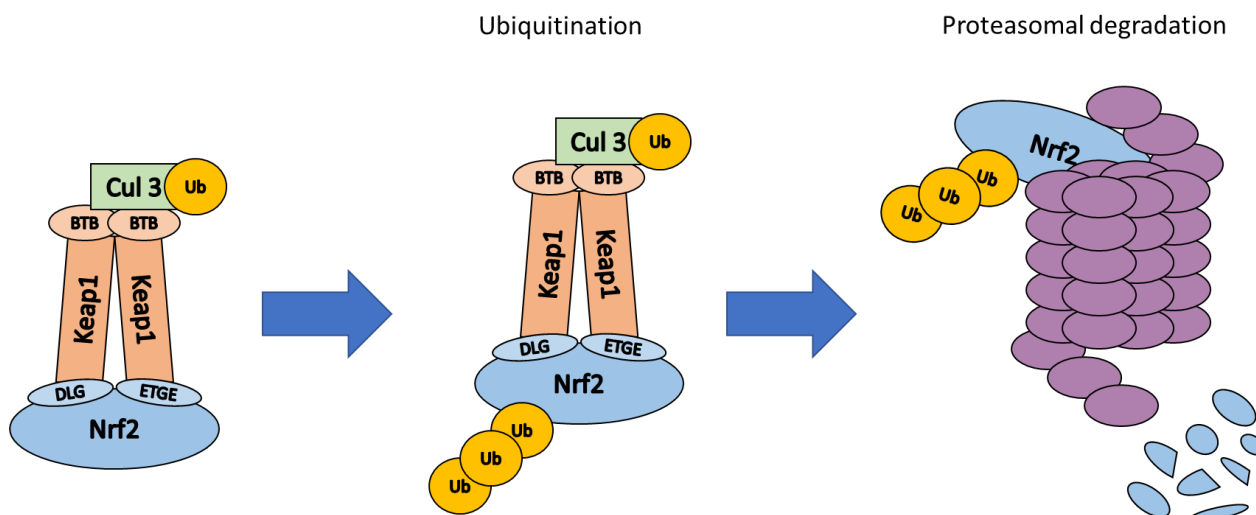


**Figure 1.5 Basal response of Nrf2**

Under basal conditions, Nrf2 is bound to Keap1 via a strong interaction with the DLG and ETGE regions of Nrf2. The cullin-dependent E3 ubiquitin ligase complex binds to a Keap1 homodimer, following an interaction with the BTB region of Keap1. This subsequent heterodimer then facilitates ubiquitination and subsequent proteasomal degradation of Nrf2.

Owing to its ability to regulate Nrf2, and subsequently both oxidative, and chemical, stress within the body, Keap1 is highly sensitive to changes in the cellular redox state. This sensitivity is a result of the plethora of cysteine residues located on the functional domains, allowing Nrf2 to be non-specifically activated by a wide range of compounds, or stimuli, following alterations to such cysteine residues and Keap1 (Canning et al., 2015). The discovery of specific cysteine residues led to the proposal of the “cysteine code” hypothesis, with an aim to convert sets of cysteine modifications into specific biological effects (Kobayashi et al., 2009). With this comes the potential to decipher the cysteine code for each activator of Nrf2, thus providing valuable insight and understanding of its therapeutic and/or toxic effects.

### 1.5.2 Activation of Nrf2

The mechanism in which Keap1 regulates Nrf2 is commonly referred to as the hinge and latch hypothesis. As mentioned previously, Nrf2 is repressed by Keap1 due to high-affinity interactions between the two DGR domains of Keap1 and the Neh2 domain of Nrf2, specifically the DLG and ETGE motifs, where binding to ETGE is referred to as the hinge and binding to DLG is referred to as the latch. Under basal conditions, both the hinge and latch remain bound, however following modification of specific cysteine residues within Keap1, the latch is released. This prevents Keap1 from repressing Nrf2, meaning ubiquitination and proteasomal degradation is avoided (Itoh et al., 1997). As a result, freshly synthesised Nrf2 is able to accumulate within the cytoplasm and subsequently translocate to the nucleus. Once inside the nucleus, Nrf2 forms a heterodimer with small Maf (sMaf) proteins, which exhibits high specificity and binding affinity to the antioxidant response element (ARE) (Li et al., 2008). Binding of the Nrf2/sMaf heterodimer to the ARE then occurs, triggering the transcription and subsequent upregulation of numerous antioxidant, cytoprotective and metabolic genes (Yamamoto et al., 2018; He et al., 2020).

The modification of cysteine residues within Keap1, leading to Nrf2 translocation and subsequent transcription of downstream target genes can occur due to a variety of different reasons. This can include a natural cellular response to oxidative stress stimuli, such as exposure to ROS. These highly reactive oxidants, which commonly possess oxygen molecules with unpaired electrons (Chen et al., 2015), interact with the cysteine residues within Keap1 and cause conformational changes which prevent Keap1 from repressing Nrf2. Subsequent transcription of Nrf2 target genes including antioxidants then work to remove the ROS or oxidative stress stimuli, thus working in a feedback loop (Ma, 2013).



Another way in which Nrf2 translocation and subsequent transcription of downstream target genes can occur is due to pharmacological activation of Nrf2 (Figure 1.6). Despite being referred to as pharmacological Nrf2 activators, this class of compounds commonly exert their effect by inhibiting Keap1 (Staurengo-Ferrari et al., 2019). These small electrophilic molecules form covalent bonds with the sulfhydryl groups of cysteine residues in Keap1 via oxidation or alkylation (Magesh et al., 2012), thus preventing repression of Nrf2 and allowing transient transcription of downstream Nrf2 target genes. As a result of their strong electrophilicity, such small molecules include fumaric acid esters and synthetic triterpenoids (Robledinos-Antón et al., 2019).

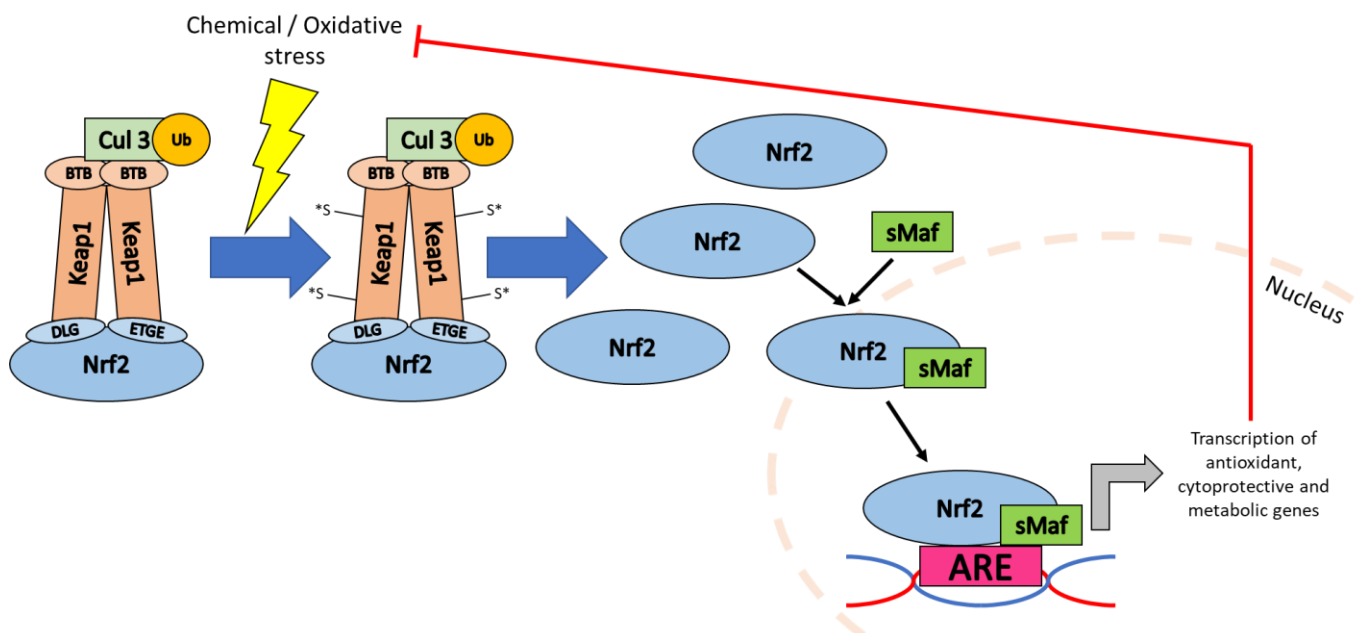


**Figure 1.6 Activation of Nrf2**

Modification of specific cysteine residues prevents Keap1 from repressing Nrf2, meaning ubiquitination and proteasomal degradation is avoided. Freshly synthesised Nrf2 is then able to translocate into the nucleus where it forms a dimer with sMaf before binding to the ARE. Transcription and subsequent upregulation of numerous antioxidant, cytoprotective and metabolic genes then occurs.

### 1.5.3 Pharmacological Nrf2 activators – past and present

Nrf2 activators have been known and documented for many years following the discovery of naturally occurring activating compounds in foods such as fruits and vegetables. Sulforaphane, initially discovered in broccoli by Zhang et al. in 1992 (Zhang et al., 1992) was one of the first of these naturally occurring compounds to be found and it remains the most potent natural activator of Nrf2. The discovery of sulforaphane paralleled the discovery and preliminary understanding of the Nrf2 pathway. Another naturally occurring Nrf2 activator is resveratrol which can be found in fruits including grapes and blueberries, although this compound is considerably less potent than sulforaphane, and its use is far less documented. Nonetheless, the discovery and understanding of such natural compounds led to the development of more potent and specific synthetic Nrf2 activators (Table 1.1).

The use of Nrf2 activators within clinical practice is very limited, with dimethyl fumarate (DMF, Tecfidera®) being one of only two compounds approved for use at the time of writing. In clinical trials, patients with relapse-remitting multiple sclerosis (RRMS) treated with DMF exhibited a 50 % reduction in the rate of relapse when compared to those treated with a placebo, resulting in its approval as the first-line oral therapy for RRMS in 2013 (Xu et al., 2015; Linker and Haghikia, 2016). Further to this, DMF has also been approved for use in moderate to severe plaque psoriasis (Blair, 2018). Despite DMF showing considerable efficacy in these disease areas, and being widely accepted as well tolerated, there are concerns of side effects associated with its use. Serious safety concerns have only been identified in less than 2 % of patients (D'Amico et al., 2018) however side effects originating from GI events are much more common and frequently include nausea and diarrhoea (Linker and Haghikia, 2016; Koulinska et al., 2018).

Furthermore, it has been shown that DMF is rapidly metabolised and converted to the bioactive compound monomethyl fumarate (MMF) (Dibbert et al., 2013) which then exerts its therapeutic effect. It is therefore unsurprising that MMF, with improved bioavailability and efficacy, is currently undergoing phase III clinical trials for MS at the time of writing (Sun et al., 2017). Although, the mechanisms of action for fumaric acid esters, including DMF and MMF are not fully understood with Keap1 and Nrf2 independent effects being illustrated, it has been reported that such compounds activate nicotinic receptors which are highly expressed in immune and gut epithelial cells, thus resulting in anti-inflammatory responses independent of the Nrf2 signalling pathway (von Glehn et al., 2018). As a result, newer synthetic Nrf2 activators may provide an enhanced therapeutic benefit both for the aforementioned disorders, and further disease areas encompassing oxidative stress and metabolic disorders.

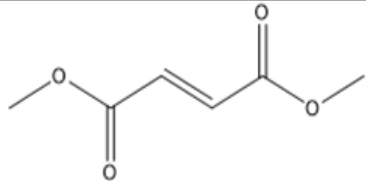
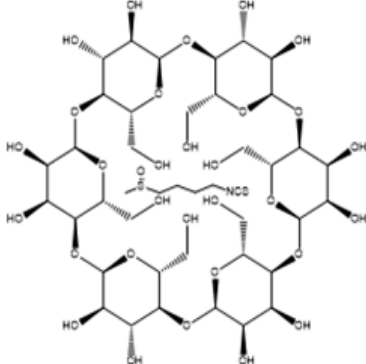
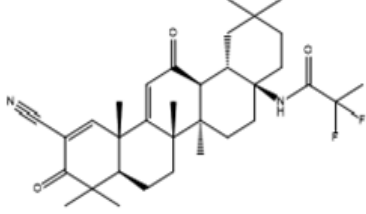
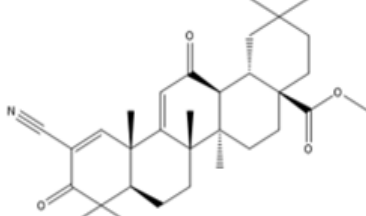
The majority of these newer compounds are currently in clinical trials for a variety of different disease areas. SFX-01, a compound formed by encapsulating the naturally occurring compound sulforaphane in a cyclodextrin complex, is in various early-stage clinical trials with a phase 1 trial in prostate cancer being of significant interest (NCT02055716 and NCT01948362). Furthermore, RTA-408 (omaveloxolone) has progressed into phase 2 trials for preventing pain and inflammation in ocular surgery (NCT02065375 and NCT02128113) and has recently been approved under the brand name Skyclarys™ for clinical use in Friedreich's ataxia, a rare genetic disorder affecting the nervous system (Dayalan Naidu and Dinkova-Kostova, 2023). As with SFX-01, it is also of significant interest that RTA-408 is in phase 2 trials for melanoma (NCT02259231) and breast cancer (NCT02142959). Bardoxolone methyl (CDDO-Me) is another Nrf2 activator in clinical trials. It is currently in phase 2/3 trials for numerous chronic kidney focused diseases in which oxidative stress and inflammation play a considerable role (NCT01351675), including Alport syndrome (NCT03019185). CDDO-Me is also in

phase 1/2 trials for liver disease (NCT00550849), hepatic impairment (NCT01563562) and advanced solid tumours (NCT00529438).

Additionally, there are numerous novel Nrf2 activators in pre-clinical development with proteolysis-targeting chimeras (PROTACs) being of considerable interest. Such molecules, also referred to as bivalent chemical protein degraders, structurally connect to the protein of interest, subsequently degrading the targeted protein through ubiquitination and the proteasome (Qi et al., 2021). Recently, two studies have highlighted the ability to create PROTACs that target Keap1 for proteasomal degradation, thus activating Nrf2 (Chen et al., 2023; Du et al., 2022). Such molecules therefore present promising leads for future development.

With further progression of such compounds, and the continuation of clinical trials, it is highly likely that Nrf2 activators will become part of routine clinical use for a vast range of diseases. CDDO-Me remains a leading compound with promising therapeutic targets including the liver and is the most potent of the clinical stage Nrf2 activators. However, given the complexity of liver regeneration, and the fears of cancer progression and recurrence arising from the nature in which liver resection takes place in patients presenting liver cancer, it is of utmost importance that CDDO-Me is tested in such environments.

**Table 1.1 Examples of pharmacological Nrf2 activators that are currently, or have been, in clinical trials**

Compound	Chemical Structure	Disease	Clinical Trial Phase	Clinical Trial Identifier
DMF		Relapse-remitting multiple sclerosis (RRMS)	Approved for clinical use	
		Severe plaque psoriasis	Approved for clinical use	
SFX-01		Prostate cancer	I	NCT02055716 & NCT01948362
RTA-408 (Omaveloxolone)		Friedreich's ataxia	Approved for clinical use	
		Inflammation and pain following ocular surgery	II	NCT02065375 & NCT02128113
		Melanoma	I/II	NCT02259231
		Breast cancer	II	NCT02142959
Bardoxolone methyl (CDDO-Me)		Chronic kidney disease	III	NCT01351675
		Alport syndrome	II/III	NCT03019185
		Liver disease	I/II	NCT00550849
		Hepatic impairment	I	NCT01563562
		Advanced solid tumours	I	NCT00529438

## 1.6 Nrf2 in the liver

Owing to the essential and diverse role of the liver in functions such as detoxification, metabolism and the maintenance of homeostasis, it is crucial that the liver remains protected from insult in order to preserve good general health. However, due to the continual exposure of the liver to insult through its routine function, it is not uncommon for liver diseases such as DILI and cirrhosis to initiate, and eventually progress to cancer if left untreated. As a result of oxidative stress being significantly implemented in liver disease, and the ability of Nrf2 to alleviate oxidative stress via transcription of various cytoprotective and antioxidant genes, it is unsurprising that the role of Nrf2 within the liver is extensively studied and reported (Xu et al., 2018), with Nrf2 activation being shown to alleviate fatty liver disease (Shin et al., 2009) and liver fibrosis (Xu et al., 2008) in mice. Furthermore, the role of Nrf2 in liver cancer has also been widely studied, with conflicting findings on the ability of Nrf2 to play an anti-tumour, and tumour-promoting, role often reported (Raghunath et al., 2018; Orrù et al., 2020). Therefore, a more secure understanding of the role of Nrf2 in these liver diseases would aid the development and use of Nrf2 targeting treatment strategies.

### 1.6.1 Nrf2 in liver regeneration

As liver regeneration requires the utilisation of several complex pathways and signalling mechanisms, it is pertinent to its success that insult from factors such as oxidative stress is kept to a minimum. Oxidative stress can result in excessive damage to hepatocytes through necrosis and apoptosis (Parola and Robino, 2001), subsequently preventing the liver from fulfilling its regenerative ability and potentially leading to further post-operative complications. As mentioned previously, Nrf2 within the liver is able to reduce the level of oxidative stress present and thus prevent unnecessary hepatocyte damage from occurring. This occurs through the transcription of various cytoprotective and antioxidant genes, which in turn utilise numerous signalling cascades to exert their effect, with some of these signalling pathways providing cross-talk to those involved with liver regeneration itself

(Wakabayashi et al., 2015). Therefore, therapies utilising pharmacological activation of Nrf2 may be beneficial for the regenerating liver, allowing liver mass and function to be restored in a preferential manner, thus reducing post-operative complications.

The role of Nrf2 in liver regeneration has been reported by numerous groups, although such reports present confictions in their findings which only complicates understanding and clarity. Beyer et al. reported that liver regeneration was significantly impaired in Nrf2 knockout mice following partial hepatectomy. As a result of Nrf2 knockout, cytoprotective enzyme expression was considerably reduced in hepatocytes, producing high levels of oxidative stress. This in turn resulted in the impairment of activating p38 mitogen-activated kinase, a key signalling cascade in liver regeneration, which subsequently enhanced the delayed proliferation and death of hepatocytes (Beyer et al., 2008). Such findings were then supported by Wakabayashi et al. in a similar Nrf2 knockout mouse model in which a partial hepatectomy was conducted. Transcriptional analysis identified interactions and cross-talking between Nrf2 and the Notch1 signalling pathway, a cascade that regulates crucial processes such as cell proliferation and cell fate decisions. Disruption of Nrf2 following knockout, lead to disruption within Notch1 and subsequently caused significant impairment of liver regeneration (Wakabayashi et al., 2010). Both of these reports therefore highlight an essential requirement of Nrf2 in the regenerating liver of mouse models.

However, in a study conducted by Hu et al. it was found that Nrf2 played a detrimental role in liver regeneration. By knocking down Keap1, the repressor of Nrf2, after performing a partial hepatectomy, the enhanced levels of Nrf2 resulted in a delay in S-phase entry, disruption of S-phase progression and loss of mitotic rhythm in replicating hepatocytes. This in turn caused severe disruption in both the redox and cell cycle of the regenerating liver, thus concluding that Nrf2 does not restore liver mass or function in a beneficial way (Hu et al., 2014). In addition, Köhler et al.

demonstrated a detrimental effect of Nrf2 on liver regeneration. Through the generation of mice expressing constitutively active Nrf2, it was found that liver regeneration was impaired following partial hepatectomy due to delayed hepatocyte proliferation and enhanced apoptosis of regenerating cells following liver injury (Köhler et al., 2014). Both of these reports therefore illustrate that liver regeneration is able to occur efficiently and to a better degree in the absence of Nrf2.

It is however crucial to note that all of these studies, irrespective of their findings, utilise transgenic mouse models in which Nrf2 is either constitutively inactivated, as is the case with an Nrf2 knockout, or activated, via Keap1 knockdown or the generation of mice expressing constitutively activated Nrf2. Such phenotypic characteristics would not be presented in a clinical setting in which transient activation or inhibition of a target pathway would be achieved with pharmacological intervention. Therefore, pharmacological approaches targeting Nrf2 still need to be investigated in liver regeneration.

### **1.6.2 Nrf2 in liver cancer**

The Nrf2 pathway is frequently implicated within various cancers, including pancreatic (Lister et al., 2011), breast (Zhang et al., 2016), and liver cancers (Raghunath et al., 2018). Genes within the pathway, including NFE2L2 itself, the repressor KEAP1, and others downstream, are commonly mutated within clinical liver (Ding et al., 2017) and colorectal cancer (Torrente et al., 2020) samples. As such, various *in vivo* models have been developed to test approaches targeting Nrf2. However, similarly to liver regeneration, the role and potential therapeutic benefit of Nrf2 in liver cancers is unclear with conflicting findings reported.



Ngo et al. demonstrated that mice deficient in Nrf2 were able to resist diethylnitrosamine (DEN)-induced hepatocarcinogenesis and that activation of Nrf2, achieved in wild-type mice, was required in order to initiate and progress DEN-induced HCC. Wild-type mice were found to have significantly more, and larger, hepatic tumours when compared to mice deficient in Nrf2. Nrf2 deficient mice were shown to have reduced expression of the pentose phosphate pathway-related enzymes, a depletion of which has been associated with a reduction in HCC incidence (Ngo et al., 2017). In addition, Zavattari et al. showed that silencing Nrf2 in rats caused inhibition in the ability of HCC tumours to grow *in vitro*, and that wild-type rats had significantly larger tumours when compared to rats with silenced Nrf2 (Zavattari et al., 2015). However, as both studies utilise transgenic models, in which Nrf2 has been constitutively inhibited through the use of Nrf2 knockout animals, they lack the clinical relevancy achieved with pharmacological intervention.

As liver cancers also encompass colorectal metastasis, it is also important to investigate the role of Nrf2 in such *in vivo* models, however the findings of which are considerably more ambiguous. It has been demonstrated that Nrf2 knockout mice were more likely to develop colorectal cancer when compared to wild-type mice due to the significant impairment of antioxidant mechanisms (Khor et al., 2008). Pharmacological manipulation of Nrf2 in colorectal cancer has also been investigated, although reported findings are contradictory. Pandurangan et al. showed that upregulating Nrf2 with the naturally occurring flavonoid, Luteolin, inhibited the development and progression of colorectal cancer (Pandurangan et al., 2014). However, pharmacological inhibition of Nrf2 in colorectal cancer cells possessing overexpressed Nrf2 was shown to elicit considerable anti-tumour properties following the xenograft of such cells into mice (Shen et al., 2019).

A more comprehensive understanding of the role of pharmacological Nrf2 activation in liver cancers would provide significant developments in treatment strategies for cancer. Furthermore, if

pharmacological Nrf2 activation is shown to not enhance liver cancer recurrence or growth, it may widen treatment options for patients undergoing tumour resection. It is essential to find a balance between the efficacious properties of pharmacological Nrf2 activation in preventing disease and post-operative complications, and the safety of manipulating a highly complicated pathway in an oncology setting.

### 1.7 Thesis aims

An ever-increasing incidence of liver cancer worldwide, coupled to significant challenges with surgical treatment approaches and subsequent post-operative complications, has led to a considerable and escalating clinical burden. In a disease in which antioxidant, inflammatory and metabolic pathways are commonly complicated, targeting such pathways may provide the potential to alleviate such clinical burden. Nrf2 activators have long been studied for their ability to upregulate a battery of antioxidant, cytoprotective and metabolic genes, and pharmacological activation of the Nrf2 pathway has since started to make its way into routine clinical use and late-stage clinical trials with promising results being reported. The role of Nrf2 in liver regeneration and liver cancer remains somewhat unknown and is often questioned by contradictory findings, however an advancement in the understanding of pharmacological Nrf2 activation in liver regeneration and liver cancer may aid future developments in treatment strategies that improve patient outcome and reduce clinical burdens. This thesis therefore seeks to investigate if pharmacological activation of Nrf2 can aid liver regeneration, whilst ensuring such treatment does not worsen the burden of liver cancer by promoting the growth of pre-existing tumours. To achieve this, the principle aims of this thesis were:

- To investigate if pharmacological activation of Nrf2 can enhance post-operative liver regeneration.
- To assess the effect of pharmacological Nrf2 activation on *in vitro* proliferation of liver cancer and colorectal cancer cell lines.

- To determine if pharmacological Nrf2 activation enhances the burden of liver cancer in an *in vivo* orthotopic tumour xenograft model.

## Chapter 2

### Pharmacological activation of Nrf2 enhances post-operative liver regeneration

## Contents

<b>2.1 Introduction</b> .....	53
<b>2.2 Methods</b> .....	55
2.2.1 Animal Experiments.....	55
2.2.1.1 Partial Hepatectomy.....	55
2.2.1.2 Animal drug treatments.....	58
2.2.1.3 Magnetic Resonance Imaging (MRI).....	58
2.2.2 Total protein quantification.....	59
2.2.3 Western blotting.....	60
2.2.4 Gene expression analysis.....	63
2.2.4.1 RNA isolation.....	63
2.2.4.2 cDNA synthesis.....	64
2.2.4.3 qPCR.....	64
2.2.5 Glutathione quantification.....	66
2.2.6 Metabolic coenzyme quantification.....	67
2.2.6.1 NADP/H quantification.....	68
2.2.6.2 NAD/H quantification.....	69
2.2.7 Primary human hepatocytes.....	70
2.2.7.1 Isolation and culture.....	70
2.2.7.2 Drug treatment.....	71
2.2.8 TempO-Seq high-throughput transcriptomics analysis.....	71
2.2.8.1 Bioinformatics.....	72
2.2.9 Statistical analysis.....	73
<b>2.3 Results</b> .....	74
2.3.1 CDDO-Me enhances restoration of liver volume.....	74
2.3.2 Molecular mechanisms driving CDDO-Me enhanced liver regeneration.....	80
2.3.3 Metabolic adaptations underpinning liver regeneration.....	86
2.3.4 Transcriptomic analysis of primary human hepatocytes.....	92
<b>2.4 Discussion</b> .....	94

## 2.1 Introduction

The regenerative ability of the liver is well documented and widely exploited in clinical oncology scenarios. Despite this, insufficient liver regeneration following hepatectomy can lead to liver failure. Post-hepatectomy liver failure (PHLF) remains a substantial clinical problem, occurring in up to 10% of patients (Ocak et al., 2020) depending upon the underlying health of the liver, as well as the type and stage of liver cancer presented (Ray et al., 2018). Furthermore, PHLF contributes significantly to the mortality rate associated with hepatectomy procedures (Zheng et al., 2017), with 40% to 60% of hepatectomy mortalities arising as a result of PHLF in the last 15 years (Balzan et al., 2005; Mullen et al., 2007; Rahbari et al., 2011), and has been shown to be the greatest cause of death following major hepatectomy (Gilg et al., 2018).

Currently, there are numerous clinical risk factors associated with the occurrence of PHLF, including the underlying pre-operative condition of the liver, such as cirrhosis or steatosis, as well as the tumour burden itself and subsequent small future liver remnant (FLR) (Sparrelid et al., 2022). Patients presenting clinical risk factors are therefore commonly deemed as inoperable, restricting standard of care options, and consequently preventing access to the only curative treatment for liver cancer. As a result, there is an unmet need to establish novel therapeutic strategies aimed at promoting post-hepatectomy liver regeneration, and adequate hepatic function, in turn reducing the burden of PHLF.

Pharmacological activation of Nuclear factor erythroid 2-related factor 2 (Nrf2) has become an encouraging strategy in therapeutic areas encompassing oxidative stress and metabolic disorder (Cuadrado et al., 2019) due to its ability to upregulate the expression of numerous cytoprotective and metabolic genes (He et al., 2020). However, the therapeutic potential of Nrf2 in liver regeneration is currently unclear due to conflicting findings on how Nrf2 impacts the regenerative

ability of the liver. Following a routine two-thirds partial hepatectomy (PHx) (Mitchell and Willenbring, 2008), some report that transgenic mice possessing constitutively inactivated Nrf2 have impaired levels of liver regeneration (Beyer et al., 2008; Wakabayashi et al., 2010), whilst others report impairment of liver regeneration with constitutively activated Nrf2 (Hu et al., 2014; Köhler et al., 2014).

The ever-expanding interest, and gradual shift towards, the clinical use of small molecules targeting Nrf2, coupled to the lack of investigation into the effect of pharmacological Nrf2 activation on liver regeneration, has provided the rationale to explore this novel therapeutic approach. I hypothesised that pharmacological activation of Nrf2 would enhance liver regeneration following a two-thirds PHx in wild-type mice. In order to test this hypothesis, wild-type C57BL/6 mice underwent a two-thirds PHx with or without administration of bardoxolone methyl (methyl-2-cyano 3,12-dioxooleano-1,9-dien-28-oate [CDDO-Me]), a small molecule and potent Nrf2 activator. Using non-invasive Magnetic Resonance Imaging (MRI), we assessed the functional restoration of liver volume, and using *in vitro* functional assays, we determined the molecular mechanisms underpinning Nrf2 driven liver regeneration. Furthermore, we aimed to address the clinical translatability of this hypothesis by using primary human hepatocytes, exposed to CDDO-Me, to explore any similarity in the underlying biological processes. Some of the content of this chapter has contributed to a published manuscript, **“Chan et al., Pharmacological Activation of Nrf2 Enhances Functional Liver Regeneration”**.

## 2.2 Methods

All reagents were purchased from Sigma Aldrich unless otherwise stated.

### 2.2.1 Animal Experiments

All animal experiments were carried out according to the Animals (Scientific Procedures) Act 1986 guidelines under the Home Office project licence P72DA1059 and approved by the University of Liverpool Animal Welfare Committee.

#### 2.2.1.1 Partial Hepatectomy

Male, wild-type C57BL/6 mice aged 8-10 weeks old, were purchased from Charles River and underwent a 5-day acclimatisation period prior to experimental work commencing. All animals were maintained in a 12-hour light/dark cycle in a temperature and humidity controlled, specific pathogen-free environment. Mice were fed CRM (P) diet (Special Diets Services) ad-libitum.

A 2/3 partial hepatectomy procedure was performed on day 0. Mice received sub-cutaneous buprenorphine (0.05 µg/g bodyweight) 1 hour prior to surgery, and 6-8 hours after surgery. General anaesthesia was achieved via induction in a chamber with 2 % isoflurane and 2 L/min oxygen flow. The abdomen was then shaved, and skin disinfected with 10 % povidone-iodine. Mice were then transferred to a heated operated table, where the body temperature was monitored, and subsequently maintained, using a rectal thermometer and thermostat. Anaesthesia was maintained on the operating table via mouthpiece with 1-1.5 % isoflurane and 1 L/min oxygen flow.



Mice were placed in the supine position and a sterile drape was placed over the abdomen. A midline laparotomy incision, 10-15 mm in length, was performed with careful entry into the peritoneal cavity. The median and left lateral lobes of the liver were separately mobilised by dissecting the attaching ligaments. Each lobe was then individually externalised, by utilising a sweeping motion, with a cautious yet firm pressure, from the animal's front legs to the midline laparotomy incision, before being stabilised with cotton buds. The median and left lateral lobes were then separately ligated at the pedicles with 4/0 silk tie before being resected (Fig 2.1). The resected median and left lateral lobes were then placed in labelled 2 mL, round-bottomed, Eppendorf tubes, before being snap frozen in liquid nitrogen. Following resection, the abdomen was closed using 6/0 Vicryl as a continuous, locking, suture for the peritoneum and a sub-cuticular suture for the skin.

Post-operatively, the mice were transferred to a heated recovery chamber and allowed to recover with regular close monitoring. Wet diet was provided as a provision to help prevent loss of bodyweight and sub-cutaneous buprenorphine (0.05 µg/g bodyweight) was administered when necessary.

Mice were culled with a rising concentration of CO<sub>2</sub>. Blood was collected via cardiac puncture using a 25 G needle and a 1 mL syringe to collect blood directly from the heart. Before decanting the blood into 1.5 mL tubes, the needle was removed to prevent haemolysis. Freshly isolated blood was left to clot at room temperature for 1 hour and centrifuged at 2000 g for 10 min in a centrifuge set at 4 °C. Serum was aspirated and stored at -80 °C. The liver was excised, weighed and photographed, and cut into multiple sections before being preserved by snap freezing in liquid nitrogen, placing in 4 % paraformaldehyde (PFA) or freezing in optimal cutting temperature (OCT) embedding matrix.

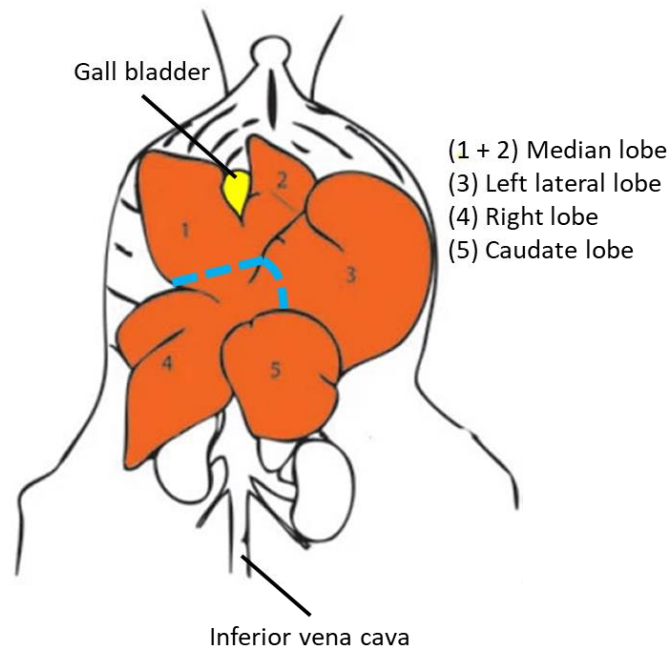


**Figure 2.1** Diagram outlining the two-thirds PHx procedure.

Anatomy of the mouse liver in relation to a two-thirds PHx being carried out. The median and left lateral lobes are removed following ligation.

Position of ligation indicated by dotted blue line. Adapted from (Boyce and Harrison, 2008; Mitchell and Willenbring, 2008).

### 2.2.1.2 Animal drug treatments

Mice were administered 3 mg/kg CDDO-Me via intraperitoneal (IP) injection. CDDO-Me was solubilised in 100 % DMSO and administered at 1 µL/g of bodyweight. Animals receiving multiple doses, received injections of CDDO-Me at 24 hours and 1 hour prior to a 2/3 partial hepatectomy being carried out, and 24 hours and 72 hours following the completion of the surgical procedure. Animals receiving a single dose, received one injection of CDDO-Me at either 24 hours prior to a 2/3 partial hepatectomy, 1 hour prior to a 2/3 partial hepatectomy, or 24 hours following the completion of a 2/3 partial hepatectomy. During a control study in which mice received either 100 % DMSO, or no drug intervention, and underwent a 2/3 partial hepatectomy, DMSO was observed to show no effect on liver regeneration. Therefore, untreated animals were used as a control in all subsequent 2/3 partial hepatectomy studies.

### 2.2.1.3 Magnetic Resonance Imaging (MRI)

Magnetic Resonance Imaging (MRI) was conducted with a 9.4 Tesla horizontal bore scanner operating the Bruker Paravision 6.1.0 software console (Bruker, Germany). Anaesthetised mice were transferred, in the prone position, into an abdominal imaging cradle with an embedded 4-channel phased array receiver coil and placed inside an 86 mm volume transit coil, centred inside the MRI scanner. Animals underwent imaging 24 hours prior to a 2/3 partial hepatectomy to provide a baseline for subsequent image analysis. Imaging was then conducted from 1 – 31 days post 2/3 partial hepatectomy.

Anaesthesia was maintained using a mouthpiece with 1-2 % isoflurane and 1 L/min oxygen flow. A warming pad with circulating warm water was placed over the dorsal aspect of the mouse. Core

body temperature was monitored throughout using a rectal thermometer and respiratory rate was monitored using a respiratory pillow placed over the thoraco-abdominal area.

Initial three-plane localiser images were obtained before multi-slice T2 weighted rapid acquisition with refocused echoes (RARE) imaging sequence covering the whole liver of the animal was performed with respiratory gating using the following parameters: echo time 24 ms, repetition time 2500 ms, number of average 3, echo spacing 8 ms, RARE factor 8, number of slices 27, slice thickness 0.5 mm, image matrix 264x264, field of view 33x33 mm<sup>2</sup>. All images were then exported in DICOM format, and the area of each slice was calculated in ImageJ using a hand-drawn region of interest (ROI) tool. For each liver slice, the area was multiplied by the slice thickness to calculate volume. Total liver volume was then calculated by summing the volumes of all 27 liver slices. At each time point, liver volume was expressed relative to the volume of the same mouse recorded 24 hours prior to surgery (baseline).

### **2.2.2 Total protein quantification**

Protein concentration was determined using the Bicinchoninic Acid (BCA) Kit for Protein Determination. 40 mg of snap frozen mouse liver tissue was added to a round-bottomed 2 mL tube, with 400  $\mu$ L radioimmunoprecipitation (RIPA) buffer and a single, metal, milling ball before being lysed using an oscillating mill for 3 min at 30 s<sup>-1</sup> (Retsch).

A standard curve was generated with bovine serum albumin (BSA) of known concentrations. A 2 mg/mL BSA solution was prepared in dH<sub>2</sub>O and subsequently diluted to produce the following concentrations: 1.5, 1, 0.75, 0.5, 0.25, 0.125 mg/mL. Mouse liver tissue lysates were diluted 1 in 100 in dH<sub>2</sub>O and briefly vortexed. 9  $\mu$ L of each standard, and 5  $\mu$ L of each liver tissue lysate were loaded

in duplicate in to a 96 well plate. A blank sample, consisting of 9  $\mu\text{L}$   $\text{dH}_2\text{O}$  was also loaded in duplicate. 2 % Copper (II) sulphate was prepared by diluting copper (II) sulphate 1 in 50 with bicinchoninic acid. The combined assay working reagent was added to the plate at 200  $\mu\text{L}$  / well before the plate was incubated at 37  $^\circ\text{C}$  for 30 min. Absorbance was measured at 562 nm using a Varioskanner Flash 3001 (ThermoScientific).

### 2.2.3 Western blotting

Mouse liver tissue lysates were prepared with a final concentration of 1  $\mu\text{g}/\mu\text{L}$ . Loading buffer was generated by combining NuPAGE 4x LDS Sample Buffer (Invitrogen) and NuPAGE 10x Sample Reducing Agent (Invitrogen) in a 7:3 ratio. 5  $\mu\text{L}$  of loading buffer was combined with 15  $\mu\text{L}$  of liver tissue lysate and incubated at 90  $^\circ\text{C}$  for 10 min to allow for protein denaturation. Following this, samples were very briefly kept on ice and then centrifuged for 30 sec at 1000 g before being loaded into wells of NuPAGE Novex 4-12 % Bis-tris Polyacrylamide Gels (Invitrogen). On each gel, one well included 5  $\mu\text{L}$  Precision-Plus Kaleidoscope Protein Standards (BioRad) to provide a reference marker. 1x 3-(N-morpholino)propanesulfonic acid (MOPS) running buffer was generated by diluting 50 mL 20x NuPAGE MOPS SDS Running Buffer (Invitrogen) in 950 mL  $\text{dH}_2\text{O}$ . Gels were resolved initially for 10 min at 90 V, followed by 70 min at 170 V in 1x MOPS running buffer.

A 10x Transfer buffer solution was produced by dissolving 150.2 g Glycine and 30.3 g Tris base in 1 L  $\text{dH}_2\text{O}$ . Once fully resolved, proteins were transferred to 0.45  $\mu\text{m}$  Nitrocellulose Membranes (GE Healthcare, Amersham) using Transfer Tanks (BioRad) and 1 L 1x Transfer buffer (100 mL 10x Transfer buffer solution, 200 mL Methanol and 700 mL  $\text{dH}_2\text{O}$ ) for 1 hour at 230 mA. Following completion of protein transfer, Nitrocellulose Membranes were incubated for 2 min in ponceau S solution to confirm successful transfer.

A 20x Tris-buffered saline (TBS) stock solution was prepared (175.2 g NaCl, 4.48 g KCl and 60.6 g Tris base in 1 L dH<sub>2</sub>O) at pH 7. A 1x TBS-Tween (TBS-T) solution was then generated (50 mL 20x TBS, 10 mL 10 % (v/v) Tween20 and 940 mL dH<sub>2</sub>O). Nitrocellulose Membranes were blocked with 10 % (w/v) Blotting grade blocker (BioRad) in 1x TBS-T for 1 hour at room temperature. Following blocking, Nitrocellulose Membranes were incubated with antibodies (Table 2.1) in 10 % (w/v) Blotting grade blocker in 1x TBS-T. Incubation with secondary antibodies (Table 2.2) was completed before membranes were washed for 4x 5 min with 1x TBS-T.

Western Lightning® Plus-ECL reagent (PerkinElmer) was used alongside Amersham Hyperfilm™ ECL X-ray film (GE Healthcare, Amersham) in a dark room for 1 – 300 sec to develop blots. X-ray film was incubated in Universal X-Ray Developer (Champion RG) for 2 min. The x-ray film was then incubated in Universal X-Ray Fixer (Champion RG) for 2 min. Once dry, films were scanned and densitometry performed using ImageJ (Schneider et al., 2012). Density of bands were normalised to the intensity of  $\beta$  actin, used as a loading control.

**Table 2.1 Primary antibodies for Western blot**

<b>Primary Antibody</b>	<b>Dilution Factor (in 10 % Blotting Grade Blocker in 1x TBS-T)</b>	<b>Incubation Time</b>	<b>Washes (using 1x TBS-T)</b>
Nrf2 (16396-1-AP, Proteintech / Rabbit / Polyclonal)	1:1,000	Overnight at 4 °C	4x 5 min
Nqo1 (ab2346, Abcam / Goat / Polyclonal)	1:2,500	Overnight at 4 °C	4x 5 min
PCNA (ab29, Abcam / Mouse / Monoclonal)	1:2,000	Overnight at 4 °C	4x 5 min
$\beta$ Actin (ab6276, Abcam / Mouse / Monoclonal)	1:10,000	1 hour at room temp	4x 5 min

**Table 2.2 Secondary antibodies for Western blot**

<b>Secondary Antibody</b>	<b>Dilution Factor (in 10 % Blotting Grade Blocker in 1x TBS-T)</b>	<b>Incubation Time</b>	<b>Washes (using 1x TBS-T)</b>
Anti-Rabbit HRP (A9169, Sigma / Goat / Polyclonal)	1:5,000	1 hour at room temp	4x 5 min
Anti-Goat HRP (P044901-2, Agilent / Rabbit / Polyclonal)	1:5,000	1 hour at room temp	4x 5 min
Anti-Mouse HRP (A9044, Sigma / Rabbit / Polyclonal)	1:5,000	1 hour at room temp	4x 5 min

### 2.2.4 Gene expression analysis

Gene expression was determined using quantitative (real-time) polymerase chain reaction (qPCR).

Isolated RNA was converted to cDNA and quantified using the SYBR green fluorescent dye. The SYBR green dye works by intercalating with double stranded DNA to produce a detectable fluorescent signal (Zipper et al., 2004).

#### 2.2.4.1 RNA isolation

Total RNA was isolated from snap frozen mouse liver tissue using a RNeasy Mini Kit (Qiagen). 20 mg of snap frozen mouse liver tissue was added a round-bottomed 2 mL tube with a single, metal, milling ball and was homogenised in 300  $\mu$ L buffer RLT using an oscillating mill for 3 min at 30  $s^{-1}$  (Retsch). Lysates were centrifuged at 18,000 g for 3 min and the resulting supernatant transferred to new tubes. 70 % (v/v) ethanol in  $dH_2O$  was prepared and 300  $\mu$ L was added to all samples prior to being vortexed and loaded onto a spin column above a 2 mL collection tube. Spin columns were then centrifuged at 8,000 g for 15 sec and the flow-through was discarded. The silica membranes were then washed two times with 700  $\mu$ L buffer RW1 and 500  $\mu$ L buffer RPE, ensuring the spin columns were centrifuged, and flow-through discarded, after the addition of each buffer. The spin columns were spun for a final time to remove residual ethanol at 8,000 g for 1 min and RNA was eluted in 30  $\mu$ L RNase-free  $dH_2O$ . RNA yield was quantified using the Nanodrop Spectrophotometer ND-1000 (Labtech International). Only RNA with a 260/280 ratio between 1.8 and 2.1 were used. All RNA samples were stored at  $-80\text{ }^{\circ}\text{C}$  until ready to be used.



#### 2.2.4.2 cDNA synthesis

Reverse transcription of RNA to cDNA was carried out using the ImProm-II Reverse Transcription System (Promega). 0.5 µg RNA was added to a semi-skirted RNase free 96 well plate (Starlab) along with random primer (0.5 µg/reaction) and made up to 5 µL with nuclease free dH<sub>2</sub>O. The plate was sealed and incubated for 5 min at 70 °C and then immediately cooled on ice for 5 min. A reverse transcription reaction mix was generated (4 µL ImProm-II 5x reaction buffer, 3 µL 4 mM MgCl<sub>2</sub>, 1 µL dNTP mix, 20 units recombinant RNasin ribonuclease inhibitor, 1 µL ImProm-II reverse transcriptase) and made up to 15 µL with nuclease free dH<sub>2</sub>O per reaction. 15 µL transcription reaction mix was added to each well to give a final reaction volume of 20 µL. The plate was then sealed and incubated for 5 min at 25 °C to allow annealing, incubated for 1 hour at 42 °C to allow for extension, and incubated for 15 min at 70 °C to inactivate the reverse transcriptase enzyme. All cDNA samples were stored at -20 °C until ready to be used.

#### 2.2.4.3 qPCR

qPCR analysis was performed using Power SYBR Green (Thermo Fisher Scientific) on a ViiA7 qPCR system (Applied Biosystems). Lyophilised forward and reverse primers (sequences outlined in Table 2.3) were rehydrated in nuclease free dH<sub>2</sub>O to produce 100 µM stocks and diluted to produce 10 µM working solutions. Reaction master mix was prepared for each primer pair (5 µL Power SYBR Green master mix, 0.5 µL 10 µM forward primer, 0.5 µL 10 µM reverse primer) and made up to 8 µL with nuclease free dH<sub>2</sub>O. 8 µL of reaction master mix was added to each well of an RNase free 384 well plate. cDNA was diluted 1 in 5 with nuclease free dH<sub>2</sub>O and 2 µL was loaded per well, creating a final reaction volume of 10 µL. Each sample was ran in duplicate. The plate was analysed using the ViiA7 qPCR system (program outlined in Table 2.4). For each sample, Ct values were averaged and normalised to *Gapdh* prior to the generation of fold changes using the formula  $2^{-\Delta\Delta Ct}$ .

**Table 2.3 Mouse qPCR primer sequences**

Gene	Primer	Sequence
Mouse <i>Pcna</i>	Fwd	5'- TAC AGC TTA CTC TGC GCT CC -3'
	Rev	5'- TTG GAC ATG CTG GTG AGG TTC -3'
Mouse <i>Nqo1</i>	Fwd	5'- TTT AGG GTC GTC TTG GCA AC -3'
	Rev	5'- GTC TTC TCT GAA TGG GCC AG -3'
Mouse <i>Pgd</i>	Fwd	5'- GCG TTT CTT CCT CCT CGA CT -3'
	Rev	5'- TTC ACA AGC AGG ATG ACC CG -3'
Mouse <i>Scd1</i>	Fwd	5'- TTC TTG CGA TAC ACT CTG GTG C -3'
	Rev	5'- CGG GAT TGA ATG TTC TTG TCG T -3'
Mouse <i>Gapdh</i>	Fwd	5'- TGT CCG TCG TGG ATC TGA C -3'
	Rev	5'- CCT GCT TCA CCA CCT TCT TG -3'

**Table 2.4 qPCR program**

Cycle Step	Temperature	Time	Cycles
Initial Denaturation	95 °C	60 sec	1
Denaturation	95 °C	15 sec	40
Extension	60 °C	30 sec	

### 2.2.5 Glutathione quantification

Total glutathione (GSH) was quantified by utilising the 5-5'-Dithiobis(2-nitrobenzoic acid) (DTNB) method (Vandeputte et al., 1994).

Glutathione stock buffer was produced by dissolving 8.58 g sodium dihydrogen phosphate monohydrate ( $\text{NaH}_2\text{PO}_4 \cdot 2\text{H}_2\text{O}$ ) and 1.17 g Ethylenediaminetetraacetic acid (EDTA) in 450 mL  $\text{dH}_2\text{O}$  at pH 7.4. 50 mg of snap frozen mouse liver tissue was added to a round-bottomed 2 mL tube with a single, metal, milling ball and was homogenised in 800  $\mu\text{L}$  GSH stock buffer and 200  $\mu\text{L}$  6.5 % (w/v) sulfosalicylic acid (SSA), using an oscillating mill for 3 min at  $30 \text{ s}^{-1}$  (Retsch). Samples were then left on ice for 10 min to facilitate deproteinization before being centrifuged at 18,400 g for 5 min at 4 °C. All supernatants were stored at -80 °C until ready to be used. The protein pellets were dissolved in 1 mL 1 M NaOH at 60 °C for 1 hour before being stored at -80 °C until ready to be used. Protein content of the dissolved pellets was determined using the BioRad Protein Assay kit (BioRad), which utilises a dye-binding method based on the Bradford assay.

1 mM glutathione was prepared in GSH stock buffer and then diluted further in GSH stock buffer to produce solutions for a standard curve, with the following concentrations: 50, 40, 20, 10, 5, 2, 1 nmol/mL. Supernatants were defrosted on ice, diluted 1 in 10 in GSH stock buffer and briefly vortexed. 20  $\mu\text{L}$  of each standard and supernatant sample were loaded in duplicate in to a 96 well plate. A blank sample, consisting of 20  $\mu\text{L}$  GSH stock buffer was also loaded in duplicate.

The assay working reagent was produced by dissolving DTNB and NADPH in GSH stock buffer before combining in equal volumes to give 25 mL final volume (10 mg DTNB in 12.5 mL GSH stock buffer, 7

mg NADPH in 12.5 mL GSH stock buffer). Glutathione reductase was diluted in GSH stock buffer to give a final volume of 10 mL, according to the following calculation:

$$\text{Volume } (\mu\text{L}) = [(6.96 \text{ units/mL} \times 10 \text{ mL}) / (\text{Units/mL of stock reductase})] \times 1000$$

Both the assay working reagent and diluted glutathione reductase were kept on ice until ready to be used. 200  $\mu\text{L}$  assay working reagent was added to each well using a multi-channel pipette, and incubated at room temperature for 5 min. Following this, 50  $\mu\text{L}$  glutathione reductase was added to each well, again using a multi-channel pipette. Immediately after, the optical density (OD) was measured by kinetic assay at 412 nm using the Varioskanner Flash 3001. All samples were normalised to their respective protein content.

### **2.2.6 Metabolic coenzyme quantification**

The levels of the metabolic coenzymes, Nicotinamide adenine dinucleotide phosphate (NADP/H) and Nicotinamide adenine dinucleotide (NAD/H), were measured by utilising a luciferase-based assay. A bicarbonate buffer comprising 20 mM sodium bicarbonate, 100 mM sodium carbonate, 10 mM nicotinamide, 0.5 % dodecyltrimethylammonium bromide and 0.05 % Triton X-100 was produced. 20 mg of snap frozen mouse liver tissue was added to round-bottomed 2 mL tube with a single, metal, milling ball and was homogenised in 400  $\mu\text{L}$  bicarbonate buffer using an oscillating mill for 3 min at  $30 \text{ s}^{-1}$  (Retsch). Lysates were then centrifuged at 10,000 g for 20 min at  $4 \text{ }^{\circ}\text{C}$  and supernatant transferred to new, labelled, 1.5 mL tubes.

### 2.2.6.1 NADP/H quantification

Nicotinamide adenine dinucleotide phosphate (NADP<sup>+</sup>), and its reduced form NADPH, was quantified using the NADP/NADPH-Glo™ assay kit (Promega). Prior to quantification, liver tissue homogenate was diluted 1 in 25 in phosphate buffered saline (PBS) and briefly vortexed. Samples were then pre-treated to allow quantification. To quantify NADP<sup>+</sup>, 25 µL of 0.4 N HCl was added to labelled 0.5 mL tubes containing 50 µL of diluted liver tissue homogenate, prior to incubation at 60 °C for 15 min and room temperature for a further 10 min. Following this, 25 µL of 0.5 M Trizma base was added. To quantify NADPH, 50 µL of diluted liver homogenate was incubated in labelled 0.5 mL tubes at 60 °C for 15 min and room temperature for a further 10 min, before 50 µL of 0.2 N HCl/0.25 M Trizma base solution was added.

A standard curve was generated with purified NADP<sup>+</sup> and NADPH of known concentrations. 10 µM stocks of NADP<sup>+</sup> and NADPH were prepared in PBS and subsequently diluted in PBS to produce the following concentrations: 5, 10, 25, 50, 100, 200, 400 nM. All standards received the same pre-treatment for NADP<sup>+</sup> and NADPH as the relevant liver homogenates.

Liver tissue homogenates and standards treated for NADP<sup>+</sup> were loaded into a separate plate to those treated for NADPH to prevent contamination. 50 µL of each liver tissue homogenate, and standard, treated for NADP<sup>+</sup> and NADPH, were loaded in duplicate in to clear 96 well plates respectively. A blank sample consisting of 50 µL untreated PBS was also loaded in duplicate to each clear 96 well plate. NADP/NADPH-Glo™ detection reagent was prepared (1 mL reconstituted luciferin detection reagent, 5 µL reductase, 5 µL reductase substrate, 5 µL NADP cycling enzyme, 5 µL NADP cycling substrate) and 50 µL was added to each well ensuring a 1:1 ratio of sample to detection reagent. The plates were then shaken for 2 min at 65 rpm before being incubated in the dark for 30

min at room temperature. Following this 50  $\mu$ L of reaction solution was transferred to a white 96 well plate (Greiner Bio-One) and luminescence was quantified using a Varioskanner Flash 3001 (ThermoScientific). NADP<sup>+</sup> and NADPH concentrations were then normalised to the total protein content of the liver tissue. Total protein concentration was determined using the Bicinchoninic Acid (BCA) Kit for Protein Determination, as previously explained in section 2.2.2.

### 2.2.6.2 NAD/H quantification

Nicotinamide adenine dinucleotide (NAD<sup>+</sup>), and its reduced form NADH, was quantified using the NAD/NADH-Glo™ assay kit (Promega). Prior to quantification, liver tissue homogenate was diluted 1 in 25 in phosphate buffered saline (PBS) and briefly vortexed. Samples were pre-treated for NAD<sup>+</sup> and NADH quantification following the same method for NADP<sup>+</sup> and NADPH respectively, as outlined previously in section 2.2.6.1.

A standard curve was generated with purified NAD<sup>+</sup> and NADH of known concentrations. 10  $\mu$ M stocks of NAD<sup>+</sup> and NADH were prepared in PBS and subsequently diluted in PBS to produce the following concentrations: 5, 10, 25, 50, 100, 200, 400 nM. All standards received the same pre-treatment for NAD<sup>+</sup> and NADH as the relevant liver homogenates.

Liver tissue homogenates and standards treated for NAD<sup>+</sup> were loaded into a separate plate to those treated for NADH to prevent contamination. 50  $\mu$ L of each liver tissue homogenate, and standard, treated for NAD<sup>+</sup> and NADH, were loaded in duplicate in to clear 96 well plates respectively. A blank sample consisting of 50  $\mu$ L untreated PBS was also loaded in duplicate to each clear 96 well plate. NAD/NADH-Glo™ detection reagent was prepared (1 mL reconstituted luciferin detection reagent, 5  $\mu$ L reductase, 5  $\mu$ L reductase substrate, 5  $\mu$ L NAD cycling enzyme, 25  $\mu$ L NAD cycling substrate) and

50  $\mu\text{L}$  was added to each well ensuring a 1:1 ratio of sample to detection reagent. Luminescence was then quantified as previously outlined in section 2.2.6.1.  $\text{NAD}^+$  and  $\text{NADH}$  concentrations were then normalised to the total protein content of the liver tissue. Total protein concentration was determined using the Bicinchoninic Acid (BCA) Kit for Protein Determination, as previously explained in section 2.2.2.

### **2.2.7 Primary human hepatocytes**

Excess liver tissue was obtained from routine hepatobiliary surgery, carried out by medical professionals at Aintree University Hospital (Liverpool, UK). All patients gave informed written consent. The protocol (11/NW/0327) was approved by the National Health Service North West–Liverpool Central Research Ethics Committee and adhered to the ethical guidelines of the 1975 Declaration of Helsinki.

#### **2.2.7.1 Isolation and culture**

Resected liver tissue was kept on ice in perfusion buffer (10 mM HEPES, 5 mM KCl, 136 mM NaCl and 0.5 % (w/v) glucose (Thermo-Fisher Scientific) in  $\text{dH}_2\text{O}$ ) during transport to the University laboratories. Primary human hepatocytes (PHH) were kindly isolated by Dr Rowena Sison-Young by utilising the two-stage collagenase digestion method detailed by LeCluyse et al. (LeCluyse et al., 2005). The liver tissue was weighed, cannulated, and then perfused with ice cold perfusion buffer to remove any excess blood from the tissue.

The liver tissue was again cannulated and perfused with digestion buffer (0.5 mg/mL Collagenase IV and 700  $\mu\text{M}$   $\text{CaCl}_2$  in perfusion buffer) at a flow rate of between 15 and 30 mL/min for no longer than 25 min. Once the tissue has softened, indicating complete digestion, the Glisson's capsule was gently

torn open using sterile tissue forceps and scissors. The resulting cell suspension was then passed through a 125 µm mesh (Clarcor) to filter out undigested material and connective tissue. The cell suspension was then centrifuged at 75 g for 5 min at 4 °C, supernatant discarded, and cell pellet gently resuspended in Williams E medium. The viability of the resulting cell suspension was then determined and only suspensions with ≥ 75 % viability were used. The cell pellet was resuspended in complete medium (1 % (v/v) insulin-transferrin-selenium (Life Technologies), 2 mM L-glutamine, 100 nM dexamethasone and 1 % (v/v) penicillin/streptomycin in Williams E medium) and seeded onto Type I Collagen-coated plates (Becton Dickinson), at a density of  $1 \times 10^6$  cells/mL, before being maintained at 37 °C in a 5 % CO<sub>2</sub> environment.

#### **2.2.7.2 Drug treatment**

Isolated PHH cells were left for 16 hours, to allow complete adherence, prior to the commencement of drug treatment. CDDO-Me was prepared to a concentration of 20 µM in 100 % DMSO, then diluted 1 in 200 in complete medium to produce a final CDDO-Me concentration of 100 nM, and a DMSO content of 0.5 %. Control media, with a DMSO content of 0.5 %, was produced by diluting 100 % DMSO 1 in 200 in complete medium. Existing media was then aspirated from the plate and replaced with either CDDO-Me-treated, or control, media for 24 hours.

#### **2.2.8 TempO-Seq high-throughput transcriptomics analysis**

TempO-Seq high-throughput transcriptomics analysis (House et al., 2017) was carried out by BioClavis (Glasgow, UK). Primary human hepatocytes (PHH) from 3 donors were isolated, cultured and treated as outlined in section 2.2.7. Total RNA was isolated and purified from PHH as outlined in section 2.2.4.1. 10 µL of each purified RNA sample (70 – 200 ng/µL) was transferred to a conical-



bottom 384 well plate and frozen at  $-80^{\circ}\text{C}$ , before being packaged on dry ice and transported to BioClavis.

TempO-Seq was performed as described by Chan et al. (Chan et al., 2021). FASTQ files were generated and aligned to the Human Whole Transcriptome v2.0 panel, consisting of 22,537 probes, using Bowtie (Everett et al., 2022) in the TempO-SeqR software package (BioSpyder Technologies).

### 2.2.8.1 Bioinformatics

Normalisation and differential expression analysis of FASTQ files was performed using the DESeq2 package (v1.30.0) in R, as outlined by Love et al. (Love et al., 2014). For each gene, the raw counts were normalised by utilising the estimateSizeFactors function. The variance across the mean was then stabilised by applying the variance stabilising transformation (vst) (Anders and Huber, 2010). Limma batch effect correction was then applied to remove unwanted batch effects and further power the differential expression analysis (Ritchie et al., 2015).

Sample variability was then assessed by principal component analysis. As the number of samples were limited, an unadjusted P value  $< 0.05$  was considered statistically significant. As outlined by Yu et al. (Yu et al., 2012), gene set enrichment analysis (GSEA) was carried out using ClusterProfiler package (v3.18.0) on the differentially expressed genes (DEGs) ranked by  $\log_2$  fold-change. The number of permutations was set to 10,000. Normalised Enrichment Score (NES) was then calculated by dividing the positive and negative enrichment scores by the mean of positive or negative permutation enrichment scores (pES) respectively. Gene ontology (GO) biological processes (Ashburner et al., 2000) were considered significant with an unadjusted P value  $< 0.05$  and absolute Normalised Enrichment Score (NES)  $> 1.5$ . Finally, similarities between GO terms were identified, and

the parent terms were visualised using the REVIGO based rrvgo R package (v1.2.0) (Supek et al., 2011). Significant GO terms were then presented with respective NES and P value.

### **2.2.9 Statistical analysis**

As indicated in each figure legend, statistical analysis was carried out using Stats Direct 3 software. P values are reported to three decimal places. For Student t tests and Mann-Whitney U tests, two-tailed P values are reported. Differences were considered significant at  $P \leq 0.05$ .

## 2.3 Results

### 2.3.1 CDDO-Me enhances restoration of liver volume

We first verified that untreated, wild-type, C57BL/6 mice would act as a suitable negative control for assessing restoration of liver volume following two-thirds PHx. This is opposed to wild-type C57BL/6 mice receiving 100 % DMSO, the vehicle used for delivery of CDDO-Me, as means of a negative control. In order to achieve this, we used MRI, a non-invasive imaging technique, to measure liver volume before and after a two-thirds PHx, in untreated mice and those treated with 100 % DMSO (Fig 2.2). Mice were treated or not with 100 % DMSO on days -1, 0, 1 and 3, PHx was carried out on day 0, and liver volume quantified by MRI, relative to day -1 baseline, on days 1, 2, 3 and 7. Following PHx, liver volume increased in both untreated mice, and those treated with 100 % DMSO, in a time-dependent manner. No significant difference was observed between the two groups at all time points measured by unpaired t-test ( $P = 0.139, 0.711, 0.901, 0.127$  respectively). Therefore, untreated mice were used as a negative control in all further PHx experiments to better mimic the current clinical setting.

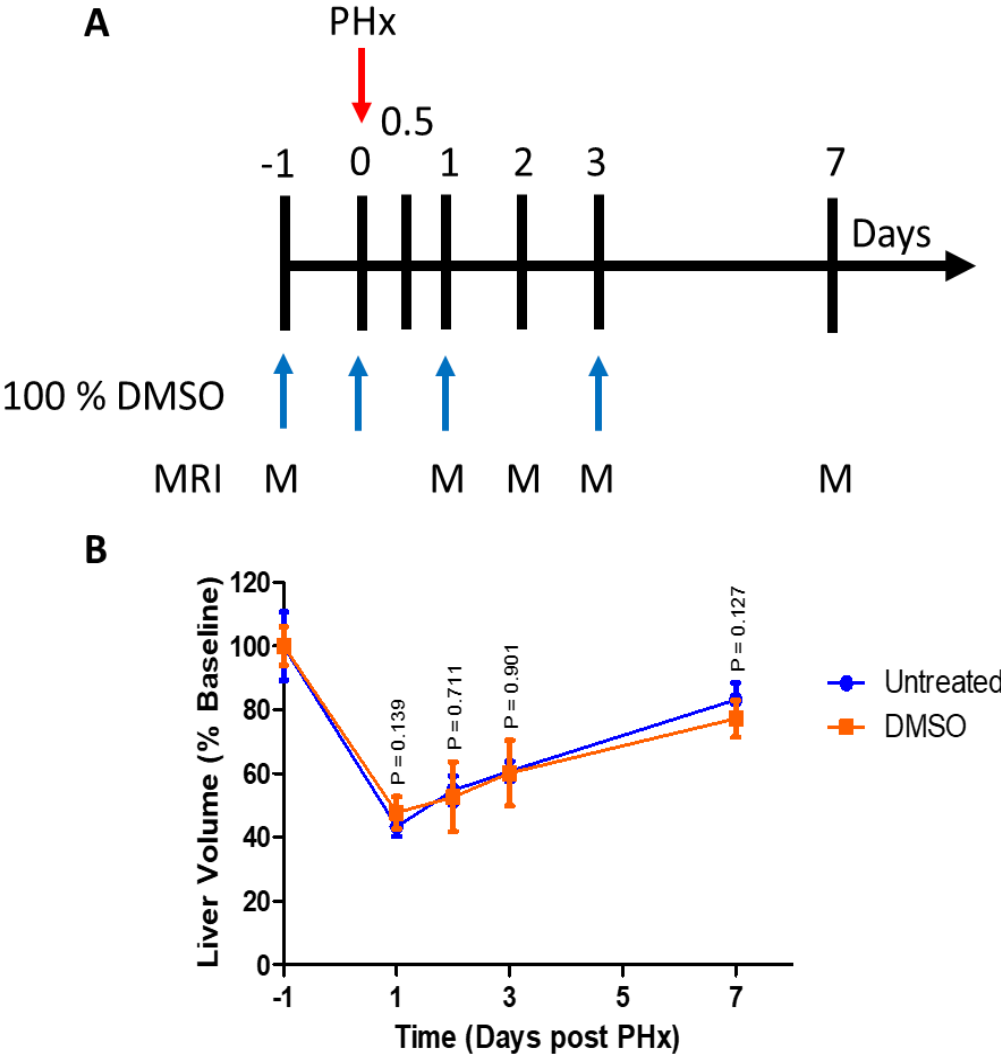


**Figure 2.2 Restoration of liver volume following PHx in untreated and DMSO treated wild-type C57BL/6 mice.**

(A) Study design. Mice were treated or not with 100 % DMSO on days -1, 0, 1 and 3, PHx was carried out on day 0, and liver volume quantified by MRI, relative to day -1 baseline, on days 1, 2, 3 and 7. (B) Liver volume in wild-type mice imaged for 7 days following PHx. Unpaired t-test, untreated vs DMSO at each time point. Data analysis represents mean  $\pm$  SD of n=5 animals per treatment group.

We then assessed the effect of multiple doses of CDDO-Me, administered before and after PHx to ensure greatest Nrf2 activation, on the restoration of liver volume following two-thirds PHx (Fig 2.3). Mice were treated or not with 3 mg/kg CDDO-Me, on days -1, 0, 1 and 3, PHx was carried out on day 0, and liver volume quantified by MRI, relative to day -1 baseline, on days 1, 2, 3, 7, 14 and 31. Immediately following PHx, liver volume increased in a time-dependent manner in both groups up to day 14, at which point liver volume plateaued close to pre-surgery levels ( $90.27 \pm 5.58$  % in control,  $96.19 \pm 2.88$  % in CDDO-Me). Interestingly, mice treated with CDDO-Me had a significantly faster rate of liver volume restoration than control mice at days 1, 2, 3 and 7 ( $P = 0.022, 0.006, 0.016$  and  $0.003$  respectively).

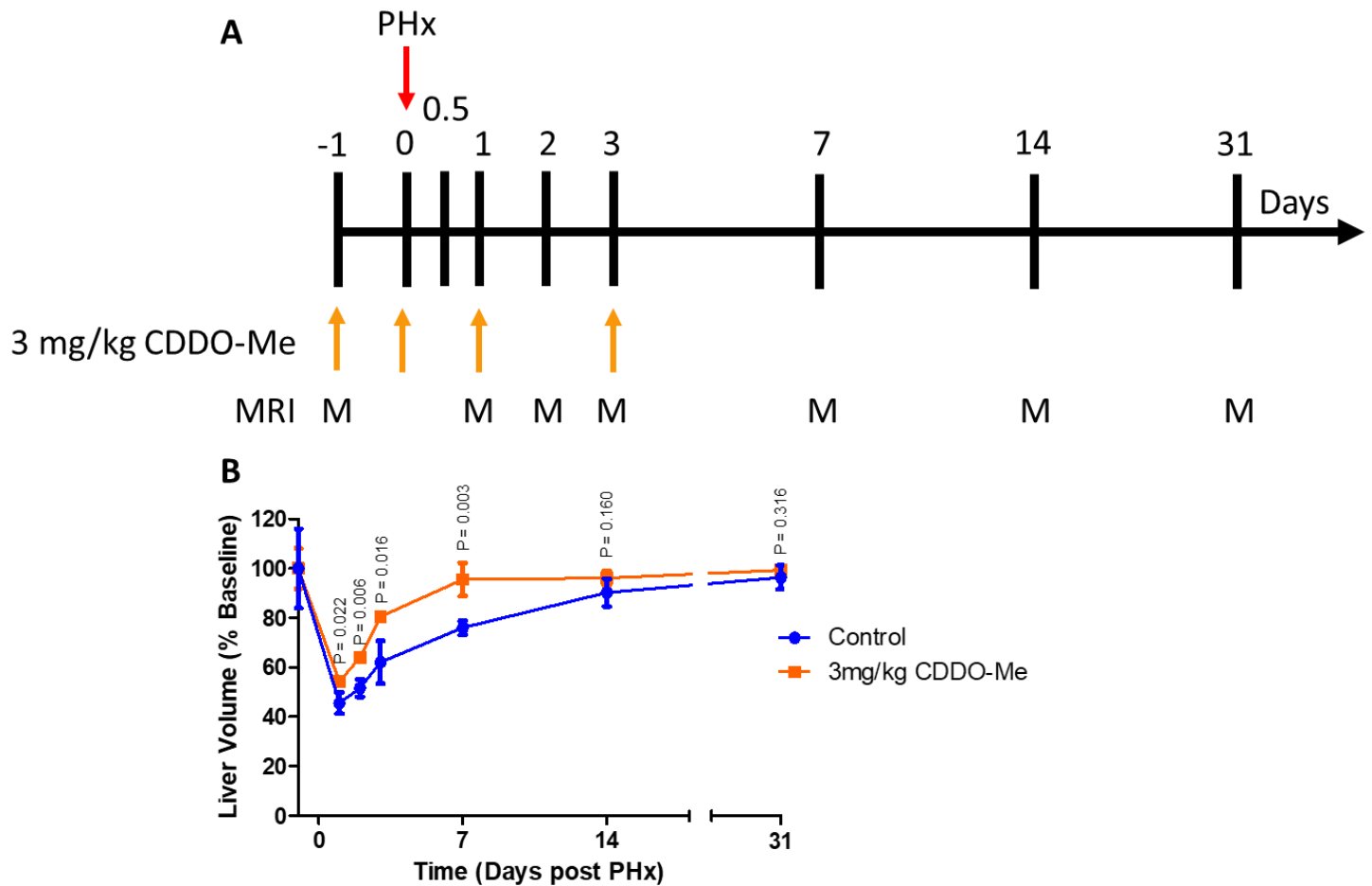


**Figure 2.3 Multiple doses of CDDO-Me enhances restoration of liver volume following two-thirds PHx in wild-type C57BL/6 mice.**

(A) Study Design. Mice were treated or not with 3 mg/kg CDDO-Me on days -1, 0, 1 and 3, PHx was carried out on day 0, and liver volume quantified by MRI, relative to day -1 baseline, on days 1, 2, 3, 7, 14 and 31. (B) Liver volume in wild-type mice imaged for 31 days following PHx. Unpaired t-test, control vs CDDO-Me at each time point. Data analysis represents mean  $\pm$  SD of n=3-5 animals per treatment group.

As administration of a single therapeutic dose would be more practical in a clinical setting, we then assessed the effect of a single CDDO-Me dose, and the timing at which this was administered in relation to surgery, on the restoration of liver volume following two-thirds PHx (Fig 2.4). Mice were treated or not with a single 3 mg/kg CDDO-Me dose on day -1 (denoted as pre-op), day 0, 1 hour prior to surgery commencing (denoted as intra-op) or day 1 (denoted as post-op). PHx was carried out on day 0, and liver volume quantified by MRI, relative to day -1 baseline, on days 1, 3 and 7. Intra-op administration of CDDO-Me significantly enhanced the rate of liver volume restoration compared to untreated animals at day 1 and 3 ( $P = 0.011$  and  $0.004$  respectively). By day 7, this significance was lost. No significant differences in restoration of liver volume were observed in either pre-op CDDO-Me or post-op CDDO-Me, when compared to untreated animals, at all time points measured.

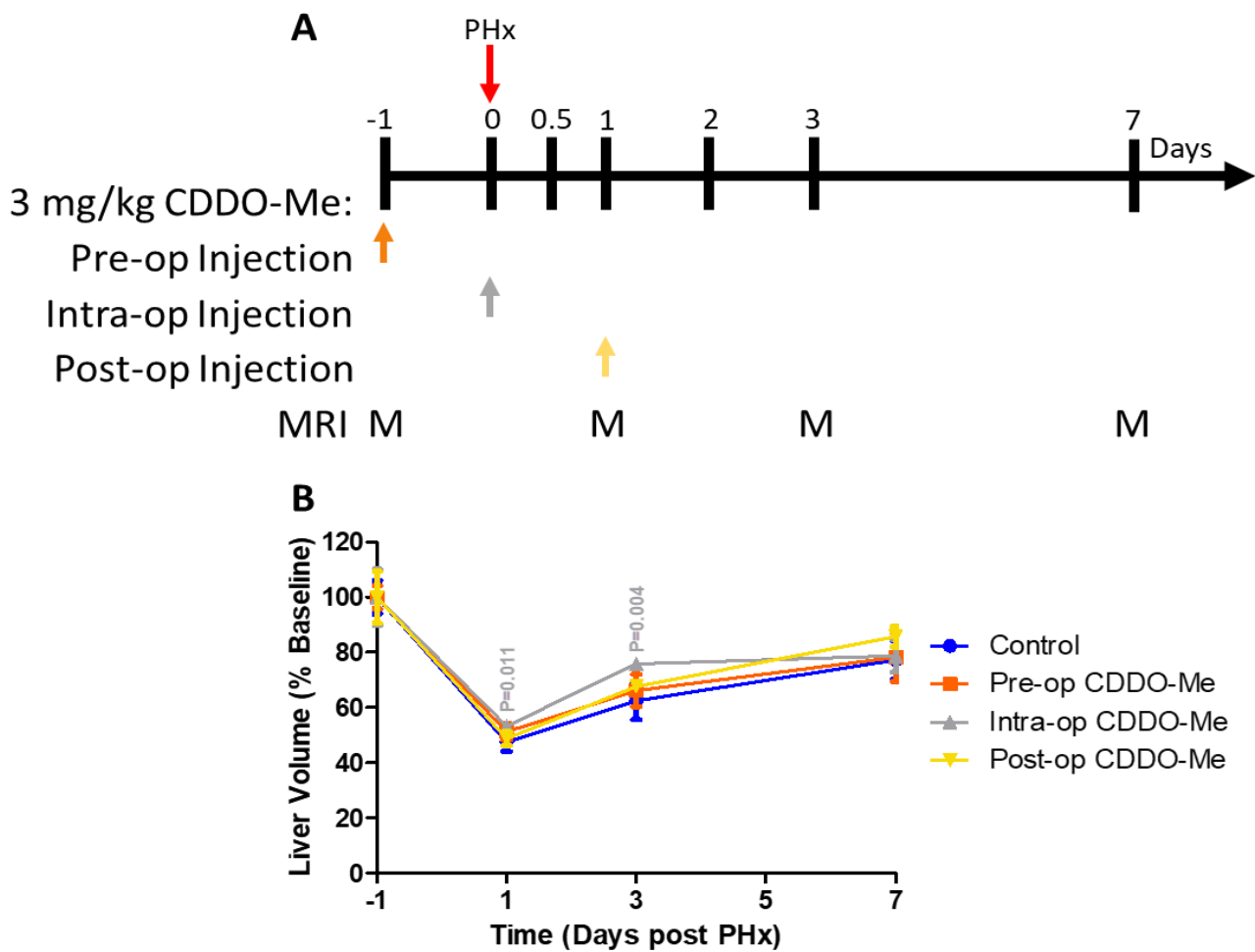


**Figure 2.4** The impact of a single dose of CDDO-Me on the restoration of liver volume following two-thirds PHx in wild-type C57BL/6 mice.

(A) Study design. Mice were treated or not with a single 3 mg/kg CDDO-Me dose on day -1 (denoted as pre-op), day 0, 1 hour prior to surgery commencing (denoted as intra-op) or day 1 (denoted as post-op). PHx was carried out on day 0, and liver volume quantified by MRI, relative to day -1 baseline, on days 1, 3 and 7. (B) Liver volume in wild-type mice imaged for 7 days following PHx. Unpaired t-test, control vs CDDO-Me at each time point. Data analysis represents mean  $\pm$  SD of  $n=3-5$  animals per treatment group. Where no P value is reported, no significant difference was observed.



### 2.3.2 Molecular mechanisms driving CDDO-Me enhanced liver regeneration

Gene expression levels of NAD(P)H dehydrogenase, quinone 1 (*Nqo1*), an established target gene of Nrf2 commonly utilised to monitor the activity of the Nrf2 pathway (Mutter et al., 2015), and proliferating cell nuclear antigen (*Pcna*), a well-known marker of cellular proliferation (Kelman, 1997), were quantified in the livers of mice following PHx in the presence or absence of multiple doses of 3 mg/kg CDDO-Me, using quantitative (real-time) polymerase chain reaction (qPCR) (Fig 2.5).

Understandably, PHx alone increased the expression of *Pcna* (Chen et al., 2019), however this was further enhanced, although not statistically significantly, in mice treated with CDDO-Me at 8, 24 and 96 hours ( $P = 0.413, 0.905$  and  $0.064$  respectively) (Fig 2.5 A). Furthermore, mice treated with CDDO-Me had significantly higher expression levels of *Nqo1* when compared to untreated animals at 8, 24, 48 and 96 hours ( $P = 0.005, < 0.001, < 0.001, < 0.001$  respectively). This enhanced level of expression in CDDO-Me treated mice was lost by 168 hours (Fig 2.5 B).

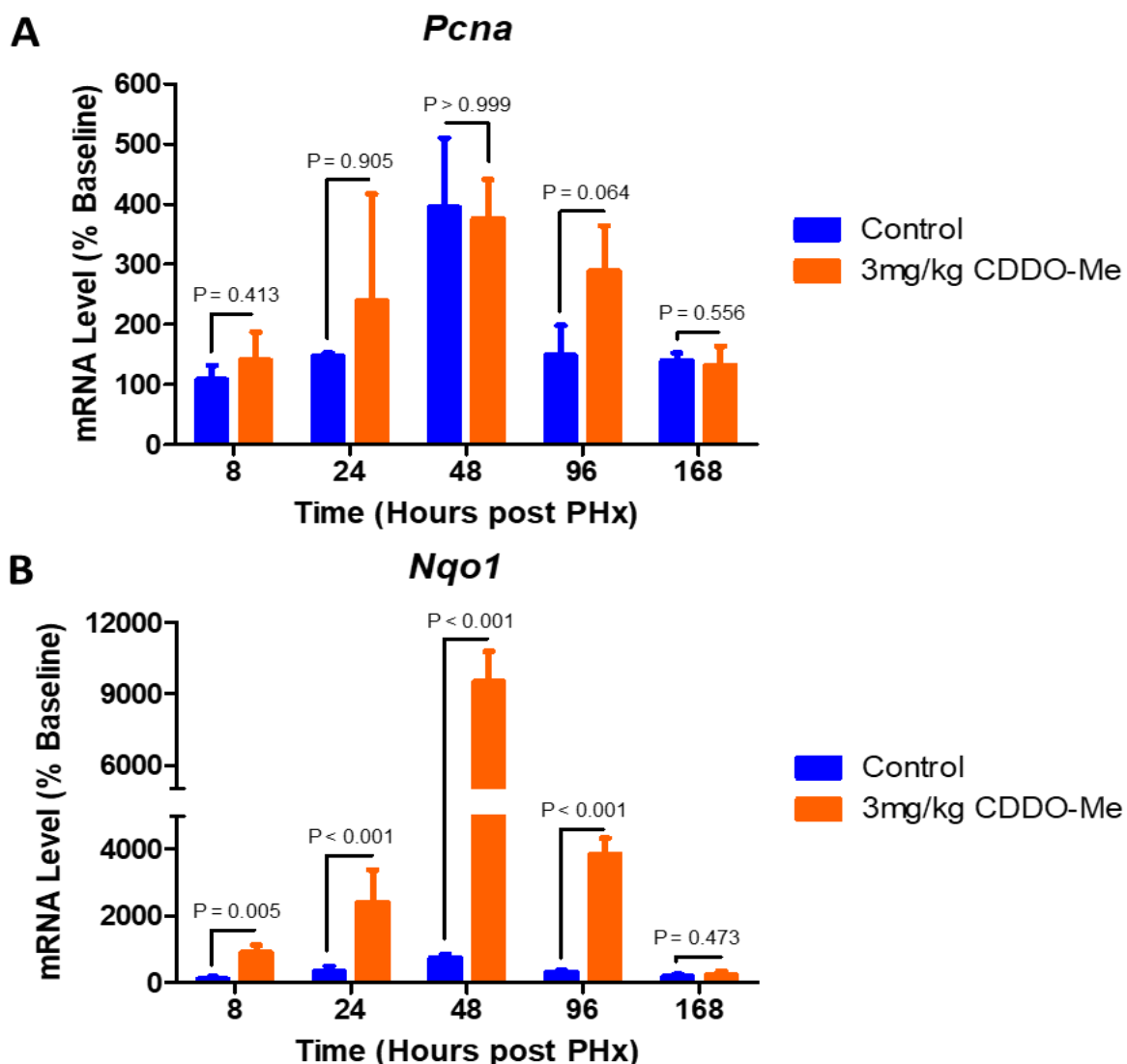


**Figure 2.5** The impact of multiple doses of CDDO-Me on the gene expression levels of *Pcna* and *Nqo1* in mouse livers following two-thirds PHx.

Gene expression levels of (A) *Pcna* and (B) *Nqo1* were normalised to *Gapdh* and presented as a % of the average day -1, untreated, mRNA level. (A) Mann-Whitney U test, control vs CDDO-Me at each time point, (B) Unpaired t-test, control vs CDDO-Me at each time point. Data analysis represents mean  $\pm$  SD of n=4-5 animals per treatment group. Abbreviations: *Gapdh*, glyceraldehyde-3-phosphate dehydrogenase; *Pcna*, proliferating cell nuclear antigen; *Nqo1*, NAD(P)H dehydrogenase, quinone 1.

Following this, protein expression levels of Nqo1 and PcnA in the livers of mice following PHx, in the presence or absence of multiple doses of 3 mg/kg CDDO-Me, were quantified by western blotting, to investigate if the changes in gene expression translated to protein (Fig 2.6). PHx alone caused an increase in PcnA protein expression after 48 hours, peaking at this time point. This was then further enhanced at all time points in animals treated with CDDO-Me, with significantly higher levels seen at 48 hours ( $P = 0.016$ ). Increased PcnA protein expression was also observed earlier, at 24 hours, in CDDO-Me treated mice. Treatment with CDDO-Me prolonged the expression of PcnA protein, with significantly increased levels observed at 168 hours when compared to untreated mice at the same time point ( $P = 0.032$ ) (Fig 2.6 A and B). Nqo1 protein expression increased following PHx in both groups, peaking at 48 hours in untreated and 96 hours in CDDO-Me treated. In addition, mice treated with CDDO-Me had significantly higher Nqo1 protein expression at all time points observed ( $P = 0.016, 0.016, 0.008, 0.008, 0.016$  respectively) (Fig 2.6 A and C).

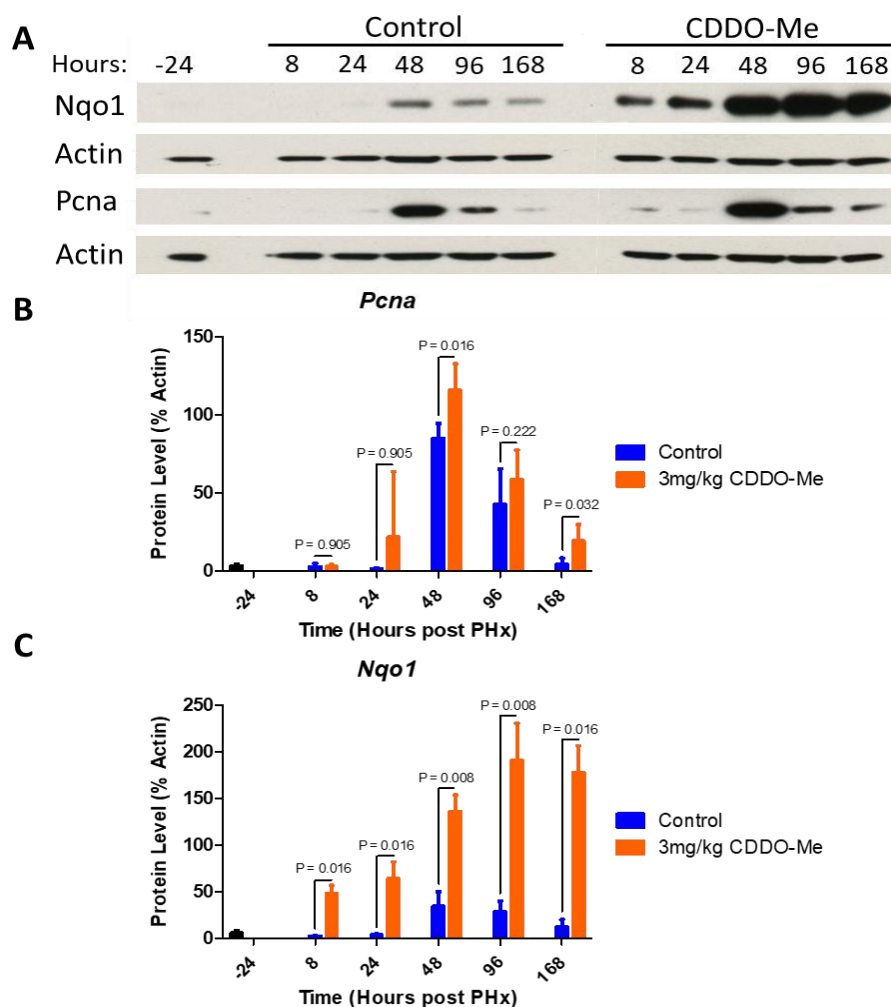


**Figure 2.6** The impact of multiple doses of CDDO-Me on the protein expression levels of *Pcna* and *Nqo1* in mouse livers following two-thirds PHx.

(A) Western blot for *Pcna* and *Nqo1* of representative liver lysates at indicated time points in relation to PHx. (B) Densitometry of *Pcna* immunoblotting from all liver lysates at indicated time points in relation to PHx, normalised to Actin. (C) Densitometry of *Nqo1* immunoblotting from all liver lysates at indicated time points in relation to PHx, normalised to Actin. (B and C) Mann-Whitney U test, control vs CDDO-Me at each time point. Data analysis represents mean  $\pm$  SD of  $n=4-5$  animals per treatment group. Abbreviations: *Pcna*, proliferating cell nuclear antigen; *Nqo1*, NAD(P)H dehydrogenase, quinone 1.

Furthermore, Nqo1 protein expression was quantified in the livers of mice 7 days following a two-thirds PHx, in the presence or absence of a single 3 mg/kg dose of CDDO-Me administered at different time points in relation to surgery being carried out. Mice were treated or not with a single 3 mg/kg CDDO-Me dose on day -1 (denoted as pre-op), day 0, 1 hour prior to surgery commencing (denoted as intra-op) or day 1 (denoted as post-op). PHx was carried out on day 0, and livers were harvested on day 7. A single dose of CDDO-Me caused an increase in the levels of Nqo1 protein, regardless of when the dose was administered. Predictably, as animals treated post-operatively with CDDO-Me were culled closest to the point of drug administration, peak Nqo1 levels were achieved in mice treated with CDDO-Me post-operatively (Fig 2.7 A and B). Significantly enhanced Nqo1 protein expression was observed in mice treated intra-operatively and post-operatively ( $P = 0.015$  and  $< 0.001$  respectively).

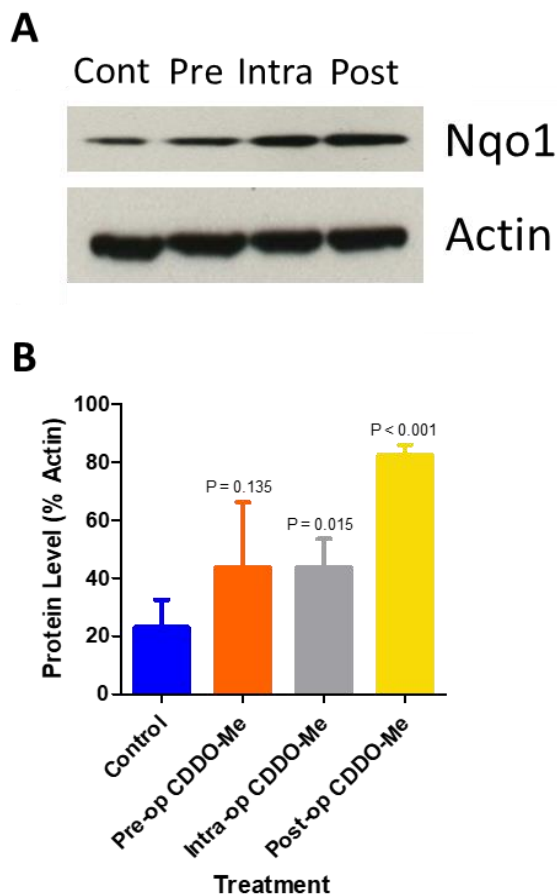


**Figure 2.7** The impact of a single dose of CDDO-Me, administered at different time points in relation to surgery, on the protein expression levels of Nqo1 in mouse livers 7 days following two-thirds PHx.

(A) Western blot for Nqo1 of pooled liver lysates harvested 7 days post PHx.

(B) Nqo1 immunoblotting from all liver lysates harvested 7 days following PHx, normalised to Actin. Mice were treated or not with a single 3 mg/kg CDDO-Me dose on day -1 (denoted as pre-op), day 0, 1 hour prior to surgery commencing (denoted as intra-op) or day 1 (denoted as post-op). PHx was carried out on day 0. (B) Unpaired t-test control vs CDDO-Me. Data analysis represents mean  $\pm$  SD of n=4-5 animals per treatment group.

Abbreviations: Nqo1, NAD(P)H dehydrogenase, quinone 1.

### 2.3.3 Metabolic adaptations underpinning liver regeneration

It is widely reported that the remodelling of key metabolic processes contributes to the initiation and maintenance of liver regeneration (Caldez et al., 2018; Verma et al., 2021), and that Nrf2 functions as a regulator of metabolism (Hayes and Dinkova-Kostova, 2014; He et al., 2020). Therefore, we set out to better understand the metabolic adaptations underpinning the enhanced liver regeneration observed following pharmacological activation of Nrf2. In order to achieve this, hepatic glutathione levels were quantified in mice following two-thirds PHx when treated or not with multiple doses of 3 mg/kg CDDO-Me. Immediately following PHx, glutathione levels decreased in untreated animals before returning to baseline levels at day 7. Interestingly, such decrease in levels was not observed in mice treated with CDDO-Me, with significantly higher levels of glutathione seen at 8 and 48 hours ( $P = 0.013$  and  $0.037$  respectively) (Fig 2.8).

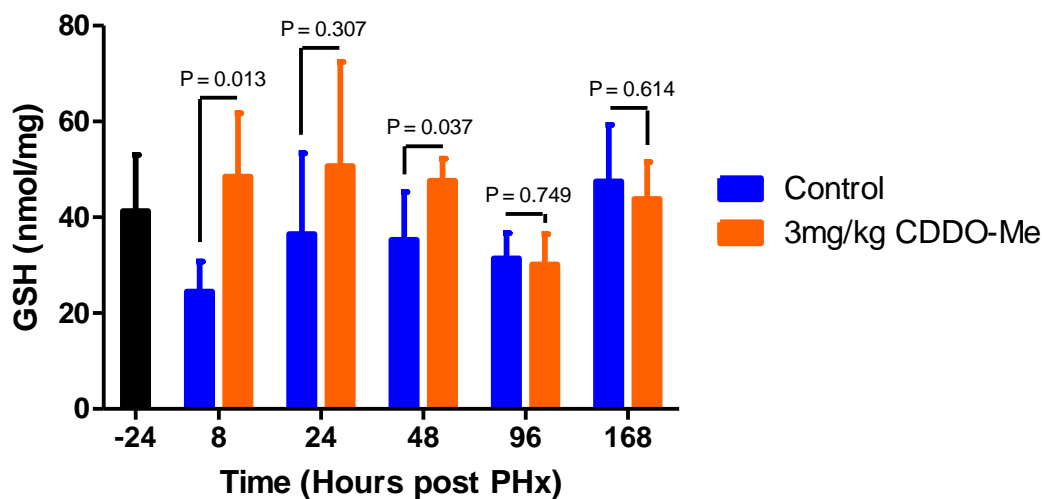


**Figure 2.8 Hepatic glutathione levels in mice following two-thirds PHx.**

Hepatic glutathione levels at indicated time points in mice, treated with or without multiple doses of 3 mg/kg CDDO-Me, following two-thirds PHx. Normalised to total protein content. PHx was carried out on day 0. Unpaired t-test control vs CDDO-Me at each time point. Data represents mean  $\pm$  SD of n=4-5 animals per treatment group.

Abbreviation: GSH, glutathione.



We also investigated the effect of PHx, in the presence of Nrf2 activation, on two enzymes, crucial to cellular metabolism and the maintenance of homeostasis, which have also been previously shown to be regulated by Nrf2 (Huang et al., 2010; Hayes and Ashford, 2012). Therefore, the gene expression levels of stearoyl-CoA desaturase 1 (*Scd1*), involved in lipogenesis, and phosphogluconate dehydrogenase (*Pgd*), involved in amino acid biosynthesis via the pentose phosphate pathway, were measured in the livers of mice following two-thirds PHx, when treated or not with CDDO-Me, using quantitative (real-time) polymerase chain reaction (qPCR) (Fig 2.9). The expression levels of *Scd1* decreased immediately following PHx in untreated animals before peaking at 96 hours post-surgery. These levels were then further, and significantly, reduced in mice treated with CDDO-Me at 8, 24, 48 and 96 hours ( $P = 0.008, 0.008, 0.003$  and  $0.007$  respectively), before returning to the level observed in untreated mice at 168 hours post PHx (Fig 2.9 A).

On the other hand, *Pgd* levels were seen to increase in a time dependent manner following PHx in untreated mice, before dropping at 168 hours post-surgery. CDDO-Me further enhanced this time dependent increase, with significantly greater expression levels measured at 8, 24, 48 and 96 hours ( $P = 0.001, 0.001, < 0.001$  and  $0.032$  respectively). Similarly to untreated mice, *Pgd* expression levels in CDDO-Me treated mice then dropped at 168 hours post-surgery, resulting in significantly lower expression levels compared to control animals ( $P = 0.014$ ) (Fig 2.9 B).

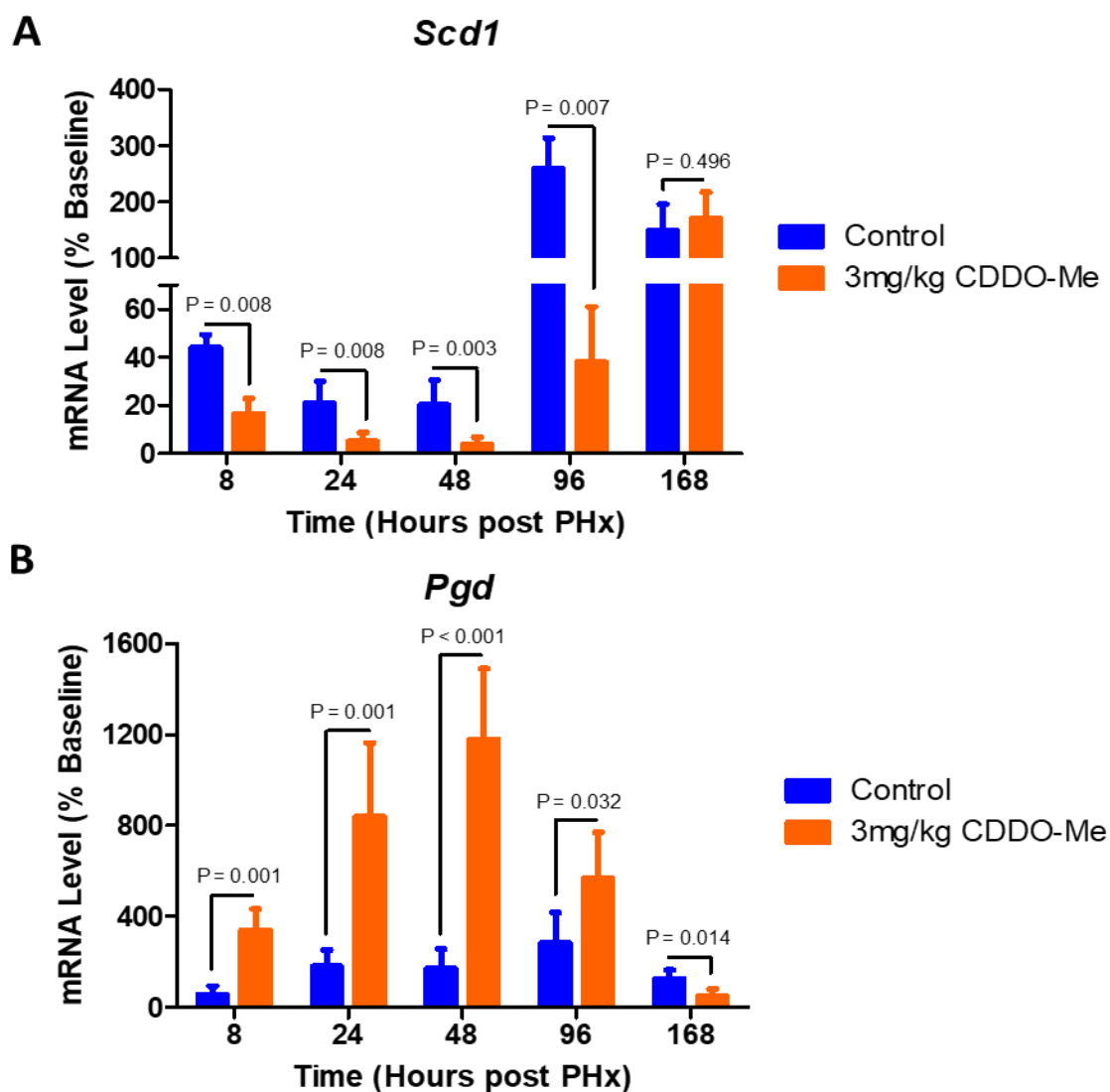


**Figure 2.9** Gene expression levels of (A) *Scd1* and (B) *Pgd* in mice following two-thirds PHx when treated or not with CDDO-Me.

Gene expression levels of (A) *Scd1* and (B) *Pgd* were normalised to *Gapdh* and presented as a % of the average day -1, untreated, mRNA level. Unpaired t-test, control vs CDDO-Me at each time point.

Data analysis represents mean  $\pm$  SD of n=4-5 animals per treatment group. Abbreviations: *Gapdh*, glyceraldehyde-3-phosphate dehydrogenase; *Scd1*, stearyl-CoA desaturase 1; *Pgd*, phosphogluconate dehydrogenase.

Considering the importance of co-enzymes in metabolic processes, and the adaptations in co-enzyme expression that occurs following liver regeneration, and as a result of crosstalk with Nrf2 (Dinkova-Kostova and Abramov, 2015), it was pertinent to quantify the levels of Nicotinamide adenine dinucleotide (NAD<sup>+</sup>) and Nicotinamide adenine dinucleotide phosphate (NADP<sup>+</sup>), as well as the reduced forms, NADH and NADPH. In untreated mice, NAD<sup>+</sup> levels peaked at 8 hours post PHx before gradually dropping back to baseline levels. In CDDO-Me treated mice however, NAD<sup>+</sup> levels peaked at 24 hours post PHx and remained higher than those in untreated animals for all other time points with significantly higher levels observed at 48 hours ( $P = 0.016$ ) (Fig 2.10 A). Understandably, NADH levels followed a very similar pattern, with levels peaking at 8 hours in untreated mice and 24 hours in CDDO-Me treated. CDDO-Me prevented the loss of NADH and treated mice possessed higher NADH levels at all other time points, though no significant differences were seen (Fig 2.10 B).

PHx alone caused an increase in the levels of NADP<sup>+</sup>, peaking at 8 hours post-surgery in untreated animals. CDDO-Me further enhanced this increase in NADP<sup>+</sup> levels, peaking at 96 hours post-surgery, with significantly higher levels at 48 hours when compared to control ( $P = 0.018$ ) (Fig 2.10 C).

Similarly, NADPH levels increased immediately following PHx, peaking at 8 hours in both control and treated animals. CDDO-Me then further enhanced NADPH content, with higher levels measured at all time points and significantly higher levels at 48 hours post-surgery ( $P = 0.032$ ) (Fig 2.10 D).

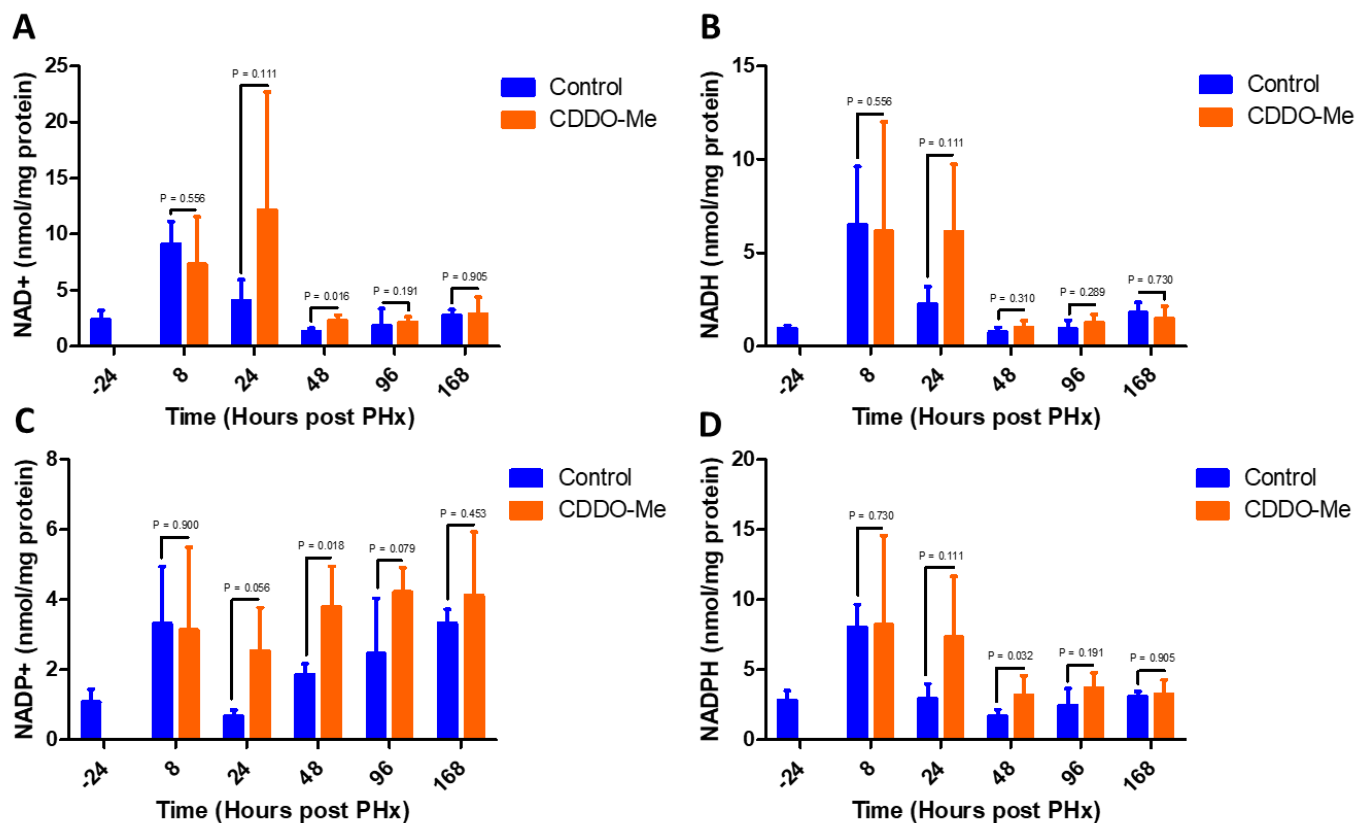


**Figure 2.10 Levels of metabolic co-enzymes (A) NAD<sup>+</sup> (B) NADH (C) NADP<sup>+</sup> and (D) NADPH.**

Hepatic levels of the metabolic co-enzymes (A) NAD<sup>+</sup> (B) NADH (C) NADP<sup>+</sup> and (D) NADPH at indicated time points in mice, treated with or without multiple doses of 3 mg/kg CDDO-Me, following two-thirds PHx. Normalised to total protein content. PHx was carried out on day 0. Mann-Whitney U test (A, B and D) or unpaired t-test (C) control vs CDDO-Me at each time point. Data represents mean  $\pm$  SD of n=4-5 animals per treatment group.

### 2.3.4 Transcriptomic analysis of primary human hepatocytes

To assess the translatability of our findings in mice, we carried out transcriptomics analysis on primary human hepatocytes (PHH) from 3 donors, treated or not with CDDO-Me in vitro. GO terms were considered significant with an unadjusted P value  $< 0.05$  and absolute Normalised Enrichment Score (NES)  $> 1.5$ . Treatment with CDDO-Me produced a negative NES score, and downregulation of genes associated with NAD metabolic process (GO:0019674). Predictably, treatment with CDDO-Me caused upregulation of genes associated with adaptation to oxidative stress as seen by positive NES scores in oxidation-reduction process, cellular response to oxidative stress and cell redox homeostasis (GO:0055114, GO:0034599 and GO:0045454 respectively). An increase in NADPH regeneration was also observed, as well as processes associated with pentose metabolism (Fig 2.11). However, CDDO-Me didn't alter the expression of level of genes associated with cell proliferation.

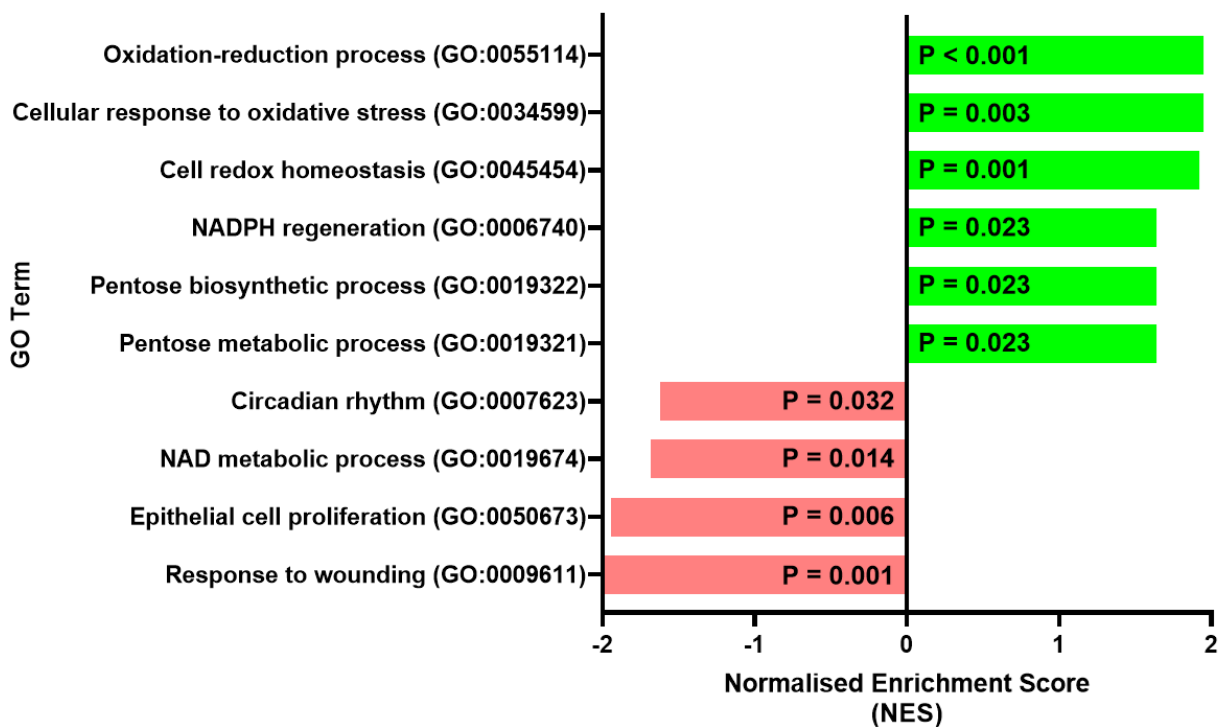


**Figure 2.11** Transcriptomic analysis of primary human hepatocytes treated or not with CDDO-Me.

Normalised Enrichment Scores (NES) of selected GO terms found to be significantly enriched following transcriptomic analysis of primary human hepatocytes from 3 donors that were treated or not with 100 nM CDDO-Me for 24 hours. P values, indicating significance of enrichment, are included within the figure.

## 2.4 Discussion

As post-hepatectomy liver failure (PHLF) remains a substantial clinical problem (Ocak et al., 2020), and there is an ever-increasing burden of liver disease (Asrani et al., 2019), there remains an unmet need for novel therapeutic strategies to promote post-hepatectomy liver regeneration, and adequate hepatic function. In recent years, Nrf2 has become an encouraging strategy in therapeutic areas encompassing oxidative stress and metabolic disorder (Cuadrado et al., 2019; Yagishita et al., 2020), with several clinical trials ongoing in numerous disease areas (Robledinos-Antón et al., 2019). Coupled to a continued interest in the clinical use of small molecule therapies, there is the potential for pharmacological Nrf2 activators to resolve this unmet need. The role of Nrf2 in liver regeneration is widely disputed and often contradicting (Beyer et al., 2008; Wakabayashi et al., 2010; Hu et al., 2014; Köhler et al., 2014), however these previous studies all utilise transgenic models, in which mice possess constitutively altered Nrf2 activity, a phenotype that would not be presented in a clinical setting. Therefore, this chapter, supported by the findings communicated by our group (Chan et al., 2021), outlines a more clinically relevant approach to understanding the role of Nrf2 in liver regeneration, whilst presenting a promising therapeutic approach.

The findings of this chapter show that CDDO-Me, and subsequent activation of the Nrf2 pathway, enhances liver regeneration following two-thirds PHx in wild-type mice. In addition, the observed plateau in liver volume indicates that, despite significantly faster rates of regeneration, successful and routine termination of liver regeneration, a crucial stage in the process (Michalopoulos, 2007; Miyaoka and Miyajima, 2013), is achieved following treatment with CDDO-Me. Interestingly however, despite a limited significant increase in liver regeneration following a single, intra-operative injection, this enhanced, CDDO-Me driven, restoration of liver volume was only achievable following multiple doses. It is therefore evident that enhanced liver regeneration can only occur with maximal Nrf2 activation which is achieved following prolonged exposure to CDDO-Me treatment. The exact

number of doses at which this prolonged exposure is achieved requires further delineation. We have demonstrated that four doses can provide sufficient exposure, but it would be of clinical interest to reduce the number of doses, potentially reducing the number of invasive injections and in turn improving a patient's overall treatment. Therefore, it would be pertinent to optimise the dosing schedule in future studies.

It is widely accepted that hepatocyte proliferation is one of the driving mechanisms of liver regeneration (Michalopoulos, 2007; Fujiiyoshi and Ozaki, 2011), with *Pcna* commonly reported as a robust marker (Kelman, 1997) due to its conservation and translatability across human (Hoffmann et al., 2020), rat (Assy et al., 1998) and mouse (Zhao et al., 2021). *Pcna* stimulates the remnant liver parenchyma to synthesise DNA and enter the cell cycle, thus promoting hepatocyte proliferation and driving liver regeneration to restore normal, pre-operative, liver volume. It was shown that PHx alone resulted in upregulation of *Pcna*, and that Nrf2 activation further enhanced expression, both at the gene and protein level. Consequently, the findings of this chapter confirm the importance of hepatic cell proliferation in liver regeneration, and that proliferation is enhanced following pharmacological activation of Nrf2.

In addition, the biochemical analyses conducted in this chapter provide evidence for metabolic remodelling in the livers of mice treated with CDDO-Me. Activation of Nrf2 prevented the loss of glutathione, a crucial redox factor, that was observed in control mice, and the trend seen in hepatic GSH levels matched that of Nqo1 protein expression following PHx in mice that had been treated with CDDO-Me. Gene expression analysis showed an immediate decrease in the levels of *Scd1*, but an increase in *Pgd*, which was later reversed, indicating a short-term shift towards pentose phosphate driven metabolism. The observed changes in the levels of both co-enzymes, NAD/H and NADP/H further confirms this due to the involvement of NADP/H in the pentose phosphate pathway



(Xiao et al., 2018), and again the trend observed in the levels of both co-enzymes matched that of Nqo1 protein expression following PHx in mice that had been treated with CDDO-Me. It has been previously demonstrated that Nrf2 regulates genes within numerous redox and metabolic pathways essential for the maintenance of homeostasis in the liver (Kitteringham et al., 2010; Hayes and Dinkova-Kostova, 2014) and that such pathways are essential for efficient liver regeneration immediately following PHx (Huang and Rudnick, 2014; Caldez et al., 2018). Others have also demonstrated a crosstalk between Nrf2 and NADP/H (Wu et al., 2011; Dinkova-Kostova and Abramov, 2015), allowing for a direct interaction between antioxidant response and metabolic activity (Heiss et al., 2013). Taken together, it is apparent that the mouse liver undergoes significant metabolic adaptations to provide the essential cellular building blocks, and energy, required to support hepatic function during restoration of liver mass, and that such metabolic remodelling is enhanced by pharmacological activation of Nrf2 and its ability to regulate, or interact with, numerous redox and metabolic signalling pathways.

This chapter has also highlighted the potential translatability of such a model testing the effect of pharmacological Nrf2 activation on liver regeneration. Through the exposure of primary human hepatocytes to CDDO-Me, we have shown that pharmacological activation of Nrf2 modulates many of the biochemical and transcriptional processes associated with enhanced regeneration in the livers of mice treated with CDDO-Me. Understandably, redox processes remain significantly enriched following exposure to CDDO-Me, confirming the ability of Nrf2 to maintain an antioxidant response. In addition, the observed upregulation of NADPH regeneration and downregulation of NAD metabolic processes, suggests a similar shift, or adaptation, in metabolism that was seen in mice, further emphasising the promising nature of this therapy. It was seen that CDDO-Me did not alter the expression of level of genes associated with cell proliferation. However, this is not surprising, or of

concern, due to the inherent and well documented proliferative resistance of primary hepatocytes *in vitro* (Guguen-Guillouzo and Guillouzo, 2010; Garnier et al., 2018).

To summarise, the findings of this chapter, coupled to the increasing interest of small molecules targeting Nrf2 (Cuadrado et al., 2019), demonstrate the therapeutic potential of pharmacological Nrf2 activation to improve post-operative liver regeneration. Such a therapeutic approach could significantly alleviate the current clinical burden seen with PHLF, and associated liver disease, whilst potentially expanding treatment options to allow for curative resection in liver cancer patients that would normally be deemed inoperable. There is further potential to expand this model by inducing liver damage, either by fibrosis or cirrhosis, prior to a two-thirds PHx being carried out in the presence of CDDO-Me. This would help better mimic the typical liver parenchyma health seen in patients undergoing tumour resection and thus provide further insight into the capability of pharmacological Nrf2 activation to aid regeneration in a true clinical setting. As pharmacological Nrf2 activators can be administered close to surgery without the need to constitutively activate the pathway, the risk of enhancing tumorigenicity seen with hyperactivation of Nrf2 (Raghunath et al., 2018), is theoretically reduced. Nevertheless, in order to progress pharmacological Nrf2 activation as a therapeutic approach in the context of liver tumour surgery, it is essential to ensure the safety of this therapy in an oncology setting, both in primary hepatocellular carcinoma (HCC) and secondary metastasis arising from colorectal cancer.

## Chapter 3

**Pharmacological activation of Nrf2 does not promote *in vitro* proliferation of liver cancer cell lines**

## Contents

<b>3.1 Introduction</b> .....	100
<b>3.2 Methods</b> .....	102
3.2.1 Cell culture.....	102
3.2.1.1 Drug treatments.....	103
3.2.2 ATP proliferation assay.....	103
3.2.3 Western blotting.....	104
3.2.4 Statistical analysis.....	107
<b>3.3 Results</b> .....	108
3.3.1 Justification of cell lines.....	108
3.3.2 Effect of CDDO-Me on <i>in vitro</i> ATP content of human HCC and CRC cell lines.....	113
3.3.3 CDDO-Me upregulates Nrf2 <i>in vitro</i> following serum starving of human HCC and CRC cell lines.....	121
<b>3.4 Discussion</b> .....	125

### 3.1 Introduction

Cancer research has utilised *in vitro* models as a primary investigative tool for many years, with 2D monolayer based approaches playing a significant role. Although these models possess disadvantages when compared to *in vivo* models, such as the inability to fully recapitulate cancer heterogeneity and the true physiological conditions, they are frequently utilised due to the wide availability of cell lines, the relative ease of use and the ability to perform high-throughput analysis (Katt et al., 2016). Liver cancer is no outlier to this with routine use, and continued development, of cell line-based approaches (Chang and Hughes-Fulford, 2009). In recent years, such models have evolved significantly from 2D, monolayer, cell cultures, to co-cultures, 3D cultures, including spheroids and organoids, and even precision-cut liver slices (Ijssennagger et al., 2016). Despite this, 2D cell culture remains the most used type of *in vitro* cancer model (Yip and Cho, 2013), providing crucial insight into the development of cancer and targeted therapies against such malignancies.

As liver cancer encompasses both primary hepatocellular carcinoma (HCC) and secondary colorectal metastasis, it is essential that any *in vitro* approach utilises numerous different cell lines derived from both hepatocellular carcinoma (HCC) and colorectal cancer (CRC). This subsequently allows multiple genotypes to be investigated simultaneously, whilst better mimicking the current clinical setting, and facilitating the transition towards the further development of personalised medicine.

The role of Nrf2 in the proliferation of liver cancer cell lines *in vitro* is currently unclear and is commonly referred to as a double-edged sword (Wu et al., 2019), due mainly to the context dependant nature in which data is reported. It has been reported that Nrf2 promotes proliferation and invasion in HCC cell lines, using Nrf2 expression plasmids (Zhang et al., 2015), and constitutive pathway activation (Haque et al., 2020). Furthermore, similar processes have been reported in colorectal cancer cell lines. Zhao et al. highlighted that Nrf2 promotes resistance to chemotherapy

and subsequently enhances proliferation in colorectal cell lines following epigenetic modification in the promoter DNA of Nrf2 (Zhao et al., 2015). However, the overriding majority of studies reporting enhanced proliferation utilise genetically modified cells, in which Nrf2 is being constitutively activated through mutations in the cell's genetic material, as opposed to acute and pulsatile pharmacological activation of Nrf2 through therapeutic intervention in wild-type cell lines.

Interestingly the use of CDDO-Me, a pharmacological Nrf2 activator, has been shown to elicit an anti-tumour effect in numerous wild-type HCC cell lines (Gee et al., 2018; Baer-Dubowska et al., 2021). It is therefore crucial to further investigate the role of pharmacological Nrf2 activation on the proliferation of cells *in vitro*.

I hypothesised that pharmacological Nrf2 activation would not promote *in vitro* proliferation in liver cancer and colorectal cancer cell lines. In order to test this hypothesis, the proliferative ability of the HCC cell lines, HepG2 and Huh7, as well as the CRC cell lines, HCT116 and SW480, were investigated when treated or not with CDDO-Me.

## 3.2 Methods

All reagents were purchased from Sigma Aldrich unless otherwise stated.

### 3.2.1 Cell culture

All cell lines were maintained in an incubator set at 37 °C and 5 % CO<sub>2</sub>. HepG2, SW480 and HCT116 cells were cultured in Dulbecco's Modified Eagle's medium (DMEM), supplemented with 10 % (v/v) Fetal Bovine Serum (FBS) and 1 % (v/v) Penicillin-Streptomycin. Huh7 cells were cultured in Roswell Park Memorial Institute (RPMI) medium, supplemented with 10 % (v/v) FBS and 1 % (v/v) Penicillin-Streptomycin.

Once confluency had been reached, cells were dissociated from the surface of culture flasks using trypsin. The monolayer culture was briefly, and gently, washed with PBS before 2 mL 0.25 % Trypsin-EDTA was added to each flask. Flasks were then incubated at 37 °C for 5-8 min before 8 mL of appropriate culture media was added to inactivate trypsin, preventing cell damage. Cells were aspirated and transferred to a labelled 15 mL Falcon, and then centrifuged at 300 g for 5 min. Media was then aspirated and replaced with 10 mL fresh, appropriate culture media, before cells were resuspended and dissociated to a single cell solution using a 21G needle. Cells were then counted by the trypan blue exclusion method, which utilises dye to determine the number of viable cells in a suspension (Strober, 2015). 50 µL resuspended cells were added to a tube containing 450 µL 0.4 % Trypan blue, diluting cells 1 in 10. 10 µL was then loaded onto a haemocytometer before being counted. Cells were passaged twice weekly up to 20 passages before being discarded. All cell lines were routinely tested for mycoplasma using a qPCR-based mycoplasma kit, as outlined by Corral-Vázquez et al. (Corral-Vázquez et al., 2017).

### 3.2.1.1 Drug treatments

Cells were seeded at least 24 hours prior to any treatment, to allow complete adherence. CDDO-Me was prepared in 100 % DMSO at a concentration 300x higher than the desired final working concentration. All drug stocks were then diluted 1 in 300 in appropriate culture media, and drug-treated media used to replace existing media. The final DMSO concentration was 0.33 %.

### 3.2.2 ATP proliferation assay

*In vitro* proliferation was measured by quantifying the ATP content of cells using the CellTiter-Glo<sup>®</sup> Luminescent Cell Viability Assay kit (Promega). This kit utilises luminescence signal to detect cellular ATP. The luminescence produced is proportional to the ATP present, which in turn is directly proportional to the number of cells present.

Cells were seeded in a 96 well plate at 5,000 cells per well in 100  $\mu$ L of culture media and left for 24 hours to allow complete adherence. Culture media containing differing low concentrations of FBS, these being 0, 0.1, 0.25, 0.5, 0.75, 1 and 5 % FBS, were produced. Cells then underwent a serum starve. To achieve this, full growth media containing 10 % FBS was aspirated off, cells briefly washed with PBS, and low FBS containing media, 0-5 % as outlined previously, was added. The process of serum starving induces synchronisation of the cell cycle (Pirkmajer & Chibalin, 2011), thus allowing the proliferative effect of drugs to be monitored without the interference of high FBS on growth. Cells were then returned to the incubator for a further 24 hours. Following this, the low FBS containing media was aspirated off and cells briefly washed with PBS. Cells were then exposed for 72 hours to either fresh low FBS containing media, low FBS containing media supplemented with DMSO, or low FBS containing media supplemented with CDDO-Me at a final concentration of 10, 30 or 100 nM. DMSO and CDDO-Me supplemented media were produced as described in section 3.2.1.1. Cells



that were kept in full growth media containing 10 % FBS throughout the entire assay were used as a control for normal proliferation and all results are normalised to this condition.

Cells were then subject to quantification of ATP content. CellTiter-Glo<sup>®</sup> reagent was produced by adding 10 mL CellTiter-Glo<sup>®</sup> Buffer to 10 g CellTiter-Glo<sup>®</sup> Substrate and thoroughly vortexed to allow complete solubilisation. As CellTiter-Glo<sup>®</sup> reagent is light sensitive, vials containing solubilised reagent were kept in the dark until ready to use to avoid exposure to light. 96 well plates were removed from the incubator and incubated at room temperature for 10 min. 25  $\mu$ L of CellTiter-Glo<sup>®</sup> reagent was added to each well, before shaking at 500 rpm for 5 min, to allow complete lysis of cells. 75  $\mu$ L of resulting lysate / CellTiter-Glo<sup>®</sup> reagent mixture was transferred to a white 96 well plate before wrapping in aluminium foil to prevent exposure to light. Luminescence was then measured using a Varioskanner Flash 3001 (ThermoScientific). To provide a standard curve of ATP content against cell number, cells were plated in a separate 96 well plate at known seeding densities ranging from 500-100,000 cells per well in 100  $\mu$ L of media containing 10 % FBS, 8 hours prior to luminescence quantification, determined as outlined previously.

### **3.2.3 Western blotting**

Western blotting was conducted using cell lysates. Cells cultured and treated in 6 well plates were removed from the incubator and left at room temperature for 10 min. Media was aspirated and cells briefly, and gently, washed with PBS. 300  $\mu$ L Ice cold radioimmunoprecipitation assay (RIPA) buffer was added to each well and the plate incubated on ice for 5 min. Using a plastic cell scraper, each well was thoroughly scraped, the cells collected, and transferred to labelled 0.5 mL tubes before being centrifuged at 16,000 g for 20 min at 4 °C. The resulting supernatant was transferred to a new, labelled 0.5 mL tube and cell pellet discarded.

Total protein content was determined as previously described in section 2.2.2 and cell lysates were prepared to a final concentration of 1  $\mu\text{g}/\mu\text{L}$ . Western blotting was then performed, up to the point of development, as previously described in section 2.2.3 using the antibodies listed in Table 3.1 and Table 3.2.

For development, chemiluminescence was quantified using the ChemiDoc system (BioRad). Western Lightning<sup>®</sup> Plus-ECL reagent (PerkinElmer) was prepared and added to nitrocellulose membranes before being placed onto a Blot/UV/Stain-Free sample tray (BioRad) inside the ChemiDoc instrument. The chemiluminescence protocol was selected and auto-optimal exposure time used for all blots. Images were exported as JPEG files and densitometry performed using ImageJ (Schneider et al., 2012). Density of bands were normalised to the intensity of  $\beta$  actin, used as a loading control.

**Table 3.1 Primary antibodies for Western blot**

<b>Primary Antibody</b>	<b>Dilution Factor (in 10 % Blotting Grade Blocker in 1x TBS-T)</b>	<b>Incubation Time</b>	<b>Washes (using 1x TBS-T)</b>
Nqo1 (ab2346, Abcam / Goat / Polyclonal)	1:2,500	Overnight at 4 °C	4x 5 min
$\beta$ Actin (ab6276, Abcam / Mouse / Monoclonal)	1:10,000	1 hour at room temp	4x 5 min

**Table 3.2 Secondary antibodies for Western blot**

<b>Secondary Antibody</b>	<b>Dilution Factor (in 10 % Blotting Grade Blocker in 1x TBS-T)</b>	<b>Incubation Time</b>	<b>Washes (using 1x TBS-T)</b>
Anti-Goat HRP (P044901-2, Agilent / Rabbit / Polyclonal)	1:5,000	1 hour at room temp	4x 5 min
Anti-Mouse HRP (A9044, Sigma / Rabbit / Polyclonal)	1:5,000	1 hour at room temp	4x 5 min

### 3.2.4 Statistical analysis

As indicated in each figure legend, statistical analysis was carried out using Stats Direct 3 software. P values are reported to three decimal places. For Student t tests and Mann-Whitney U tests, two-tailed P values are reported. For analysis of variance, Kruskal-Wallis tests were used with a Conover-Iman post-hoc test and two-tailed P values are reported. Differences were considered significant at  $P \leq 0.05$ .

### 3.3 Results

#### 3.3.1 Justification of cell lines

There are numerous different HCC and CRC cell lines, each with their own phenotypic characteristics. It is therefore essential that when selecting a model cell line, these characteristics are considered, and potential mutation profiles ideally matched to those observed in a clinical setting. It is also of key importance to consider how commonly used each model is within the literature, as well as the availability of cell lines and the ease at which these cells can be routinely cultured, without the need of specialist equipment or containment.

The most frequent mutations observed in clinical HCC tumours include telomere maintenance (TERT) at 47.1 %, tumour protein 53 (TP53) at 28-36 % and AT-rich interaction domain-containing protein 1A (ARID1A) at 16.8 % (Ding et al., 2017). Additionally, mutations in NFE2L2, specifically inhibiting the binding of Keap1 to the DLG and ETGE motifs (Guichard et al., 2012), and mutations in Keap1 itself, decreasing expression of the repressor protein (Cleary et al., 2013), have been reported in clinical HCC tumours with frequencies of 6.4 % and 8 % respectively. As both HepG2 and Huh7 cell lines originate from differentiated HCC and correlate closely to the mutation profiles observed in clinical tumours, with Huh7 possessing mutations in TP53 and ARID1A (Harmonizome, 2021), and HepG2 being reported as the most highly correlated by Chen et al. (Chen et al., 2015), these cell lines were selected. Whilst HepG2 also possess mutations in several oncogenes including KRAS and NRAS, and Huh7 possess mutations in FLI1 and ROS1 (Table 3.3), neither cell line possesses mutations in either Nrf2 or Keap1. Furthermore, both cell lines were readily available, easy to culture and commonly used as *in vitro* models of HCC initiation and proliferation (Bagi and Andresen, 2010; Krelle et al., 2013; Harjumäki et al., 2019).

The most frequent mutations observed in clinical CRC tumours include TP53 at 44 %, (Ki-ras2 Kirsten rat sarcoma viral oncogene homolog (KRAS) at 32 % and v-raf murine sarcoma viral oncogene homolog B1 (BRAF) at 12 %. The frequency of NFE2L2 and Keap1 mutations in CRC tumours is far less than HCC, at 1.6 % and 1.7 % respectively (Cosmic, 2021). With regards to CRC cell lines, and their use as a model for secondary colorectal metastasis within the liver, HCT116 and SW480 were selected. Both cell lines are highly correlated to mutations seen in clinical tumours, with mutations in KRAS present in both as well as PTEN and APC tumour suppressors in HCT116 and SW480 respectively (Harmonizome, 2021) (Table 3.3). Similarly, neither cell line possesses mutations in either Nrf2 or Keap1. Again, both cell lines were readily available and easy to culture, with HCT116 being well established in many oncology models (Rajput et al., 2008; Wahab et al., 2017).

Table 3.3 Characteristics of selected cell lines

Cell Line	Disease	Origin	Correlated Clinical Mutations	Justification
HepG2	Highly differentiated hepatocellular carcinoma.	15-year-old Caucasian male.	Oncogenes/proto-oncogenes: <ul style="list-style-type: none"> <li>• ABL2</li> <li>• FGFR1OP</li> <li>• FLI1</li> <li>• MAF</li> <li>• KRAS</li> <li>• NRAS</li> <li>• RET</li> </ul> Tumour suppressors: <ul style="list-style-type: none"> <li>• LATS2</li> </ul>	<ul style="list-style-type: none"> <li>• Readily available and simple to culture.</li> <li>• Highly correlated to mutations present in clinical hepatocellular carcinoma.</li> <li>• Identified as the best cell line for a hepatocellular carcinoma model due to high correlation (Chen et al., 2015).</li> </ul>
Huh7	Differentiated hepatocellular carcinoma.	57-year-old Asian male.	Oncogenes/proto-oncogenes: <ul style="list-style-type: none"> <li>• FLI1</li> <li>• ROS1</li> </ul>	<ul style="list-style-type: none"> <li>• Simple to culture.</li> <li>• Correlated to mutations present in clinical hepatocellular carcinoma.</li> </ul>
HCT116	Dukes' grade A/D colorectal carcinoma.	Male of unknown age and race.	Oncogenes/proto-oncogenes: <ul style="list-style-type: none"> <li>• FOS</li> <li>• KRAS</li> <li>• LCK</li> <li>• MET</li> <li>• REL</li> </ul> Tumour suppressors: <ul style="list-style-type: none"> <li>• PTEN</li> <li>• LRP1B</li> </ul>	<ul style="list-style-type: none"> <li>• Readily available and simple to culture.</li> <li>• Highly correlated to mutations present in clinical colorectal cancer.</li> <li>• Well established cell line in oncology models.</li> </ul>
SW480	Dukes' grade B colorectal adenocarcinoma.	50-year-old Caucasian male.	Oncogenes/proto-oncogenes: <ul style="list-style-type: none"> <li>• KRAS</li> <li>• FLI1</li> <li>• MYB</li> <li>• ROS1</li> </ul> Tumour suppressors: <ul style="list-style-type: none"> <li>• APC</li> </ul>	<ul style="list-style-type: none"> <li>• Readily available and simple to culture.</li> <li>• Correlated to mutations present in clinical colorectal adenocarcinoma.</li> </ul>

Other cell lines were considered for both HCC and CRC, including Hep3B, PLC/PRF/5, Gp2D and HCT15. However, these cell lines commonly require specialist containment facilities and culture techniques due to the integration of the hepatitis B virus in the genome. It is also increasingly difficult to obtain such cell lines and the lack of reported use in proliferative HCC and CRC models further supports excluding their use (Table 3.4).



Table 3.4 Characteristics of excluded cell lines

Cell Line	Disease	Origin	Justification
Hep3B	Hepatocellular carcinoma with epithelial morphology.	8-year-old black male.	<ul style="list-style-type: none"> <li>• Difficult to purchase.</li> <li>• Cells contain an integrated hepatitis B virus genome.</li> <li>• Specialist BSL 2 required for culture.</li> <li>• Hepatitis B vaccination recommended.</li> </ul>
PLC/PRF/5	Liver hepatoma, Alexander cell.	Unknown.	<ul style="list-style-type: none"> <li>• Not commonly cited in HCC implant models.</li> <li>• Can be difficult to culture.</li> <li>• Cells produce hepatitis B antigen.</li> <li>• Specialist BSL 2 required for culture.</li> <li>• Hepatitis B vaccination recommended.</li> </ul>
Gp2D	Dukes' grade B colon carcinoma, diploid.	71-year-old Caucasian female.	<ul style="list-style-type: none"> <li>• Difficult to culture.</li> <li>• Rarely cited in literature for implant models.</li> </ul>
SKCO-1	Colorectal adenocarcinoma, derived from metastatic site.	65-year-old Caucasian male.	<ul style="list-style-type: none"> <li>• Not commonly cited in implant models.</li> <li>• Can be difficult to culture.</li> </ul>
HCT15	Dukes' grade C colorectal adenocarcinoma.	Male of unknown age and race.	<ul style="list-style-type: none"> <li>• Not commonly cited in implant models.</li> </ul>

### 3.3.2 Effect of CDDO-Me on *in vitro* ATP content of human HCC and CRC cell lines

*In vitro* proliferation was measured by quantifying the ATP content of cells. Prior to treatment with CDDO-Me, cells underwent a serum starve process to induce synchronisation of the cell cycle and thus allow any proliferative effect of CDDO-Me to be monitored without the interference of high FBS on growth. In HepG2 cells, the ATP content increased in a FBS concentration dependent manner as the concentration of FBS within media increased from 0 to 10 %. Treatment with 100 nM CDDO-Me produced significantly higher ATP content when compared to DMSO control following serum starving with 0 % and 0.5 % FBS containing media ( $P = 0.013$  and  $0.004$  respectively). However, despite significantly enhanced proliferation with 100 nM CDDO-Me in these cells, the ATP content did not reach that of cells maintained in full, 10 % FBS, growth media throughout. HepG2 cells treated with 10 nM and 30 nM CDDO-Me, that were maintained in 10 % FBS containing media, had significantly higher ATP content when compared to DMSO ( $P = 0.024$  and  $0.001$  respectively). However, again, the ATP content did not reach the levels observed in cells maintained in normal full growth media conditions. This indicates that CDDO-Me did not enhance proliferation beyond normal cell culture growth.

Interestingly, HepG2 cells treated with CDDO-Me following serum starving at 0.1 % and 1 % FBS, had significantly lower ATP levels when compared with cells treated with DMSO ( $P = 0.001$  at 30 nM CDDO-Me and  $P = 0.040$  at 100 nM CDDO-Me in 0.1 % FBS, and  $P < 0.001$  at 100 nM CDDO-Me in 1 % FBS). This indicates that these cells underwent inhibition of proliferation. No significant differences were observed in HepG2 cells serum starved at 0.25 % FBS (Fig 3.1).

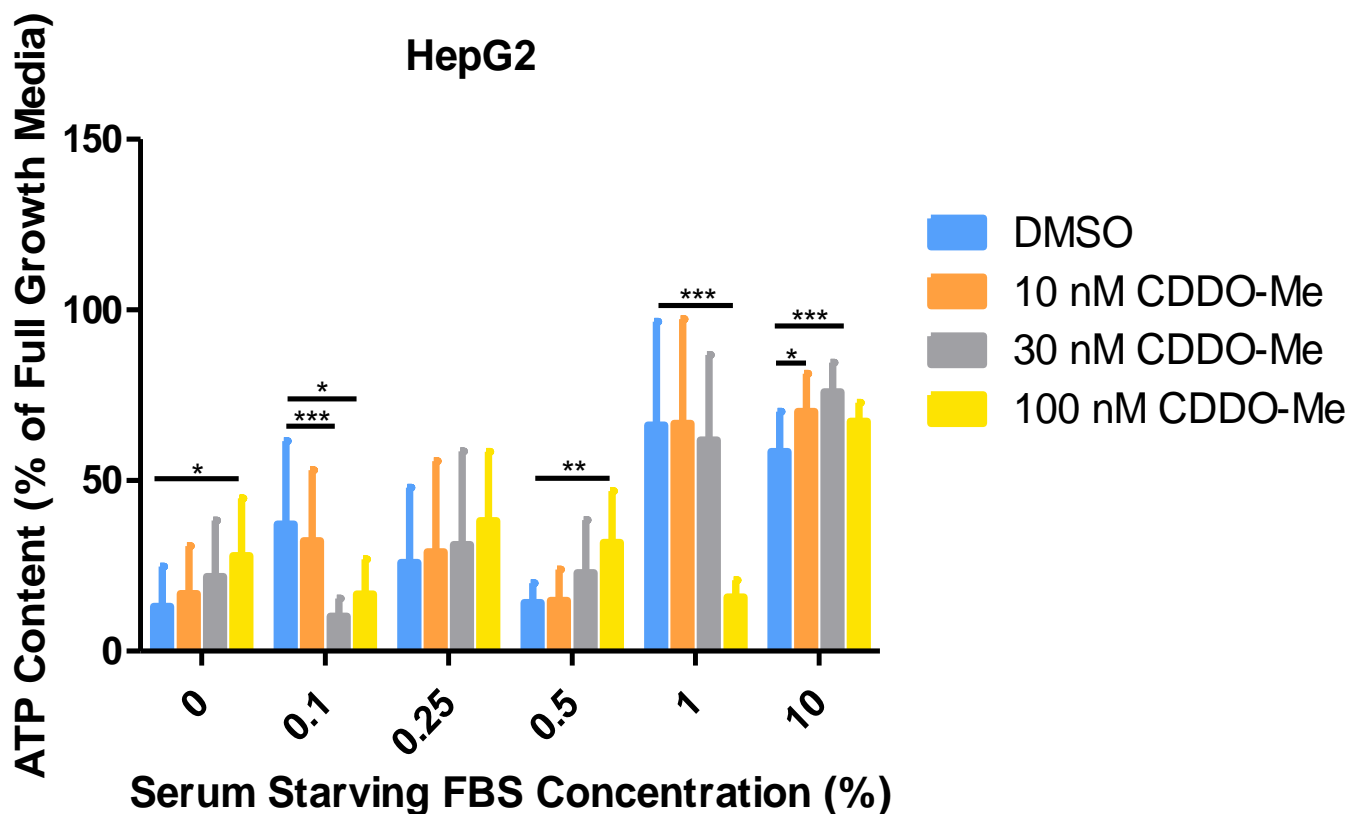


**Figure 3.1** Effect of CDDO-Me on *in vitro* ATP content in HepG2 cells

HepG2 cells were serum starved in the indicated concentrations of FBS containing media prior to being exposed to DMSO or CDDO-Me. ATP content was quantified and is directly proportional to the number of cells present, therefore allowing proliferation to be assessed. ATP content is normalised to control cells that were maintained in full, 10 % FBS, growth media throughout, simulating normal culture and proliferation. Non-parametric Kruskal-Wallis with a Conover-Iman post-hoc test, DMSO vs CDDO-Me at each serum starving FBS concentration. Data analysis represents mean  $\pm$  SD of triplicate wells from n=3 samples. Levels of significance are indicated as follows: \* = 5 % (P = 0.05), \*\* = 1 % (P = 0.01), \*\*\* = 0.1 % (P = 0.001).

In Huh7 cells, the ATP content of serum starved cells, in the presence or absence of CDDO-Me, remained below 50 % of control cells maintained in full growth media at all serum starving FBS concentrations except 10 %. In addition, treatment with 100 nM CDDO-Me following serum starving resulted in lower ATP contents than DMSO treated cells in 0.1, 0.25 and 1 % FBS containing media, with significantly lower levels observed at 0.1 % and 1 % ( $P < 0.001$  for both). Significantly lower ATP levels were also seen with 30 nM CDDO-Me in 0.1 % FBS containing media when compared to DMSO treated cells ( $P = 0.015$ ). Treatment with CDDO-Me in 0 % and 0.5 % FBS containing media produced higher ATP content in Huh7 cells, however no significant differences were observed when compared to DMSO treated cells.

Huh7 cells treated with 10, 30 and 100 nM CDDO-Me in 10 % FBS containing media had significantly higher ATP levels when compared to DMSO treated cells ( $P = 0.001$ ,  $< 0.001$  and  $0.027$  respectively). Despite this, treatment with CDDO-Me in 10 % FBS containing media did not produce ATP levels higher than control cells maintained in full growth media throughout, highlighting that CDDO-Me does not enhance proliferation beyond that of routine cell culture (Fig 3.2). Taken together, this indicates inhibition of proliferation in media containing FBS at concentrations lower than 10 %, with enhanced inhibition observed following treatment with CDDO-Me at selected low FBS concentrations.

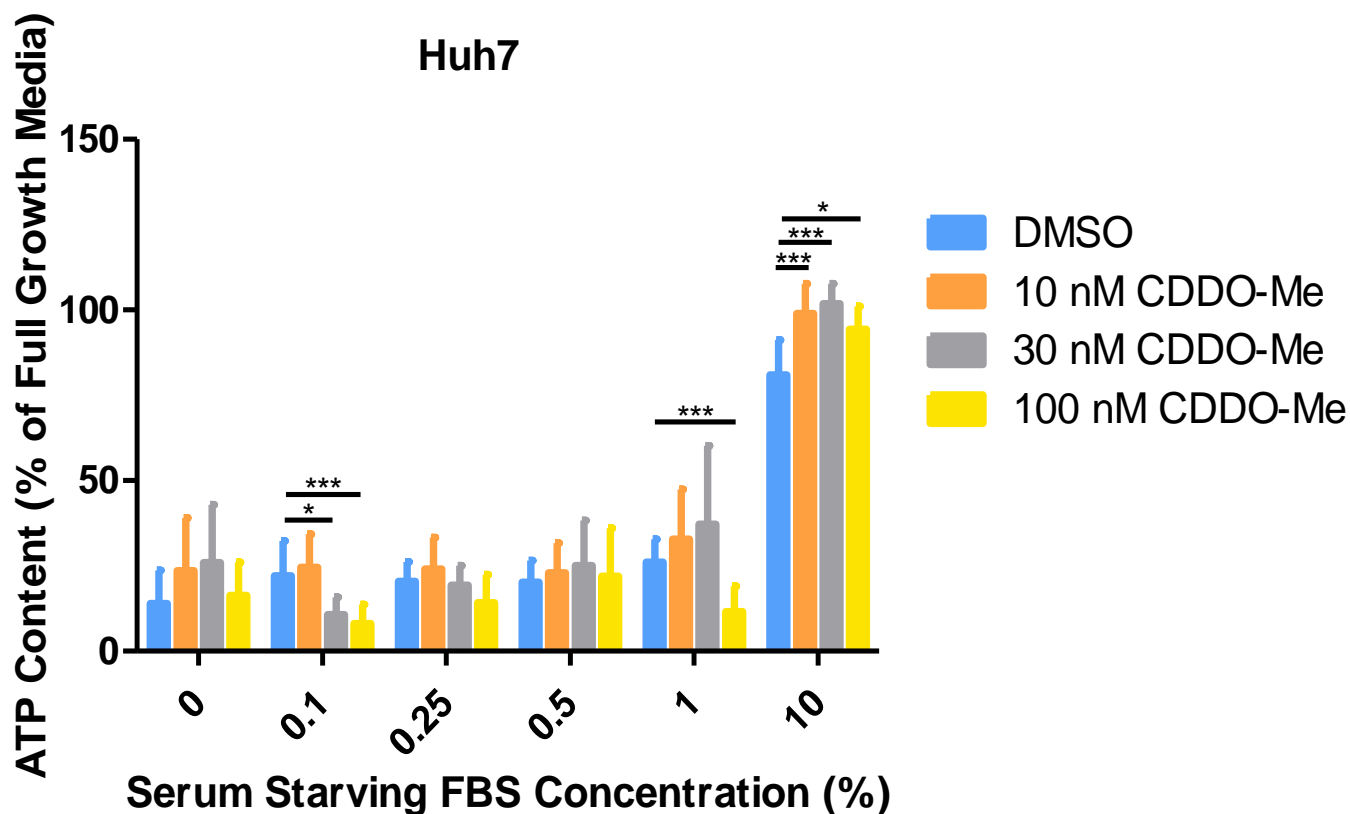


**Figure 3.2** Effect of CDDO-Me on *in vitro* ATP content in Huh7 cells

Huh7 cells were serum starved in the indicated concentrations of FBS containing media prior to being exposed to DMSO or CDDO-Me. ATP content was quantified and is directly proportional to the number of cells present, therefore allowing proliferation to be assessed. ATP content is normalised to control cells that were maintained in full, 10 % FBS, growth media throughout, simulating normal culture and proliferation. Non-parametric Kruskal-Wallis with a Conover-Iman post-hoc test, DMSO vs CDDO-Me at each serum starving FBS concentration. Data analysis represents mean  $\pm$  SD of triplicate wells from  $n=3$  samples. Levels of significance are indicated as follows: \* = 5 % ( $P = 0.05$ ), \*\* = 1 % ( $P = 0.01$ ), \*\*\* = 0.1 % ( $P = 0.001$ ).

In HCT116 cells, the ATP content increased in a FBS concentration dependent manner as the concentration of FBS within media increased for 0 to 10 %. Treatment with CDDO-Me in 0 % FBS containing media produced higher ATP levels when compared to DMSO treated cells, with significantly higher levels observed following treatment with 30 nM CDDO-Me ( $P = 0.049$ ). Similar increases in ATP content were seen following treatment with CDDO-Me in 0.25 % and 0.5 % FBS containing media when compared to DMSO treated cells, although no significance was observed. Interestingly, HCT116 cells treated with CDDO-Me produced lower ATP levels in 0.1 % and 1 % FBS containing media when compared to DMSO treated cells, with significantly lower levels following 30 nM and 100 nM CDDO-Me treatment at 0.1 % FBS ( $P = 0.024$  and  $0.001$  respectively) and 100 nM CDDO-Me treatment at 1 % FBS ( $P = 0.003$ ).

Treatment with CDDO-Me in 10 % FBS containing media produced ATP levels similar to those from DMSO treated cells, with no significant differences observed (Fig 3.3) and such levels did not reach those of control cells maintained in full growth media throughout. Therefore CDDO-Me does not promote proliferation of HCT116 cells beyond that observed in routine cell culture.

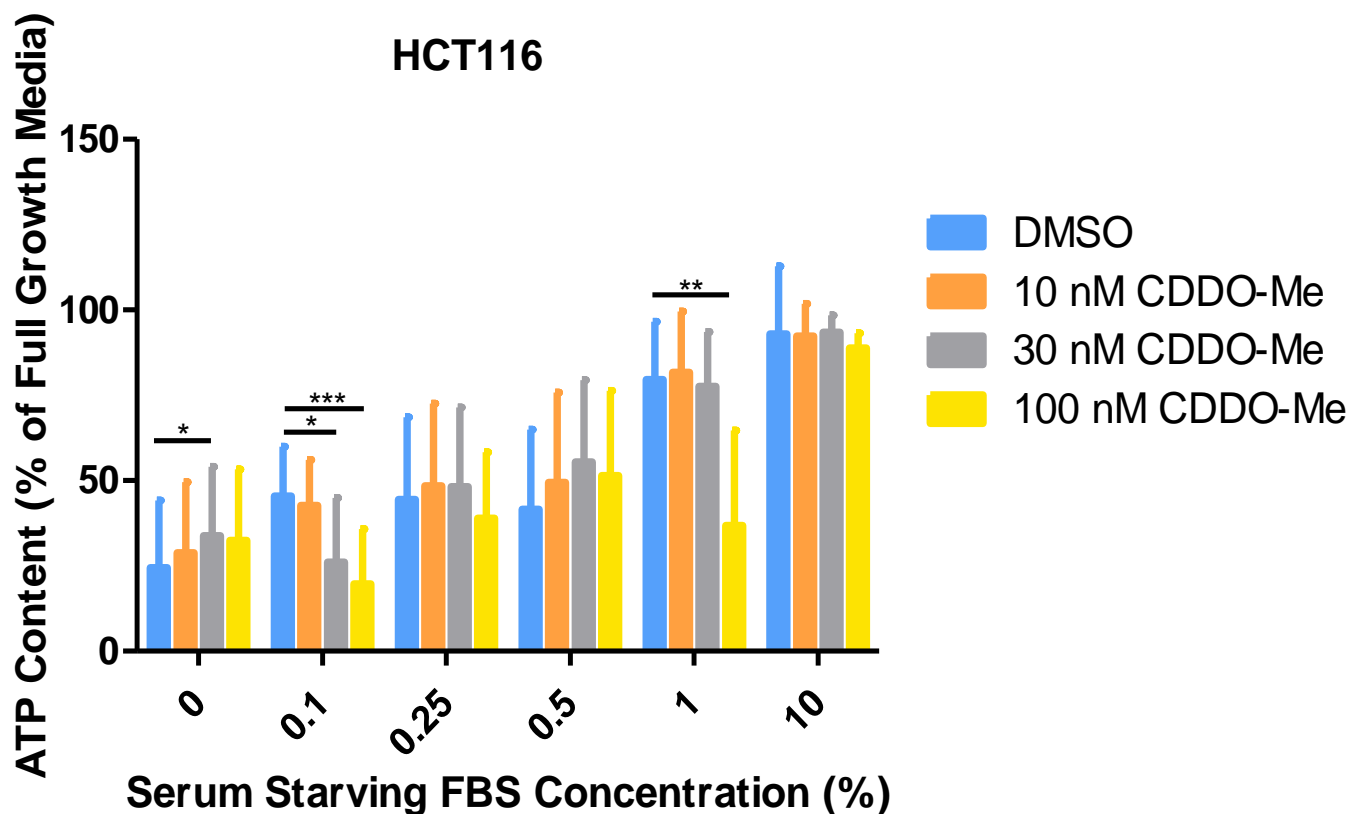


**Figure 3.3** Effect of CDDO-Me on *in vitro* ATP content in HCT116 cells

HCT116 cells were serum starved in the indicated concentrations of FBS containing media prior to being exposed to DMSO or CDDO-Me. ATP content was quantified and is directly proportional to the number of cells present, therefore allowing proliferation to be assessed. ATP content is normalised to control cells that were maintained in full, 10 % FBS, growth media throughout, simulating normal culture and proliferation. Non-parametric Kruskal-Wallis with a Conover-Iman post-hoc test, DMSO vs CDDO-Me at each serum starving FBS concentration. Data analysis represents mean  $\pm$  SD of triplicate wells from n=3 samples. Levels of significance are indicated as follows: \* = 5 % (P = 0.05), \*\* = 1 % (P = 0.01), \*\*\* = 0.1 % (P = 0.001).

In SW480 cells, the ATP content increased in a FBS concentration dependent manner as the concentration of FBS within media increased from 0 to 10 %. Treatment with 10 nM and 30 nM CDDO-Me produced higher levels of ATP when compared to DMSO treated cells in 0, 0.25, 0.5, 1 and 10 % FBS containing media, with significantly higher levels observed with 10 nM CDDO-Me in 1 % FBS media ( $P = 0.015$ ) and 30 nM CDDO-Me in 10 % FBS media ( $P = 0.026$ ). Treatment with 100 nM CDDO-Me produced lower ATP content at all FBS concentrations when compared to DMSO treated cells, with significantly lower ATP levels seen at 0.1, 0.25 and 1 % FBS ( $P < 0.001$ , 0.049 and  $< 0.001$  respectively) (Fig 3.4).

Treatment with CDDO-Me following serum starving did not produce ATP levels higher than those produced from control cells maintained in full, 10 % FBS, growth media throughout. This indicates that CDDO-Me does not promote proliferation of SW480 cells beyond that of routine cell culture.



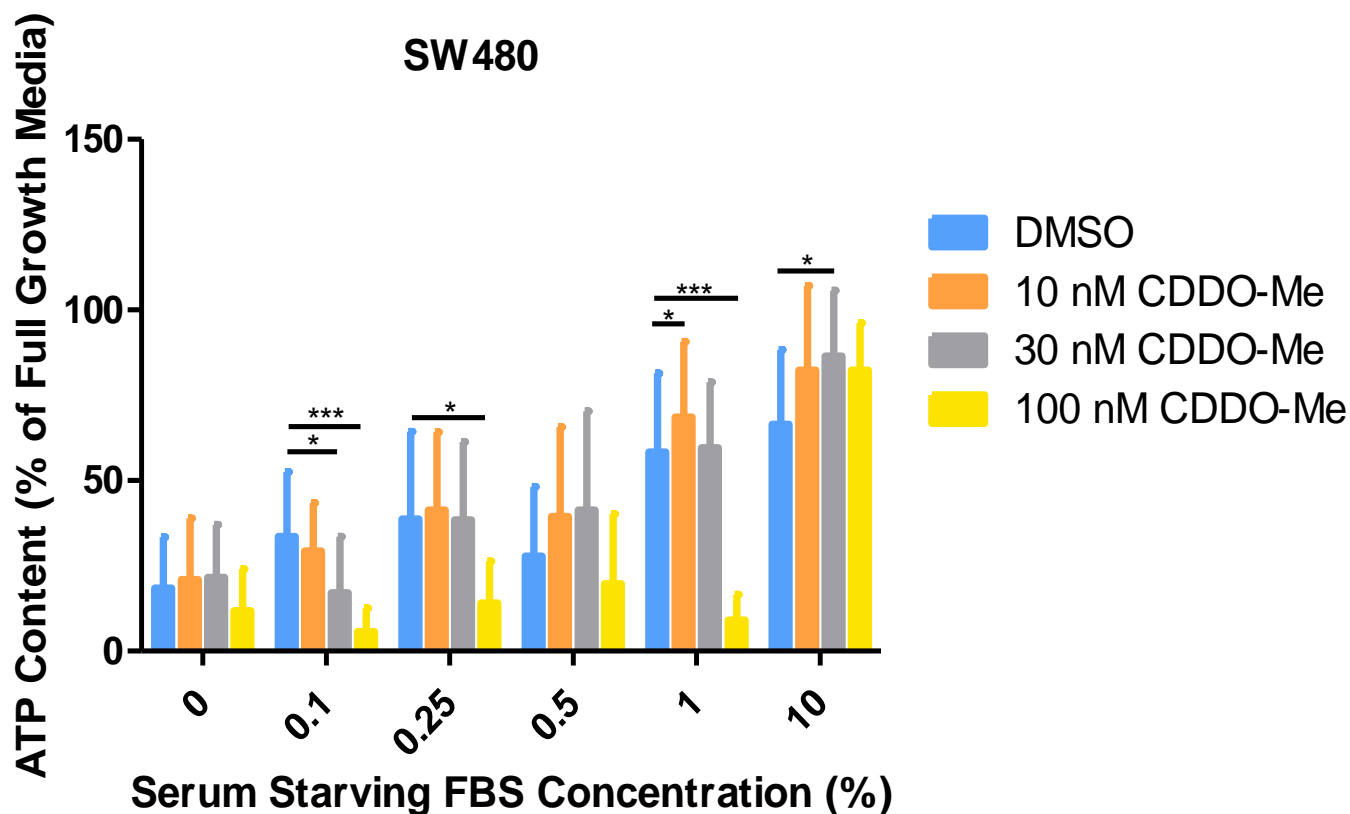


**Figure 3.4** Effect of CDDO-Me on *in vitro* ATP content in SW480 cells

SW480 cells were serum starved in the indicated concentrations of FBS containing media prior to being exposed to DMSO or CDDO-Me. ATP content was quantified and is directly proportional to the number of cells present, therefore allowing proliferation to be assessed. ATP content is normalised to control cells that were maintained in full, 10 % FBS, growth media throughout, simulating normal culture and proliferation. Non-parametric Kruskal-Wallis with a Conover-Iman post-hoc test, DMSO vs CDDO-Me at each serum starving FBS concentration. Data analysis represents mean  $\pm$  SD of triplicate wells from n=3 samples. Levels of significance are indicated as follows: \* = 5 % (P = 0.05), \*\* = 1 % (P = 0.01), \*\*\* = 0.1 % (P = 0.001).

### 3.3.3 CDDO-Me upregulates Nrf2 *in vitro* following serum starving of human HCC and CRC cell lines

To mimic the conditions used in the ATP proliferation assays, HepG2, Huh7, HCT116 and SW480 cells were serum starved in 0, 1 and 10 % FBS containing media using the same method as outlined previously in section 3.2.2. All cells were then exposed or not to 100 nM CDDO-Me for 72 hours, prior to quantification of protein expression via western blotting against NQO1, an established target gene of Nrf2 (Mutter et al., 2015), to assess upregulation of the Nrf2 pathway in the *in vitro* proliferative assay.

HepG2 cells possessed similar expression levels of NQO1 at all FBS concentrations following control treatment with DMSO. Treatment with 100 nM CDDO-Me significantly enhanced NQO1 protein expression levels at all FBS concentrations ( $P = 0.029$ ), with peak expression levels achieved in 0 % FBS containing media (Fig 3.5 B). As HepG2 cells naturally possess high protein expression levels of NQO1 (Haefeli et al., 2011; Chhetri et al., 2022), further enhancement of protein expression via pharmacological intervention is difficult to observe prior to routine normalisation to the intensity of  $\beta$  actin loading control.

In Huh7 cells treated with DMSO control, the protein expression levels of NQO1 decreased as the concentration of FBS within the media increased from 0 to 10 %. Treatment with 100 nM CDDO-Me produced significantly higher levels of NQO1 protein at all FBS concentrations when compared to DMSO treated cells ( $P = 0.029$ ), with levels peaking in 0 % FBS containing media. As with DMSO treated cells, those treated with 100 nM CDDO-Me had decreasing levels of NQO1 protein as the concentration of FBS increased from 0 to 10 % (Fig 3.5 D).

In HCT116 cells treated with DMSO, the level of NQO1 protein decreased as the concentration of FBS within the media increased from 0 to 10 %. Treatment with 100 nM CDDO-Me produced significantly higher levels of NQO1 protein at all FBS concentrations ( $P = 0.029$ ), with NQO1 levels peaking in 0 % FBS containing media (Fig 3.6 B).

SW480 cells had similar NQO1 protein expression levels at all FBS concentrations. Following treatment with 100 nM CDDO-Me, the protein levels of NQO1 were higher at all FBS concentrations, with significantly higher expression levels observed in 0 % and 1 % FBS containing media ( $P = 0.001$  and  $0.002$  respectively) (Fig 3.6 D).

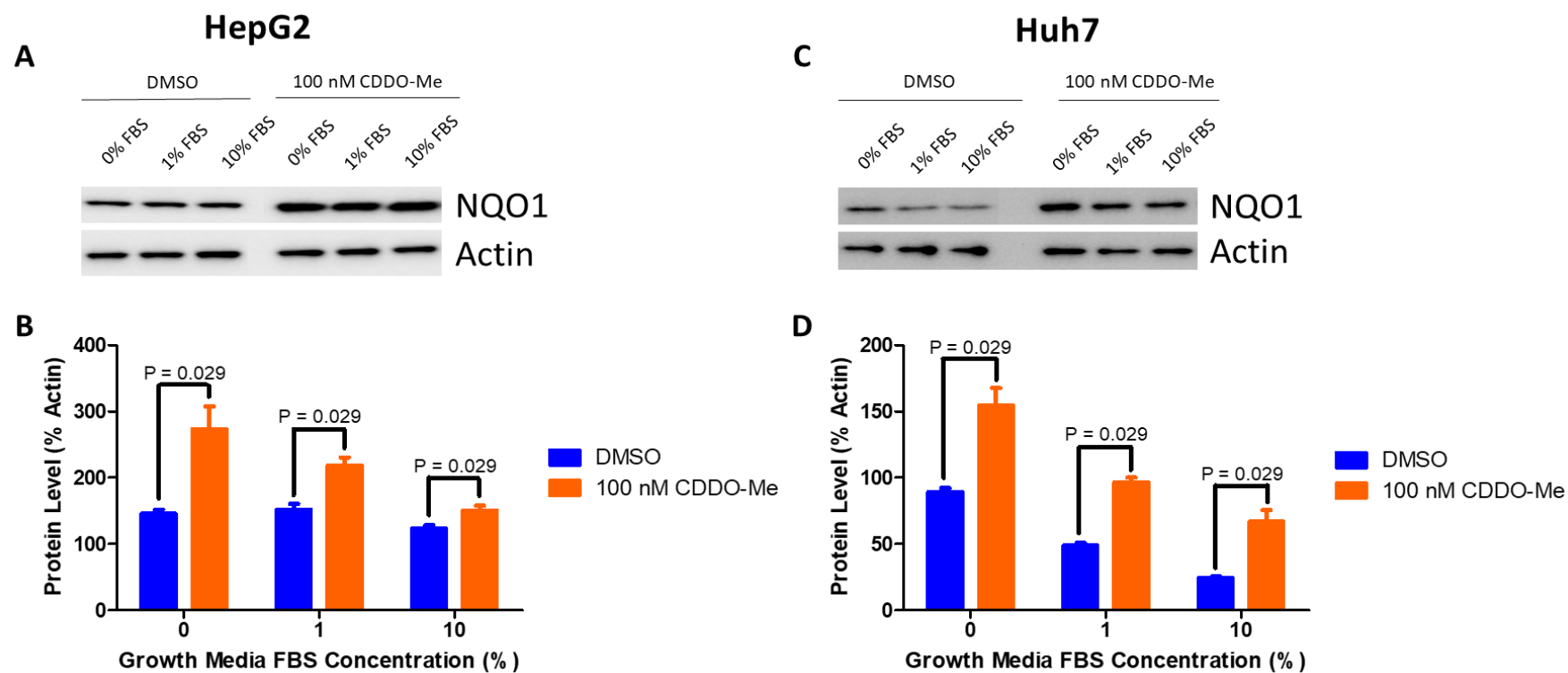


**Figure 3.5 Effect of CDDO-Me on the protein expression levels of NQO1 in human HCC cell lines following serum starving.**

Western blot for NQO1 of representative (A) HepG2 and (C) Huh7 cell lysates that were serum starved in media containing the indicated concentrations of FBS prior to treatment with or without 100 nM CDDO-Me. Densitometry of NQO1 immunoblotting from all (B) HepG2 and (D) Huh7 cell lysates, normalised to  $\beta$  actin. (B and D) Mann-Whitney U test, DMSO vs CDDO-Me at each FBS concentration. Data analysis represents mean  $\pm$  SD of triplicate wells from n=3 samples.

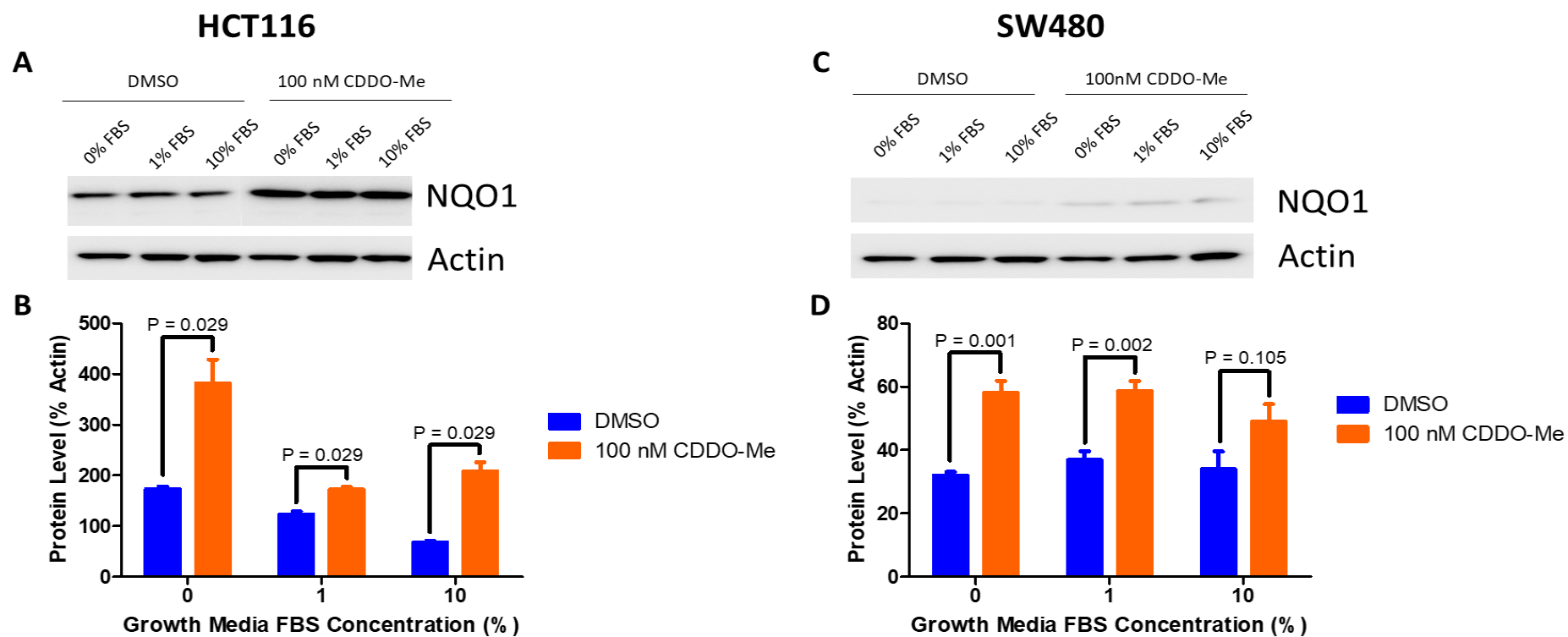


**Figure 3.6 Effect of CDDO-Me on the protein expression levels of NQO1 in human CRC cell lines following serum starving.**

Western blot for NQO1 of representative (A) HCT116 and (C) SW480 cell lysates that were serum starved in media containing differing concentrations of FBS prior to treatment with or without 100 nM CDDO-Me. Densitometry of NQO1 immunoblotting from all (B) HCT116 and (D) SW480 cell lysates, normalised to  $\beta$  actin. (B) Mann-Whitney U test and (D) Unpaired t-test, DMSO vs CDDO-Me at each FBS concentration. Data analysis represents mean  $\pm$  SD of triplicate wells from n=3 samples.

### 3.4 Discussion

For many years, cancer research has utilised numerous *in vitro*, cell based, models to better the understanding of cancer initiation, development, and treatment strategies (Ferreira et al., 2013; Kitaeva et al., 2020; Ayuso et al., 2021). Although *in vitro* models lack the ability to recapitulate cancer homogeneity and the true physiological conditions of disease as seen with *in vivo* models, their continued use is largely due to the wide availability of cells, relative ease of use in larger scale studies (Gillet et al., 2013), ability to perform high throughput analysis (Katt et al., 2016; Antunes et al., 2022) and the ability of cell lines to provide an almost infinite source of biological material for experimental use (Mirabelli et al., 2019).

*In vitro* models have been used for many years to assess Nrf2 and its role in the proliferation of liver cancer cell lines, however this still remains unclear, with Nrf2 commonly being referred to as a double-edged sword (Wu et al., 2019). Several reports show enhanced proliferation and invasion in both HCC cell lines (Zhang et al., 2015; Haque et al., 2020) and CRC cell lines (Zhao et al., 2015), through the use of genetically modified cell lines and constitutive activation of the Nrf2 pathway. Interestingly however, a more clinically relevant approach, utilising pharmacological Nrf2 activation in wild-type HCC cell lines has been shown to elicit an anti-tumour effect (Gee et al., 2018; Baer-Dubowska et al., 2021). Therefore, this chapter provides further investigation into the role of Nrf2 in the proliferation of liver cancer *in vitro* using a clinically relevant therapeutic strategy.

It was essential to select appropriate HCC and CRC cell lines to best mimic the current clinical setting for both primary liver cancer and secondary colorectal metastasis. As previously outlined in section 3.3.1, this was achieved through the use of cell lines closely correlated to the

genotypes of clinical tumours (Chen et al., 2015), which are well established *in vitro* models for investigating the initiation and development of such cancers (Wahab et al., 2017; Schicht et al., 2022). The exclusion of other cell lines was primarily due to the practical limitations of obtaining and culturing such cells without the necessary isolation and specialist culture requirements associated with the integrated hepatitis B virus genome. However, the use of these cell lines has recently become more widely accepted and such models provide considerable insight into their respective malignancies. The Hep3B cell line is a useful *in vitro* model for HCC progression (Blidisel et al., 2021) and associated therapeutic strategies (Skonieczna et al., 2022), meanwhile the HCT15 cell line acts as a suitable model for colorectal cancer tumorigenesis (Tang et al., 2022) and metastatic behaviour (Brás et al., 2022). Therefore, owing to the heterogeneity of both HCC (Lu et al., 2016; Zhang et al., 2020) and CRC (Sagaert et al., 2018), including metastasis to the liver (Blank et al., 2018), it would be advantageous to use such models in future studies.

The findings of this chapter highlight the potential of CDDO-Me to elicit an anti-tumour effect in both human HCC and CRC cell lines *in vitro*, thus supporting previously published findings. Gee et al. (Gee et al., 2018) demonstrated that exposure of HepG2 and Huh7 cells to CDDO-Me at concentrations of 1.25-20  $\mu\text{M}$  led to a significant decrease in cell viability after 24 hours, as measured using the 3-(4,5-dimethylthiazol2-yl)-2,5-diphenyl tetrazolium bromide (MTT) assay. In addition, CDDO-Me treatment in Huh7 cells led to an increase in the number of apoptotic cells, suggesting that the observed loss of cell viability in response to CDDO-Me was due to the activation of apoptotic pathways. Similarly, pharmacological Nrf2 activation, achieved via treatment with sulforaphane, provoked an anti-proliferative effect in HepG2 cells, as measured by lower viability in MTT assay, as well as the formation of fewer colonies in a colony formation assay, relative to cells treated with DMSO vehicle control (Liu et al., 2018).

These findings in HCC cell lines are also supported in CRC cell lines, with Hao et al. demonstrating a dose-dependent loss of viability with MTT assay in SW480 cells after treatment with sulforaphane for 24, 48 and 72 hours. Furthermore, sulforaphane treated cells exhibited less staining for EdU, a stain that preferentially binds to newly synthesised DNA. This supports the findings that the impact on cell viability is due to a reduction in the proliferative rate of cells following treatment with the Nrf2 activator (Hao et al., 2020). Additionally, Pharmacological activation of Nrf2 using the natural activator, 2-(Pro-1-ynyl)-5-(5,6-dihydroxypenta-1,3-diynyl) thiophene (PYDDT), in SW620, SW480 and HCT116 cells, caused a dose-dependent loss of cell viability at 24 and 48 hours, and an increase in the apoptotic markers, cleaved caspase-3 and cleaved PARP (Xu et al., 2015). Although this data is consistent with the findings from Gee et al, it is highly likely that the observed loss of cell viability is due to cytotoxicity resulting from the considerably high drug concentrations used in these studies, as opposed to pharmacological Nrf2 activation driving the activation of apoptotic mechanisms.

However, it is important to consider the limitations. The process of serum starving cells, although widely used as a means of reducing basal cell activity (Codeluppi et al., 2011) to produce a homogenous population of quiescent cells (van Rechem et al., 2010; Pontarin et al., 2011), is highly inconsistent and lacks a standardised protocol (Pirkmajer & Chibalin, 2011). In addition, serum starving can promote dysregulation of numerous cellular signalling pathways, subsequently reducing the expression of crucial proteins such as GAPDH and promoting cell death via apoptotic pathways (Pirkmajer & Chibalin, 2011; Rashid & Coombs, 2019). Furthermore, it has been shown that fetal bovine serum (FBS) can alter the bioavailability of some compounds in *in vitro* assays (Hestermann et al., 2000). As a result of its viscosity, high levels of FBS can bind small molecules, holding them within culture media and preventing efficient uptake into cells. Taken together, the observed inhibition of proliferation in this chapter



could be attributed to the prolonged exposure of cells to culture media containing low FBS, or to alterations in the bioavailability of CDDO-Me in culture media as a result of differing FBS levels during the serum starving process. Further optimisation of this assay, including an assessment of caspase and apoptotic activity following serum starvation of cells, would allow a more comprehensive understanding of the effect of CDDO-Me on HCC and CRC cell proliferation, and could help further support the findings of Gee et al. and Xu et al. as discussed previously.

In order to further expand the findings and understandings of this chapter, it would be highly beneficial to incorporate 3D cell models. Spheroids are known to better recreate the *in vivo* physiology (Romualdo et al., 2021) and therefore would better encapsulate the knowledge surrounding the role of Nrf2 in liver cancer proliferation. Additionally, a colony formation assay could be utilised to enhance understanding. Although this is routinely used to assess cell death (Brix et al., 2020), it could be optimised to investigate proliferative ability of cells, thus providing an additional and powerful tool for assessing *in vitro* proliferative ability. The use of such an assay was attempted, however due to a number of technical difficulties encountered during the development and optimisation of a colony formation assay with the HCC and CRC cell lines outlined in this chapter, an *in vitro* ATP proliferation was preferably used to assess cellular proliferation following treatment with CDDO-Me.

To summarise, the findings of this chapter highlight the potential use of CDDO-Me to enhance liver regeneration without adversely affecting HCC or CRC cell proliferation. However, the limitations of this chapter, coupled to the further development of *in vitro* cell based approaches (Romualdo et al., 2021; Shao et al., 2022), illustrates the need for further investigation, and the incorporation of more advanced *in vitro* models including 3D spheroids, to better encapsulate

the knowledge surrounding the role of Nrf2 in liver cancer proliferation. Furthermore, it is also essential to investigate this role of Nrf2 in relevant using *in vivo* models of liver cancer.

## Chapter 4

**Pharmacological activation of Nrf2 does not promote the proliferation of tumours forming from an orthotopic xenograft of human HCC and CRC cells in an *in vivo* model**

## Contents

<b>4.1 Introduction</b> .....	133
<b>4.2 Methods</b> .....	136
4.2.1 Cell culture.....	136
4.2.1.1 Production of luciferase expressing cell lines.....	136
4.2.1.2 Confirmation of luciferase expression.....	139
4.2.2 Animal experiments.....	140
4.2.2.1 <i>In vivo</i> model selection.....	140
4.2.2.2 Orthotopic tumour xenograft cell preparation.....	142
4.2.2.3 Orthotopic tumour xenograft.....	143
4.2.2.4 Bioluminescence imaging.....	145
4.2.2.5 Animal drug treatments.....	148
4.2.3 Western blotting.....	149
4.2.4 Histological examinations.....	151
4.2.5 Statistical analysis.....	152
<b>4.3 Results</b> .....	153
4.3.1 Puromycin dose response.....	153
4.3.2 Confirmation of luciferase presence in cells using an <i>in vitro</i> luciferase assay.....	155
4.3.3 Confirmation of luciferase presence in cells using IVIS bioluminescence imaging.....	158
4.3.4 <i>In vivo</i> model selection.....	161
4.3.5 Preliminary orthotopic tumour xenograft and <i>in vivo</i> bioluminescence imaging.....	163
4.3.5.1 IVIS bioluminescence imaging.....	163
4.3.5.2 Immunoblotting.....	165
4.3.5.3 Macroscopic analysis of tumour mass.....	167
4.3.5.4 Histological examination.....	169
4.3.6 Optimisation of orthotopic tumour xenograft and <i>in vivo</i> bioluminescence imaging.....	171
4.3.6.1 IVIS bioluminescence imaging.....	171
4.3.6.2 Immunoblotting.....	177
4.3.7 CDDO-Me does not promote growth of tumours <i>in vivo</i> .....	180
4.3.8 Protein expression analysis following orthotopic tumour xenograft.....	187
4.3.9 Histological examinations of HepG2-luc and HCT116-luc tumours.....	191

4.4 Discussion..... 196

#### 4.1 Introduction

Owing to the livers remarkable ability to regenerate following surgical insult, current curative treatments for liver cancer frequently involve surgical resection of the affected liver tissue. Although, in some cases, liver regeneration does not occur efficiently, resulting in post-operative complications such as PHLF. The findings of chapter 2 illustrate that pharmacological activation of Nrf2, through treatment with CDDO-Me, can significantly enhance liver regeneration in a rodent two-thirds PHx model. However, it has been observed that genes within the Nrf2 pathway, including NFE2L2 itself, the repressor KEAP1, and others downstream, are commonly mutated within clinical HCC (Guichard et al., 2012; Cleary et al., 2013; Ding et al., 2017) and CRC (Sameer, 2013; Torrente et al., 2020) tumours, thus raising concerns about the use of therapies involving Nrf2 stimulation in the context of liver tumour surgery.

Numerous *in vivo* models have been developed and reported, in which Nrf2 has been manipulated in rodents possessing HCC or CRC. Wild-type mice, in which normal Nrf2 levels were observed, possessing HCC, induced via administration of the well-established hepatocarcinogen Diethylnitrosamine (DEN), were shown to have significantly more, and larger, hepatic tumours when compared to Nrf2 knockout mice that effectively resisted DEN-induced hepatocarcinogenesis (Ngo et al., 2017). In addition, wild-type rats were observed to possess significantly larger HCC tumours compared to rats possessing silenced Nrf2 (shNrf2) (Zavattari et al., 2015). Both studies therefore highlight the negative impact of Nrf2 on HCC initiation and subsequent growth. However, it is important to note that both models reported utilise transgenic rodent models and lack a more clinically relevant method of modulating Nrf2, such as pharmacological intervention.

With regards to *in vivo* rodent models of CRC in which the effects of Nrf2 manipulation have been investigated, the reported findings are considerably more ambiguous. Numerous studies have shown that Nrf2 knockout mice were more likely to develop colorectal cancer when compared to wild-type mice (Khor et al., 2008; Hammad et al., 2019), due to impairment of antioxidant mechanisms and significant increases in the inflammatory response. Furthermore, it has been shown that pharmacological upregulation of Nrf2, through the use of the flavonoid, Luteolin, can inhibit the tumorigenic development and progression of Azoxymethane/Dextran sodium sulphate (AOM/DSS) induced colorectal cancer (Pandurangan et al., 2014). Interestingly however, pharmacological inhibition of Nrf2, both in a xenograft model of human HCT116 cells stably transfected to overexpress Nrf2 (Shen et al., 2019), and in a xenograft model of wild-type murine CT26 (Evans et al., 2018) was shown to elicit anti-tumour properties and suppress Nrf2-mediated chemoresistance.

Taken together, the concerns arising from the use of Nrf2 stimulation in a clinical liver tumour setting, and the often conflicting and ambiguous findings reported in *in vivo* models of Nrf2 activation in liver cancer, highlights the need to assess the safety of Nrf2 targeting therapies, by investigating the effect of pharmacological Nrf2 activation on the burden of pre-existing tumours. Such assessment would therefore address one of the risks of stimulating Nrf2 in cancer patients to boost access to curative surgery.

I hypothesised that acute pharmacological activation of Nrf2 would not promote proliferation of liver cancer in an *in vivo* orthotopic tumour xenograft model. In order to test this hypothesis, human HCC and CRC cell lines were transfected to constitutively express luciferase, prior to an orthotopic, subcapsular intrahepatic, xenograft taking place in BALB/c Nude mice. Owing to the bioluminescent properties of xenografted cells, mice treated or not with CDDO-Me then underwent non-invasive

bioluminescence imaging to assess the effect of pharmacological Nrf2 activation on tumour growth  
*in vivo*.



## 4.2 Methods

All reagents were purchased from Sigma Aldrich unless otherwise stated.

### 4.2.1 Cell culture

HepG2, Huh7, SW480 and HCT116 cells were maintained in an incubator set at 37 °C and 5 % CO<sub>2</sub>. All cell lines were cultured as previously outlined in section 3.2.1.

#### 4.2.1.1 Production of luciferase expressing cell lines

Luciferase expressing cell lines were produced following stable transfection with the pEF6 Firefly Luciferase P2A plasmid (Fig 4.1). Luciferase expressing cell lines produce light in the presence of ATP and luciferin substrate, allowing cells to be visualised via non-invasive bioluminescence imaging techniques. Transfection with such plasmid allows for selection of successfully transfected cells, owing to the presence of a puromycin resistance gene. Therefore prior to the commencement of stable transfection, the maximum tolerated dose of puromycin in each un-transfected cell line was determined, such that a normally toxic dose could be used to drive selection of cells possessing plasmid DNA.

In order to determine the maximum tolerated dose of puromycin, a dose response curve was generated for each cell line. Cells were seeded in a 96 well plate at 25,000 cells per well in 100 µL culture media and left for 24 hours in an incubator to allow complete adherence. Following this, cells were treated with puromycin. Culture media containing puromycin was produced such that the final concentrations of puromycin were 9, 6, 3, 2.4, 1.8, 1.2, 0.6, 0.3 and 0.1 µg/mL. Culture media was aspirated off each well and replaced with media containing puromycin. Culture media containing no

puromycin was used as a control. This process was repeated every two days for four times total, allowing continual exposure of the cells to puromycin. After eight days, an ATP assay was carried out utilising the CellTiter-Glo® Luminescent Cell Viability Assay kit (Promega) as outlined previously in section 3.2.3. The concentration of puromycin that resulted in > 90 % cell death, was then used as a culture media supplement once plasmid transfection had been carried out, allowing culture of transfected cells only.

Cells were stably transfected with the pEF6 Firefly Luciferase P2A plasmid using jetPEI™ (Polyplus). Cells were seeded in a 6 well plate at 500,000 cells per well in 2 mL of culture media and left for 24 hours in an incubator to allow complete adherence. DNA was diluted to 45 ng/μL in 150 mM NaCl. jetPEI was produced at 2 μL per 1 μg DNA, 3 μL per 1 μg DNA and 4 μL per 1 μg DNA in 150 mM NaCl in separate tubes, allowing for the production of three different clones per cell line: 2JP clone 2, 3JP clone 3 and 4JP clone 4 respectively. All solutions were vortexed before each concentration of jetPEI was added to DNA in a 1:1 volume ratio. The resulting solution was again vortexed and centrifuged for 30 sec at 1000 g, before being incubated at room temperature for 20 min. During this time, culture media was aspirated from each well and replaced with fresh culture media. 200 μL of jetPEI/DNA solution was then added per well in a dropwise fashion before the plate was returned to the incubator. After 24 hours, all cells were visually checked using a standard light microscope to assess cell viability and culture media was replaced with culture media containing 1.8 μg/mL puromycin. Media was then subsequently refreshed every two days and confluency assessed. Once confluent in a 6 well plate, cells were detached using trypsin as outlined previously in section 3.2.1 and transferred to a T25 cell culture flask. This was repeated upon confluency until cells were able to be grown in a T175 cell culture flask.



Figure 4.1 pEF6 Firefly Luciferase P2A plasmid map

#### 4.2.1.2 Confirmation of luciferase expression

Successful transfection of cells with the pEF6 Firefly Luciferase P2A plasmid was confirmed by comparing the luminescence signal produced from wild-type, non-transfected, and transfected cells. Initially wild-type cells were seeded alongside the three transfected clones: 2JP clone 2, 3JP clone 3 and 4JP clone 4 in a 96 well plate at 25,000 cells per well in 100  $\mu$ L of culture media or culture media containing puromycin respectively. All cells were then left to adhere for 24 hours.

Cells were removed from the incubator and left at room temperature for 10 min. Luminescence was then quantified using the Bright-Glo™ Luciferase Assay System (Promega). 100  $\mu$ L Bright-Glo reagent was added to each well before plates were sealed with aluminium foil and shaken for 2 min at 500 rpm. 100  $\mu$ L from each well of the resulting cell lysate/Bright-Glo reagent was transferred to a white 96 well plate and Luminescence was then measured using a Varioskanner Flash 3001 (ThermoScientific). The luminescence signal of transfected cells was normalised to that of wild-type cells.

To then further confirm successful transfection and investigate if the luminescent signal produced was dependent on the density of cells seeded, the three transfected clones were seeded in a 96 well plate at 250,000, 100,000, 50,000, 25,000, 10,000, 5,000 and 2,500 cells per well in 100  $\mu$ L culture media containing puromycin. All cells were then left to adhere for 24 hours. Following this, luminescence was quantified using the Bright-Glo™ Luciferase Assay System (Promega) according to the same protocol as outlined previously. Wells containing only culture media, with no cells, were used as control and to normalise luminescence signal.

## 4.2.2 Animal experiments

All animal experiments were carried out according to the Animals (Scientific Procedures) Act 1986 guidelines under the Home Office project licence PC195FABD and approved by the University of Liverpool Animal Welfare Committee.

### 4.2.2.1 *In vivo* model selection

As human cancer cell lines were used for all *in vivo* orthotopic tumour xenograft work, it was essential to utilise an immunodeficient mouse strain. In order to select the most appropriate strain, a small pilot study was conducted using mouse strains with differing degrees of immunodeficiency (Table 4.1).

Immunodeficient male CB17-SCID, NOD-SCID, BALB/c Nude and immunocompetent male C57BL/6JRj, used as a reference control to the two-thirds PHx model outlined in chapter 2, were purchased from Janvier aged 8-10 weeks, and underwent a 5-day acclimatisation period prior to experimental work commencing. All animals were maintained in a 12-hour light/dark cycle in a temperature and humidity controlled, specific pathogen-free environment. Mice were fed CRM (P) diet (Special Diets Services) ad-libitum.

All animals received a single dose of either 3 mg/kg CDDO-Me or 100 % DMSO via intraperitoneal (IP) injection, administered at 1  $\mu$ L/g of bodyweight. All animals were then culled with a rising concentration of CO<sub>2</sub>, 24 hours post dose. The liver was excised, weighed, and preserved by snap freezing in liquid nitrogen for downstream analysis.

**Table 4.1 Phenotypic characteristics of immunodeficient mice**

<b>Mouse Strain</b>	<b>T Lymphocytes</b>	<b>B Lymphocytes</b>	<b>NK Cells</b>	<b>Dendritic Cells</b>	<b>Macrophages</b>
CB-17 SCID	Absent	Absent	Low	Low	Dysfunctional
NOD-SCID	Absent	Absent	Dysfunctional	Low	Dysfunctional
BALB/c Nude	Absent	Normal	Normal	Normal	Normal

#### 4.2.2.2 Orthotopic tumour xenograft cell preparation

Prior to the commencement of any *in vivo* study using luciferase expressing cells, all cell lines underwent biologics screening to ensure they were free of infectious agents, that can infect mice post-inoculation, potentially impacting the animal's welfare and compromising valuable research data. To achieve this, all transfected cells were passaged without antibiotics, washed twice in PBS and then subsequently re-suspended in PBS to produce 200  $\mu$ L aliquots containing a minimum of  $5 \times 10^6$  cells per mL. Aliquots were frozen at  $-20^\circ\text{C}$  before being shipped on dry ice to Charles River (UK). Here, the aliquots underwent PCR testing against a mouse essential CLEAR panel, which includes various targets of known rodent infection.

Upon confirmation that all cell lines were negative for all infectious targets on the mouse essential CLEAR panel, cells were prepared for orthotopic tumour xenograft. HepG2-luc and HCT116-luc cells, produced as outlined in section 4.2.1.1 were prepared fresh 1 hour prior to orthotopic tumour xenografts taking place. Cells were dissociated from the surface of culture flasks and subsequently counted using trypan blue as previously outlined in section 3.2.1. Cells were pelleted, washed twice in PBS, and then resuspended in Matrigel<sup>®</sup> Basement Membrane Matrix, growth factor reduced (GFR), phenol red-free (Corning), such that the final cell inoculum in 30  $\mu$ L Matrigel was either  $2 \times 10^6$ ,  $1 \times 10^6$ ,  $5 \times 10^5$  or  $2.5 \times 10^5$  cells. Once resuspended in Matrigel, all cell suspensions were maintained on ice.

#### 4.2.2.3 Orthotopic tumour xenograft

Male, BALB/c Nude mice aged 8-10 weeks old, were purchased from Janvier and underwent a 5-day acclimatisation period prior to experimental work commencing. All animals were maintained in a 12-hour light/dark cycle in a temperature and humidity controlled, specific pathogen-free environment. Mice were fed CRM (P) diet (Special Diets Services) ad-libitum.

An orthotopic tumour xenograft, similar to that carried out by Kasashima et al. (Kasashima et al., 2020), was performed on day 0. Mice received sub-cutaneous buprenorphine (0.05 µg/g bodyweight) 1 hour prior to surgery. General anaesthesia was achieved via induction in a chamber with 2 % isoflurane and 2 L/min oxygen flow. The abdominal skin was disinfected with 10 % povidone-iodine. Mice were then transferred to a heated operating table, where the body temperature was monitored, and subsequently maintained, using a rectal thermometer and thermostat. Anaesthesia was maintained on the operating table via mouthpiece with 1-1.5 % isoflurane and 1 L/min oxygen flow.

Immediately prior to surgery commencing, HepG2-luc 2JP clone 2 and HCT116-luc 2JP clone 2 cells suspended in Matrigel, produced and prepared as outlined in sections 4.2.1.1 and 4.2.2.2, were carefully agitated with a 1 mL pipette, whilst on ice, to ensure a homogenous suspension was maintained. 30 µL of cell/Matrigel suspension was then loaded into a Hamilton syringe with a 30 G needle attached. The syringe was then briefly placed on the heated operating table, whilst surgery commenced, to allow the Matrigel to begin solidifying.

Mice were placed in the supine position and a sterile drape was placed over the abdomen. A midline laparotomy incision, 10-15 mm in length, was performed with careful entry into the peritoneal cavity.



The left lateral lobe was carefully externalised before being stabilised with cotton buds. The Hamilton syringe was then held parallel to the left lateral lobe and 30 G needle slowly traversed 3-5 mm under the liver capsule. 30  $\mu$ L of cell/Matrigel suspension was then very slowly injected under the liver capsule and the needle held in position for 1 min to ensure complete solidification of the Matrigel, providing a plug which prevents bleeding and the loss of cells. Successful subcapsular implantation caused the surrounding liver surface to turn white. In the event of leaking cell/Matrigel suspension, the needle was removed and re-inserted at another adjacent site, 2-3 mm away, before the remaining volume of suspension was injected.

Upon successful implantation, the needle was carefully and slowly removed. Following this, the abdomen was closed using 6/0 Vicryl as a continuous, locking, suture for the peritoneum and a subcuticular suture for the skin.

Post-operatively, the mice were transferred to a heated recovery chamber and allowed to recover with regular close monitoring. When necessary, wet diet was provided to help prevent loss of bodyweight.

Mice were culled with a rising concentration of CO<sub>2</sub>. Blood was collected via cardiac puncture using a 25 G needle and a 1 mL syringe to collect blood directly from the heart. Before decanting the blood into 1.5 mL tubes, the needle was removed to prevent haemolysis. Freshly isolated blood was left to clot at room temperature for 1 hour and centrifuged at 2000 g for 10 min in a centrifuge set at 4 °C. Serum was aspirated and stored at -80 °C. The liver, and incorporated tumour, was excised, weighed and weight recorded, and photographed. If the presenting tumour was large enough, a small section was removed and preserved by snap freezing in liquid nitrogen. Remaining tumour, or in cases where

a small tumour was presented, was left intact with the left lateral lobe, and preserved in PFA. Healthy liver tissue, defined as lobes unaffected by the implantation of cells, with no visible tumours, was also collected and cut into multiple sections before being preserved by snap freezing in liquid nitrogen or by placing in PFA. In animals where local metastasis was observed, affected tissue was collected and preserved in PFA.

#### 4.2.2.4 Bioluminescence imaging

Bioluminescence imaging was conducted using the *in vivo* imaging system (IVIS) spectrum (PerkinElmer). The IVIS system not only allows for non-invasive imaging of live mice and quantification of bioluminescence signal, but also imaging and quantification of cells.

Prior to the commencement of *in vivo* imaging, all luciferase expressing cell lines were imaged in the IVIS machine to ensure the cells produced sufficient bioluminescence to be detected and quantified. Cells were seeded in a black 96 well plate at 250,000, 100,000, 50,000, 25,000, 10,000, 5,000, 2,500 and 1,000 cells per well in 100  $\mu$ L cell culture media. *In vivo* grade Beetle Luciferin, Potassium Salt (Promega) was suspended in diH<sub>2</sub>O to produce a 30 mg/mL stock solution. This stock solution was then diluted 1 in 200 in culture media, giving a final luciferin concentration of 150  $\mu$ g/mL. Culture media was then aspirated from cells and replaced with culture media containing luciferin reagent. Plates were sealed with aluminium foil and left to incubate at room temperature in the dark for 10 min. Plates were orientated centrally in the IVIS machine and images taken using Living Image<sup>®</sup> software and the following parameters: exposure time auto, binning medium, F/stop 1, excitation filter closed, emission filter open. An ROI tool, set to the circumference of each well was then used to calculate average radiance (photons/sec/cm<sup>2</sup>/sr). As the same size ROI tool was used for all images,

average radiance was converted to bioluminescence total flux (photons/sec) by the Living Image® software (Fig 4.2).

To quantify the bioluminescence signal *in vivo*, mice were imaged on days -1, 2, 7, 14, 21, 28 (Fig 4.3), with the day of cell implantation defined as day 0. Mice were firstly anaesthetised using an induction chamber with 2 % isoflurane and 2 L/min oxygen flow. Anaesthetised mice were then weighed and administered 150 mg/kg *in vivo* grade luciferin at 10 µL/g of bodyweight via IP injection. After 7.5 min, mice were transferred to the IVIS machine where anaesthesia was maintained via mouthpiece with 1-1.5 % isoflurane and 1 L/min oxygen flow. Mice were placed in the supine position and images taken using Living Image® software and the following parameters: exposure time auto, binning medium, F/stop 1, excitation filter closed, emission filter open. Following completion of imaging, mice were transferred to a heated recovery chamber and allowed to recover with regular close monitoring. An ROI tool, set to the size of the abdomen was then used to calculate average radiance (photons/sec/cm<sup>2</sup>/sr). As the same size ROI tool was used for all images, average radiance was converted to bioluminescence total flux (photons/sec) by the Living Image® software (Fig 4.2).

Bioluminescence was also observed in organs *ex vivo*. Following cull, the liver was removed, briefly rinsed in PBS and subsequently incubated with 500 µL 150 µg/mL *in vivo* grade luciferin (in PBS) at room temperature for 1 min. The liver was then placed on black card and placed inside the IVIS machine before images were taken using Living Image® software. The liver was then washed briefly in PBS and preserved as outlined previously in section 4.2.2.3. In mice where metastasis was observed in initial, whole-body imaging, the animal underwent full dissection after cull and all organs were subsequently imaged. Any organs in which bioluminescence was detected, were then washed in PBS, and preserved in PFA.

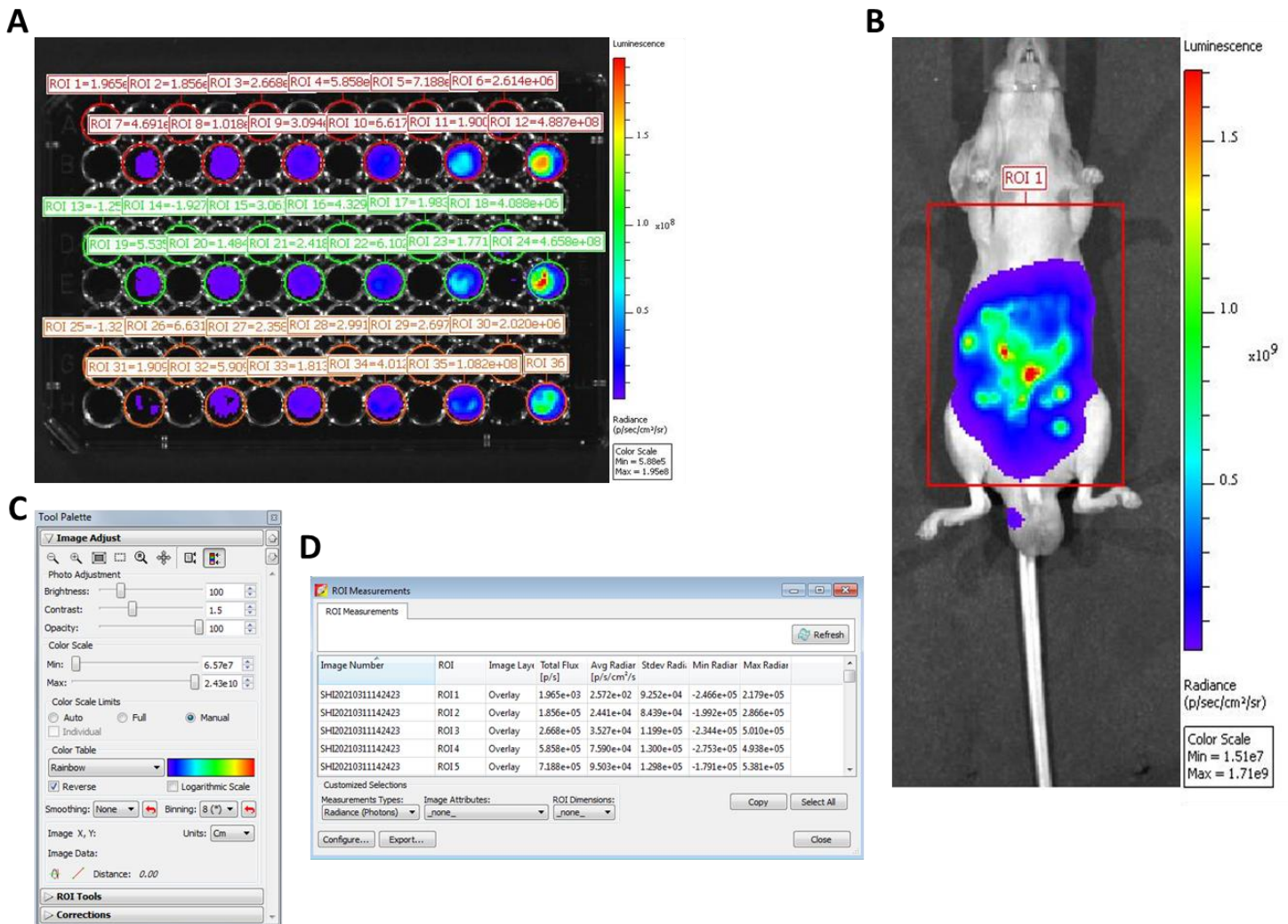


**Figure 4.2 Calculation of bioluminescence total flux using a region of interest (ROI) tool**

The ROI was set to (A) each well containing luciferase tagged cells, where 2JP clone 2 is indicated by red ROIs, 3JP clone 3 is indicated by green ROIs and 4JP clone 4 is indicated by orange ROIs, or (B) the abdomen of each mouse. (C) Image adjust settings were used to set the minimum and maximum colour scales to the same range for all quantification within the same experiment. (D) Total flux (p/s) was calculated from the average radiance obtained from each defined ROI.

#### 4.2.2.5 Animal drug treatments

Mice were administered with 3 mg/kg CDDO-Me via intraperitoneal (IP) injection. CDDO-Me was solubilised in 100 % DMSO and administered at 1  $\mu$ L/g of bodyweight. Animals received injections of CDDO-Me at day 14, 15, 16 and 19 post orthotopic tumour xenograft (Fig 4.3). Dosing reflects the same regimen used in the PHx model outlined in chapter 2 in which enhanced liver regeneration was observed. 100 % DMSO was used as a control in all studies.

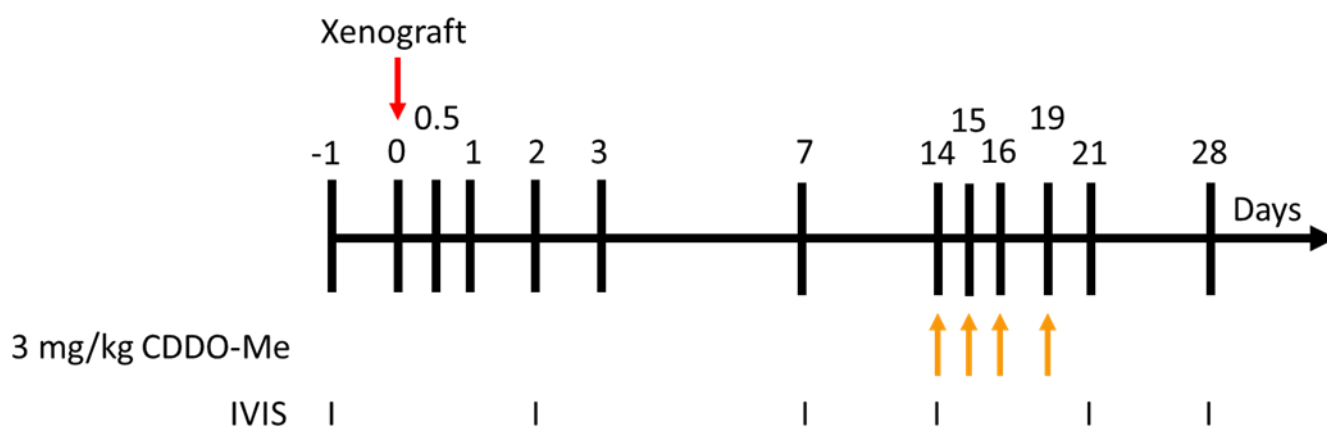


**Figure 4.3 Orthotopic tumour xenograft and bioluminescence imaging study design**

Study design. Mice underwent an orthotopic tumour xenograft on day 0. Mice were treated or not with 3 mg/kg CDDO-Me on days 14, 15, 16 and 19. Bioluminescence was conducted on days -1, 2, 7, 14, 21 and 28.

### 4.2.3 Western blotting

Western blotting was conducted using mouse liver tissue lysates. Total protein content was quantified as previously outlined in section 2.2.2 and liver tissue lysates were prepared to a final concentration of 1  $\mu\text{g}/\mu\text{L}$ .

Western blotting was then conducted as previously described in section 2.2.3 using the antibodies listed in Table 4.2 and Table 4.3.

**Table 4.2 Primary antibodies for Western blot**

<b>Primary Antibody</b>	<b>Dilution Factor (in 10 % Blotting Grade Blocker in 1x TBS-T)</b>	<b>Incubation Time</b>	<b>Washes (using 1x TBS-T)</b>
Nrf2 (16396-1-AP, Proteintech / Rabbit / Polyclonal)	1:1,000	Overnight at 4 °C	4x 5 min
Nqo1 (ab2346, Abcam / Goat / Polyclonal)	1:2,500	Overnight at 4 °C	4x 5 min
PCNA (ab29, Abcam / Mouse / Monoclonal)	1:2,000	Overnight at 4 °C	4x 5 min
$\beta$ Actin (ab6276, Abcam / Mouse / Monoclonal)	1:10,000	1 hour at room temp	4x 5 min

**Table 4.3 Secondary antibodies for Western blot**

<b>Secondary Antibody</b>	<b>Dilution Factor (in 10 % Blotting Grade Blocker in 1x TBS-T)</b>	<b>Incubation Time</b>	<b>Washes (using 1x TBS-T)</b>
Anti-Rabbit HRP (A9169, Sigma / Goat / Polyclonal)	1:5,000	1 hour at room temp	4x 5 min
Anti-Goat HRP (P044901-2, Agilent / Rabbit / Polyclonal)	1:5,000	1 hour at room temp	4x 5 min
Anti-Mouse HRP (A9044, Sigma / Rabbit / Polyclonal)	1:5,000	1 hour at room temp	4x 5 min

#### 4.2.4 Histological examinations

Healthy liver tissue, liver tissue containing tumours from xenografted cells and organs in which metastasis was observed were fixed in 4 % Paraformaldehyde (PFA) before being sectioned and embedded in paraffin wax. Sections were then routinely stained with haematoxylin-eosin (HE).

Processing and staining was carried out by Dr. Julie Haigh, Histology Laboratories, Department of Veterinary Pathology and Public Health, Institute of Veterinary Sciences, University of Liverpool.

HE-stained sections were then examined for pathological alterations consistent with the proliferative and non-proliferative lesions of the mouse hepatobiliary system and scored according to the scoring system published by Thoolen et al. (Thoolen et al., 2010). Examination of HE-stained sections was carried out by Dr. Emanuele Ricci, Histology Laboratories, Department of Veterinary Pathology and Public Health, Institute of Veterinary Sciences, University of Liverpool. In addition, all sections were examined for tumour fibrosis and necrosis, and scored accordingly. Mitotic index was calculated by counting the number of mitoses in 10 randomly chosen non-overlapping high-power fields (HPFs). The number of masses were counted, and average size of each mass calculated in microns ( $\mu\text{m}$ ), in 10 randomly chosen non-overlapping HPFs.



#### 4.2.5 Statistical analysis

As indicated in each figure legend, statistical analysis was carried out using Stats Direct 3 software. P values are reported to three decimal places. For Student t tests and Mann-Whitney U tests, two-tailed P values are reported. Differences were considered significant at  $P \leq 0.05$ .

## 4.3 Results

### 4.3.1 Puromycin dose response

In all wild-type, non-transfected cells: HepG2, Huh7, HCT116 and SW480, the ATP content decreased as the concentration of puromycin increased from 0 to 9  $\mu\text{g}/\text{mL}$ , indicating cell death. In all cells, 1.8  $\mu\text{g}/\text{mL}$  puromycin was effective in producing an ATP content  $< 10\%$  of the level of untreated cells, indicating sufficient cell death of  $> 90\%$  for successful selection of transfected cells (Fig 4.4)

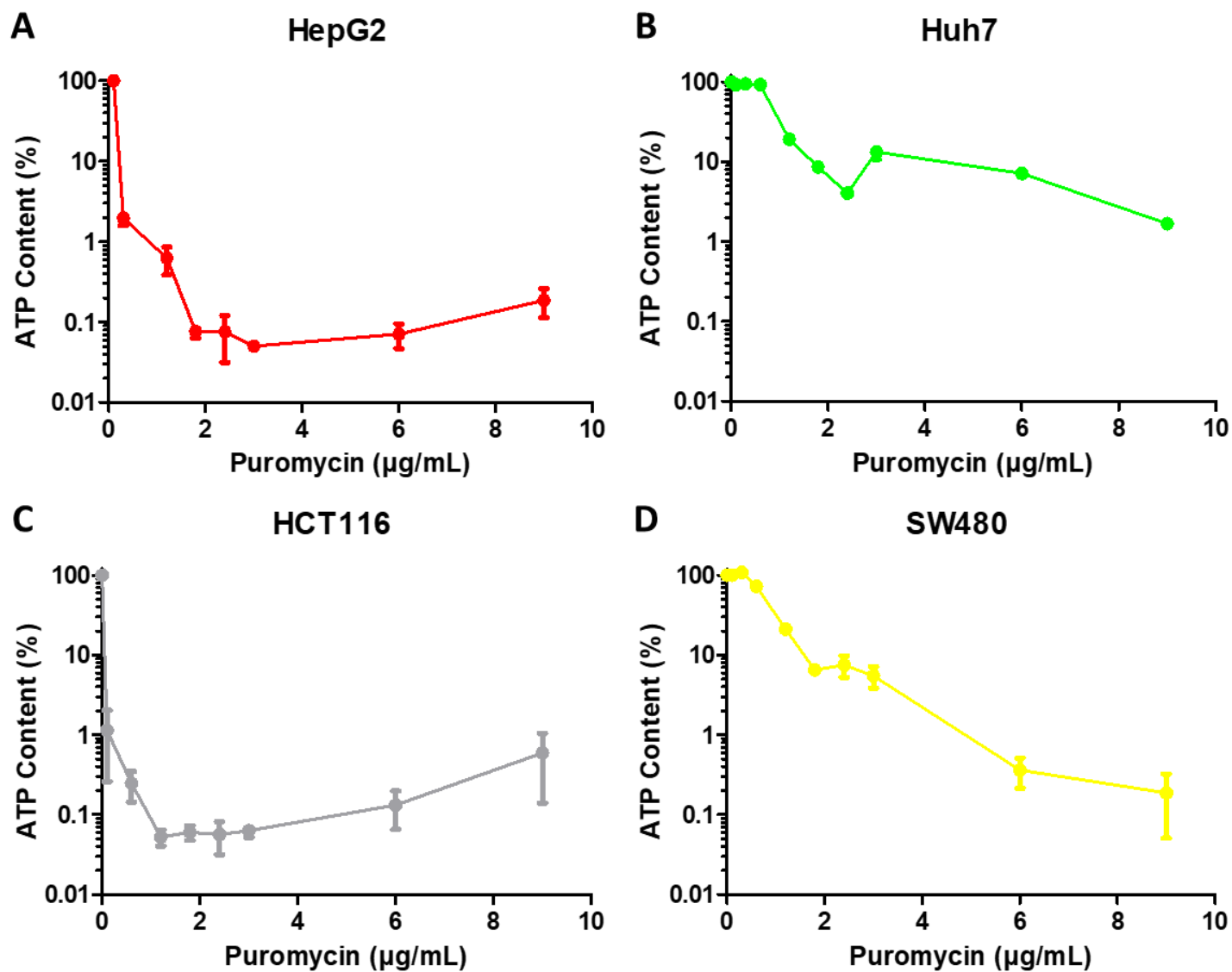


**Figure 4.4** Dose response curves of wild-type, non-transfected HepG2, Huh7, HCT116 and SW480 cells in response to treatment with puromycin.

Dose response curve of wild-type, non-transfected (A) HepG2, (B) Huh7, (C) HCT116 and (D) SW480 cells in response to treatment with puromycin. Data analysis represents mean  $\pm$  SD of triplicate wells, n=1.

### 4.3.2 Confirmation of luciferase presence in cells using an *in vitro* luciferase assay

Initially wild-type cells were seeded alongside the three transfected clones: 2JP clone 2, 3JP clone 3 and 4JP clone 4. Luminescence was then quantified using the Bright-Glo™ Luciferase Assay System (Promega). In transfected HepG2 cells, 2JP clone 2 possessed higher luciferase content than 3JP clone 3, and due to the cells not growing, the luciferase content was not determined for 4JP clone 4. Following transfection of Huh7 cells, only 2JP clone 2 cells grew and thus luciferase content was only determined for this clone. In transfected HCT116 cells, luciferase content peaked in 3JP clone 3 cells, with 2JP clone 2 and 4JP clone 4 producing lower levels of luciferase. Similarly, in transfected SW480 cells, luciferase content peaked in 3JP clone 3 cells with 2JP clone 2 and 4JP clone 4 cells producing slightly lower levels of luciferase (Fig 4.5).

To then further confirm successful transfection and investigate if the luminescent signal produced was dependent on the density of cells seeded, the three transfected clones were seeded in a 96 well plate at numerous cell densities. In transfected HepG2 cells, both 2JP clone 2 and 3JP clone 3 cells produced luciferase in a cell density dependent manner, with luciferase content increasing as the number of cells seeded increased. Peak luciferase content was observed in HepG2 2JP clone 2 cells (Fig 4.6 A). In Huh7 transfected cells, the luciferase content of 2JP clone 2 cells increased in a cell density dependent manner (Fig 4.6 B). In transfected HCT116 cells, the luciferase content of all three transfected clones increased in a cell density dependent manner, with 3JP clone 3 producing the highest level of luciferase (Fig 4.6 C). Similarly, in transfected SW480 cells, the luciferase content of all three clones increased in a cell density dependent manner, with 3JP clone 3 producing the highest level of luciferase (Fig 4.6 D).

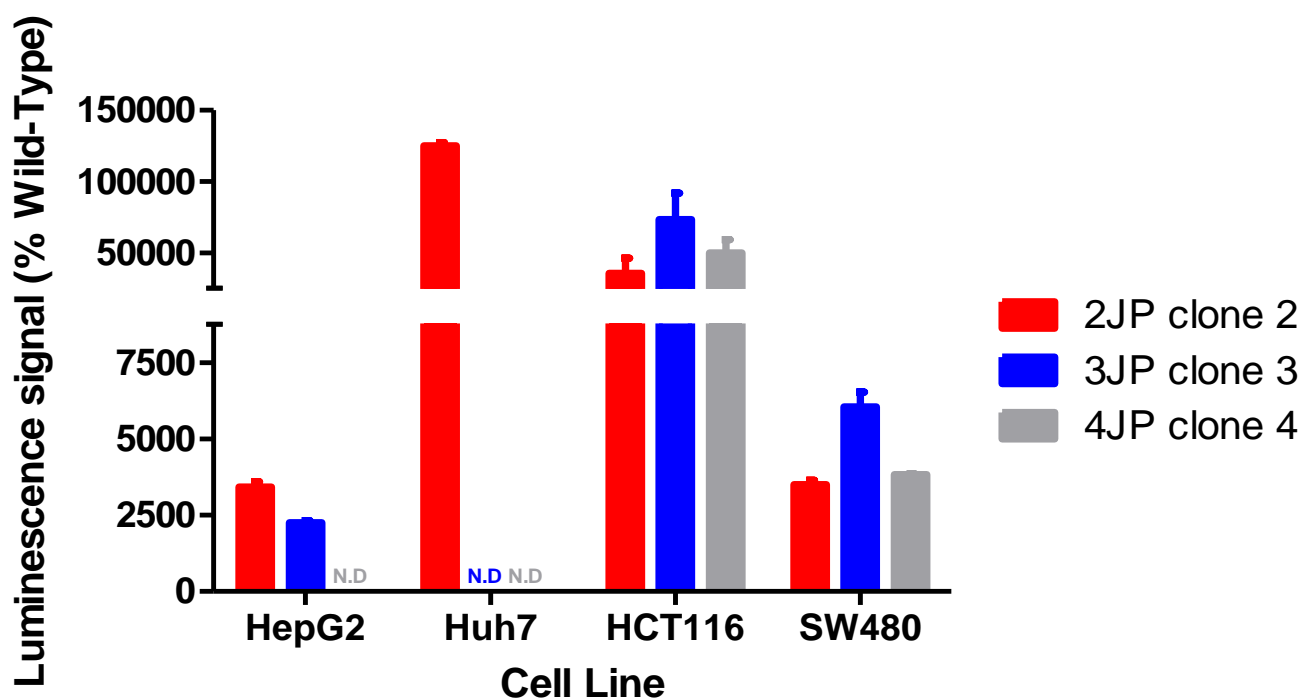
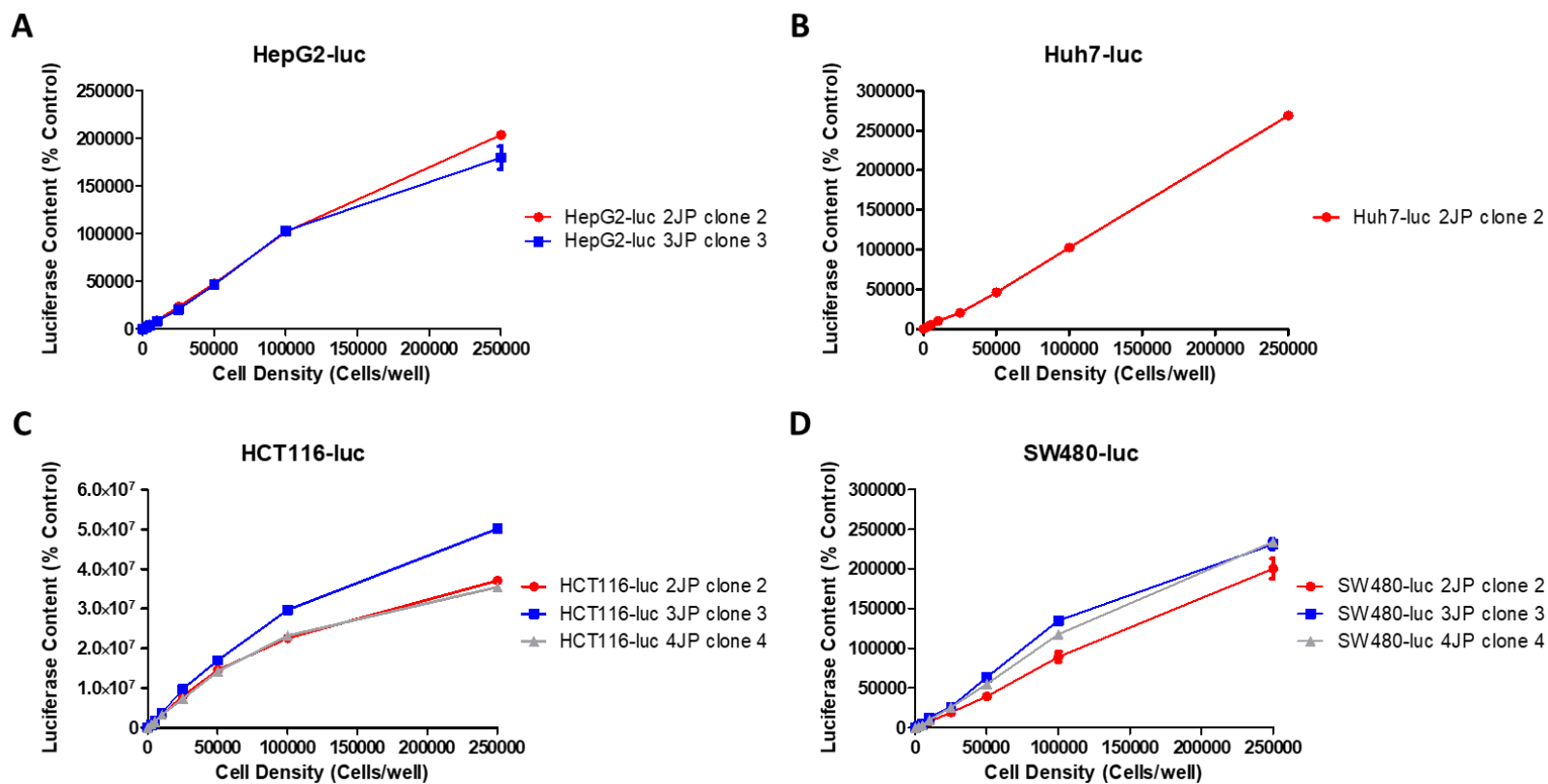


Figure 4.5 Luminescence signal of transfected HepG2, Huh7, HCT116 and SW480 cells

For each cell line, three luciferase clones were produced: 2JP clone 2, 3JP clone 3 and 4JP clone 4.

Cells were plated in a 96 well plate at 25,000 cells per well prior to quantification of luciferase content. Luciferase content of transfected cells was normalised to that of wild-type, non-transfected, cells. N.D represents non-determined values. Data analysis represents mean  $\pm$  SD of triplicate wells, n=1.



**Figure 4.6 Cell density dependent luciferase content of transfected HepG2, Huh7, HCT116 and SW480 cells**

Three luciferase clones, 2JP clone 2, 3JP clone 3 and 4JP clone 4, were plated in a 96 well plate at 250,000, 100,000, 50,000, 25,000, 10,000, 5,000 and 2,500 cells per well prior to quantification of luciferase content. Luciferase content of transfected cells was normalised to that of wells containing culture media only. Data analysis represents mean  $\pm$  SD of triplicate wells, n=1.

### 4.3.3 Confirmation of luciferase presence in cells using IVIS bioluminescence imaging

Luciferase transfected cells were seeded in a black 96 well plate at 250,000, 100,000, 50,000, 25,000, 10,000, 5,000, 2,500 and 1,000 cells per well. *In vivo* grade luciferin was then added to all wells prior to IVIS imaging and subsequent ROI analysis using Living Image<sup>®</sup> software. In transfected HepG2 cells, the total flux increased in a cell density dependent manner in both clones, with 2JP clone 2 producing higher total flux levels (Fig 4.7 A and B). In transfected Huh7 cells, the total flux in 2JP clone 2 increased in a cell density dependent manner (Fig 4.7 C and D). Again, as only 2JP clone 2 cells grew in the Huh7 cell line, total flux was only determined for this clone. In transfected HCT116 cells, the total flux increased in a cell density dependent manner for all three luciferase clones, with 2JP clone 2 producing the greatest level of total flux (Fig 4.8 A and B). In transfected SW480 cells, the total flux increased in all three luciferase clones in a cell density dependent manner with 3JP clone 3 producing the greatest level of total flux (Fig 4.8 C and D).

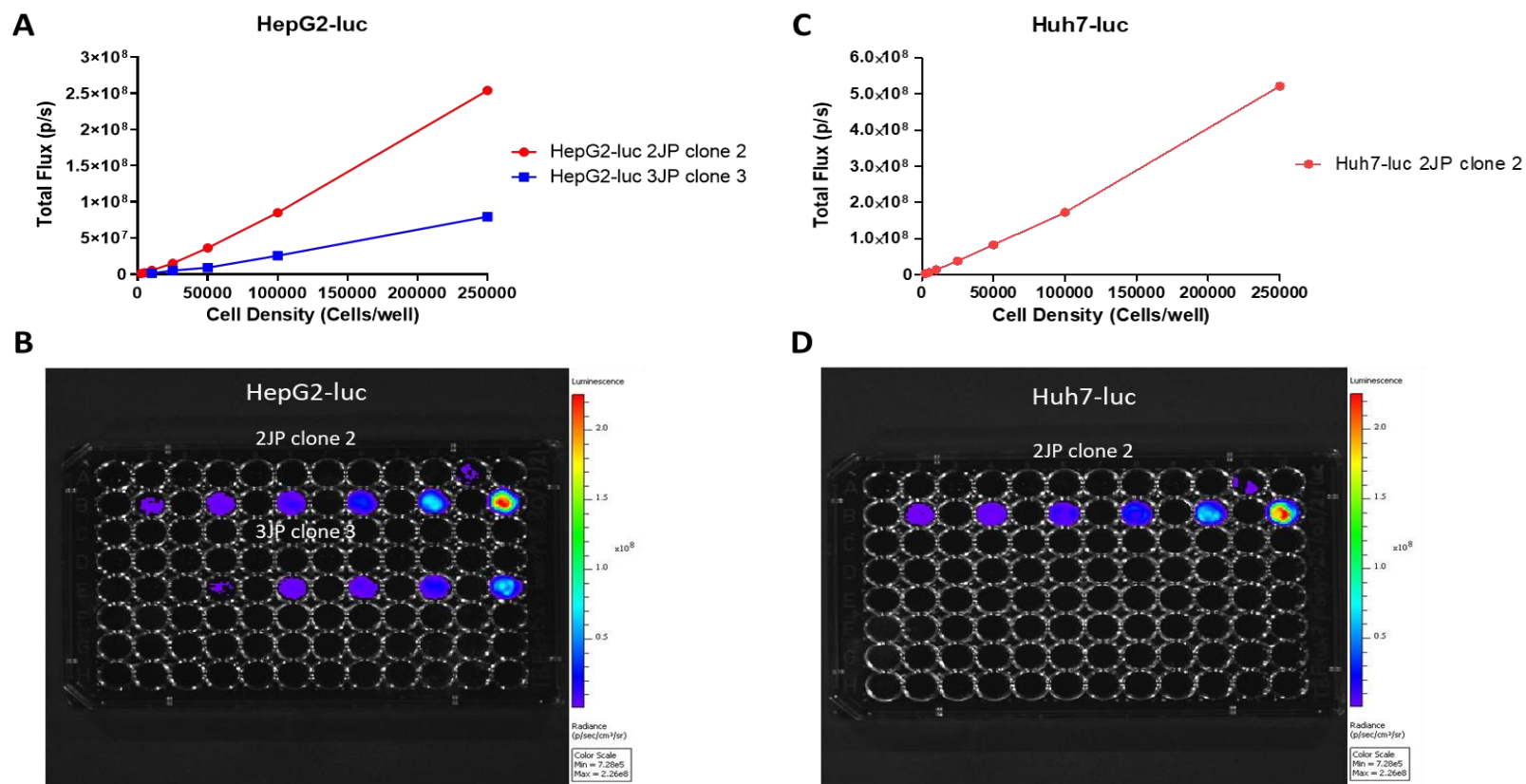


**Figure 4.7** Luciferase content of luciferase transfected HCC HepG2 and Huh7 cells quantified via IVIS bioluminescence imaging

Three luciferase clones, 2JP clone 2, 3JP clone 3 and 4JP clone 4, were plated in a black 96 well plate at 250,000, 100,000, 50,000, 25,000, 10,000, 5,000, 2,500 and 1,000 cells per well prior to quantification of luciferase content, represented as total flux (p/s), via IVIS bioluminescence imaging and subsequent ROI analysis. Data represents values from a single well, n=1.



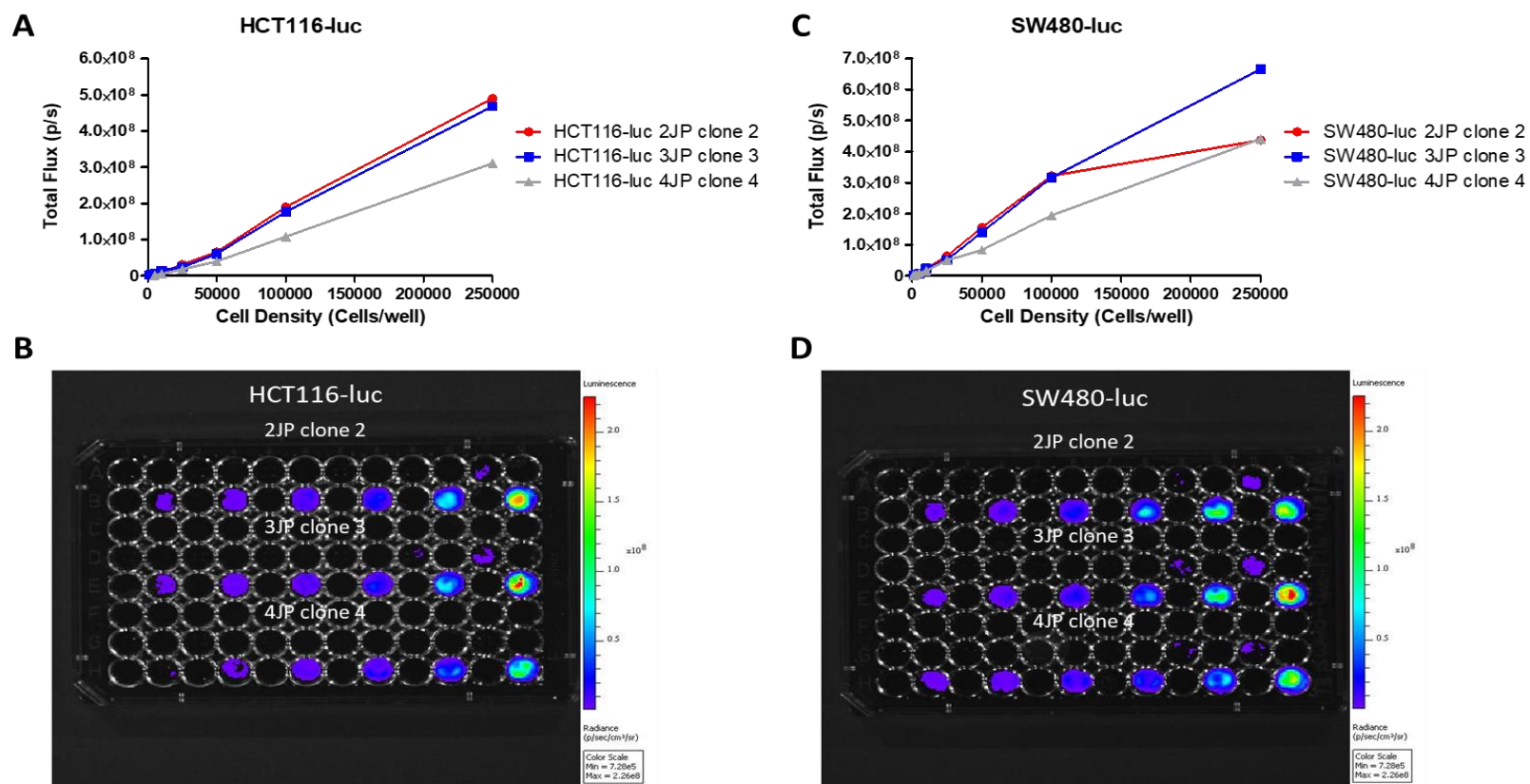


**Figure 4.8** Luciferase content of luciferase transfected CRC HCT116 and SW480 cells quantified via IVIS bioluminescence imaging

Three luciferase clones, 2JP clone 2, 3JP clone 3 and 4JP clone 4, were plated in a black 96 well plate at 250,000, 100,000, 50,000, 25,000, 10,000, 5,000, 2,500 and 1,000 cells per well prior to quantification of luciferase content, represented as total flux (p/s), via IVIS bioluminescence imaging and subsequent ROI analysis. Data represents values from a single well, n=1.

#### 4.3.4 *In vivo* model selection

Male CB17-SCID, NOD-SCID, BALB/c Nude and C57BL/6JRj received a single IP dose of either 3 mg/kg CDDO-Me or 100 % DMSO prior to being culled 24 hours post dose. The livers of mice were snap frozen and immunoblotting against Nrf2 and NQO1 was performed.

Treatment with CDDO-Me produced higher protein expression levels of Nrf2 in all strains of mice, when compared to treatment with DMSO, with significantly higher levels observed in BALB/c Nude and NOD-SCID mice ( $P = 0.013$  and  $< 0.001$  respectively). Treatment with CDDO-Me produced the highest Nrf2 protein expression levels in CB17-SCID mice, however this was not significantly higher than treatment with DMSO. Similarly, treatment with CDDO-Me produced significantly higher protein expression levels of NQO1 in all strains of mice when compared to treatment with DMSO ( $P = 0.001$  in C57BL/6JRj,  $P = 0.002$  in BALB/c Nude,  $P = 0.060$  in NOD-SCID and  $P = 0.036$  in CB17-SCID). Protein expression level of NQO1 was highest in NOD-SCID and CB17-SCID mice following treatment with CDDO-Me (Fig 4.9).

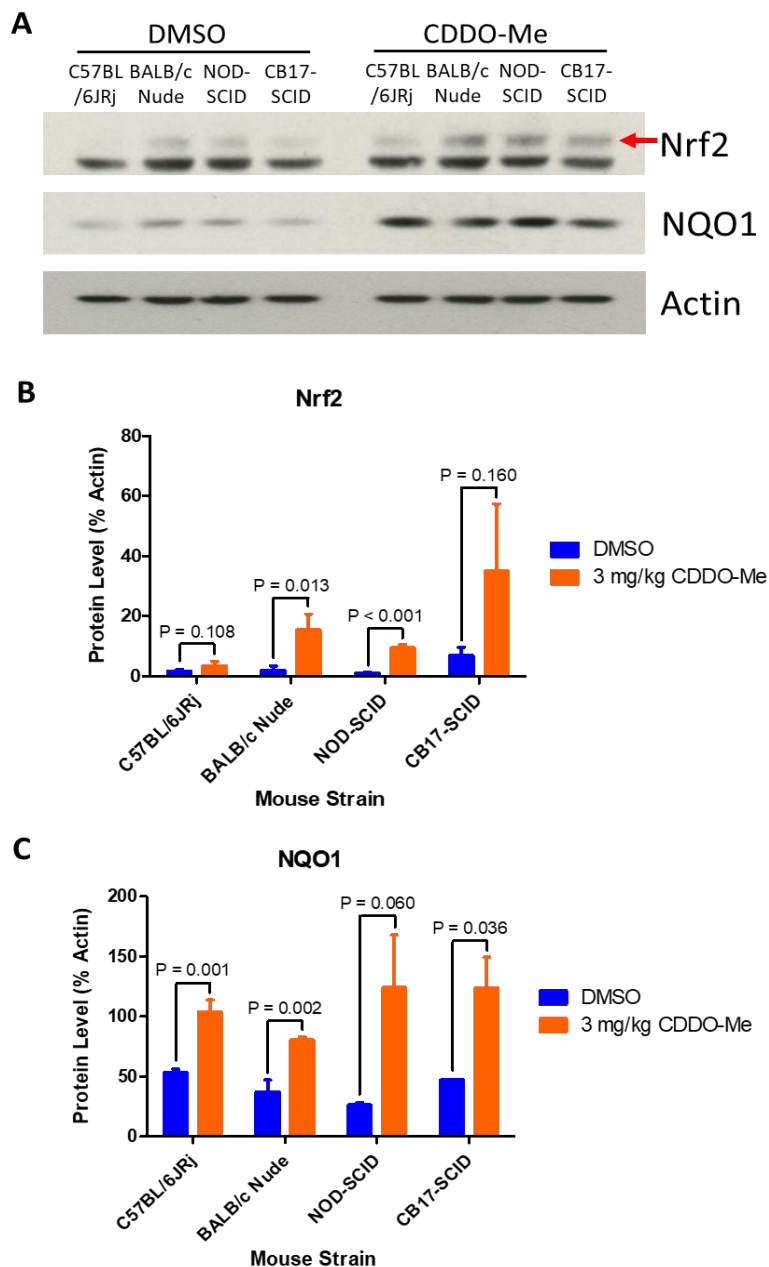


**Figure 4.9 Immunoblotting of livers from male CB17-SCID, NOD-SCID, BALB/c Nude and C57BL/6JRj mice following treatment with CDDO-Me**

(A) Western blot for Nrf2 and NQO1 of pooled liver lysates from male CB17-SCID, NOD-SCID, BALB/c Nude and C57BL/6JRj mice that were treated with DMSO or CDDO-Me. (B) Densitometry of Nrf2 immunoblotting from all liver lysates from male CB17-SCID, NOD-SCID, BALB/c Nude and C57BL/6JRj mice, normalised to Actin. (C) Densitometry of NQO1 immunoblotting from all liver lysates from male CB17-SCID, NOD-SCID, BALB/c Nude and C57BL/6JRj mice, normalised to Actin. (B and C) Unpaired t-test DMSO vs CDDO-Me. Data analysis represents mean  $\pm$  SD of n=3 animals per group.

### 4.3.5 Preliminary orthotopic tumour xenograft and *in vivo* bioluminescence imaging

#### 4.3.5.1 IVIS bioluminescence imaging

Initially, preliminary work involved xenografting HepG2-luc 2JP clone 2 and HCT116-luc 2JP clone 2 cells into the liver of BALB/c Nude mice at  $2 \times 10^6$  cells per mouse in 30  $\mu$ L Matrigel. HepG2-luc 2JP clone 2 cells were selected for the HCC cell line as they had far better transfection efficiency than Huh7-luc, with two clones being successfully produced. HCT116-luc 2JP clone 2 cells were selected for the CRC cell line as although the luminescence signal in SW480-luc cells was comparable, the signal in HCT116 was far more consistent, producing a much more linear curve (Fig 4.8 A). All mice then underwent IVIS bioluminescence imaging. As expected, the bioluminescent total flux increased with time for both xenografted cell lines, indicating tumour growth, with peak signal achieved on the final day of the study, 28 days post implantation of cells. HCT116-luc cells produced a greater total flux signal at all timepoints when compared to HepG2-luc cells. However, due to an unsuccessful xenograft in one of the mice receiving HCT116-luc cells, and subsequent large variation in total flux, there was no significant differences in total flux between the two cell lines (Fig 4.10 A). Following the xenograft of both cell lines, no adverse effects on animal body weight (Fig 4.10 B) or behaviour were observed.

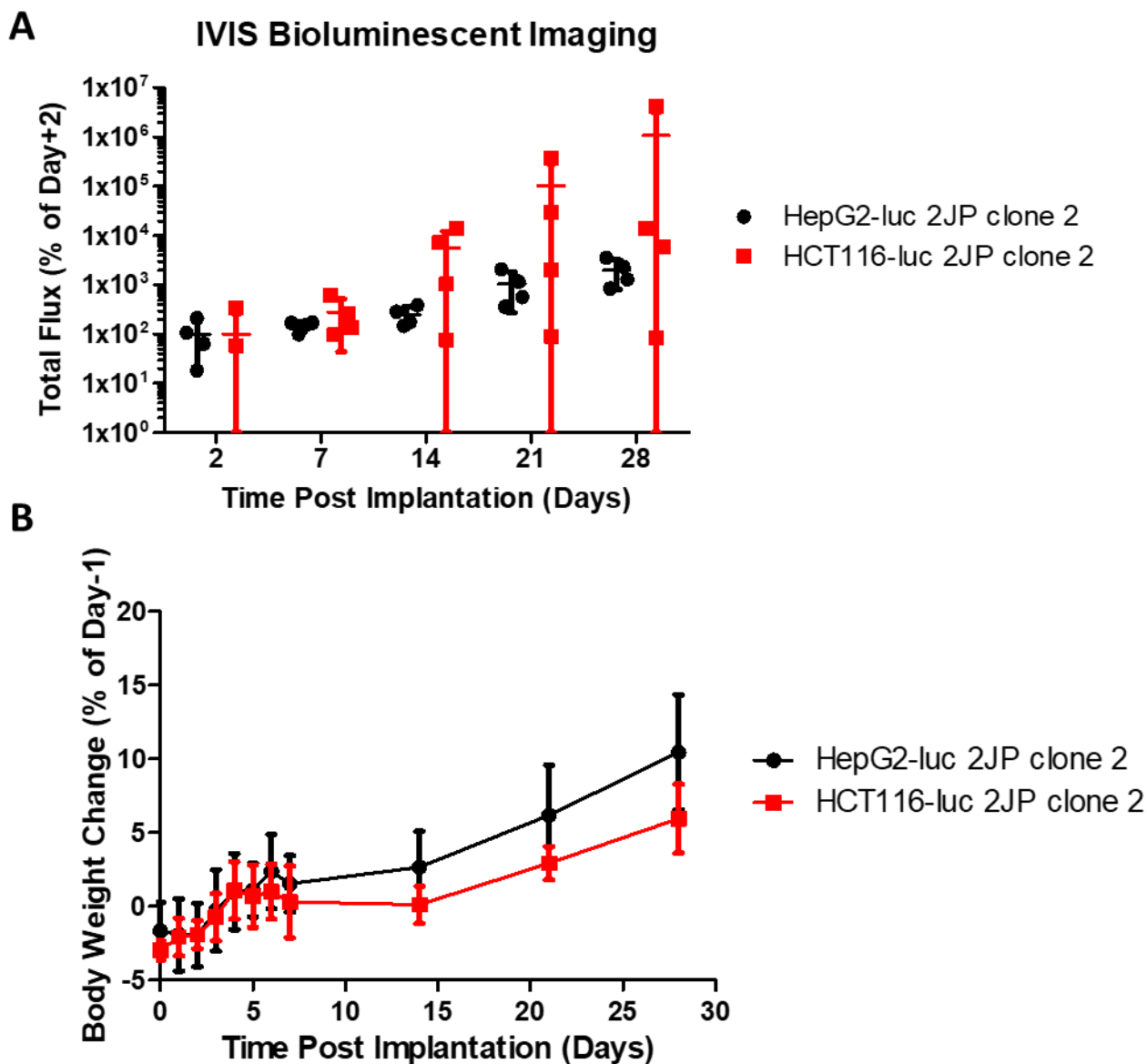
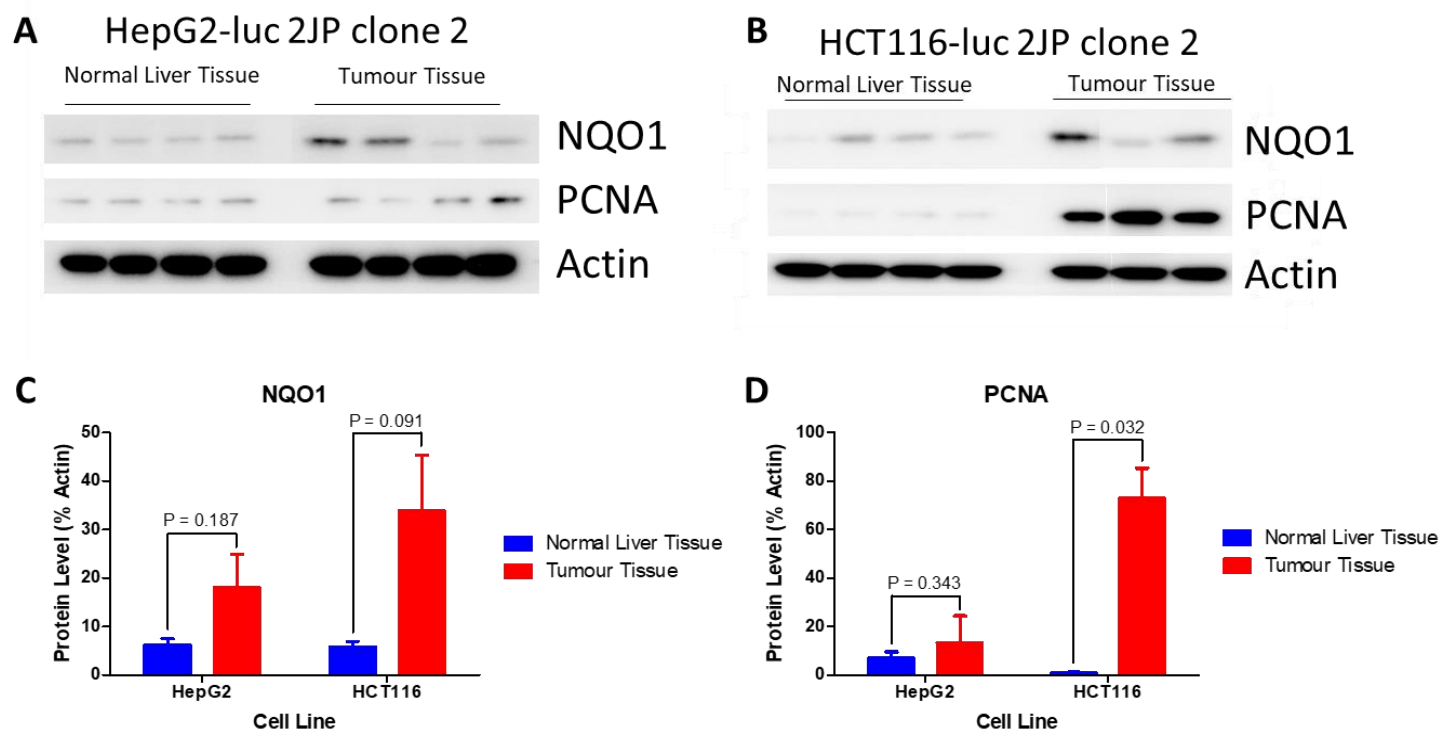


Figure 4.10 Preliminary *in vivo* bioluminescence imaging of mice xenografted with HepG2-luc or HCT116-luc cells.

(A) Total flux calculated following ROI analysis, of mice xenografted with HepG2-luc 2JP clone 2 or HCT116-luc 2JP clone 2 cells at indicated time points, normalised to total flux obtained at day 2. (B) Animal bodyweight change of mice xenografted with HepG2-luc 2JP clone 2 or HCT116-luc 2JP clone 2 cells at indicated time points. Data analysis represents mean  $\pm$  SD of  $n=4$  animals per group.

#### 4.3.5.2 Immunoblotting

Immunoblotting was then carried out against NQO1 and PCNA from lysates produced from normal liver tissue and tumour tissue formed from xenografted HepG2-luc 2JP clone 2 and HCT116 2JP clone 2 cells. In mice xenografted with HepG2-luc cells, tumour tissue possessed higher levels of NQO1 and PCNA, when compared to normal liver tissue, though these differences did not achieve statistical significance (Fig 4.11 A, C, D). In mice xenografted with HCT116-luc, tumour tissue possessed higher protein expression levels of NQO1 and PCNA when compared to normal liver tissue, with significantly higher levels of PCNA observed ( $P = 0.032$ ). Statistical significance was not observed in the protein expression levels of NQO1 (Fig 4.11 B, C, D).



**Figure 4.11 Immunoblotting of healthy liver tissue and liver tumour tissue from male BALB/c Nude xenografted with HepG2-luc or HCT116-luc cells**

Western blot for NQO1 and PCNA of normal liver, and tumour, lysates from male BALB/c Nude mice xenografted with (A) HepG2-luc 2JP clone 2 or (B) HCT116-luc 2JP clone 2 cells. (C) Densitometry of NQO1 immunoblotting from normal liver and tumour lysates, normalised to Actin. (D) Densitometry of PCNA immunoblotting from normal liver and tumour lysates, normalised to Actin. (C and D) Unpaired t-test healthy liver vs liver tumour. Data analysis represents mean  $\pm$  SD of n=3-4 animals per group.

#### **4.3.5.3 Macroscopic analysis of tumour mass**

Following cull and dissection, photos of the liver and inclusive tumour formed from xenografting either HepG2-luc 2JP clone 2 or HCT116-luc 2JP clone 2 cells, were taken. Xenografted HepG2-luc cells formed very small tumours, localised to the subcapsular location within the lobe they were implanted into (Fig 4.12 A). In contrast, xenografted HCT116-luc cells formed large tumour masses which extended far beyond both the subcapsular implant location, and the entire liver itself, expanding into the abdominal cavity below the liver (Fig 4.12 B).



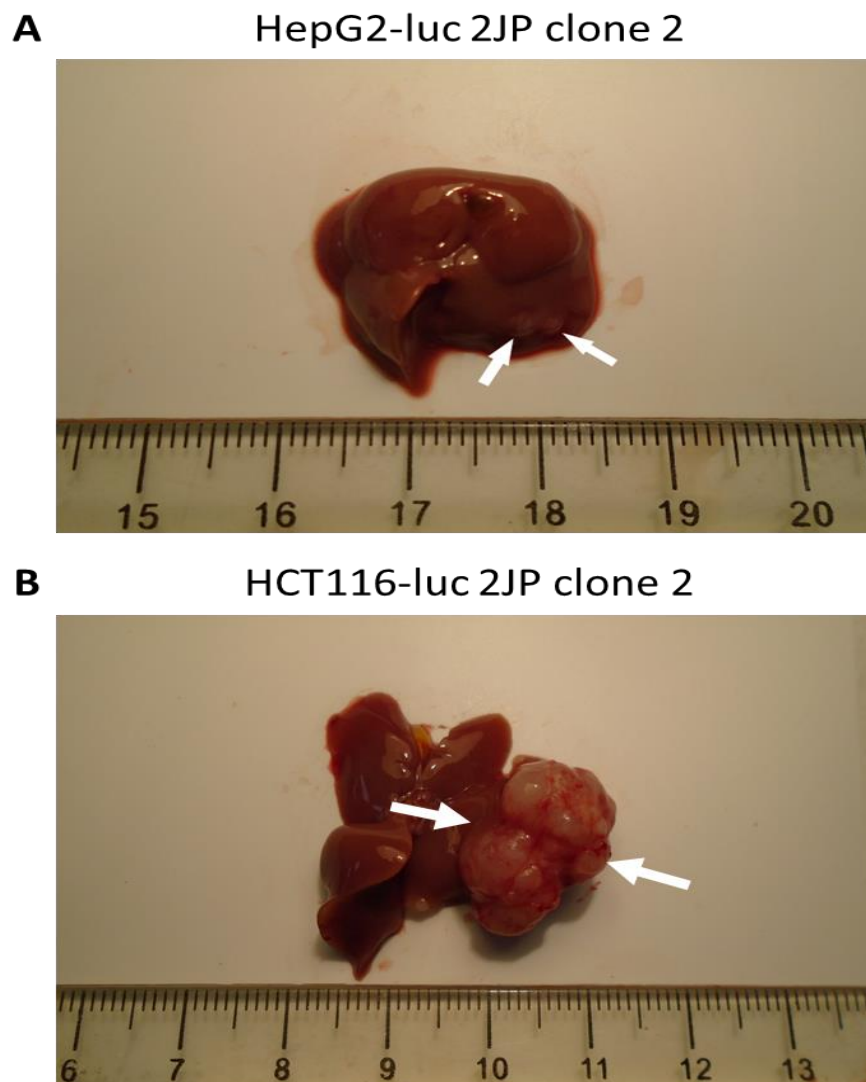


**Figure 4.12** *Ex vivo* photographs of tumours resulting from orthotopic xenograft of HepG2-luc or HCT116-luc cells in male BALB/c Nude mice.

*Ex vivo* Photographs of mouse liver and inclusive tumour, resulting from orthotopic xenograft of (A) HepG2-luc 2JP clone 2 or (B) HCT116-luc 2JP clone 2 cells in male BALB/c Nude mice. White arrows indicate location of tumour mass.

#### 4.3.5.4 Histological examination

Preliminary histological examinations were also carried out on the livers and inclusive tumours from mice xenografted with either HepG2-luc or HCT116-luc cells. It was found that both cell lines were viable and capable of inducing neoplastic masses within murine tissue. Tumours formed from HepG2-luc cells were commonly observed within the hepatic parenchyma, more often within or in close proximity to the portal spaces. Furthermore, tumours formed from HepG2-luc cells possessed an average mitotic index of 3 and an average scoring grade of 1, indicating marginal/minimal severity and a very small proportion of tissue affected (Table 4.4).

In contrast, tumours formed from HCT116-luc cells were almost exclusively present in close contact with thin collagenous strands of the peritoneum and mesentery, and commonly infiltrating the organs from a primary implantation site. Tumours formed from HCT116-luc cells created frequent large lakes of coagulative necrosis at the centre of neoplastic nodules and were more frequently accompanied by mild lymphocytic infiltration and local tissue reaction (mesothelial hyperplasia and neoangiogenesis). In addition, consistent with observations made via IVIS bioluminescence imaging and photographed tumours following cull, HCT116-luc tumours consistently induced a 'carcinomatosis-like' implantation and dissemination pattern across both peritoneal serosa and pleura, forming neoplastic masses many-fold larger than the ones created from HepG2-luc cells. The average mitotic index of tumours formed from HCT116-luc cells was 5.75 and the average scoring grade was 3, indicating moderate/severe severity and a medium proportion of tissue affected (Table 4.4). Furthermore, HCT116-luc xenografted cells were capable of metastasising across, and within, organs via intravascular metastasis and embolization via adherence to hepatic endothelial cells, with metastases observed in the lungs, spleen, bowel, stomach, and large intestine.

**Table 4.4 Parenchymal lesion scoring criteria**

From (Thoolen et al., 2010)

<b>Severity</b>	<b>Proportion of Affected Tissue</b>	<b>Grade</b>	<b>Quantifiable Finding</b>	<b>Quantifiable Finding (%)</b>
Marginal/minimal	Very small amount	1	1-2 foci	1-20 %
Slight/few	Small amount	2	3-6 foci	21-40 %
Moderate/several	Medium amount	3	7-12 foci	41-60 %
Marked/many	Large amount	4	> 12 foci	61-80 %
Severe	Very large amount	5	Diffuse	> 80 %

**Table 4.5 Tumour fibrosis and necrosis scoring criteria**

<b>Scoring Criteria</b>	<b>Grade / Severity</b>		
	<b>1 / Mild</b>	<b>2 / Moderate</b>	<b>3 / Severe</b>
<b>Tumour Fibrosis</b>	Just thin, supportive stroma. Small amount of collagen fibres	Fibroblasts and collagen fibres mixed in various ratios	Mainly compromised of hyalinised collagen fibres
<b>Tumour Necrosis</b>	Sparse, small foci	Some masses have up to 50 % of necrosis	More than half of masses have 50 % of necrotic surface

### 4.3.6 Optimisation of orthotopic tumour xenograft and *in vivo* bioluminescence imaging

#### 4.3.6.1 IVIS bioluminescence imaging

Optimisation involved xenografting HepG2-luc 2JP clone 2 and HCT116-luc 2JP clone 2 cells into BALB/c Nude mice at  $1 \times 10^6$ ,  $5 \times 10^5$  or  $2.5 \times 10^5$  cells per mouse in 30  $\mu$ L Matrigel. All mice then underwent IVIS bioluminescence imaging. Mice xenografted with  $1 \times 10^6$  cells were treated or not with 3 mg/kg CDDO-Me on days 14, 15, 16 and 19 post orthotopic tumour xenograft. Such dosing pattern reflected the regimen used in the PHx model outlined in chapter 2 in which enhanced liver regeneration was observed. Initially, to assess luciferin kinetics and determine the most appropriate time to conduct IVIS bioluminescence imaging post luciferin administration, a luciferin time course was performed. Mice xenografted with HCT116-luc 2JP clone 2 cells were imaged at different time points post luciferin administration and total flux calculated via ROI analysis.

The level of total flux was found to increase with time, until 20 minutes post luciferin administration at which point a short plateau and subsequent decline in total flux was observed (Fig 4.13). In order to best capture total flux, an imaging time of 7.5 mins post luciferin was selected for all subsequent experimental images.

As expected, the bioluminescent total flux increased with time, with higher cell inoculums producing greater total flux in both xenografted cell lines. Animals xenografted with HepG2-luc 2JP clone 2 cells produced peak signal at 28 days post implantation in all cell inoculums (Fig 4.14 A). Interestingly, treatment with CDDO-Me, administered on days 14, 15, 16 and 19 post xenograft, had no impact on the level of total flux and no significant difference was observed when compared to untreated animals that were xenografted with the same number of cells (Fig 4.14 B). Animals xenografted with HCT116-luc 2JP clone 2 cells also produced peak signal at 28 days post implantation in all cell

inoculums (Fig 4.15 A). Treatment with CDDO-Me produced significantly higher levels of total flux at 28 days post implantation when compared to untreated animals that were xenografted with the same number of cells ( $P = 0.021$ ) (Fig 4.15 B). Following the xenograft of both cell lines, no adverse effects on animal bodyweight were observed in all cell inoculums or in those animals that were treated with 3 mg/kg CDDO-Me (Fig 4.16).

### Luciferin Kinetics

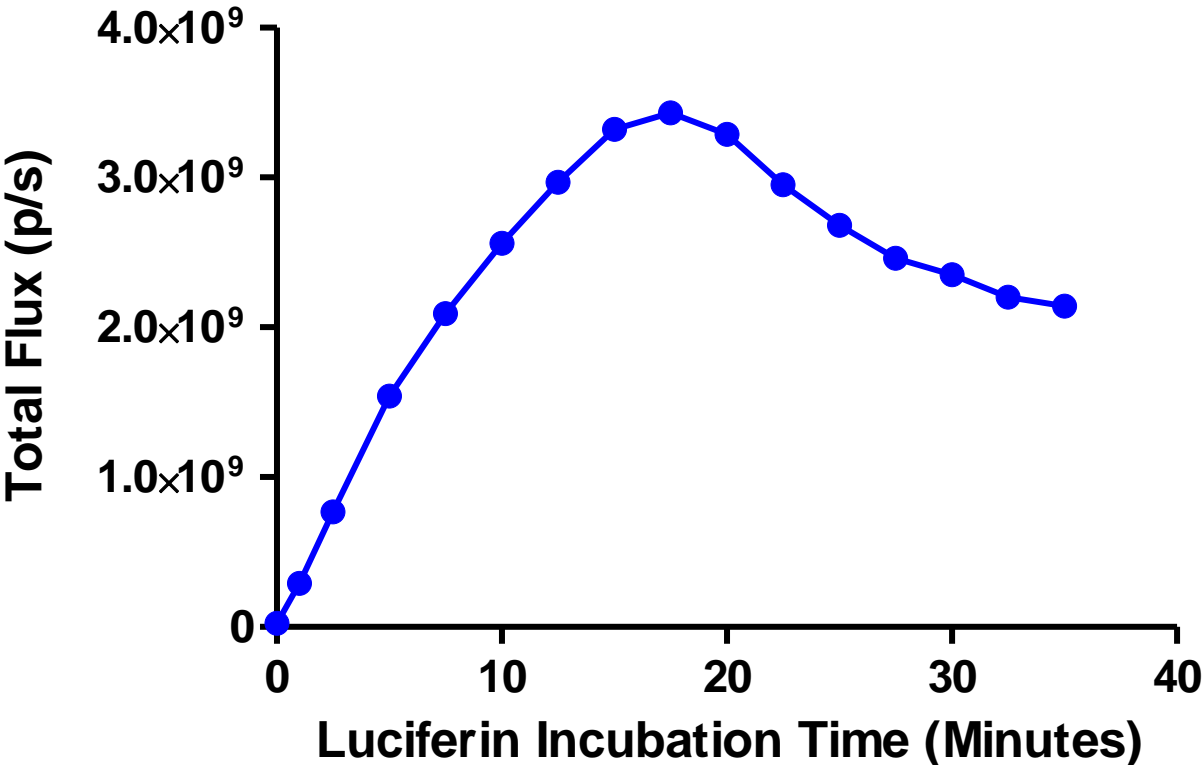
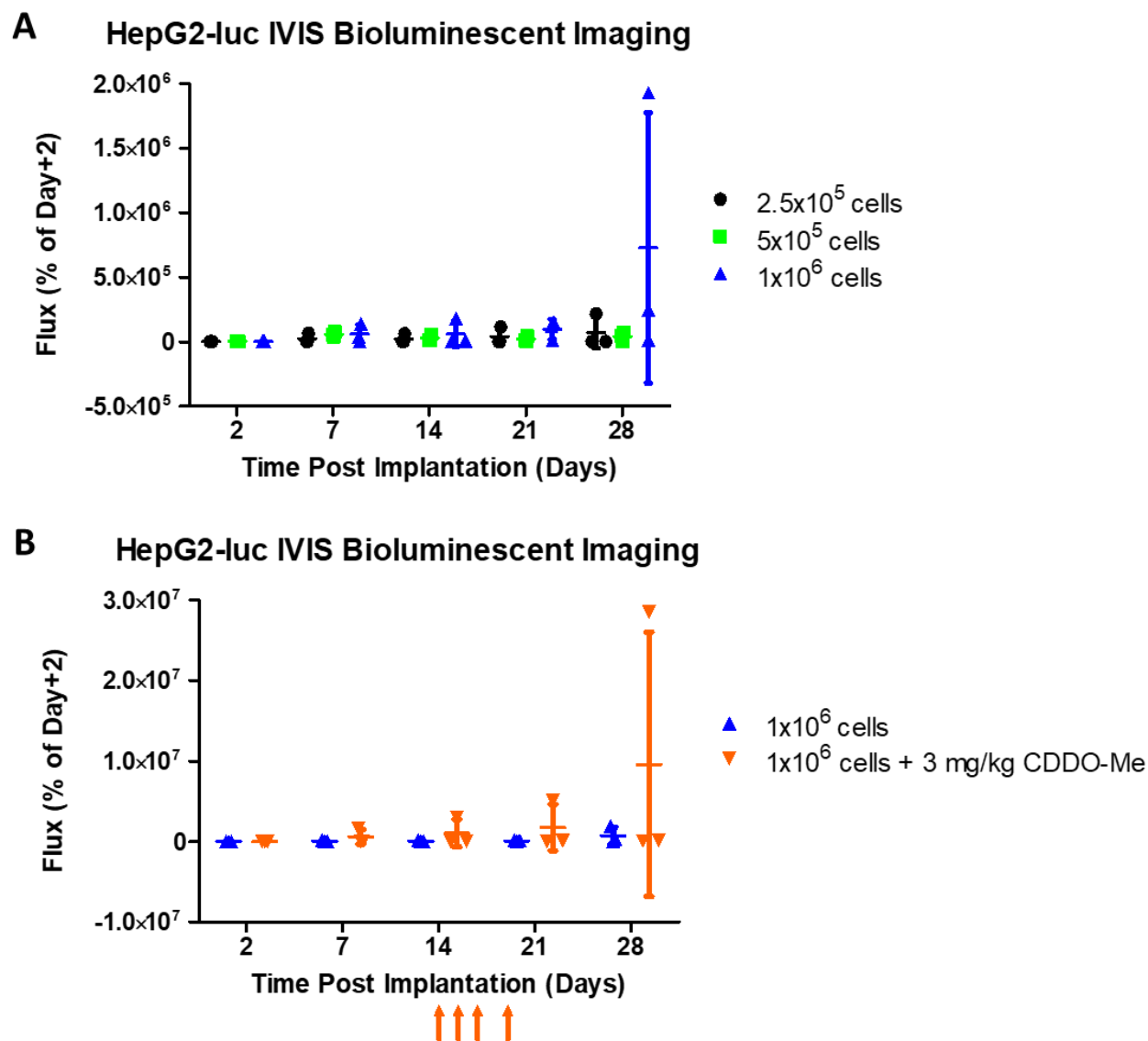


Figure 4.13 Luciferin kinetics of BALB/c Nude mice xenografted with HCT116-luc 2JP clone 2 cells

BALB/c Nude mice xenografted with HCT116-luc 2JP clone 2 cells were imaged at the indicated time points post luciferin administration and total flux calculated via ROI analysis. Data represents values from a single mouse, n=1.



**Figure 4.14 Optimisation of *in vivo* bioluminescence imaging of mice xenografted with HepG2-luc cells.**

(A) Untreated BALB/c Nude mice were xenografted with HepG2-luc 2JP clone 2 cells at the indicated cell inoculums prior to total flux being calculated following IVIS bioluminescence imaging at the indicated time points.

(B) BALB/c Nude mice, treated or not with 3 mg/kg CDDO-Me, were xenografted with  $1 \times 10^6$  cells prior to total flux being calculated following IVIS bioluminescence imaging at the indicated time points. Total flux was normalised to the total flux obtained at day 2. (B) Arrows indicate CDDO-Me administration at days 14, 15, 16 and 19. Unpaired t-test untreated vs CDDO-Me. Data analysis represents mean  $\pm$  SD of  $n=3$  animals per group.

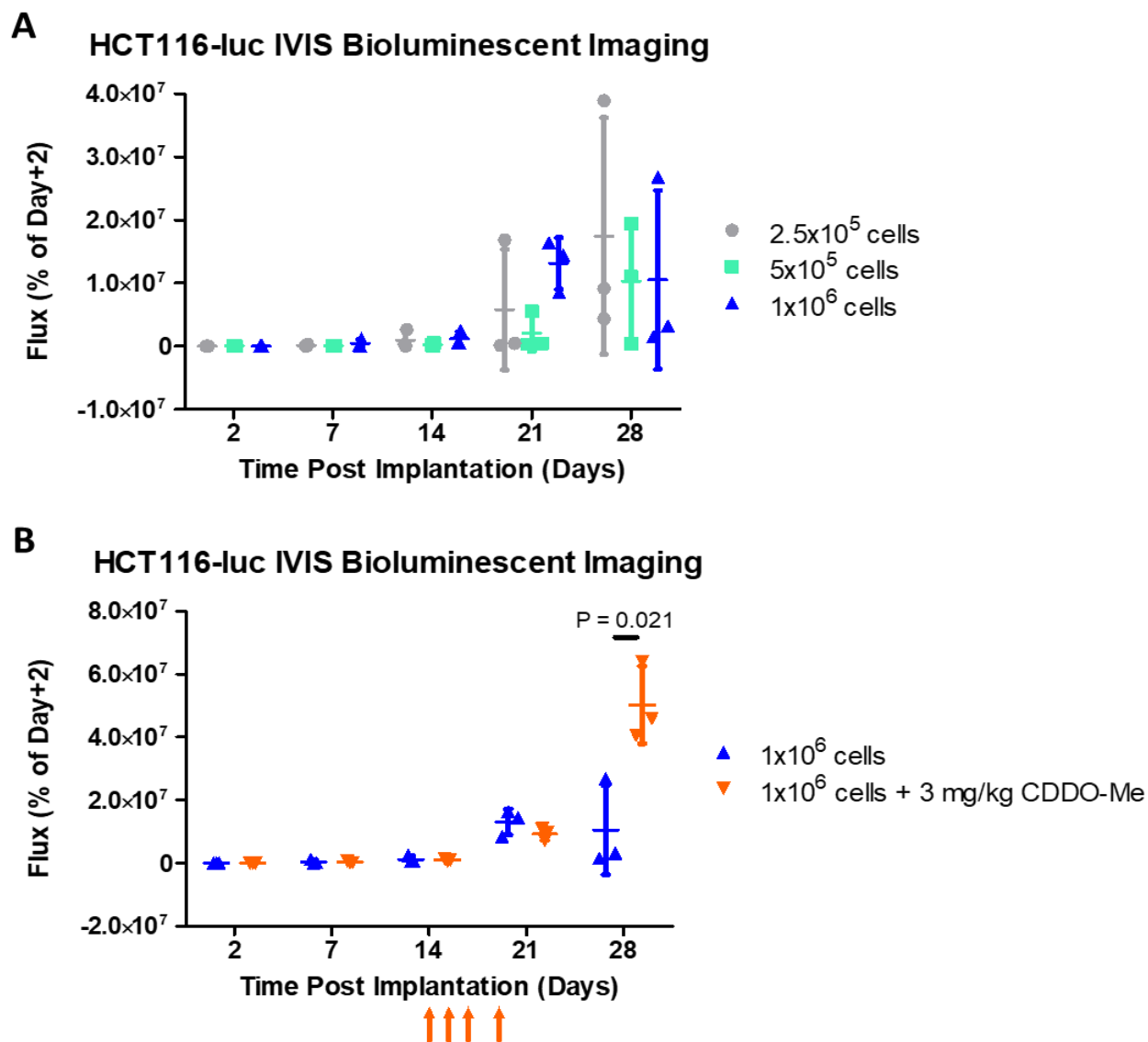


**Figure 4.15 Optimisation of *in vivo* bioluminescence imaging of mice xenografted with HCT116-luc cells.**

(A) Untreated BALB/c Nude mice were xenografted with HCT116-luc 2JP clone 2 cells at the indicated cell inoculums prior to total flux being calculated following IVIS bioluminescence imaging at the indicated time points.

(B) BALB/c Nude mice, treated or not with 3 mg/kg CDDO-Me, were xenografted with  $1 \times 10^6$  cells prior to total flux being calculated following IVIS bioluminescence imaging at the indicated time points. Total flux was normalised to the total flux obtained at day 2. (B) Arrows indicate CDDO-Me administration at days 14, 15, 16 and 19. Unpaired t-test untreated vs CDDO-Me. Data analysis represents mean  $\pm$  SD of  $n=3$  animals per group.



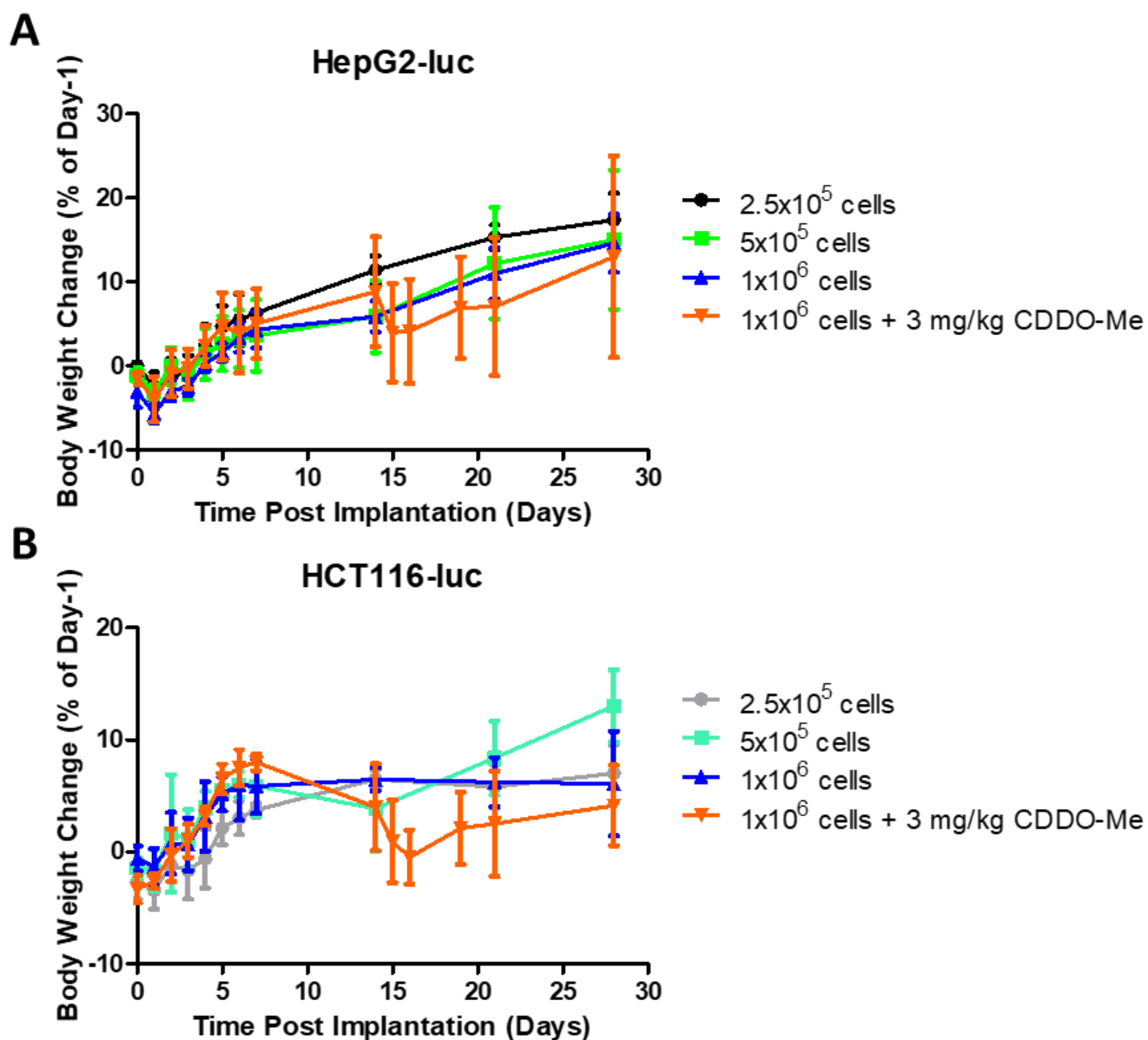


Figure 4.16 Bodyweight change of BALB/c Nude mice xenografted with HepG2-luc or HCT116-luc cells

Bodyweight change of mice xenografted with (A) HepG2-luc 2JP clone 2 or (B) HCT116-luc 2JP clone 2 cells at indicated cell inoculums at indicated time points. Data analysis represents mean  $\pm$  SD of n=3 animals per group.

#### 4.3.6.2 Immunoblotting

Immunoblotting was then carried out against NQO1 and PCNA from lysates produced from healthy liver tissue and liver tumour tissue formed from xenografted HepG2-luc 2JP clone 2 and HCT116-luc 2JP clone 2 cells. Mice xenografted with HepG2-luc cells had lower protein expression levels of NQO1 in tumour tissue when implanted with  $2.5 \times 10^5$  cells, but greater expression at all other cell inoculums when compared to healthy liver tissue, though these differences did not achieve statistical significance (Fig 4.17 A and B). Similarly, protein expression levels of PCNA were lower in tumour tissue following implantation of  $2.5 \times 10^5$  cells, but higher at all other inoculums when compared to healthy liver tissue. Again, none of these differences achieved statistical significance (Fig 4.17 A and C). Interestingly, treatment with CDDO-Me did not significantly alter the levels of either NQO1 or PCNA in tumour tissue when compared to healthy liver tissue.

Mice xenografted with HCT116-luc cells had higher protein expression levels of NQO1 in tumour tissue at all cell inoculums when compared to healthy liver tissue, though these differences did not reach statistical significance (Fig 4.18 A and B). Similarly, protein expression levels of PCNA were greater in tumour tissue at all cell inoculums when compared to healthy liver tissue, with significantly higher levels observed in mice implanted with  $2.5 \times 10^5$  cells and  $1 \times 10^6$  cells with CDDO-Me treatment ( $P = 0.031$  and  $< 0.001$  respectively) (Fig 4.18 A and C).

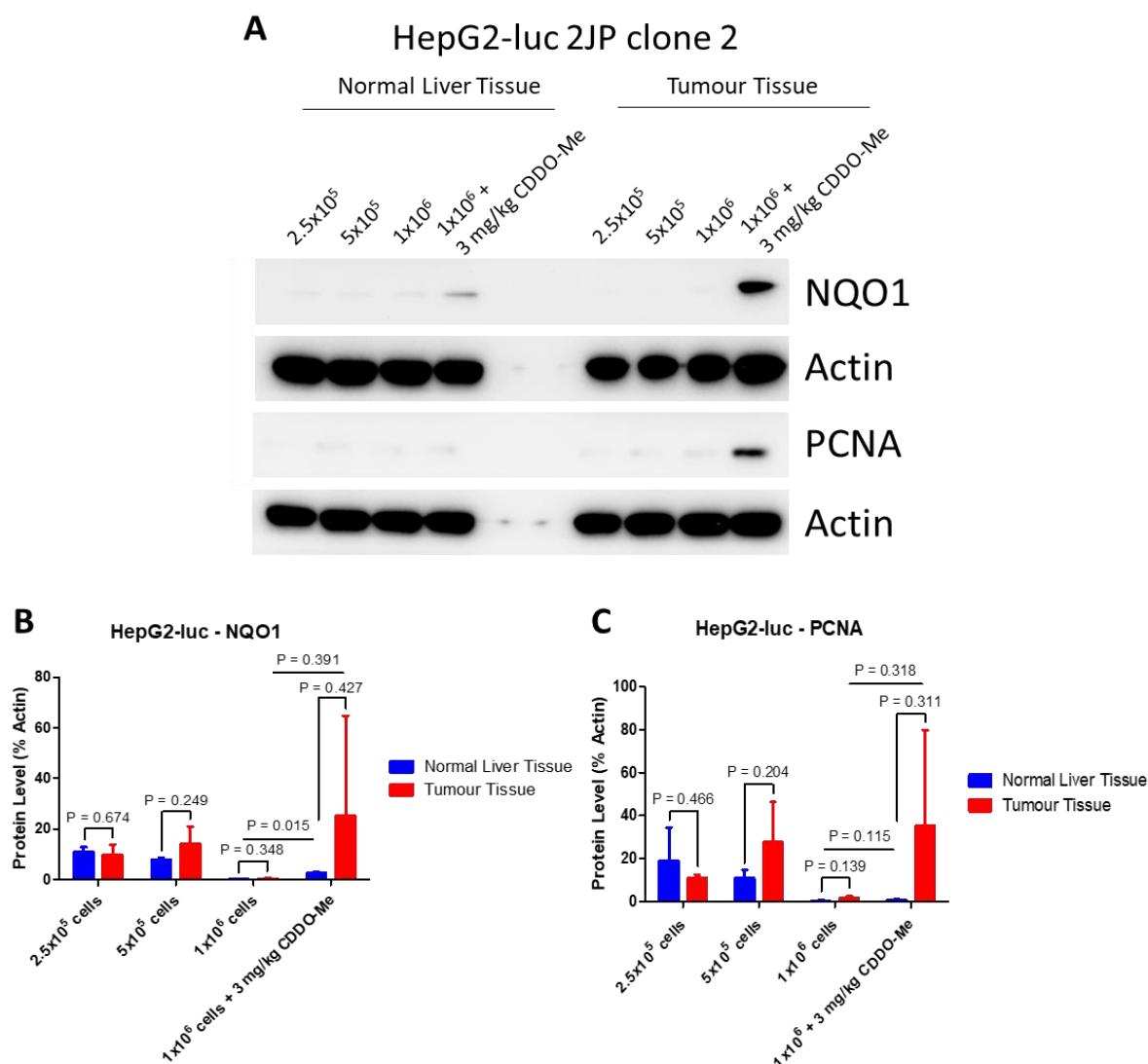


**Figure 4.17 Immunoblotting of healthy liver tissue and liver tumour tissue from male BALB/c Nude xenografted with HepG2-luc cells**

(A) Western blot for NQO1 and PCNA of healthy liver, and liver tumour, pooled lysates from male BALB/c Nude mice xenografted with HepG2-luc 2JP clone 2 cells at the indicated cell inoculums. Mice xenografted with 1x10<sup>6</sup> were treated or not with 3 mg/kg CDDO-Me. (B) Densitometry of NQO1 immunoblotting from healthy liver and liver tumour lysates, normalised to Actin. (C) Densitometry of PCNA immunoblotting from healthy liver and liver tumour lysates, normalised to Actin. (B and C) Unpaired t-test healthy liver vs liver tumour. Data analysis represents mean  $\pm$  SD of n=3 animals per group.

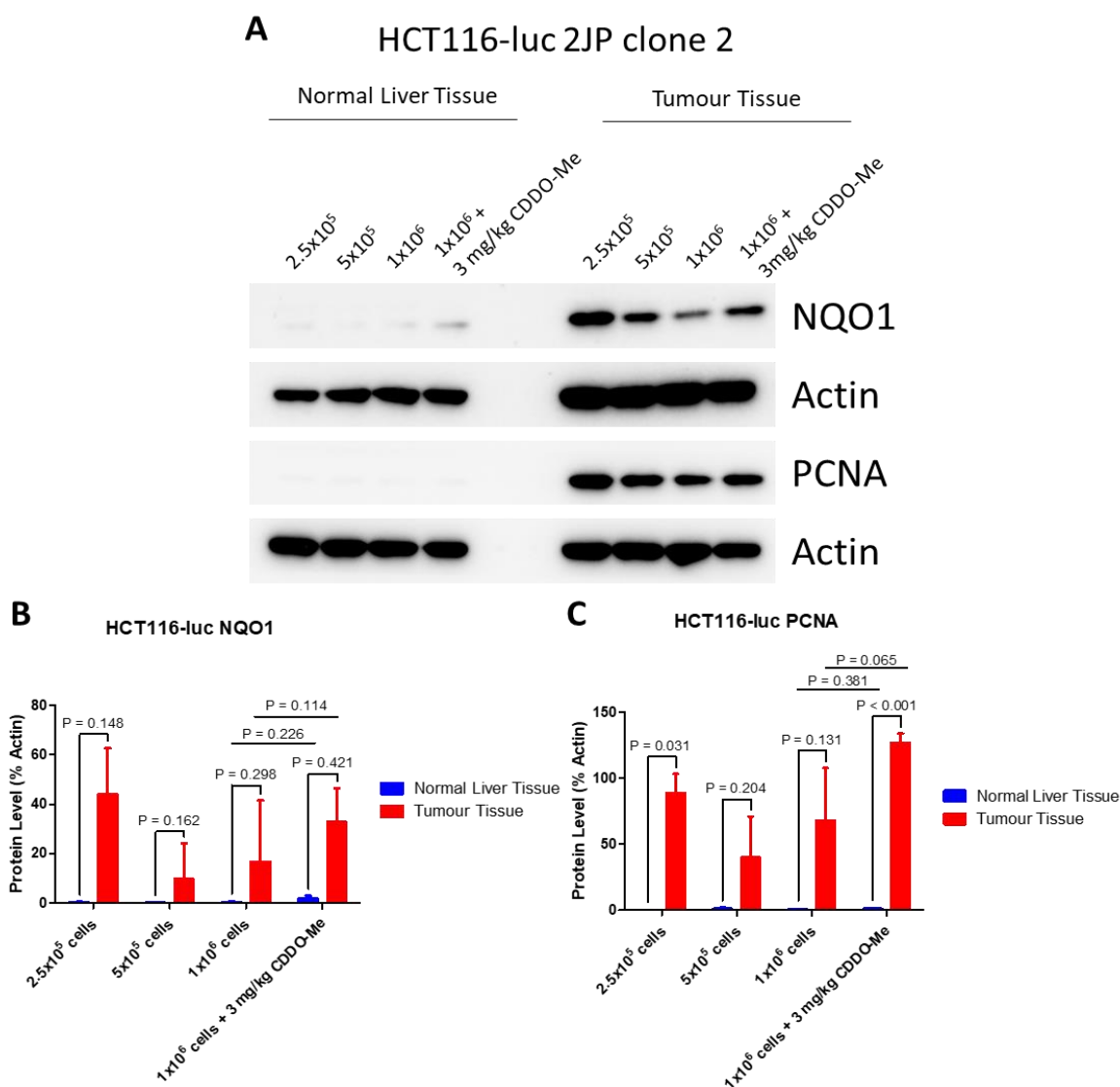


**Figure 4.18 Immunoblotting of healthy liver tissue and liver tumour tissue from male BALB/c Nude xenografted with HCT116-luc cells**

(A) Western blot for NQO1 and PCNA of healthy liver, and liver tumour, pooled lysates from male BALB/c Nude mice xenografted with HCT116-luc 2JP clone 2 cells at the indicated cell inoculums. Mice xenografted with 1x10<sup>6</sup> were treated or not with 3 mg/kg CDDO-Me. (B) Densitometry of NQO1 immunoblotting from healthy liver and liver tumour lysates, normalised to Actin. (C) Densitometry of PCNA immunoblotting from healthy liver and liver tumour lysates, normalised to Actin. (B and C) Unpaired t-test healthy liver vs liver tumour. Data analysis represents mean  $\pm$  SD of n=3 animals per group.

#### 4.3.7 CDDO-Me does not promote growth of tumours *in vivo*

As determined by the optimisation of orthotopic xenografts in section 4.3.6, a cell inoculum of  $1 \times 10^6$  cells was selected for all further xenograft work. This was due to this inoculum providing the strongest luminescence signal across both cell lines, whilst producing reasonably sized tumours to allow for *ex vivo* imaging. HepG2-luc 2JP clone 2 or HCT116-luc 2JP clone 2 cells at  $1 \times 10^6$  cells per mouse in 30  $\mu$ L Matrigel were xenografted into the livers of male BALB/c Nude mice prior to the commencement of IVIS bioluminescence imaging. Treatment with CDDO-Me commenced on day 14 post-implantation of cells, with the dosing pattern reflecting the regimen used in the PHx model outlined in chapter 2, which enhanced liver regeneration. Total flux was calculated using ROI analysis and healthy liver, as well as liver tumours, were preserved for downstream analysis. In mice xenografted with HepG2-luc 2JP clone 2 cells, a bioluminescent signal was detected in the mid-abdominal region as early as 2 days post-implantation of cells. The localised bioluminescent signal then increased in size in a time dependent manner but remained in the mid-abdominal region. The bioluminescent signal was comparable between DMSO and CDDO-Me treated mice. *Ex vivo* imaging, conducted at day 28, confirmed localisation of the tumour xenograft within a single lobe of the liver and illustrated the small size of tumours formed following the xenograft of HepG2-luc 2JP clone 2 cells. A larger bioluminescent signal was observed in DMSO treated mice, compared with CDDO-Me treated mice, *ex vivo* (Fig 4.19).

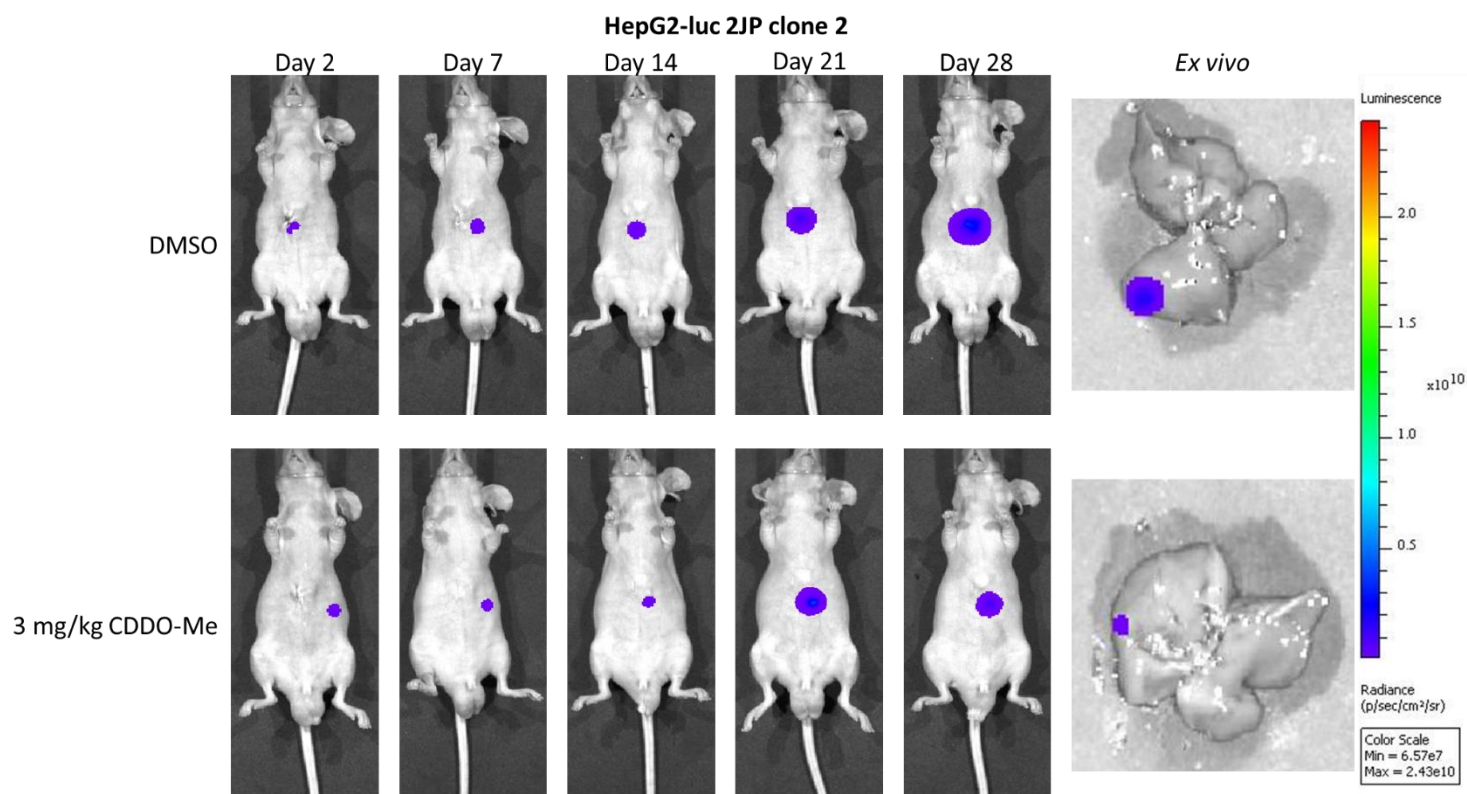


**Figure 4.19 IVIS bioluminescence images of BALB/c Nude mice orthotopically xenografted with HepG2-luc cells and treated with DMSO or CDDO-Me**

Representative *in* and *ex vivo* IVIS bioluminescence images of male BALB/c Nude mice following an orthotopic xenograft of HepG2-luc 2JP clone 2 cells at the indicated time points. Xenografts took place on day 0. Mice received either DMSO or 3 mg/kg CDDO-Me at days 14, 15, 16 and 19. For *ex vivo* images, livers were excised, briefly washed in PBS, and incubated in *in vivo* grade luciferin (150  $\mu$ g/mL in PBS) for 1 min prior to imaging. Images are of the same animal from each group throughout.

Mice xenografted with HCT116-luc 2JP clone 2 cells had a bioluminescent signal within the mid-abdominal region as early as 2 days post-implantation of cells. The bioluminescent signal then increased in size in a time dependent manner, and it was seen to spread across the entire abdominal region within both DMSO and CDDO-Me treated mice. CDDO-Me treated mice appeared to have a larger bioluminescent signal than DMSO treated mice at days 21 and 28, with the size and intensity of signal reaching peak levels at day 28. *Ex vivo* imaging, conducted at day 28, illustrated the large size of tumours present in mice treated with both DMSO and CDDO-Me following the xenograft of HCT116-luc 2JP clone 2. Furthermore, a greater level and intensity of bioluminescent signal appeared present in CDDO-Me treated mice, confirming the observations seen during whole body imaging (Fig 4.20).

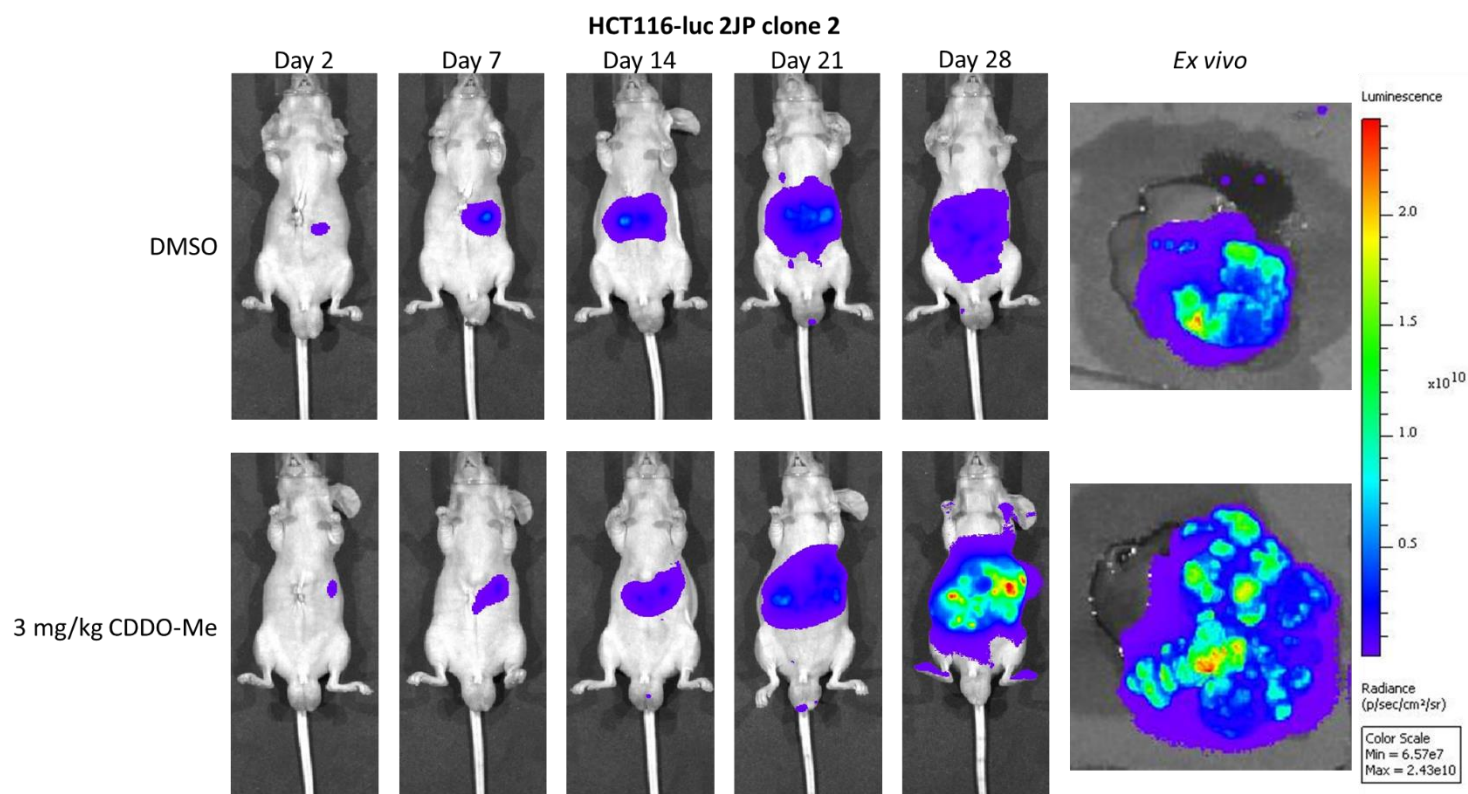


**Figure 4.20 IVIS bioluminescence images of BALB/c Nude mice orthotopically xenografted with HCT116-luc cells and treated with DMSO or CDDO-Me**

Representative *in* and *ex vivo* IVIS bioluminescence images of male BALB/c Nude mice following an orthotopic xenograft of HCT116-luc 2JP clone 2 cells at the indicated time points. Xenografts took place on day 0. Mice received either DMSO or 3 mg/kg CDDO-Me at days 14, 15, 16 and 19. For *ex vivo* images, livers were excised, briefly washed in PBS, and incubated in *in vivo* grade luciferin (150  $\mu\text{g}/\text{mL}$  in PBS) for 1 min prior to imaging. Images are of the same animal from each group throughout.



Following ROI analysis, total flux increased in a time dependent manner in mice xenografted with HepG2-luc 2JP clone 2 cells. Prior to the commencement of CDDO-Me treatment, total flux levels were comparable between treated and control groups, with no significant differences observed. Treatment with CDDO-Me from day 14, once tumours were established, caused higher levels of total flux to be observed at day 21, when compared to animals treated with DMSO, though significance was not achieved. Moreover, this increase in total flux was lost by day 28, with DMSO treated mice producing greater total flux than those treated with CDDO-Me. Again however, significance was not achieved (Fig 4.21 A).

ROI analysis showed that total flux increased in a time dependent manner in mice xenografted with HCT116-luc 2JP clone 2 cells. Prior to treatment with CDDO-Me, the levels of total flux in both groups of mice were comparable with no significant differences observed. Treatment with CDDO-Me from day 14, once tumours were established, caused higher levels of total flux to be observed at days 21 and 28 when compared to mice treated with DMSO, however significance was not achieved (Fig 4.21 B). No adverse effects on animal bodyweight were observed following the xenograft of either HepG2-luc or HCT116-luc cells or following treatment with CDDO-Me (Fig 4.22).

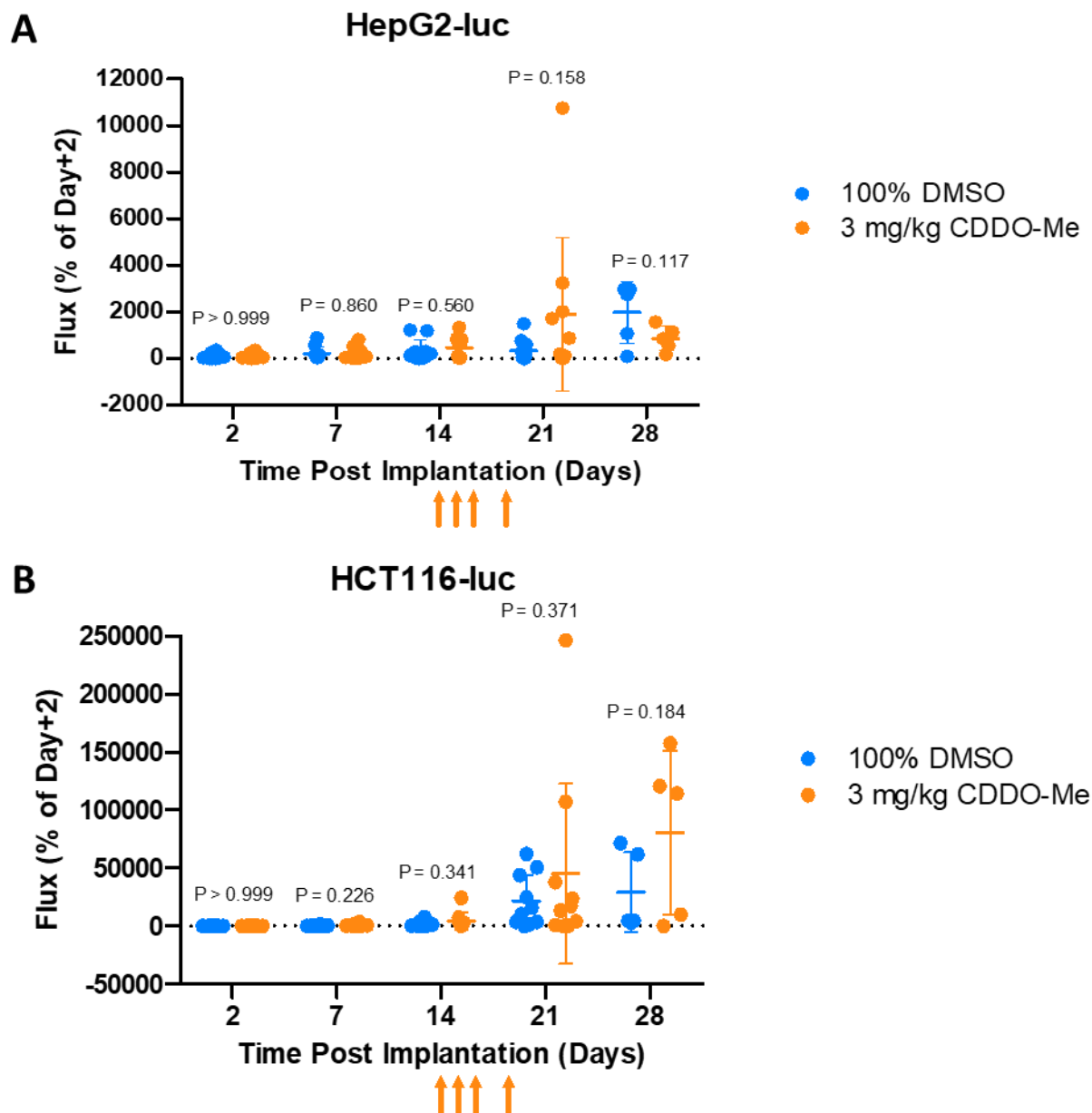


**Figure 4.21** Total flux of BALB/c Nude mice xenografted with HepG2-luc or HCT116-luc cells and treated with DMSO or CDDO-Me

Total flux of BALB/c Nude xenografted with (A) HepG2-luc 2JP clone 2 or (B) HCT116-luc 2JP clone 2 cells. Mice xenografted with  $1 \times 10^6$  cells were treated or not with 3 mg/kg CDDO-Me. Total flux was normalised to the total flux obtained at day 2. Arrows indicate CDDO-Me administration at days 14, 15, 16 and 19. (A and B) Unpaired t-test DMSO vs CDDO-Me at each time point. Data analysis represents mean  $\pm$  SD of n=5 animals per group.

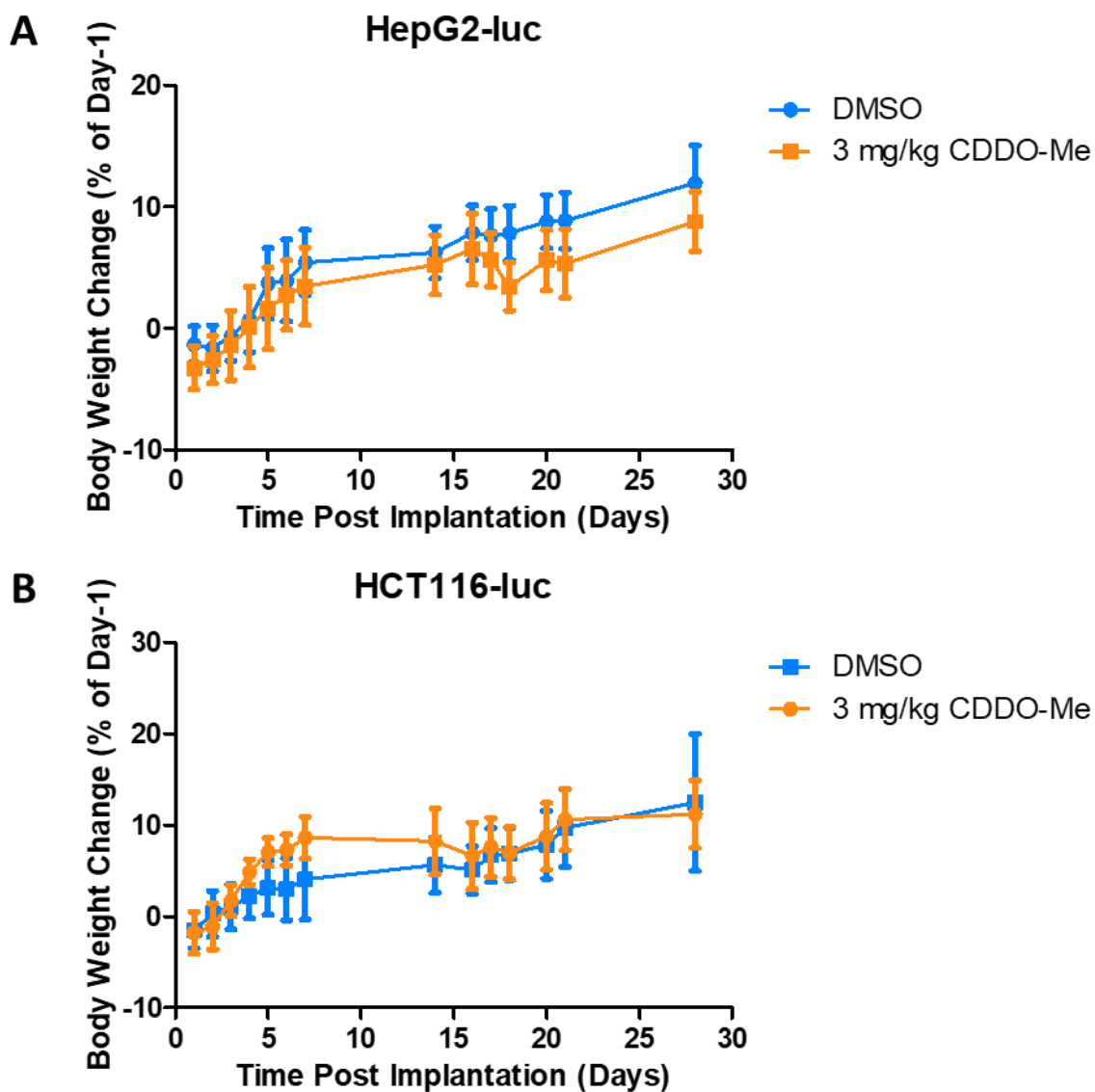


Figure 4.22 Bodyweight change of BALB/c Nude mice xenografted with HepG2-luc or HCT116-luc cells

Bodyweight change of mice xenografted with (A) HepG2-luc 2JP clone 2 or (B) HCT116-luc 2JP clone 2 cells at indicated time points. Data analysis represents mean  $\pm$  SD of n=3 animals per group.

#### 4.3.8 Protein expression analysis following orthotopic tumour xenograft

Following the completion of IVIS bioluminescence imaging, as outlined in the previous section, 4.3.7, mice were culled 21- or 28-days post-implantation of cells. Normal liver and tumour tissue was preserved before immunoblotting against NQO1 and PCNA was conducted. Livers from mice culled prior to the implantation of cells was used as a control. As the tumours resulting from HepG2-luc xenograft were localised within the subcapsular region in which they were implanted, and subsequently too small to section prior to histological examination, only lysates of healthy liver tissue were obtained from mice xenografted with HepG2-luc cells. PCNA is a proliferative marker (Kelman, 1997) and was used as a marker for tumour growth. As no tumour tissue could be obtained for protein expression analysis from mice xenografted with HepG2-luc, only immunoblotting against NQO1 was carried out in such mice.

Mice culled 21-days after being xenografted with HepG2-luc cells possessed significantly higher NQO1 protein expression levels in healthy liver tissue following treatment with CDDO-Me, when compared with DMSO treated mice ( $P = 0.008$ ). Mice treated with CDDO-Me and culled 28-days after xenograft also possessed significantly higher NQO1 protein expression when compared with DMSO treated mice ( $P = 0.024$ ). However, the NQO1 protein expression levels at day 28 were considerably lower than the levels observed in mice culled 21-days post-xenograft, indicating wash-out of CDDO-Me following the final treatment on day 19 (Fig 4.23).

The tumour tissue of mice xenografted with HCT116-luc cells possessed higher NQO1 protein expression levels in all groups regardless of treatment or time of cull, with significantly higher levels observed in day 21 cull DMSO, day 21 cull CDDO-Me and day 28 cull DMSO ( $P < 0.001$ ,  $P = 0.016$  and  $0.008$  respectively), when compared to healthy liver tissue from the same mouse. Mice xenografted

with HCT116-luc cells and treated with CDDO-Me possessed significantly higher levels of NQO1 protein expression in healthy liver tissue at both 21- and 28-days post-xenograft, when compared to mice treated with DMSO ( $P = 0.008$  for both). In tumour tissue, treatment with CDDO-Me produced higher NQO1 protein expression levels at both 21- and 28-days post-xenograft when compared to treatment with DMSO, though significance was not achieved (Fig 4.24 A and B).

Tumour tissue of mice xenografted with HCT116-luc cells possessed higher protein expression levels of PCNA in all groups regardless of treatment or time of cull, with significantly higher levels observed in day 21 cull CDDO-Me, day 28 cull DMSO and day 28 cull CDDO-Me ( $P = 0.016, 0.008$  and  $0.008$  respectively), when compared to healthy liver tissue from the same mouse. In healthy liver tissue, treatment with CDDO-Me produced lower levels of PCNA at 21-days, but higher levels at 28-days post-xenograft when compared to treatment with DMSO, though significance was not achieved. Similarly, in tumour tissue, treatment with CDDO-Me produced lower levels of PCNA at 21-days, but higher levels at 28-days post-xenograft when compared to treatment with DMSO, though these differences were not significant (Fig 4.24 A and C).

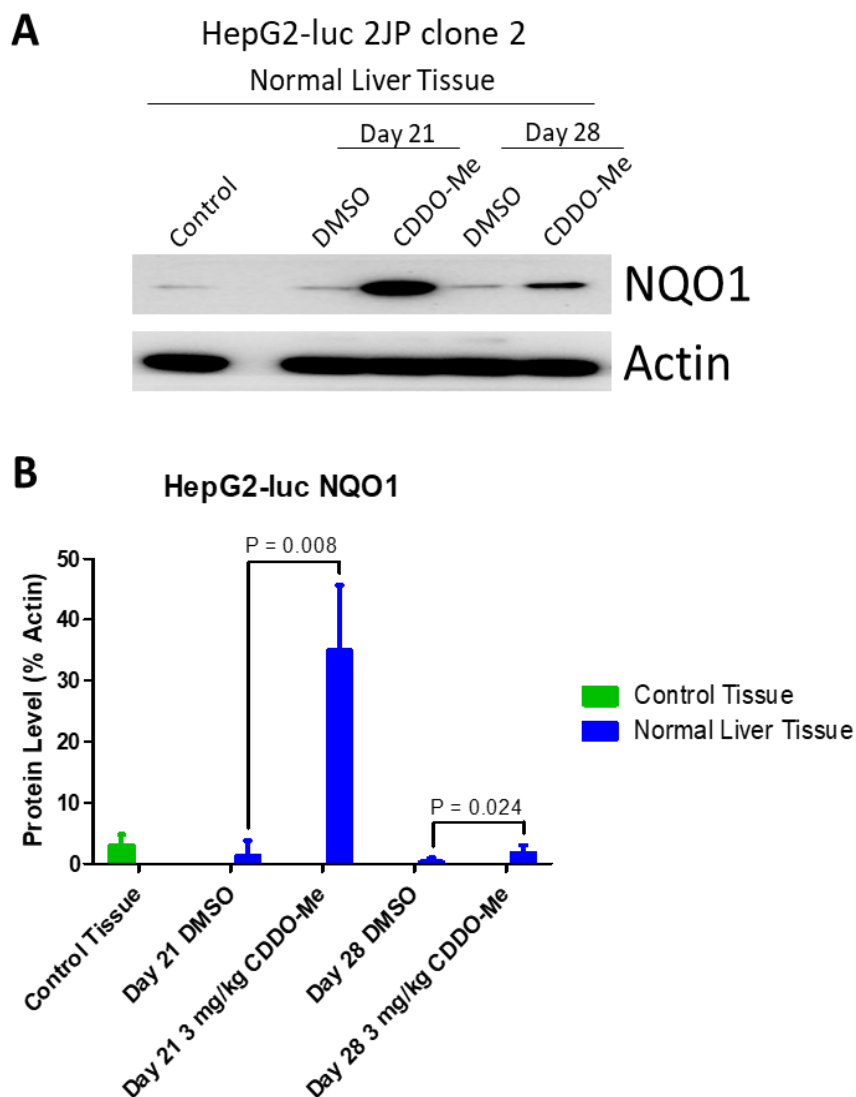


**Figure 4.23 Immunoblotting of healthy liver tissue from male BALB/c Nude mice xenografted with HepG2-luc cells and treated or not with CDDO-Me**

(A) Western blot for NQO1 of pooled healthy liver lysates from male BALB/c Nude mice that were xenografted with HepG2-luc 2JP clone 2 cells, treated or not with 3 mg/kg CDDO-Me and then culled at either 21- or 28-days post-xenograft. (B) Densitometry of NQO1 immunoblotting from all healthy liver lysates. (A and B) Livers from mice culled prior to the implantation of cells were used as a control. Mann-Whitney U test DMSO vs CDDO-Me at 21- and 28-days post-xenograft cull. Data analysis represents mean  $\pm$  SD of n=5 animals per group.

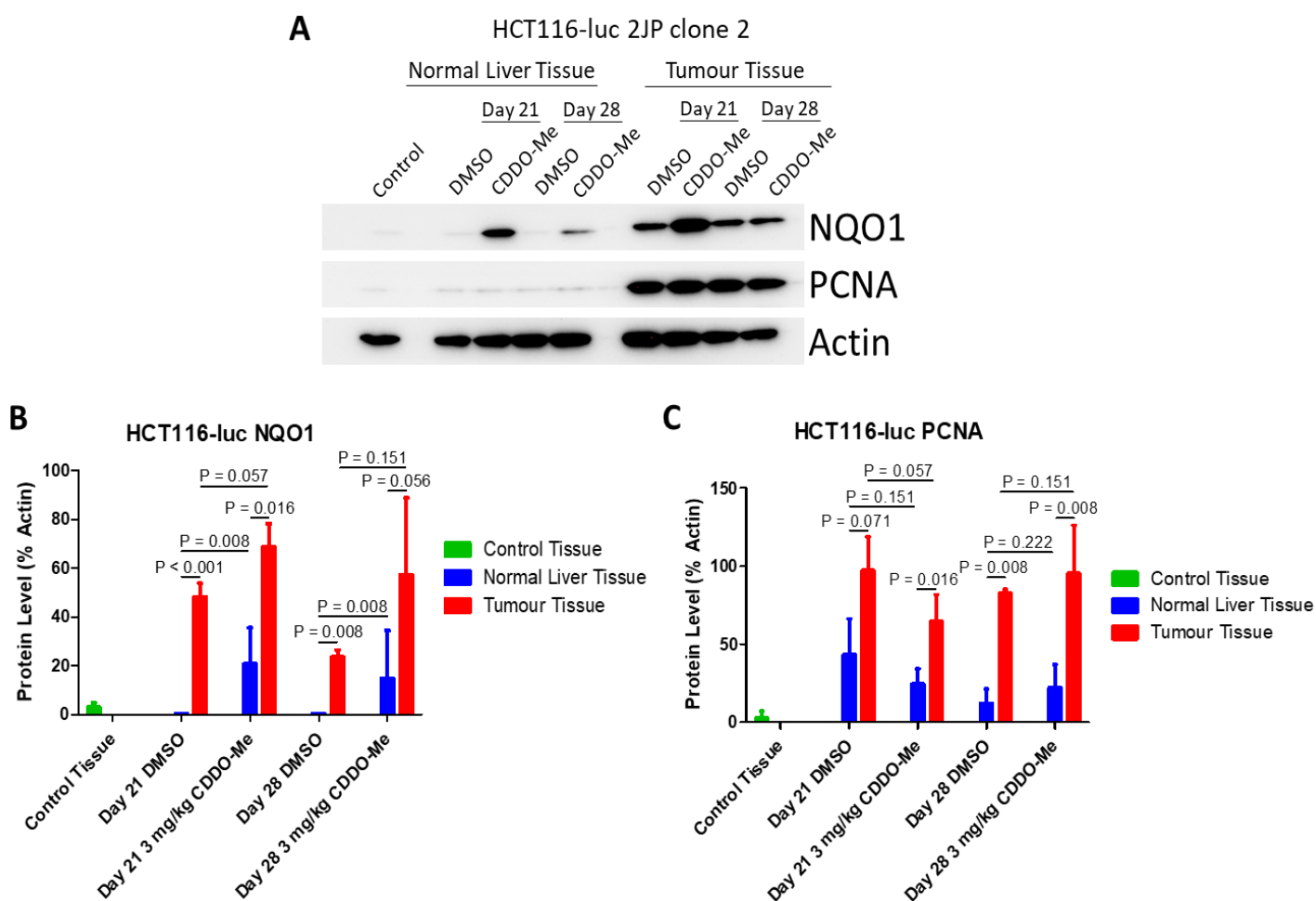


**Figure 4.24 Immunoblotting of healthy liver and tumour tissue from male BALB/c Nude mice xenografted with HCT116-luc cells and treated or not with CDDO-Me**

(A) Western blot for NQO1 and PCNA of pooled healthy liver and tumour tissue lysates from male BALB/c Nude mice that were xenografted with HCT116-luc 2JP clone 2 cells, treated or not with 3 mg/kg CDDO-Me and then culled at either 21- or 28-days post-xenograft. Densitometry of immunoblotting from all healthy liver and tumour tissue lysates against (B) NQO1 and (C) PCNA. (A, B and C) Livers from mice culled prior to the implantation of cells were used as a control. Mann-Whitney U test healthy tissue vs tumour tissue; DMSO vs CDDO-Me in healthy tissue at 21- and 28-days post-xenograft cull; DMSO vs CDDO-Me in tumour tissue at 21- and 28-days post-xenograft cull. Data analysis represents mean  $\pm$  SD of n=5 animals per group.

#### 4.3.9 Histological examinations of HepG2-luc and HCT116-luc tumours

Following the completion of IVIS bioluminescence imaging, as outlined in section 4.3.7, mice were culled 21- and 28-days post implantation of cells. The livers of these mice were harvested, preserved in 4 % PFA, sectioned and then stained with HE. HE-stained sections from liver tissue containing tumours from HepG2-luc or HCT116-luc xenografted cells underwent histological examination to determine if treatment with CDDO-Me, irrespective of the time of cull, enhanced any pathological alterations consistent with the proliferative and non-proliferative lesions of the mouse hepatobiliary system, when compared to treatment with DMSO. All sections were scored for parenchymal lesions, tumour fibrosis and tumour necrosis. Furthermore, mitotic index was calculated and the number, and average size, of masses reported.

It was found that both cell lines were viable and animals from both experimental groups presented neoplastic masses, but that the morphological phenotypes of the two neoplastic populations was recognisably different. Implantation of HepG2-luc produced numerous, small masses, scattered within the parenchyma (Fig 4.25 A). HepG2-luc cells were always associated with abundant fibrin precipitating around and amongst neoplastic cells, increasing the size of the small nodules as well as their overall number, to the point that some of the masses were almost entirely composed of dense polymerised fibrin. Such cells had a cuboidal profile, moderate amount of basophilic cytoplasm and a central round nucleus with coarsely stippled chromatin and a single basophilic nucleolus. Central areas of coagulative necrosis were rarely seen at the centre of neoplastic nodules. Tumours formed from HepG2-luc cells were consistently present below the endothelium of the portal veins, in some cases bulging into the lumina of portal veins, causing enlargement of the vein and often partial occlusion as a result of the intraluminal growth of the neoplastic masses (Fig 4.25 B). Occasionally, small emboli were seen detaching into the portal vein blood supply, providing potential for metastatic activity (Fig 4.25 C).



Treatment with CDDO-Me was shown to have little to no effect on the general parenchymal lesions, tumour fibrosis and tumour necrosis scores of tumours formed from HepG2-luc cells (Fig 4.27 A-C). Similarly, CDDO-Me did not appear to alter the mitotic index of xenografted HepG2-luc cells, nor did it enhance the number of masses present or the size of such neoplastic masses (Fig 4.27 D-F).

In contrast, implantation of HCT116-luc produced much larger masses, with higher a mitotic index. Such masses were scattered within the parenchyma but were also observed within the portal area, growing in an expansile pattern inside the hepatic lobule (Fig 4.26 A). HCT116-luc cells were arranged in tightly packed nests in association with scant fibrovascular stroma. Cells had a vaguely cuboidal profile, moderate amount of basophilic cytoplasm, a central round nucleus with finely stippled chromatin and up to 3 small basophilic nucleoli. HCT116-luc cells were associated with evident liquefactive necrosis at the centre of the masses, creating pseudo-cystic cavities in a large proportion of masses (Fig 4.26 B). In apparent correlation with the size of the mass, necrosis extended to account for up to 60 % of the neoplastic mass. Occasionally, subcapsular masses were seen pushing against the mostly intact liver capsule, causing the mass to bulge, or protrude, outside the profile of the liver, providing the potential for metastasis through direct contact with other tissue (Fig 4.26 C). Smaller masses were rarely found within the lymphatic system.

Treatment with CDDO-Me was shown to have little to no effect on the general parenchymal lesions, tumour fibrosis and tumour necrosis scores of tumours formed from HCT116-luc cells (Fig 4.27 A-C). Similarly, CDDO-Me did not appear to alter the mitotic index of xenografted HCT116-luc cells or the number and size of neoplastic masses present (Fig 4.27 D-F).

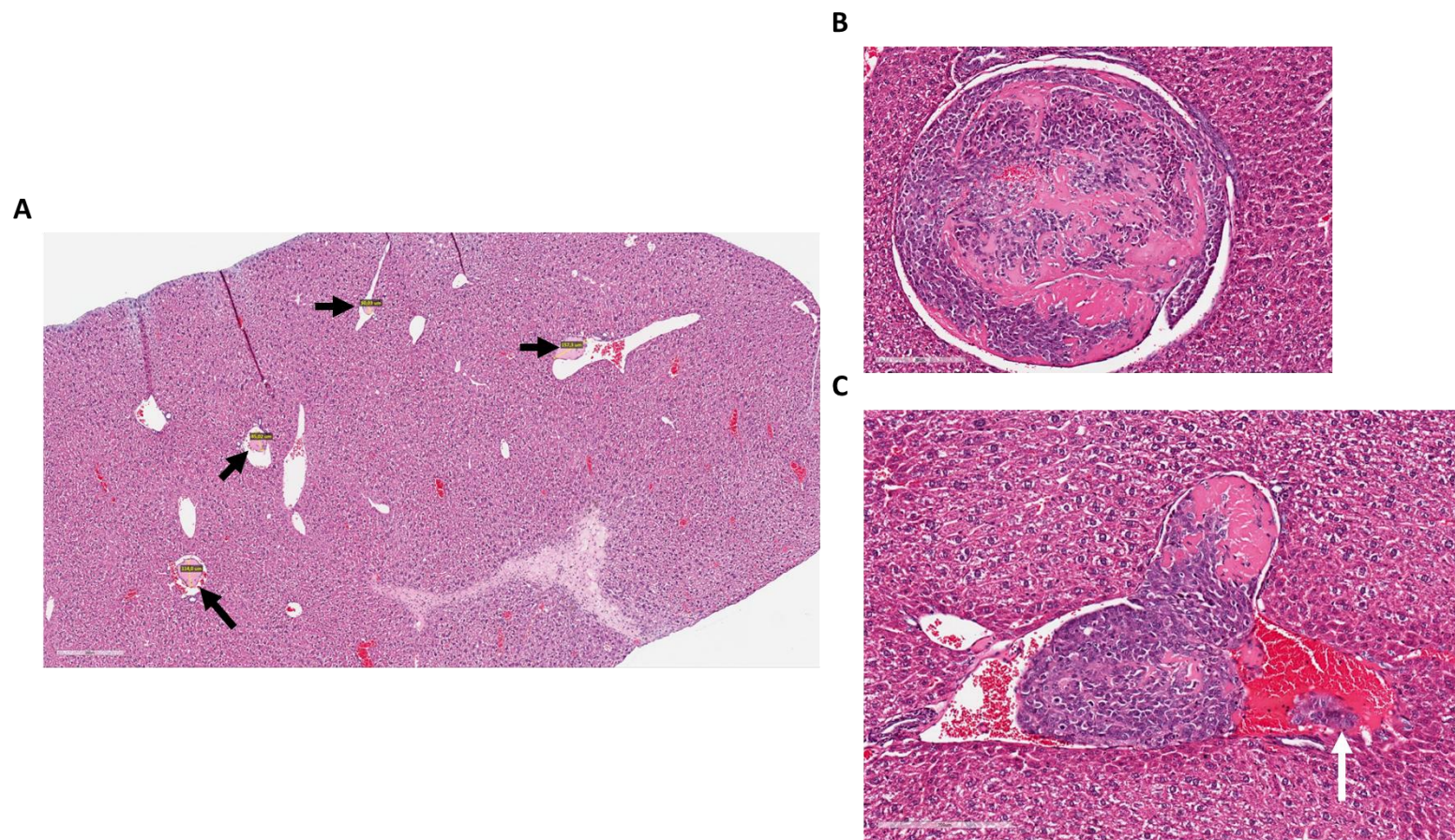


**Figure 4.25 HE-stained sections from liver tissue containing tumours formed from HepG2-luc xenografts**

HE-stained sections showing (A) numerous small masses scattered within the parenchyma and portal vein regions. Black arrows indicate tumours. (B)

Occlusion of the portal vein resulting from the intraluminal growth of the neoplastic masses. (C) Small emboli detaching into the portal vein blood supply,

providing potential for metastatic activity. White arrow indicates emboli encompassing viable HepG2-luc cells.

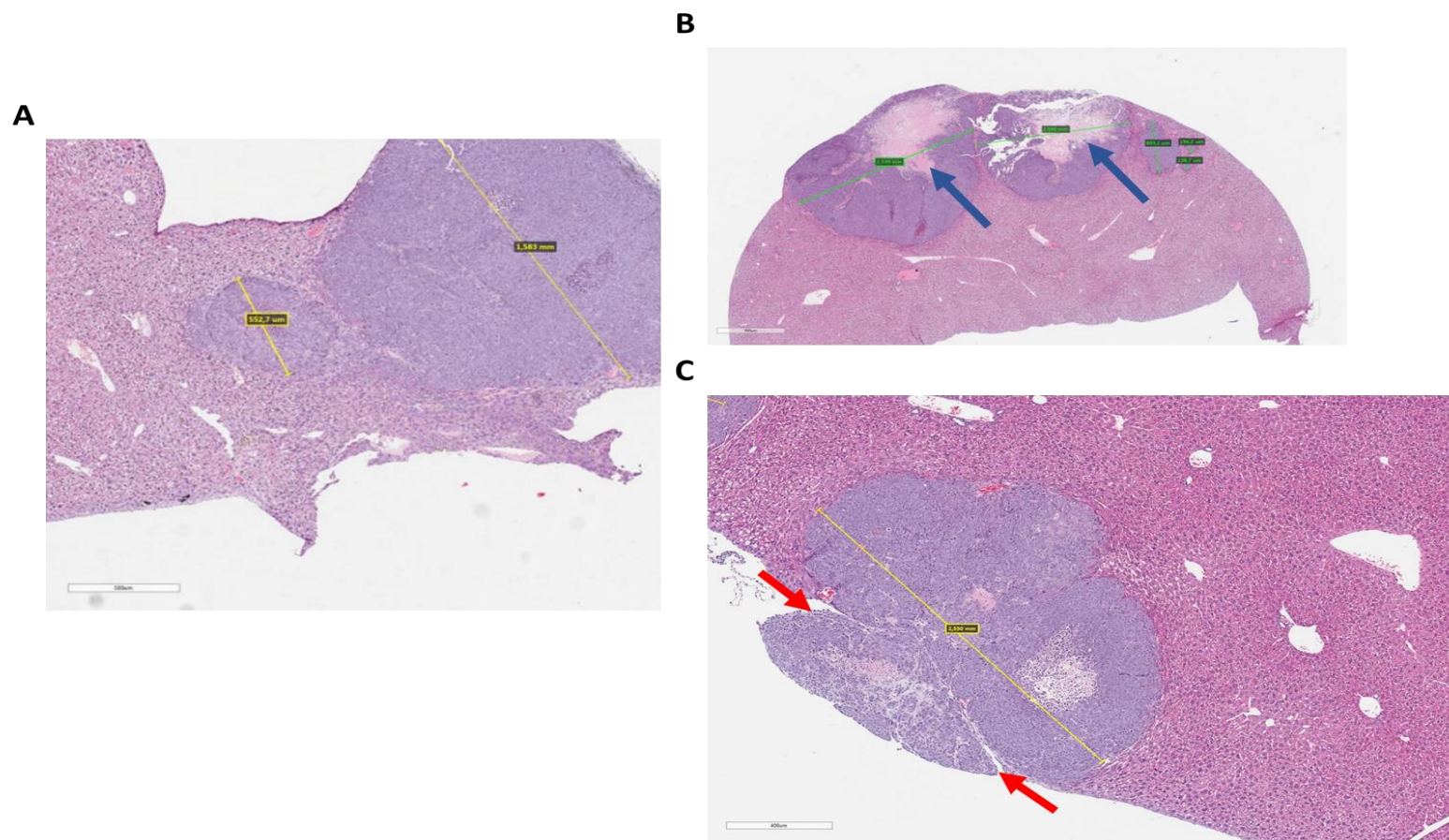


**Figure 4.26 HE-stained sections from liver tissue containing tumours formed from HCT116-luc xenografts**

HE-stained sections showing (A) Large masses within the parenchyma. (B) Large areas of liquefactive necrosis, creating pseudo-cystic cavities. Blue arrows indicate regions of necrosis. (C) Subcapsular mass pushing against the mostly intact liver capsule, causing the mass to protrude outside the profile of the liver. Red arrows indicate the point at which the mass protrudes beyond the capsule of the liver.

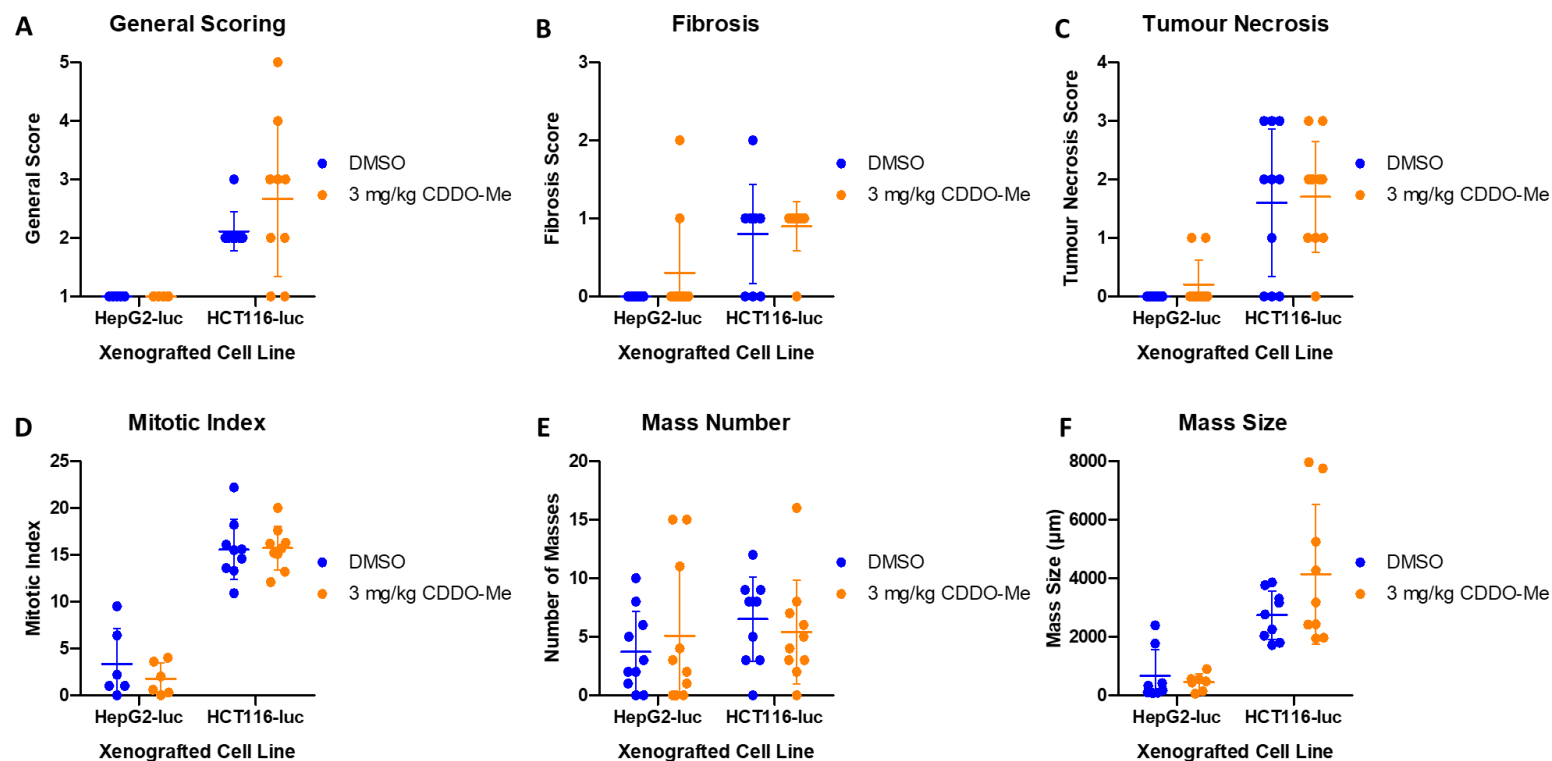


**Figure 4.27** Quantified histological examinations of HepG2-luc and HCT116-luc tumours in mice treated or not with CDDO-Me

(A) General parenchymal lesions scoring (B) Tumour fibrosis scoring and (C) Tumour necrosis scoring of HepG2-luc and HCT116-luc tumours in mice treated or not with 3 mg/kg CDDO-Me. (D) Mitotic index, quantified by counting the number of mitoses in 10 randomly chosen non-overlapping high-power fields (HPFs). (E) Number of masses quantified in 10 randomly chosen non-overlapping HPFs (F) Size of masses, in microns ( $\mu\text{m}$ ), observed in 10 randomly chosen non-overlapping HPFs. Data represents mean  $\pm$  SD of n=10 samples per group.

#### 4.4 Discussion

Patients presenting liver cancer commonly undergo surgical resection as a means of removing affected liver tissue. This is made possible due to the liver's remarkable ability to regenerate following surgical insult. Despite this, in some cases liver regeneration does not occur efficiently, resulting in severe post-operative complications such as PHLF. The findings of chapter 2 demonstrate that pharmacological activation of Nrf2 can significantly enhance liver regeneration in a rodent two-thirds PHx model. However, the role of Nrf2 in liver cancer has been studied for many years due to the incidence of clinical tumours possessing mutations in Nrf2 itself or downstream targets (Gao et al., 2013; Ziv et al., 2020). Due to its antioxidant and protective abilities, mutations associated with Nrf2 in cancer cells can create an environment that allows for abnormal cellular growth, leading to cancer progression (Zimta et al., 2019; Haque et al., 2020), and protection against treatment strategies such as radiotherapy and chemotherapeutic agents (Choi and Kwak, 2016; Islam et al., 2022; Matsuoka et al., 2022). As a result, there is considerable concern around the use of therapies involving Nrf2 stimulation in the context of liver tumour surgery.

The development of numerous *in vivo* models, in which Nrf2 has been manipulated in rodents possessing HCC or CRC has generated findings that are often conflicted and ambiguous. Some studies demonstrate the negative impact of Nrf2 on HCC initiation and subsequent tumour growth (Ngo et al., 2017; Zavattari et al., 2015), however others report Nrf2 eliciting an anti-tumour role (Wu et al., 2019; Emanuele et al., 2021). Therefore, taken together, the concerns arising from the use of Nrf2 stimulation in a clinical liver tumour setting, and the often conflicting and ambiguous findings reported *in vivo*, highlights the need to assess the safety of Nrf2 targeting therapies, by investigating the effect of pharmacological Nrf2 activation on the burden of pre-existing tumours. Such assessment would therefore address one of the risks of stimulating Nrf2 in cancer patients to boost access to curative surgery.

Cancer cell lines stably expressing luciferase are widely used due to the imaging capabilities they possess (Brennan et al., 2018) and have become powerful tools for liver cancer research (Hu et al., 2009; Woodfield et al., 2017). In order to xenograft human liver cancer cell lines expressing luciferase into mice, it is essential to utilise an immunodeficient mouse strain. A previous study conducted by Yang et al. (Yang et al., 2011) has highlighted the suitability of BALB/c Nude mice as a host for xenografting, and subsequently imaging, the luciferase tagged human liver cancer cell line HepG2. The lack of a thymus prevents rejection of xenografted human cell lines and the hairless, albino background provides the ideal foundation for non-invasive bioluminescence imaging by preventing the attenuation of bioluminescent signal that is observed in mice possessing hair or non-albino backgrounds (Curtis et al., 2011). When using bioluminescent cell lines, thereby ruling out the need for tumour caliper measurements, the use of an orthotopic xenograft, as opposed to a subcutaneous one, is advantageous due to the ability to replicate the true tumour microenvironment (He et al., 2015). With regards to orthotopic liver xenografts, an intrasplenic injection of cells is commonly used to best mimic the secondary liver metastasis that is witnessed in clinical settings (Dafflon et al., 2020; Marvin et al., 2021). However, the use of a subcapsular intrahepatic implantation produces a far better and considerably more consistent xenograft. Indeed, although natural metastasis of cells from the spleen to liver is not achieved with subcapsular intrahepatic injections, the engraftment yield is higher, mortality rate lower, and chance of extrahepatic tumours considerably less (Wu et al., 2016). It is for these reasons that a subcapsular intrahepatic injection method was used in this chapter, with the implantation of human colorectal cancer cells used as a viable alternative to mimic secondary liver metastasis. This chapter has therefore highlighted the production and use of a reproducible model for assessing the growth of primary and secondary liver tumours *in vivo*.

Through the use of non-invasive IVIS bioluminescence imaging, the findings of this chapter show that CDDO-Me does not promote the growth of tumours formed from the orthotopic xenograft of HepG2-

luc or HCT116-luc cells in mice. In addition, histological examination confirmed these findings and illustrated that treatment with CDDO-Me does not alter how the tumours grow *in vivo*. As a high and sustained rate of proliferation is a hallmark of cancer (Hanahan and Weinberg, 2011; Gutschner and Diederichs, 2012), the mitotic index of tumours is a key prognostic tool in HCC (Ha et al., 2016). The findings of this chapter show that the mitotic index of both xenografted cell lines was comparable across treated and non-treated mice indicating that CDDO-Me does not promote a high and sustained rate of proliferation in such tumours. Both tumour fibrosis and necrosis are often associated with aggressive development of cancer and poor patient prognosis (Liu and Jiao, 2020; Piersma et al., 2020). CDDO-Me did not contribute to greater levels of tumour fibrosis or necrosis in either xenografted cell line, further indicating that tumours from treated mice did not differ to those from un-treated mice. Although treatment with CDDO-Me was seen to cause a slight increase in the number of tumours formed from HepG2-luc cells, and an increase in the size of tumours formed from HCT116-luc cells, such HepG2-luc tumours were smaller in size and fewer HCT116-luc tumours were observed. Therefore, the overall tumour burden, defined as the total amount of cancer in the body (Dall'Olio et al., 2022), remains comparable between treated and un-treated mice.

Immunoblotting against PCNA further confirmed the mitotic index findings as CDDO-Me did not enhance the levels of this crucial proliferative marker in tumour tissue. In addition, treatment with CDDO-Me successfully upregulated the Nrf2 pathway in both healthy liver and tumour tissue in mice xenografted with HCT116-luc cells. As expected, due to CDDO-Me treatment ending on day 19, protein expression levels of NQO1 were higher at day 21, with a subsequent decline in protein expression by day 28 as a result of drug washout. Interestingly however, tumour tissue still possessed considerably high levels of NQO1 at day 28, potentially indicating a higher basal level in HCT116 cells. To date, there are no reported mutations associated with the Nrf2 pathway in HCT116 cells, although clinical CRC tumour samples have shown mutations in such genes (Sameer, 2013; Torrente et al.,

2020), thus it would be of interest to perform transcriptomics analysis on the tumours resulting from HCT116-luc cells to identify any novel mutations. As the tumours formed from HepG2-luc cells were considerably smaller, histological examinations were prioritised and a sample was not collected for protein analysis. Additional work, either through immunohistochemistry analysis of sectioned tumours, or via the generation of further HepG2 tumours, would therefore be required in order to assess the effect of CDDO-Me treatment on tumour protein expression levels.

There is however further potential to expand and improve this model. As fibrosis and cirrhosis are risk factors, and common causes of early liver cancer development (Lotfollahzadeh et al., 2022), induction of liver fibrosis or cirrhosis by use of a hepatotoxic agent (Brown et al., 2018) prior to conducting an orthotopic xenograft would provide a model of better clinical relevance. In addition, further optimisation of cell inoculums for xenograft would provide better insight into the effect of CDDO-Me on tumour burden. Bioluminescence imaging relies on oxygen in order to produce a light signal (Syed and Anderson, 2021), something that is not present in the large necrotic areas observed in tumours arising from HCT116-luc cells. Large tumours, which are unrealistic in size when compared to the natural tumour burden observed in patients, possessed vast areas of necrosis which can therefore compromise the bioluminescent signal produced, hence further refinement of cell inoculum would provide a beneficial effect for the production of bioluminescent signal. Furthermore, the recent development, and more common use, of red-shifted luciferase provides a better tool for *in vivo* bioluminescence imaging. By producing a brighter signal as a result of its near infrared emission spectra (Love et al., 2023), red-shifted luciferase yields better tissue penetration, allowing better visualisation of orthotopically implanted cells and subsequently better quantification of tumour burden (Yeh et al., 2017).



Current clinical biomarkers for HCC and CRC, these being alpha-fetoprotein (AFP) (Piñero et al., 2020; Song et al., 2021) and carcinoembryonic antigen (CEA) (Alves Martins et al., 2019; Ogunwobi et al., 2020) respectively, are only able to detect later stage malignancies. However, more recent studies have shown the beneficial use of more sensitive markers such as arginase-1 in tissue (Wang et al., 2020) and glypican-3 in blood for HCC (Zhou et al., 2018; Pan et al., 2020), as well as cytokeratin-20 in blood for CRC (Ji et al., 2017), which are able to detect early-stage malignancies with far better accuracy. With this in mind, in future there is the potential to investigate the presence of key HCC and CRC biomarkers within the blood of animals xenografted with HepG2-luc or HCT116-luc cells.

Finally, the experimental design of the *in vivo* orthotopic xenograft model outlined in this chapter could be improved through the addition of a positive control which is known to increase tumour burden in rodents following the implantation of cells. This would allow any impact of pharmacological Nrf2 activation on tumour burden to be placed into the context of a known pro-oncogenic compound. However, there is a lack of published literature in which such compound or method has been utilised. It is far more common to pre-treat rodents with a known hepatocarcinogen before xenografting cells as this provides a clinically relevant environment of cirrhosis and fibrosis, which in turn enhances tumour growth. Furthermore, the use of such pro-oncogenic compounds in rodents would be difficult to achieve due to the ethical complications of knowingly accelerating tumour growth beyond that of normal physiological conditions.

To summarise, the findings of this chapter illustrate that pharmacological activation of Nrf2, achieved through the transient use of CDDO-Me, does not appear to promote the growth of liver tumours *in vivo*. With these findings, and the additional support provided from the further work outlined, there is the potential to use CDDO-Me to enhance treatment strategies for other clinical burdens, such as

PHLF, in patients who previously had, or currently have, liver cancer with confidence that such transient treatment with CDDO-Me will not cause recurrence or further development of cancer.

## **Chapter 5**

### **General discussion**

## **Contents**

<b>5.1 Introduction.....</b>	<b>204</b>
<b>5.2 Key aims and major findings.....</b>	<b>205</b>
<b>5.3 General discussion of findings.....</b>	<b>206</b>
5.3.1 Expanding current liver cancer treatment approaches.....	206
5.3.2 Addressing safety concerns of pharmacological Nrf2 activation in liver cancer.....	207
5.3.3 The future of Nrf2 therapies in liver cancer.....	209
<b>5.4 Conclusions and future directions.....</b>	<b>211</b>

## 5.1 Introduction

The clinical burden of liver cancer continues to escalate due to an increasing incidence of the disease per se and the significant challenges that can arise from post-operative complications following the use of surgical treatment approaches (Are et al., 2017). Owing to the implication of antioxidant, inflammatory and metabolic pathways in such post-operative complications, Nrf2 activators targeting such pathways may effectively reduce the occurrence of complications and thus help to alleviate the clinical burden. The use of Nrf2 activators has increased considerably in recent years with several compounds making their way into routine clinical use and late-stage clinical trials with promising and efficacious results being observed (Robledinos-Antón et al., 2019). However, the role of Nrf2 in liver regeneration and liver cancer is still somewhat unknown with contradictory findings often causing further confusion. More recently, there have been several reports that support activation of Nrf2 exerting an anti-proliferative effect in cancer, both *in vitro* and *in vivo*. Sajadimajd et al. demonstrated that pharmacological Nrf2 activation, achieved via treatment with resveratrol, caused a significant increase in cytotoxicity in breast cancer cell lines, thus exhibiting an anti-cancer effect (Sajadimajd et al., 2023). This has been supported in HCC as Moghadam et al. showed that HepG2 cells treated with resveratrol possessed significantly decreased cell viability compared to control treated cells (Moghadam et al., 2023). Similar findings have also been reported *in vivo* as Moerland et al. illustrated that mice possessing lung tumours had significantly lower tumour burdens when treated with the pharmacological Nrf2 activator, CDDO-Me (Moerland et al., 2023).

Therefore, further expansion on the findings of these studies will provide a more solid understanding of pharmacological Nrf2 activation in liver regeneration and liver cancer, and may support the establishment of new treatment approaches, as well as the further development of existing therapeutic strategies, to improve patient outcome and subsequently reduce clinical burdens. This thesis therefore aimed to investigate if pharmacological activation of Nrf2 can aid liver regeneration,

whilst ensuring such treatment does not worsen the burden of liver cancer by promoting the growth of pre-existing tumours.

## 5.2 Key aims and major findings

The key aims of this thesis were:

- To investigate if pharmacological activation of Nrf2 can enhance post-operative liver regeneration.
- To assess the effect of pharmacological Nrf2 activation on *in vitro* proliferation of liver and colorectal cancer cell lines.
- To determine if pharmacological Nrf2 activation enhances the burden of liver cancer in an *in vivo* orthotopic tumour xenograft model.

The major findings of this thesis were:

- Pharmacological activation of Nrf2, achieved through treatment with CDDO-Me, significantly enhanced the rate of liver regeneration following partial hepatectomy in mice, and promoted metabolic remodelling and the maintenance of liver homeostasis.
- Transcriptomic analysis of primary human hepatocytes exposed to CDDO-Me revealed modulation of many of the same biochemical and transcriptional processes associated with enhanced liver regeneration in wild-type mice treated with CDDO-Me, thus highlighting the clinical translatability of this *in vivo* model.
- Data from an *in vitro* ATP proliferation assay demonstrated that pharmacological activation of Nrf2, achieved through treatment with CDDO-Me, does not promote *in vitro* proliferation of selected HCC and CRC cell lines.
- Non-invasive bioluminescence IVIS imaging showed that treatment with CDDO-Me, and subsequent pharmacological Nrf2 activation, does not promote the growth of tumours

formed from an orthotopic, subcapsular intrahepatic xenograft of human HCC or CRC cells in immunocompromised mice. Histological examination of tumours confirmed these findings through analysing mitotic index, tumour fibrosis and necrosis, and overall tumour burden.

### **5.3 General discussion of findings**

#### **5.3.1 Expanding current liver cancer treatment approaches**

Despite the surgical resection of tumours being a well-established, and routinely practiced, treatment strategy for liver cancer, the associated post-operative complications can cause considerable difficulties. In addition, the risk of these complications' limits access to potentially curative surgery to those patients with less advanced tumour burdens. The most serious of these complications is PHLF, occurring in up to 10% of patients (Ocak et al., 2020) and contributing significantly to the mortality rate associated with hepatectomy procedures (Balzan et al., 2005; Mullen et al., 2007; Rahbari et al., 2011). As current PHLF treatment approaches lack application in the clinical setting, and prevention of PHLF carries its own risks following further patient exposure to invasive procedures, it is evident that PHLF remains a substantial clinical burden with an unmet need for novel therapeutic strategies to promote post-hepatectomy liver regeneration and adequate hepatic function.

Pharmacological activation of Nrf2 has become a promising therapeutic approach in a wide range of disease areas with several Nrf2 activating compounds reaching late-stage clinical trials and even clinical approval (Robledinos-Antón et al., 2019). The findings of chapter 2 show that treatment with CDDO-Me, a pharmacological Nrf2 activator, enhances the rate of liver regeneration following a two-thirds PHx in wild-type mice, without interfering with the crucial termination phase of the regenerative process. In addition, treatment with CDDO-Me was shown to enhance hepatocyte

proliferation, a pivotal driving mechanism of regeneration, as well as promote metabolic remodelling and the maintenance of liver homeostasis. It is therefore apparent that pharmacological activation of Nrf2 with CDDO-Me provides a key advantage to the regenerating liver of wild-type mice.

Furthermore, the findings of chapter 2 highlight the translatability of such a model investigating the effect of pharmacological Nrf2 activation on liver regeneration, with transcriptomic analysis of primary hepatocytes exposed to CDDO-Me revealing modulation of many of the same biochemical and transcriptional processes associated with enhanced liver regeneration in wild-type mice treated with CDDO-Me.

Taken together, pharmacological activation of Nrf2 with CDDO-Me offers huge potential for enhancing liver regeneration in patients undergoing surgical resection of liver cancer, with the therapeutic benefit spanning both pre-surgery, by boosting RLV, and post-surgery, by enhancing the rate of regeneration and allowing for more efficient restoration of hepatic architecture and function. With this, it may therefore be possible to increase the post-resectional outcome, decrease the risk of PHLF and expand current treatment options to cancer patients that would normally be deemed inoperable, thus reducing the clinical burden of liver cancer.

### **5.3.2 Addressing safety concerns of pharmacological Nrf2 activation in liver cancer**

Within the clinic, genes within the Nrf2 pathway are commonly mutated in liver (Ding et al., 2017) and colorectal (Torrente et al., 2020) tumour samples. Coupled to the numerous conflicting findings of the role of Nrf2 in liver cancer, in both *in vitro* and *in vivo* models, it is unsurprising that pharmacological activation of Nrf2 in liver cancer setting raises hypothetical safety concerns surrounding the risk of enhancing tumour growth. However, in order to provide a therapeutic benefit for liver regeneration and the associated post-operative complications following surgical resection of



liver cancer, it is essential that pharmacological Nrf2 activation is safe to use in the context of liver tumour surgery, ensuring that tumour growth is not enhanced.

The findings of chapter 3 demonstrate that pharmacological activation of Nrf2, achieved through treatment with CDDO-Me, does not enhance *in vitro* proliferation of selected HCC and CRC cell lines. As *in vitro* cell based assays have been routinely used for decades for first-line cancer research (Kitaeva et al., 2020; Ayuso et al., 2021), this offers a key initial understanding into how pharmacological Nrf2 activation can be used safely in a liver cancer setting. Furthermore, the use of such *in vitro* models provides crucial insight into the development, and use, of more clinically relevant *in vivo* systems.

The data presented in chapter 4, achieved through the use of non-invasive IVIS bioluminescence imaging, shows that treatment with CDDO-Me does not promote the growth of tumours formed from an orthotopic, subcapsular intrahepatic xenograft of human HCC or CRC cells in immunocompromised mice. Furthermore, histological examination of tumours confirmed that treatment with CDDO-Me did not enhance the mitotic index, tumour fibrosis and necrosis, or overall tumour burden. As a result, it can be concluded that acute treatment with CDDO-Me and subsequent pharmacological activation of Nrf2 can be achieved safely in a liver cancer setting, and that such therapy has the potential to enhance treatment strategies for PHLF in patients undergoing surgical resection for liver tumours, with the confidence that further tumour development will not occur.

### 5.3.3 The future of Nrf2 therapies in liver cancer

Pharmacological Nrf2 activators have been known and tested for several years, with the discovery of naturally occurring activating compounds such as sulforaphane being the first documented (Zhang et al., 1992). This initial discovery then led the way for the development of numerous synthetic, small molecule, Nrf2 activating compounds, including DMF, SFX-01 and CDDO-Me, with the majority of such compounds now in clinical trials or even routine clinical use for a variety of differing disease areas (Robledinos-Antón et al., 2019). Furthermore, there are also some promising small molecule compounds in pre-clinical development with Keap1-Nrf2 protein-protein interaction (PPI) inhibitors being at the forefront. Such compounds are considered to be more specific than cysteine targeting electrophilic Nrf2 activators. One example is the phenyl bis-sulfonamide PPI inhibitors, which mimic the Keap1-Nrf2 ETGE peptide complex (Georgakopoulos et al., 2022). As a result of this distinct binding profile, phenyl bis-sulfonamide PPI inhibitors are able to bind to Keap1 at submicromolar concentrations, thus reducing the required therapeutic dose and subsequently improving its safety profile (Dinkova-Kostova and Copple, 2023). In addition, recent pre-clinical developments in proteolysis-targeting chimeras (PROTACs) has led to the creation of Keap1 targeting PROTACs, promoting proteasomal degradation of Keap1 and subsequent activation of Nrf2 (Chen et al., 2023; Du et al., 2022). Taken together, it is therefore likely that the approval and routine clinical use of Nrf2 activators will continue to progress in years to come, presenting promising therapeutic leads.

In addition to small molecules, recently there has been considerable advances in the development of oligonucleotide-based therapies in oncology following a wider understanding of the roles of genes and transcription pathways within different cancers (Gregory and Copple, 2023). Such novel therapeutic approaches utilise modified or unmodified short nucleic acid molecules and can include small interfering RNA (siRNAs), small activating RNA (saRNAs) and microRNA (miRNAs) (Xiong et al., 2021). Although each of these oligonucleotide-based strategies have a unique mechanism of action,

simply put these therapeutics specifically alter the expression of the affected gene, either through induction or inhibition. This specificity, and the ability to easily predict off-target activity due to the nature by which these therapeutics act, significantly reduces the occurrence of off-target effects, something that is incredibly difficult to achieve with small molecule compounds. Such therapeutic approaches could allow for a Nrf2 targeting oligonucleotide that could deliver the required acute modification of Nrf2. The use of a *N*-acetylgalactosamine (GalNAc) conjugation system could then be used to target uptake of Nrf2 targeting oligonucleotides specifically in hepatocytes, through binding with the highly expressed asialoglycoprotein receptor (Debacker et al., 2020), thus providing the therapeutic benefit to liver regeneration whilst removing concerns of tumour Nrf2 being altered.

In conclusion, there is vast potential for the future of Nrf2 therapies in liver cancer both with small molecules and novel oligonucleotide-based approaches. However, there are numerous challenges that need to be overcome in order for such therapies to be successful, with one of these challenges being the current lack of a specific Nrf2 biomarker. Discovery of a clinically relevant, non-invasive, biomarker would significantly enhance the development of Nrf2 activating compounds and allow for better understanding of how such therapeutics work mechanistically. Another challenge, especially with the use of small molecules, is target specificity. As most Nrf2 activators are electrophilic compounds, which aim primarily to target the cysteine residues in Keap1, the lack of specificity allows such therapeutics to widely interact with cysteines present in many other proteins, affecting protein function and activity (Liby and Sporn, 2012). Refining specificity may allow for a more targeted approach, reducing off-target effects and lowering the required dose of an Nrf2 activator. Finally, as a novel approach, oligonucleotide-based therapies are not exempt from undesirable properties, with immunogenicity (Rogers et al., 2021) and difficulties with effective delivery systems (Roberts et al., 2020) raising concerns. Addressing such concerns would drastically accelerate the use and expansion of such therapeutics to a wider range of disease areas.

#### 5.4 Conclusions and future directions

There is an unmet need for a novel therapeutic approach that can reduce the clinical burden of liver cancer and the post-operative complications that can arise from the associated surgical treatment strategies. This thesis has investigated the use of pharmacological Nrf2 activation on enhancing liver regeneration and its safety in a liver cancer setting, utilising both *in vitro* and *in vivo* models. The use of an *in vivo* model of liver regeneration with translatable findings to primary human hepatocytes allows a crucial insight into how clinical patients could benefit from such therapy. The use of well-established *in vitro* cell based proliferation assays as a first-line investigation provided an understanding of how pharmacological Nrf2 activation would affect tumours in their true physiological conditions. This was then expanded upon through the use of an *in vivo* non-invasive bioluminescence imaging model of liver cancer proliferation. Such a model has allowed for an in-depth assessment of the safety of pharmacological Nrf2 activation with regards to its effect on the growth of liver tumours.

In order to further build upon, and validate the findings of this thesis, several further studies should be conducted, the details of which are outlined within each respective experimental chapter.

To expand beyond the scope of this thesis, the *in vivo* model utilised in chapter 4 could be further developed to better recapitulate the clinical setting to include risk factors and common causes for early liver cancer development. This could be achieved by inducing liver fibrosis or cirrhosis by use of a hepatotoxic agent prior to the orthotopic xenografting of cells. In addition, combining the two-thirds PHx *in vivo* model used in chapter 2, with an *in vivo* orthotopic intrasplenic xenograft model, could allow for tumour recurrence to be measured with clinical relevancy. Xenografting human HCC or CRC cells into the spleen would allow for liver metastases to occur, and such metastases would be

homogenous across the liver. The incorporation of luciferase expression would allow for the visualisation of xenografted cells by IVIS bioluminescence imaging, as outlined in this thesis. Liver tissue possessing obvious lesions could then be removed following a two-thirds PHx and any subsequent recurrence monitored with non-invasive IVIS bioluminescence imaging. Alternatively, tumour recurrence could be measured by combining a two-thirds PHx model with chemical induction of HCC through the use of a hepatocarcinogen such as DEN. Following administration of DEN and the establishment of liver tumours, affected tissue could be removed by two-thirds PHx. Due to a lack of luciferase expression, remaining tumour burden and potential recurrence could instead be monitored using MRI imaging.

Furthermore, the findings of this thesis could be expanded by monitoring the levels of crucial clinically relevant HCC and CRC biomarkers following the use of the *in vivo* xenograft model outlined in chapter 4. Blood samples collected via terminal cardiac puncture could be analysed through the use of an Enzyme-linked immunosorbent assay (ELISA) for markers such as alpha-fetoprotein (AFP) or glypican-3 (Zhou et al., 2018). Furthermore, tumour tissue could be analysed via immunohistochemistry (IHC) for markers of tumour growth and invasiveness, such as arginase-1 (Wang et al., 2020) and cytokeratin-20 (Ji et al., 2017).

Further crucial preclinical work could also be completed beyond this thesis to improve the clinical translatability. This could be achieved through the use of a human *ex vivo* study utilising perfusion of discarded liver tissue. As demonstrated by Schurink et al. it is possible to maintain stable liver function *ex vivo* for up to 7 days by using a normothermic machine perfusion (NMP) device, providing physiological levels are maintained (Schurink et al., 2020). Such method of perfusion allowed for a gradual decrease in nonviable cells and an increase in dividing cells, indicating the initiation and presence of liver regeneration, thus potentially providing a highly valuable platform to

test the efficacy of Nrf2 targeting therapies in regenerating human liver tissue prior to clinical trials. Additionally, discarded liver tissue from routine surgical resection of liver tumours may contain small HCC or CRC metastatic lesions, which would also allow for the safety of pharmacological Nrf2 activation to be assessed in this perfused liver system.

Following the development of a clinically translatable model, it would be pertinent to progress into clinical trials. In the first instance, it would be highly beneficial to utilise DMF as the pharmacological Nrf2 activator as it is already clinically approved for other disease areas encompassing oxidative stress and thus has a well-established safety profile. Although DMF is not the most potent Nrf2 activator, repurposing an already approved drug is significantly easier and cheaper than the development of a pre-clinical compound. In addition, it is essential that the correct patient cohort is selected, with patients possessing intermediate or advanced stage HCC providing an ideal foundation as they are typically borderline eligible for surgery or without other treatment options. Therefore, it may be possible reduce the burden of complications in patients undergoing surgery, whilst boosting RLV and subsequently eligibility of curative resection for those who were previously deemed inoperable.

In order to monitor response to treatment, it would be crucial to consider both short- and long-term responses. Due to the nature of post-operative complications and PHLF, short-term monitoring would involve assessing the risk of such complications, through the use of routine liver function tests or even MRI imaging, and whether this risk is prevented or significantly reduced with pharmacological Nrf2 intervention. Long-term monitoring would then involve assessing the recurrence of cancer, however given the potentially acute therapeutic intervention required, and the numerous other risk factors associated with tumour recurrence, it may be that the correlation of recurrence over time is utilised as a means of long-term assessment. In any situation, it would be essential to develop a

balance between the efficacy of enhancing liver regeneration and reducing PHLF, and the safety of preventing tumour recurrence.

Finally, it would be incredibly difficult to not directly compare the efficacy and safety of any Nrf2 based therapy with PVE as it remains the most widely used and accepted method of preventing PHLF. It may therefore be that both therapeutic strategies are utilised in harmony with a prior assessment of risk factors used to determine the safest and most appropriate approach. It is already essential to exercise caution with PVE due to the associated risks and complications in certain patient cohorts, therefore the introduction, and use, of a complementary treatment would only expand current treatment options and eligibility.

To conclude, the findings of this thesis, coupled with the discussed further work and future directions, provides a solid foundation in understanding how Nrf2 activating therapies can play a novel role in enhancing liver regeneration in patients following tumour resection. The development of such a therapeutic approach, whereby liver regeneration is enhanced and the risk of PHLF is reduced, would drastically improve the treatment options for patients with liver cancer by reducing the burden of complications and expanding the eligibility of existing curative liver cancer treatments. This field of work is still in its infancy but provides exciting and promising opportunities for future research.

## References

- Abdel-Misih, S.R.Z., and Bloomston, M. (2010). Liver Anatomy. *Surgical Clinics of North America* 90: 643–653.
- Abreu, P., Gorgen, A., Oldani, G., Hibi, T., and Sapisochin, G. (2019). Recent advances in liver transplantation for cancer: The future of transplant oncology. *JHEP Reports* 1: 377–391.
- Akerman, P., Cote, P., Yang, S.Q., McClain, C., Nelson, S., Bagby, G.J., et al. (1992). Antibodies to tumor necrosis factor-alpha inhibit liver regeneration after partial hepatectomy. *American Journal of Physiology-Gastrointestinal and Liver Physiology* 263: G579–G585.
- Akinyemiju, T., Abera, S., Ahmed, M., Alam, N., Alemayohu, M.A., Allen, C., et al. (2017). The Burden of Primary Liver Cancer and Underlying Etiologies From 1990 to 2015 at the Global, Regional, and National Level. *JAMA Oncol* 3: 1683.
- Alves Martins, B.A., Bulhões, G.F. de, Cavalcanti, I.N., Martins, M.M., Oliveira, P.G. de, and Martins, A.M.A. (2019). Biomarkers in Colorectal Cancer: The Role of Translational Proteomics Research. *Front Oncol* 9.
- Ananthakrishnan, A., Gogineni, V., and Saeian, K. (2006). Epidemiology of Primary and Secondary Liver Cancers. *Semin Intervent Radiol* 23: 047–063.
- Anders, S., and Huber, W. (2010). Differential expression analysis for sequence count data. *Genome Biol* 11: R106.
- Antunes, N., Kundu, B., Kundu, S.C., Reis, R.L., and Correlo, V. (2022). In Vitro Cancer Models: A Closer Look at Limitations on Translation. *Bioengineering (Basel)* 9: 166.
- Aragon, R.J., and Solomon, N.L. (2012). Techniques of hepatic resection. *J Gastrointest Oncol* 3: 28–40.
- Are, C., Meyer, B., Stack, A., Ahmad, H., Smith, L., Qian, B., et al. (2017). Global trends in the burden of liver cancer. *J Surg Oncol* 115: 591–602.
- Ashburner, M., Ball, C.A., Blake, J.A., Botstein, D., Butler, H., Cherry, J.M., et al. (2000). Gene Ontology: tool for the unification of biology. *Nat Genet* 25: 25–29.
- Asrani, S.K., Devarbhavi, H., Eaton, J., and Kamath, P.S. (2019). Burden of liver diseases in the world. *J Hepatol* 70: 151–171.
- Assy, N., Gong, Y., Zhang, M., Pettigrew, N.M., Pashniak, D., and Minuk, G.Y. (1998). Use of proliferating cell nuclear antigen as a marker of liver regeneration after partial hepatectomy in rats. *J Lab Clin Med* 131: 251–256.
- Ayoub, J.P., Hess, K.R., Abbruzzese, M.C., Lenzi, R., Raber, M.N., and Abbruzzese, J.L. (1998). Unknown primary tumors metastatic to liver. *Journal of Clinical Oncology* 16: 2105–2112.
- Ayuso, J.M., Park, K.-Y., Virumbrales-Muñoz, M., and Beebe, D.J. (2021). Toward improved *in vitro* models of human cancer. *APL Bioeng* 5: 010902.
- Azoulay, D., Castaing, D., Smail, A., Adam, R., Cailliez, V., Laurent, A., et al. (2000). Resection of Nonresectable Liver Metastases From Colorectal Cancer After Percutaneous Portal Vein Embolization. *Ann Surg* 231: 480–486.



- Baer-Dubowska, W., Narożna, M., and Krajka-Kuźniak, V. (2021). Anti-Cancer Potential of Synthetic Oleanolic Acid Derivatives and Their Conjugates with NSAIDs. *Molecules* 26: 4957.
- Bagi, C.M., and Andresen, C.J. (2010). Models of hepatocellular carcinoma and biomarker strategy. *Cancers (Basel)* 2: 1441–52.
- Bahirwani, R., and Reddy, K. (2014). Drug-Induced Liver Injury due to Cancer Chemotherapeutic Agents. *Semin Liver Dis* 34: 162–171.
- Balzan, S., Belghiti, J., Farges, O., Ogata, S., Sauvanet, A., Delefosse, D., et al. (2005). The '50-50 criteria' on postoperative day 5: An accurate predictor of liver failure and death after hepatectomy. *In Annals of Surgery*, pp 824–829.
- Berghe, G. van den (1991). The Role of the Liver in Metabolic Homeostasis: Implications for Inborn Errors of Metabolism. *In Journal of Inherited Metabolic Disease*, (Dordrecht: Springer Netherlands), pp 407–420.
- Beyer, T.A., Xu, W., Teupser, D., Auf Dem Keller, U., Bugnon, P., Hildt, E., et al. (2008). Impaired liver regeneration in Nrf2 knockout mice: Role of ROS-mediated insulin/IGF-1 resistance. *EMBO Journal* 27: 212–223.
- Blair, H.A. (2018). Dimethyl Fumarate: A Review in Moderate to Severe Plaque Psoriasis. *Drugs* 78: 123–130.
- Blank, A., Roberts, D.E., Dawson, H., Zlobec, I., and Lugli, A. (2018). Tumor Heterogeneity in Primary Colorectal Cancer and Corresponding Metastases. Does the Apple Fall Far From the Tree? *Front Med (Lausanne)* 5: 234.
- Blidisel, A., Marcovici, I., Coricovac, D., Hut, F., Dehelean, C.A., and Cretu, O.M. (2021). Experimental Models of Hepatocellular Carcinoma-A Preclinical Perspective. *Cancers (Basel)* 13.
- Böhm, F., Köhler, U.A., Speicher, T., and Werner, S. (2010). Regulation of liver regeneration by growth factors and cytokines. *EMBO Mol Med* 2: 294–305.
- Bosch, F.X., Ribes, J., Díaz, M., and Cléries, R. (2004). Primary liver cancer: Worldwide incidence and trends. *Gastroenterology* 127: S5–S16.
- Boyce, S., and Harrison, D. (2008). A detailed methodology of partial hepatectomy in the mouse. *Lab Anim (NY)* 37: 529–532.
- Brar, G., and Tsukamoto, H. (2019). Alcoholic and non-alcoholic steatohepatitis: global perspective and emerging science. *J Gastroenterol* 54: 218–225.
- Brás, M.M., Cruz, T.B., Maia, A.F., Oliveira, M.J., Sousa, S.R., Granja, P.L., et al. (2022). Mechanical Properties of Colorectal Cancer Cells Determined by Dynamic Atomic Force Microscopy: A Novel Biomarker. *Cancers (Basel)* 14: 5053.
- Brennan, T. v, Lin, L., Huang, X., and Yang, Y. (2018). Generation of Luciferase-expressing Tumor Cell Lines. *Bio Protoc* 8.
- Brix, N., Samaga, D., Hennel, R., Gehr, K., Zitzelsberger, H., and Lauber, K. (2020). The clonogenic assay: robustness of plating efficiency-based analysis is strongly compromised by cellular cooperation. *Radiation Oncology* 15: 248.

- Broek, M.A.J. Van Den, Olde Damink, S.W.M., Dejong, C.H.C., Lang, H., Malagó, M., Jalan, R., et al. (2008). Liver failure after partial hepatic resection: definition, pathophysiology, risk factors and treatment. *Liver International* 28: 767–780.
- Brown, Z.J., Heinrich, B., and Greten, T.F. (2018). Mouse models of hepatocellular carcinoma: an overview and highlights for immunotherapy research. *Nat Rev Gastroenterol Hepatol* 15: 536–554.
- Bruix, J., Raoul, J.-L., Sherman, M., Mazzaferro, V., Bolondi, L., Craxi, A., et al. (2012). Efficacy and safety of sorafenib in patients with advanced hepatocellular carcinoma: Subanalyses of a phase III trial. *J Hepatol* 57: 821–829.
- Bruix, J., Reig, M., and Sherman, M. (2016). Evidence-Based Diagnosis, Staging, and Treatment of Patients With Hepatocellular Carcinoma. *Gastroenterology* 150: 835–853.
- Bruix, J., and Sherman, M. (2011). Management of hepatocellular carcinoma: An update. *Hepatology* 53: 1020–1022.
- Bucher, N.L.R. (1977). Insulin, glucagon, and the liver. *Adv Enzyme Regul* 15: 221–230.
- Buendia, M.-A., and Neuvet, C. (2015). Hepatocellular Carcinoma. *Cold Spring Harb Perspect Med* 5: a021444–a021444.
- Burton, A., Tataru, D., Driver, R.J., Bird, T.G., Huws, D., Wallace, D., et al. (2021). Primary liver cancer in the UK: Incidence, incidence-based mortality, and survival by subtype, sex, and nation. *JHEP Reports* 3: 100232.
- Cabibbo, G., Enea, M., Attanasio, M., Bruix, J., Craxi, A., and Cammà, C. (2010). A meta-analysis of survival rates of untreated patients in randomized clinical trials of hepatocellular carcinoma. *Hepatology* 51: 1274–1283.
- Caldez, M.J., Hul, N. van, Koh, H.W.L., Teo, X.Q., Fan, J.J., Tan, P.Y., et al. (2018). Metabolic Remodeling during Liver Regeneration. *Dev Cell* 47: 425–438.e5.
- Cancer Research UK (2021). BCLC staging system and the Child-Pugh system.
- Canning, P., Sorrell, F.J., and Bullock, A.N. (2015). Structural basis of Keap1 interactions with Nrf2. *Free Radic Biol Med* 88: 101–107.
- Capussotti, L., Muratore, A., Amisano, M., Polastri, R., Bouzari, H., and Massucco, P. (2005). Liver resection for hepatocellular carcinoma on cirrhosis: analysis of mortality, morbidity and survival—a European single center experience. *European Journal of Surgical Oncology (EJSO)* 31: 986–993.
- Carnovale, C.E., and Ronco, M.T. (2012). Role of nitric oxide in liver regeneration. *Ann Hepatol* 11: 636–647.
- Chakedis, J., and Schmidt, C.R. (2018). Surgical Treatment of Metastatic Colorectal Cancer. *Surg Oncol Clin N Am* 27: 377–399.
- Chan, B.K.Y., Elmasry, M., Forootan, S.S., Russomanno, G., Bunday, T.M., Zhang, F., et al. (2021). Pharmacological Activation of Nrf2 Enhances Functional Liver Regeneration. *Hepatology* 74: 973–986.
- Chan, K., Lu, R., Chang, J.C., and Kan, Y.W. (1996). NRF2, a member of the NFE2 family of transcription factors, is not essential for murine erythropoiesis, growth, and development. *Proceedings of the National Academy of Sciences* 93: 13943–13948.

- Chang, T.T., and Hughes-Fulford, M. (2009). Monolayer and Spheroid Culture of Human Liver Hepatocellular Carcinoma Cell Line Cells Demonstrate Distinct Global Gene Expression Patterns and Functional Phenotypes. *Tissue Eng Part A* 15: 559–567.
- Chen, B., Lu, Y., Chen, Y., and Cheng, J. (2015). The role of Nrf2 in oxidative stress-induced endothelial injuries. *Journal of Endocrinology* 225: R83–R99.
- Chen, H., Nguyen, N.H., Magtoto, C.M., Cobbold, S.A., Bidgood, G.M., Meza Guzman, L.G., et al. (2023). Design and characterization of a heterobifunctional degrader of KEAP1. *Redox Biology* 59: 2213–2317.
- Chen, J., Lai, L., Lin, Q., Huang, W., Cai, M., Zhu, K., et al. (2017). Hepatic resection after transarterial chemoembolization increases overall survival in large/multifocal hepatocellular carcinoma: a retrospective cohort study. *Oncotarget* 8: 408–417.
- Chen, Y., Hata, T., Rehman, F., Kang, L., Yang, L., Kim, B.Y.S., et al. (2019). Visualization of Hepatocellular Regeneration in Mice After Partial Hepatectomy. *Journal of Surgical Research* 235: 494–500.
- Chhetri, J., Dilek, J., Davies, N., Jacobson, G., Dallmann, R., and Gueven, N. (2022). NQO1 protects against clioquinol toxicity. *Front Pharmacol* 13.
- Choi, B., and Kwak, M.-K. (2016). Shadows of NRF2 in cancer: Resistance to chemotherapy. *Curr Opin Toxicol* 1: 20–28.
- Chuang, S.-C., Vecchia, C. Ia, and Boffetta, P. (2009). Liver cancer: Descriptive epidemiology and risk factors other than HBV and HCV infection. *Cancer Lett* 286: 9–14.
- Cleary, S.P., Jeck, W.R., Zhao, X., Chen, K., Selitsky, S.R., Savich, G.L., et al. (2013). Identification of driver genes in hepatocellular carcinoma by exome sequencing. *Hepatology* 58: 1693–1702.
- Codeluppi, S., Gregory, E.N., Kjell, J., Wigerblad, G., Olson, L., and Svensson, C.I. (2011). Influence of rat substrain and growth conditions on the characteristics of primary cultures of adult rat spinal cord astrocytes. *J Neurosci Methods* 197: 118–27.
- Colagrande, S., Inghilesi, A.L., Aburas, S., Taliani, G.G., Nardi, C., and Marra, F. (2016). Challenges of advanced hepatocellular carcinoma. *World J Gastroenterol* 22: 7645.
- Comar, J.F., Suzuki-Kemmelmeier, F., Constantin, J., and Bracht, A. (2010). Hepatic zonation of carbon and nitrogen fluxes derived from glutamine and ammonia transformations. *J Biomed Sci* 17: 1.
- Corral-Vázquez, C., Aguilar-Quesada, R., Catalina, P., Lucena-Aguilar, G., Ligeró, G., Miranda, B., et al. (2017). Cell lines authentication and mycoplasma detection as minimum quality control of cell lines in biobanking. *Cell Tissue Bank* 18: 271–280.
- Cosmic (2021). Cosmic Cancer Browser.
- Cuadrado, A., Manda, G., Hassan, A., Alcaraz, M.J., Barbas, C., Daiber, A., et al. (2018). Transcription Factor NRF2 as a Therapeutic Target for Chronic Diseases: A Systems Medicine Approach. *Pharmacol Rev* 70: 348–383.
- Cuadrado, A., Rojo, A.I., Wells, G., Hayes, J.D., Cousin, S.P., Rumsey, W.L., et al. (2019). Therapeutic targeting of the NRF2 and KEAP1 partnership in chronic diseases. *Nat Rev Drug Discov* 18: 295–317.

- Curtis, A., Calabro, K., Galarneau, J.-R., Bigio, I.J., and Krucker, T. (2011). Temporal variations of skin pigmentation in C57BL/6 mice affect optical bioluminescence quantitation. *Mol Imaging Biol* 13: 1114–23.
- Dafflon, C., Santamaría-Martínez, A., and Ordóñez-Morán, P. (2020). An Intrasplenic Injection Model for the Study of Cancer Stem Cell Seeding Capacity. pp 293–302.
- Dall’Olio, F.G., Marabelle, A., Caramella, C., Garcia, C., Aldea, M., Chaput, N., et al. (2022). Tumour burden and efficacy of immune-checkpoint inhibitors. *Nat Rev Clin Oncol* 19: 75–90.
- D’Amico, E., Zanghì, A., Callari, G., Borriello, G., Gallo, A., Graziano, G., et al. (2018). Comparable efficacy and safety of dimethyl fumarate and teriflunomide treatment in Relapsing-Remitting Multiple Sclerosis: an Italian real-world multicenter experience. *Ther Adv Neurol Disord* 11: 175628641879640.
- Dayalan Naidu, S., and Dinkova-Kostova, A.T. (2023). Omaveloxolone (Skyclarys™) for patients with Friedreich’s ataxia. *Trends Pharmacol Sci* 44: 394-395.
- Debacker, A.J., Voutilainen, J., Catley, M., Blakey, D., and Habib, N. (2020). Delivery of Oligonucleotides to the Liver with GalNAc: From Research to Registered Therapeutic Drug. *Molecular Therapy* 28: 1759–1771.
- Demetriou, A.A., Brown, R.S., Busuttill, R.W., Fair, J., McGuire, B.M., Rosenthal, P., et al. (2004). Prospective, Randomized, Multicenter, Controlled Trial of a Bioartificial Liver in Treating Acute Liver Failure. *Ann Surg* 239: 660–670.
- Derynck, R., and Zhang, Y.E. (2003). Smad-dependent and Smad-independent pathways in TGF- $\beta$  family signalling. *Nature* 425: 577–584.
- Desai, J.R., Ochoa, S., Prins, P.A., and He, A.R. (2017). Systemic therapy for advanced hepatocellular carcinoma: an update. *J Gastrointest Oncol* 8: 243–255.
- Díaz-González, Á., Reig, M., and Bruix, J. (2016). Treatment of Hepatocellular Carcinoma. *Digestive Diseases* 34: 597–602.
- Dibbert, S., Clement, B., Skak-Nielsen, T., Mrowietz, U., and Rostami-Yazdi, M. (2013). Detection of fumarate–glutathione adducts in the portal vein blood of rats: evidence for rapid dimethylfumarate metabolism. *Arch Dermatol Res* 305: 447–451.
- Ding, X.-X., Zhu, Q.-G., Zhang, S.-M., Guan, L., Li, T., Zhang, L., et al. (2017). Precision medicine for hepatocellular carcinoma: driver mutations and targeted therapy. *Oncotarget* 8: 55715–55730.
- Dinkova-Kostova, A.T., and Abramov, A.Y. (2015). The emerging role of Nrf2 in mitochondrial function. *Free Radic Biol Med* 88: 179–188.
- Dinkova-Kostova, A.T., and Copple, I.M. (2023). Advances and challenges in therapeutic targeting of NRF2. *Trends Pharmacol Sci* 44: 137–149.
- Dionne, S., Russo, P., Tuchweber, B., Plaa, G.L., and Yousef, I.M. (2008). The role of acinar zone 3 hepatocytes in bile formation: influence of bromobenzene treatment on bile formation in the rat. *Liver* 10: 85–93.
- Du, G., Jiang, J., Henning, N.J., Safaee, N., Koide, E., Nowak, R.P., et al. (2022). Exploring the target scope of KEAP1 E3 ligase-based PROTACs. *Cell Chem Biol* 29: 1470-1481.

- Ekberg, K., Chandramouli, V., Kumaran, K., Schumann, W.C., Wahren, J., and Landau, B.R. (1995). Gluconeogenesis and Glucuronidation in Liver in Vivo and the Heterogeneity of Hepatocyte Function. *Journal of Biological Chemistry* 270: 21715–21717.
- Emanuele, S., Celesia, A., D'Anneo, A., Lauricella, M., Carlisi, D., Blasio, A. de, et al. (2021). The Good and Bad of Nrf2: An Update in Cancer and New Perspectives in COVID-19. *Int J Mol Sci* 22: 7963.
- Emond, J.C., Renz, J.F., Ferrell, L.D., Rosenthal, P., Lim, R.C., Roberts, J.P., et al. (1996). Functional Analysis of Grafts from Living Donors. *Ann Surg* 224: 544–554.
- Erstad, D.J., and Tanabe, K.K. (2017). Hepatocellular carcinoma: early-stage management challenges. *J Hepatocell Carcinoma Volume 4*: 81–92.
- Evans, J.P., Winiarski, B.K., Sutton, P.A., Jones, R.P., Ressel, L., Duckworth, C.A., et al. (2018). The Nrf2 inhibitor brusatol is a potent antitumour agent in an orthotopic mouse model of colorectal cancer. *Oncotarget* 9: 27104–27116.
- Everett, L.J., Mav, D., Phadke, D.P., Balik-Meisner, M.R., and Shah, R.R. (2022). Impact of Aligner, Normalization Method, and Sequencing Depth on TempO-seq Accuracy. *Bioinform Biol Insights* 16: 11779322221095216.
- Fan, S.-T. (2002). Methods and related drawbacks in the estimation of surgical risks in cirrhotic patients undergoing hepatectomy. *Hepatogastroenterology* 49: 17–20.
- Fausto, N. (2000). Liver regeneration. *J Hepatol* 32: 19–31.
- Fernandez, F.G., Ritter, J., Goodwin, J.W., Linehan, D.C., Hawkins, W.G., and Strasberg, S.M. (2005). Effect of Steatohepatitis Associated with Irinotecan or Oxaliplatin Pretreatment on Resectability of Hepatic Colorectal Metastases. *J Am Coll Surg* 200: 845–853.
- Ferreira, D., Adegá, F., and Chaves, R. (2013). The Importance of Cancer Cell Lines as in vitro Models in Cancer Methylome Analysis and Anticancer Drugs Testing. In *Oncogenomics and Cancer Proteomics*, C. López-Camarillo, and E. Aréchaga-Ocampo, eds. (Rijeka: IntechOpen), p Ch. 6.
- Forbes, S.J., and Newsome, P.N. (2016). Liver regeneration — mechanisms and models to clinical application. *Nat Rev Gastroenterol Hepatol* 13: 473–485.
- Fujiyoshi, M., and Ozaki, M. (2011). Molecular mechanisms of liver regeneration and protection for treatment of liver dysfunction and diseases. *J Hepatobiliary Pancreat Sci* 18: 13–22.
- Gao, J., Aksoy, B.A., Dogrusoz, U., Dresdner, G., Gross, B., Sumer, S.O., et al. (2013). Integrative Analysis of Complex Cancer Genomics and Clinical Profiles Using the cBioPortal. *Sci Signal* 6.
- Garnier, D., Li, R., Delbos, F., Fourrier, A., Collet, C., Guguen-Guillouzo, C., et al. (2018). Expansion of human primary hepatocytes in vitro through their amplification as liver progenitors in a 3D organoid system. *Sci Rep* 8: 8222.
- Gee, M.S., Kang, S.-B., Kim, N., Choi, J., Kim, N.-J., Kim, B.-J., et al. (2018). Bardoxolone Methyl Suppresses Hepatitis B Virus Large Surface Protein Variant W4P-Related Carcinogenesis and Hepatocellular Carcinoma Cell Proliferation Via the Inhibition of Signal Transducer and Activator of Transcription 3 Signaling. *Pharmacology* 105–113.

- Georgakopoulos, N., Talapatra, S., Dikovskaya, D., Dayalan Naidu, S., Higgins, M., Gatliff, J., et al. (2022). Phenyl Bis-Sulfonamide Keap1-Nrf2 Protein–Protein Interaction Inhibitors with an Alternative Binding Mode. *J Med Chem* 65: 7380–7398.
- Georgiades, C., Geschwind, J.-F., Harrison, N., Hines-Peralta, A., Liapi, E., Hong, K., et al. (2012). Lack of Response after Initial Chemoembolization for Hepatocellular Carcinoma: Does It Predict Failure of Subsequent Treatment? *Radiology* 265: 115–123.
- Ger, R. (1989). Surgical Anatomy of the Liver. *Surgical Clinics of North America* 69: 179–192.
- Ghuri, Y., Mian, I., and Rowe, J. (2017). Review of hepatocellular carcinoma: Epidemiology, etiology, and carcinogenesis. *J Carcinog* 16: 1.
- Gilg, S., Sandström, P., Rizell, M., Lindell, G., Ardnor, B., Strömberg, C., et al. (2018). The impact of post-hepatectomy liver failure on mortality: a population-based study. *Scand J Gastroenterol* 53: 1335–1339.
- Gillet, J.-P., Varma, S., and Gottesman, M.M. (2013). The clinical relevance of cancer cell lines. *J Natl Cancer Inst* 105: 452–8.
- Glehn, F. von, Dias-Carneiro, R.P.C., Moraes, A.S., Farias, A.S., Silva, V.A.P.G., Oliveira, F.T.M., et al. (2018). Dimethyl fumarate downregulates the immune response through the HCA2/GPR109A pathway: Implications for the treatment of multiple sclerosis. *Mult Scler Relat Disord* 23: 46–50.
- Gomez, D., and Cameron, I.C. (2010). Prognostic scores for colorectal liver metastasis: clinically important or an academic exercise? *HPB* 12: 227–238.
- Gosalia, A.J., Martin, P., and Jones, P.D. (2017). Advances and Future Directions in the Treatment of Hepatocellular Carcinoma. *Gastroenterol Hepatol (N Y)* 13: 398–410.
- Gregory, G.L., and Copple, I.M. (2023). Modulating the expression of tumor suppressor genes using activating oligonucleotide technologies as a therapeutic approach in cancer. *Mol Ther Nucleic Acids* 31: 211–223.
- Guguen-Guillouzo, C., and Guillouzo, A. (2010). General Review on In Vitro Hepatocyte Models and Their Applications. In *Hepatocytes: Methods and Protocols*, P. Maurel, ed. (Totowa, NJ: Humana Press), pp 1–40.
- Guichard, C., Amaddeo, G., Imbeaud, S., Ladeiro, Y., Pelletier, L., Maad, I. Ben, et al. (2012). Integrated analysis of somatic mutations and focal copy-number changes identifies key genes and pathways in hepatocellular carcinoma. *Nat Genet* 44: 694–698.
- Guido, M., Sarcognato, S., Sacchi, D., and Ludwig, K. (2019). The Anatomy and Histology of the Liver and Biliary Tract. In *Pediatric Hepatology and Liver Transplantation*, (Cham: Springer International Publishing), pp 41–55.
- Gutschner, T., and Diederichs, S. (2012). The hallmarks of cancer: a long non-coding RNA point of view. *RNA Biol* 9: 703–19.
- Ha, S.Y., Choi, M., Lee, T., and Park, C.-K. (2016). The Prognostic Role of Mitotic Index in Hepatocellular Carcinoma Patients after Curative Hepatectomy. *Cancer Res Treat* 48: 180–189.
- Hackl, C. (2014). Liver transplantation for malignancy: Current treatment strategies and future perspectives. *World J Gastroenterol* 20: 5331.

Haefeli, R.H., Erb, M., Gemperli, A.C., Robay, D., Courdier Fruh, I., Anklin, C., et al. (2011). NQO1-dependent redox cycling of idebenone: effects on cellular redox potential and energy levels. *PLoS One* 6: e17963.

Hammad, A., Zheng, Z.-H., Gao, Y., Namani, A., Shi, H.-F., and Tang, X. (2019). Identification of novel Nrf2 target genes as prognostic biomarkers in colitis-associated colorectal cancer in Nrf2-deficient mice. *Life Sci* 238: 116968.

Hanahan, D., and Weinberg, R.A. (2011). Hallmarks of Cancer: The Next Generation. *Cell* 144: 646–674.

Hao, Q., Wang, M., Sun, N., Zhu, C., Lin, Y., Li, C., et al. (2020). Sulforaphane suppresses carcinogenesis of colorectal cancer through the ERK/Nrf2-UDP glucuronosyltransferase 1A metabolic axis activation. *Oncol Rep*.

Haque, E., Karim, M.R., Salam Teeli, A., Śmiech, M., Leszczynski, P., Winiarczyk, D., et al. (2020). Molecular Mechanisms Underlying Hepatocellular Carcinoma Induction by Aberrant NRF2 Activation-Mediated Transcription Networks: Interaction of NRF2-KEAP1 Controls the Fate of Hepatocarcinogenesis. *Int J Mol Sci* 21.

Harjumäki, R., Nugroho, R.W.N., Zhang, X., Lou, Y.-R., Yliperttula, M., Valle-Delgado, J.J., et al. (2019). Quantified forces between HepG2 hepatocarcinoma and WA07 pluripotent stem cells with natural biomaterials correlate with in vitro cell behavior. *Sci Rep* 9: 7354.

Harmonizome (2021). Huh7 CCLE Cell Line Gene Mutation Profiles.

Hayes, J.D., and Ashford, M.L.J. (2012). Nrf2 Orchestrates Fuel Partitioning for Cell Proliferation. *Cell Metab* 16: 139–141.

Hayes, J.D., and Dinkova-Kostova, A.T. (2014). The Nrf2 regulatory network provides an interface between redox and intermediary metabolism. *Trends Biochem Sci* 39: 199–218.

He, F., Antonucci, L., and Karin, M. (2020). NRF2 as a regulator of cell metabolism and inflammation in cancer. *Carcinogenesis* 41: 405–416.

He, L., Tian, D.-A., Li, P.-Y., and He, X.-X. (2015). Mouse models of liver cancer: Progress and recommendations. *Oncotarget* 6: 23306–22.

Heiss, E.H., Schachner, D., Zimmermann, K., and Dirsch, V.M. (2013). Glucose availability is a decisive factor for Nrf2-mediated gene expression. *Redox Biol* 1: 359–365.

Hestermann, E.V., Stegeman, J.J., Hahn, M.E. (2000). Serum Alters the Uptake and Relative Potencies of Halogenated Aromatic Hydrocarbons in Cell Culture Bioassays. *Toxicol Sci* 53: 316-325.

Higgins, Gm., Anderson, R.E., Higgins, Gm., and Anderson, R. (1931). Experimental pathology of liver: restoration of liver in white rat following partial surgical removal. p.

Hoffmann, K., Nagel, A.J., Tanabe, K., Fuchs, J., Dehlke, K., Ghamarnejad, O., et al. (2020). Markers of liver regeneration—the role of growth factors and cytokines: a systematic review. *BMC Surg* 20: 31.

House, J.S., Grimm, F.A., Jima, D.D., Zhou, Y.-H., Rusyn, I., and Wright, F.A. (2017). A Pipeline for High-Throughput Concentration Response Modeling of Gene Expression for Toxicogenomics. *Front Genet* 8: 168.

- Hu, J., Dong, A., Fernandez-Ruiz, V., Shan, J., Kawa, M., Martínez-Ansó, E., et al. (2009). Blockade of Wnt Signaling Inhibits Angiogenesis and Tumor Growth in Hepatocellular Carcinoma. *Cancer Res* 69: 6951–6959.
- Hu, M., Zou, Y., Nambiar, S.M., Lee, J., Yang, Y., and Dai, G. (2014). Keap1 modulates the redox cycle and hepatocyte cell cycle in regenerating liver. *Cell Cycle* 13: 2349–2358.
- Huang, D.Q., Singal, A.G., Kono, Y., Tan, D.J.H., El-Serag, H.B., and Loomba, R. (2022). Changing global epidemiology of liver cancer from 2010 to 2019: NASH is the fastest growing cause of liver cancer. *Cell Metab* 34: 969-977.e2.
- Huang, J., and Rudnick, D.A. (2014). Elucidating the Metabolic Regulation of Liver Regeneration. *Am J Pathol* 184: 309–321.
- Huang, J., Tabbi-Anneni, I., Gunda, V., and Wang, L. (2010). Transcription factor Nrf2 regulates SHP and lipogenic gene expression in hepatic lipid metabolism. *American Journal of Physiology-Gastrointestinal and Liver Physiology* 299: G1211–G1221.
- Huh, C.-G., Factor, V.M., Sánchez, A., Uchida, K., Conner, E.A., and Thorgeirsson, S.S. (2004). Hepatocyte growth factor/ *c-met* signaling pathway is required for efficient liver regeneration and repair. *Proceedings of the National Academy of Sciences* 101: 4477–4482.
- Iber, F.L., Murphy, P.A., and Connor, E.S. (1994). Age-Related Changes in the Gastrointestinal System. *Drugs Aging* 5: 34–48.
- Ijssennagger, N., Janssen, A.W.F., Milona, A., Ramos Pittol, J.M., Hollman, D.A.A., Mokry, M., et al. (2016). Gene expression profiling in human precision cut liver slices in response to the FXR agonist obeticholic acid. *J Hepatol* 64: 1158–1166.
- Imamura, H. (2003). One Thousand Fifty-Six Hepatectomies Without Mortality in 8 Years. *Archives of Surgery* 138: 1198.
- Imamura, H., Shimada, R., Kubota, M., Matsuyama, Y., Nakayama, A., Miyagawa, S., et al. (1999). Preoperative portal vein embolization: An audit of 84 patients. *Hepatology* 29: 1099–1105.
- Islam, S.S., Qassem, K., Islam, S., Parag, R.R., Rahman, M.Z., Farhat, W.A., et al. (2022). Genetic alterations of Keap1 confers chemotherapeutic resistance through functional activation of Nrf2 and Notch pathway in head and neck squamous cell carcinoma. *Cell Death Dis* 13: 696.
- Itoh, K., Chiba, T., Takahashi, S., Ishii, T., Igarashi, K., Katoh, Y., et al. (1997). An Nrf2/Small Maf Heterodimer Mediates the Induction of Phase II Detoxifying Enzyme Genes through Antioxidant Response Elements. *Biochem Biophys Res Commun* 236: 313–322.
- Itoh, K., Wakabayashi, N., Katoh, Y., Ishii, T., Igarashi, K., Engel, J.D., et al. (1999). Keap1 represses nuclear activation of antioxidant responsive elements by Nrf2 through binding to the amino-terminal Neh2 domain. *Genes Dev* 13: 76–86.
- Izzo, F., Granata, V., Grassi, R., Fusco, R., Palaia, R., Delrio, P., et al. (2019). Radiofrequency Ablation and Microwave Ablation in Liver Tumors: An Update. *Oncologist* 24: e990–e1005.
- Jadlowiec, C.C. (2016). Liver transplantation: Current status and challenges. *World J Gastroenterol* 22: 4438.



- Ji, B., Cheng, X., Cai, X., Kong, C., Yang, Q., Fu, T., et al. (2017). CK20 mRNA expression in serum as a biomarker for colorectal cancer diagnosis: A meta-analysis. *Open Medicine* 12: 347–353.
- Jia, C. (2011). Advances in the regulation of liver regeneration. *Expert Rev Gastroenterol Hepatol* 5: 105–121.
- Jianyong, L., Lunan, Y., Wentao, W., Yong, Z., Bo, L., Tianfu, W., et al. (2014). Barcelona Clinic Liver Cancer Stage B Hepatocellular Carcinoma. *Medicine* 93: e180.
- Jun, C.H., Yoon, J.H., Cho, E., Shin, S.S., Cho, S.B., Kim, H.J., et al. (2017). Barcelona clinic liver cancer-stage C hepatocellular carcinoma. *Medicine* 96: e6745.
- Jungermann, K. (1983). Functional significance of hepatocyte heterogeneity for glycolysis and gluconeogenesis. *Pharmacol Biochem Behav* 18: 409–414.
- Jungermann, K. (1986). Functional Heterogeneity of Periportal and Perivenous Hepatocytes. *Enzyme* 35: 161–180.
- Jungermann, K., and Katz, N. (1989). Functional specialization of different hepatocyte populations. *Physiol Rev* 69: 708–764.
- Karoui, M., Penna, C., Amin-Hashem, M., Mitry, E., Benoist, S., Franc, B., et al. (2006). Influence of Preoperative Chemotherapy on the Risk of Major Hepatectomy for Colorectal Liver Metastases. *Ann Surg* 243: 1–7.
- Kasashima, H., Duran, A., Cid-Diaz, T., Kudo, Y., Diaz-Meco, M.T., and Moscat, J. (2020). An Orthotopic Implantation Mouse Model of Hepatocellular Carcinoma with Underlying Liver Steatosis. *STAR Protoc* 1: 100185.
- Katt, M.E., Placone, A.L., Wong, A.D., Xu, Z.S., and Searson, P.C. (2016). In Vitro Tumor Models: Advantages, Disadvantages, Variables, and Selecting the Right Platform. *Front Bioeng Biotechnol* 4: 12.
- Kelman, Z. (1997). PCNA: structure, functions and interactions. *Oncogene* 14: 629–640.
- Khor, T.O., Huang, M.-T., Prawan, A., Liu, Y., Hao, X., Yu, S., et al. (2008). Increased susceptibility of Nrf2 knockout mice to colitis-associated colorectal cancer. *Cancer Prev Res (Phila)* 1: 187–91.
- Kietzmann, T. (2017). Metabolic zonation of the liver: The oxygen gradient revisited. *Redox Biol* 11: 622–630.
- Kirstein, M.M., and Vogel, A. (2016). Epidemiology and Risk Factors of Cholangiocarcinoma. *Visc Med* 32: 395–400.
- Kitaeva, K. V, Rutland, C.S., Rizvanov, A.A., and Solovyeva, V. V (2020). Cell Culture Based in vitro Test Systems for Anticancer Drug Screening. *Front Bioeng Biotechnol* 8.
- Kitteringham, N.R., Abdullah, A., Walsh, J., Randle, L., Jenkins, R.E., Sison, R., et al. (2010). Proteomic analysis of Nrf2 deficient transgenic mice reveals cellular defence and lipid metabolism as primary Nrf2-dependent pathways in the liver. *J Proteomics* 73: 1612–1631.
- Kobayashi, A., Kang, M.-I., Okawa, H., Ohtsuji, M., Zenke, Y., Chiba, T., et al. (2004). Oxidative Stress Sensor Keap1 Functions as an Adaptor for Cul3-Based E3 Ligase To Regulate Proteasomal Degradation of Nrf2. *Mol Cell Biol* 24: 7130–7139.

- Kobayashi, M., Li, L., Iwamoto, N., Nakajima-Takagi, Y., Kaneko, H., Nakayama, Y., et al. (2009). The Antioxidant Defense System Keap1-Nrf2 Comprises a Multiple Sensing Mechanism for Responding to a Wide Range of Chemical Compounds. *Mol Cell Biol* 29: 493–502.
- Köhler, U.A., Kurinna, S., Schwitter, D., Marti, A., Schäfer, M., Hellerbrand, C., et al. (2014). Activated Nrf2 impairs liver regeneration in mice by activation of genes involved in cell-cycle control and apoptosis. *Hepatology* 60: 670–678.
- Kokudo, N. (2001). Proliferative activity of intrahepatic colorectal metastases after preoperative hemihepatic portal vein embolization. *Hepatology* 34: 267–272.
- Koulinska, I., Riestler, K., Chalkias, S., and Edwards, M.R. (2018). Effect of Bismuth Subsalicylate on Gastrointestinal Tolerability in Healthy Volunteers Receiving Oral Delayed-release Dimethyl Fumarate: PREVENT, a Randomized, Multicenter, Double-blind, Placebo-controlled Study. *Clin Ther* 40: 2021-2030.e1.
- Kow, A.W.C. (2019). Transplantation versus liver resection in patients with hepatocellular carcinoma. *Transl Gastroenterol Hepatol* 4: 49–49.
- Krelle, A.C., Okoli, A.S., and Mendz, G.L. (2013). Huh-7 Human Liver Cancer Cells: A Model System to Understand Hepatocellular Carcinoma and Therapy. *J Cancer Ther* 04: 606–631.
- Krishna, M. (2013). Microscopic anatomy of the liver. *Clin Liver Dis (Hoboken)* 2: S4–S7.
- Krisper, P., and Stauber, R.E. (2007). Technology Insight: artificial extracorporeal liver support—how does Prometheus® compare with MARS®? *Nat Clin Pract Nephrol* 3: 267–276.
- Krueger, W.H., Tanasijevic, B., Barber, V., Flamier, A., Gu, X., Manautou, J., et al. (2013). Cholesterol-Secreting and Statin-Responsive Hepatocytes from Human ES and iPS Cells to Model Hepatic Involvement in Cardiovascular Health. *PLoS One* 8: e67296.
- Kwak, M.-K., Wakabayashi, N., Greenlaw, J.L., Yamamoto, M., and Kensler, T.W. (2003). Antioxidants Enhance Mammalian Proteasome Expression through the Keap1-Nrf2 Signaling Pathway. *Mol Cell Biol* 23: 8786–8794.
- LeCluyse, E.L., Alexandre, E., Hamilton, G.A., Viollon-Abadie, C., Coon, D.J., Jolley, S., et al. (2005). Isolation and Culture of Primary Human Hepatocytes. In *Basic Cell Culture Protocols*, C.D. Helgason, and C.L. Miller, eds. (Totowa, NJ: Humana Press), pp 207–229.
- Lee, D.H., Lee, J.M., Lee, J.Y., Kim, S.H., Yoon, J.H., Kim, Y.J., et al. (2014). Radiofrequency Ablation of Hepatocellular Carcinoma as First-Line Treatment: Long-term Results and Prognostic Factors in 162 Patients with Cirrhosis. *Radiology* 270: 900–909.
- Lee, J.K., and Abou-Alfa, G.K. (2013). An Update on Clinical Trials in the Treatment of Advanced Hepatocellular Carcinoma. *J Clin Gastroenterol* 47: S16–S19.
- Lencioni, R., Petruzzi, P., and Crocetti, L. (2013). Chemoembolization of Hepatocellular Carcinoma. *Semin Intervent Radiol* 30: 003–011.
- Levings, D.C., Wang, X., Kohlhase, D., Bell, D.A., and Slattery, M. (2018). A distinct class of antioxidant response elements is consistently activated in tumors with NRF2 mutations. *Redox Biol* 19: 235–249.

- Li, C., Mi, K., Wen, T., Yan, L., and Li, B. (2012). Safety of Patients with a Graft to Body Weight Ratio Less than 0.8% in Living Donor Liver Transplantation using Right Hepatic Lobe without Middle Hepatic Vein. *Hepatogastroenterology* 59.
- Li, W., Liang, X., Kellendonk, C., Poli, V., and Taub, R. (2002). STAT3 Contributes to the Mitogenic Response of Hepatocytes during Liver Regeneration. *Journal of Biological Chemistry* 277: 28411–28417.
- Li, W., Yu, S., Liu, T., Kim, J.-H., Blank, V., Li, H., et al. (2008). Heterodimerization with small Maf proteins enhances nuclear retention of Nrf2 via masking the NESzip motif. *Biochimica et Biophysica Acta (BBA) - Molecular Cell Research* 1783: 1847–1856.
- Liby, K.T., and Sporn, M.B. (2012). Synthetic Oleanane Triterpenoids: Multifunctional Drugs with a Broad Range of Applications for Prevention and Treatment of Chronic Disease. *Pharmacol Rev* 64: 972–1003.
- Lim, S.-C., Choi, J.E., Kang, H.S., and Si, H. (2009). Ursodeoxycholic acid switches oxaliplatin-induced necrosis to apoptosis by inhibiting reactive oxygen species production and activating p53-caspase 8 pathway in HepG2 hepatocellular carcinoma. *Int J Cancer NA-NA*.
- Lin, S., Hoffmann, K., and Schemmer, P. (2012). Treatment of Hepatocellular Carcinoma: A Systematic Review. *Liver Cancer* 1: 144–158.
- Linker, R.A., and Haghikia, A. (2016). Dimethyl fumarate in multiple sclerosis: latest developments, evidence and place in therapy. *Ther Adv Chronic Dis* 7: 198–207.
- Lister, A., Nedjadi, T., Kitteringham, N.R., Campbell, F., Costello, E., Lloyd, B., et al. (2011). Nrf2 is overexpressed in pancreatic cancer: implications for cell proliferation and therapy. *Mol Cancer* 10: 37.
- Liu, C.-Y., Chen, K.-F., and Chen, P.-J. (2015). Treatment of Liver Cancer. *Cold Spring Harb Perspect Med* 5: a021535.
- Liu, P., Wang, W., Zhou, Z., Smith, A., Bowater, R., Wormstone, I., et al. (2018). Chemopreventive Activities of Sulforaphane and Its Metabolites in Human Hepatoma HepG2 Cells. *Nutrients* 10: 585.
- Liu, Z., Jiang, Y., Yuan, H., Fang, Q., Cai, N., Suo, C., et al. (2019). The trends in incidence of primary liver cancer caused by specific etiologies: Results from the Global Burden of Disease Study 2016 and implications for liver cancer prevention. *J Hepatol* 70: 674–683.
- Liu, Z., and Jiao, D. (2020). Necroptosis, tumor necrosis and tumorigenesis. *Cell Stress* 4: 1–8.
- Livraghi, T., Meloni, F., Stasi, M. Di, Rolle, E., Solbiati, L., Tinelli, C., et al. (2007). Sustained complete response and complications rates after radiofrequency ablation of very early hepatocellular carcinoma in cirrhosis: Is resection still the treatment of choice? *Hepatology* 47: 82–89.
- Llovet, J.M., Zucman-Rossi, J., Pikarsky, E., Sangro, B., Schwartz, M., Sherman, M., et al. (2016). Hepatocellular carcinoma. *Nat Rev Dis Primers* 2: 16018.
- Lotfollahzadeh, S., Recio-Boiles, A., and Babiker, H.M. (2022). Liver Cancer.
- Love, A.C., Caldwell, D.R., Kolbaba-Kartchner, B., Townsend, K.M., Halbers, L.P., Yao, Z., et al. (2023). Red-Shifted Coumarin Luciferins for Improved Bioluminescence Imaging. *J Am Chem Soc* 145: 3335–3345.

- Love, M.I., Huber, W., and Anders, S. (2014). Moderated estimation of fold change and dispersion for RNA-seq data with DESeq2. *Genome Biol* 15: 550.
- Lu, L.-C., Hsu, C.-H., Hsu, C., and Cheng, A.-L. (2016). Tumor Heterogeneity in Hepatocellular Carcinoma: Facing the Challenges. *Liver Cancer* 5: 128–138.
- Ma, J., Wang, F., Zhang, W., Wang, L., Yang, X., Qian, Y., et al. (2019). Percutaneous cryoablation for the treatment of liver cancer at special sites: an assessment of efficacy and safety. *Quant Imaging Med Surg* 9: 1948–1957.
- Ma, Q. (2013). Role of Nrf2 in Oxidative Stress and Toxicity. *Annu Rev Pharmacol Toxicol* 53: 401–426.
- Madoff, D.C., Abdalla, E.K., and Vauthey, J.-N. (2005). Portal Vein Embolization in Preparation for Major Hepatic Resection: Evolution of a New Standard of Care. *Journal of Vascular and Interventional Radiology* 16: 779–790.
- Magesh, S., Chen, Y., and Hu, L. (2012). Small Molecule Modulators of Keap1-Nrf2-ARE Pathway as Potential Preventive and Therapeutic Agents. *Med Res Rev* 32: 687–726.
- Maida, M. (2014). Staging systems of hepatocellular carcinoma: A review of literature. *World J Gastroenterol* 20: 4141.
- Manfredi, S., Lepage, C., Hatem, C., Coatmeur, O., Faivre, J., and Bouvier, A.-M. (2006). Epidemiology and Management of Liver Metastases From Colorectal Cancer. *Ann Surg* 244: 254–259.
- Manzini, G., Henne-Bruns, D., Porzsolt, F., and Kremer, M. (2017). Is there a standard for surgical therapy of hepatocellular carcinoma in healthy and cirrhotic liver? A comparison of eight guidelines. *BMJ Open Gastroenterol* 4: e000129.
- Maor, Y., and Malnick, S. (2013). Liver Injury Induced by Anticancer Chemotherapy and Radiation Therapy. *Int J Hepatol* 2013: 1–8.
- Marengo, A., Rosso, C., and Bugianesi, E. (2016). Liver Cancer: Connections with Obesity, Fatty Liver, and Cirrhosis. *Annu Rev Med* 67: 103–117.
- Marvin, D.L., Dijke, P. ten, and Ritsma, L. (2021). An Experimental Liver Metastasis Mouse Model Suitable for Short and Long-Term Intravital Imaging. *Curr Protoc* 1.
- Matsuoka, Y., Yoshida, R., Kawahara, K., Sakata, J., Arita, H., Nkashima, H., et al. (2022). The antioxidative stress regulator Nrf2 potentiates radioresistance of oral squamous cell carcinoma accompanied with metabolic modulation. *Laboratory Investigation* 102: 896–907.
- May, B., and Madoff, D. (2012). Portal Vein Embolization: Rationale, Technique, and Current Application. *Semin Intervent Radiol* 29: 081–089.
- McMahon, M., Itoh, K., Yamamoto, M., and Hayes, J.D. (2003). Keap1-dependent Proteasomal Degradation of Transcription Factor Nrf2 Contributes to the Negative Regulation of Antioxidant Response Element-driven Gene Expression. *Journal of Biological Chemistry* 278: 21592–21600.
- Mehta, N.N., Ravikumar, R., Coldham, C.A., Buckels, J.A.C., Hubscher, S.G., Bramhall, S.R., et al. (2008). Effect of preoperative chemotherapy on liver resection for colorectal liver metastases. *European Journal of Surgical Oncology (EJSO)* 34: 782–786.
- Meunier, L., and Larrey, D. (2020). Chemotherapy-associated steatohepatitis. *Ann Hepatol* 19: 597–601.

- Michalopoulos, G.K. (2007). Liver regeneration. *J Cell Physiol* 213: 286–300.
- Michalopoulos, G.K., and Khan, Z. (2005). Liver regeneration, growth factors, and amphiregulin. *Gastroenterology* 128: 503–506.
- Mierlo, K.M.C. van, Schaap, F.G., Dejong, C.H.C., and Olde Damink, S.W.M. (2016). Liver resection for cancer: New developments in prediction, prevention and management of postresectional liver failure. *J Hepatol* 65: 1217–1231.
- Minami, Y. (2010). Radiofrequency ablation of hepatocellular carcinoma: Current status. *World J Radiol* 2: 417.
- Mirabelli, P., Coppola, L., and Salvatore, M. (2019). Cancer Cell Lines Are Useful Model Systems for Medical Research. *Cancers (Basel)* 11.
- Misiakos, E.P. (2011). Current treatment for colorectal liver metastases. *World J Gastroenterol* 17: 4067.
- Mitchell, C., Nivison, M., Jackson, L.F., Fox, R., Lee, D.C., Campbell, J.S., et al. (2005). Heparin-binding Epidermal Growth Factor-like Growth Factor Links Hepatocyte Priming with Cell Cycle Progression during Liver Regeneration. *Journal of Biological Chemistry* 280: 2562–2568.
- Mitchell, C., and Willenbring, H. (2008). A reproducible and well-tolerated method for 2/3 partial hepatectomy in mice. *Nat Protoc* 3: 1167–1170.
- Mitra, S., Gupta, S., Dahiya, D., and Saikia, U.N. (2017). A Rare Case of Primary Sarcomatous Hepatocellular Carcinoma Without Previous Anticancer Therapy. *J Clin Exp Hepatol* 7: 378–384.
- Miyaoka, Y., and Miyajima, A. (2013). To divide or not to divide: revisiting liver regeneration. *Cell Div* 8: 8.
- Moerland, J.A., Leal, A.S., Lockwood, B., Demireva, E.Y., Xie, H., Krieger-Burke, T., et al. (2023). The Triterpenoid CDDO-Methyl Ester Redirects Macrophage Polarization and Reduces Lung Tumor Burden in a Nrf2-Dependent Manner. *Antioxidants* 12: 116.
- Moghadam, D., Zarei, R., Vakili, S., Ghojoghi, R., Zarezade, V., Veisi, A., et al. (2023). The effect of natural polyphenols Resveratrol, Gallic acid, and Kuromanin chloride on human telomerase reverse transcriptase (hTERT) expression in HepG2 hepatocellular carcinoma: role of SIRT1/Nrf2 signaling pathway and oxidative stress. *Mol Biol Rep* 50: 77–84.
- Moi, P., Chan, K., Asunis, I., Cao, A., and Kan, Y.W. (1994). Isolation of NF-E2-related factor 2 (Nrf2), a NF-E2-like basic leucine zipper transcriptional activator that binds to the tandem NF-E2/AP1 repeat of the beta-globin locus control region. *Proceedings of the National Academy of Sciences* 91: 9926–9930.
- Mullen, J.T., Ribero, D., Reddy, S.K., Donadon, M., Zorzi, D., Gautam, S., et al. (2007). Hepatic Insufficiency and Mortality in 1,059 Noncirrhotic Patients Undergoing Major Hepatectomy. *J Am Coll Surg* 204.
- Mutter, F.E., Park, B.K., and Copple, I.M. (2015). Value of monitoring Nrf2 activity for the detection of chemical and oxidative stress. *Biochem Soc Trans* 43: 657–662.
- Nalesnik, M.A., Gandhi, C.R., and Starzl, T.E. (2017). Augmenter of liver regeneration: A fundamental life protein. *Hepatology* 66: 266–270.

- Namani, A., Li, Y., Wang, X.J., and Tang, X. (2014). Modulation of NRF2 signaling pathway by nuclear receptors: Implications for cancer. *Biochimica et Biophysica Acta (BBA) - Molecular Cell Research* 1843: 1875–1885.
- Narita, M., Oussoultzoglou, E., Bachellier, P., Jaeck, D., and Uemoto, S. (2015). Post-hepatectomy liver failure in patients with colorectal liver metastases. *Surg Today* 45: 1218–1226.
- Natarajan, A., Wagner, B., and Sibilía, M. (2007). The EGF receptor is required for efficient liver regeneration. *Proceedings of the National Academy of Sciences* 104: 17081–17086.
- Ngo, H.K.C., Kim, D.-H., Cha, Y.-N., Na, H.-K., and Surh, Y.-J. (2017). Nrf2 Mutagenic Activation Drives Hepatocarcinogenesis. *Cancer Res* 77: 4797–4808.
- Ocak, İ., Topaloğlu, S., and Acarli, K. (2020). Posthepatectomy liver failure. *Turk J Med Sci* 50: 1491–1503.
- Oe, S., Lemmer, E.R., Conner, E.A., Factor, V.M., Levéen, P., Larsson, J., et al. (2004). Intact signaling by transforming growth factor  $\beta$  is not required for termination of liver regeneration in mice. *Hepatology* 40: 1098–1105.
- Ogunwobi, O.O., Mahmood, F., and Akingboye, A. (2020). Biomarkers in Colorectal Cancer: Current Research and Future Prospects. *Int J Mol Sci* 21.
- Ohtsubo, T., Kamada, S., Mikami, T., Murakami, H., and Tsujimoto, Y. (1999). Identification of NRF2, a member of the NF-E2 family of transcription factors, as a substrate for caspase-3(-like) proteases. *Cell Death Differ* 6: 865–872.
- Orcutt, S.T., and Anaya, D.A. (2018). Liver Resection and Surgical Strategies for Management of Primary Liver Cancer. *Cancer Control* 25: 107327481774462.
- Organ, S.L., and Tsao, M.-S. (2011). An overview of the c-MET signaling pathway. *Ther Adv Med Oncol* 3: S7–S19.
- Orrù, C., Giordano, S., and Columbano, A. (2020). Nrf2 in Neoplastic and Non-Neoplastic Liver Diseases. *Cancers (Basel)* 12: 2932.
- Pan, Y., Chen, H., and Yu, J. (2020). Biomarkers in Hepatocellular Carcinoma: Current Status and Future Perspectives. *Biomedicines* 8.
- Pandurangan, A.K., Ananda Sadagopan, S.K., Dharmalingam, P., and Ganapasam, S. (2014). Luteolin, a bioflavonoid inhibits Azoxymethane-induced colorectal cancer through activation of Nrf2 signaling. *Toxicol Mech Methods* 24: 13–20.
- Paranjpe, S., Bowen, W.C., Bell, A.W., Nejak-Bowen, K., Luo, J.-H., and Michalopoulos, G.K. (2007). Cell cycle effects resulting from inhibition of hepatocyte growth factor and its receptor c-Met in regenerating rat livers by RNA interference. *Hepatology* 45: 1471–1477.
- Parola, M., and Robino, G. (2001). Oxidative stress-related molecules and liver fibrosis. *J Hepatol* 35: 297–306.
- Paternostro, R., Sieghart, W., Trauner, M., and Pinter, M. (2021). Cancer and hepatic steatosis. *ESMO Open* 6: 100185.

- Pecorelli, A., Lenzi, B., Gramenzi, A., Garuti, F., Farinati, F., Giannini, E.G., et al. (2017). Curative therapies are superior to standard of care (transarterial chemoembolization) for intermediate stage hepatocellular carcinoma. *Liver International* 37: 423–433.
- Piersma, B., Hayward, M.-K., and Weaver, V.M. (2020). Fibrosis and cancer: A strained relationship. *Biochim Biophys Acta Rev Cancer* 1873: 188356.
- Piñero, F., Dirchwolf, M., and Pessôa, M.G. (2020). Biomarkers in Hepatocellular Carcinoma: Diagnosis, Prognosis and Treatment Response Assessment. *Cells* 9.
- Pirkmajer, S., and Chibalin, A. v (2011). Serum starvation: caveat emptor. *American Journal of Physiology-Cell Physiology* 301: C272–C279.
- Piscaglia, F., and Ogasawara, S. (2018). Patient Selection for Transarterial Chemoembolization in Hepatocellular Carcinoma: Importance of Benefit/Risk Assessment. *Liver Cancer* 7: 104–119.
- Pocha, C., and Xie, C. (2019). Hepatocellular carcinoma in alcoholic and non-alcoholic fatty liver disease—one of a kind or two different enemies? *Transl Gastroenterol Hepatol* 4: 72–72.
- Pontarin, G., Ferraro, P., Rampazzo, C., Kollberg, G., Holme, E., Reichard, P., et al. (2011). Deoxyribonucleotide Metabolism in Cycling and Resting Human Fibroblasts with a Missense Mutation in p53R2, a Subunit of Ribonucleotide Reductase. *Journal of Biological Chemistry* 286: 11132–11140.
- Prins, H.A., Meijer, C., Boelens, P.G., Diks, J., Holtz, R., Masson, S., et al. (2004). KUPFFER CELL???DEPLETED RATS HAVE A DIMINISHED ACUTE-PHASE RESPONSE FOLLOWING MAJOR LIVER RESECTION. *Shock* 21: 561–565.
- Qi, S-M., Dong, J., Xu, Z-Y., Cheng, X-D., Zhang, W-D., and Qin, J-J. (2021). PROTAC: An Effective Targeted Protein Degradation Strategy for Cancer Therapy. *Front. Pharmacol* 12: 692574.
- Raghunath, A., Sundarraj, K., Arfuso, F., Sethi, G., and Perumal, E. (2018). Dysregulation of Nrf2 in Hepatocellular Carcinoma: Role in Cancer Progression and Chemoresistance. *Cancers (Basel)* 10: 481.
- Rahbari, N.N., Garden, O.J., Padbury, R., Brooke-Smith, M., Crawford, M., Adam, R., et al. (2011). Posthepatectomy liver failure: A definition and grading by the International Study Group of Liver Surgery (ISGLS). *Surgery* 149: 713–724.
- Rahnemai-Azar, A.A., Cloyd, J.M., Weber, S.M., Dillhoff, M., Schmidt, C., Winslow, E.R., et al. (2018). Update on Liver Failure Following Hepatic Resection: Strategies for Prediction and Avoidance of Post-operative Liver Insufficiency. *J Clin Transl Hepatol* 6: 1–8.
- Rai, R.M., Lee, F.Y.J., Rosen, A., Yang, S.Q., Lin, H.Z., Koteish, A., et al. (1998). Impaired liver regeneration in inducible nitric oxide synthasedeficient mice. *Proceedings of the National Academy of Sciences* 95: 13829–13834.
- Rajput, A., Dominguez San Martin, I., Rose, R., Beko, A., LeVea, C., Sharratt, E., et al. (2008). Characterization of HCT116 Human Colon Cancer Cells in an Orthotopic Model. *Journal of Surgical Research* 147: 276–281.
- Raoul, J.-L., Gilibert, M., and Piana, G. (2014). How to Define Transarterial Chemoembolization Failure or Refractoriness: A European Perspective. *Liver Cancer* 3: 119–124.

- Raoul, J.-L., Kudo, M., Finn, R.S., Edeline, J., Reig, M., and Galle, P.R. (2018). Systemic therapy for intermediate and advanced hepatocellular carcinoma: Sorafenib and beyond. *Cancer Treat Rev* 68: 16–24.
- Rashid, M., and Coombs, K.M. (2019). Serum-reduced media impacts on cell viability and protein expression in human lung epithelial cells. *J Cell Physiol* 234: 7718–7724.
- Ray, S., Mehta, N.N., Golhar, A., and Nundy, S. (2018). Post hepatectomy liver failure – A comprehensive review of current concepts and controversies. *Annals of Medicine and Surgery* 34: 4–10.
- Rechem, C. van, Boulay, G., Pinte, S., Stankovic-Valentin, N., Guérardel, C., and Leprince, D. (2010). Differential Regulation of HIC1 Target Genes by CtBP and NuRD, via an Acetylation/SUMOylation Switch, in Quiescent versus Proliferating Cells. *Mol Cell Biol* 30: 4045–4059.
- Reddy, S.K., Reilly, C., Zhan, M., Mindikoglu, A.L., Jiang, Y., Lane, B.F., et al. (2014). Long-term influence of chemotherapy on steatosis-associated advanced hepatic fibrosis. *Medical Oncology* 31: 971.
- Reig, M., Darnell, A., Forner, A., Rimola, J., Ayuso, C., and Bruix, J. (2014). Systemic Therapy for Hepatocellular Carcinoma: The Issue of Treatment Stage Migration and Registration of Progression Using the BCLC-Refined RECIST. *Semin Liver Dis* 34: 444–455.
- Ricart, A.D. (2017). Drug-induced liver injury in Oncology. *Annals of Oncology* 28: 2013–2020.
- Ringehan, M., McKeating, J.A., and Protzer, U. (2017). Viral hepatitis and liver cancer. *Philosophical Transactions of the Royal Society B: Biological Sciences* 372: 20160274.
- Ritchie, M.E., Phipson, B., Wu, D., Hu, Y., Law, C.W., Shi, W., et al. (2015). limma powers differential expression analyses for RNA-sequencing and microarray studies. *Nucleic Acids Res* 43: e47–e47.
- Rizvi, S., Khan, S.A., Hallemeier, C.L., Kelley, R.K., and Gores, G.J. (2018). Cholangiocarcinoma — evolving concepts and therapeutic strategies. *Nat Rev Clin Oncol* 15: 95–111.
- Roayaie, S., Obeidat, K., Sposito, C., Mariani, L., Bhoori, S., Pellegrinelli, A., et al. (2013). Resection of hepatocellular cancer  $\leq 2$  cm: Results from two Western centers. *Hepatology* 57: 1426–1435.
- Roberts, T.C., Langer, R., and Wood, M.J.A. (2020). Advances in oligonucleotide drug delivery. *Nat Rev Drug Discov* 19: 673–694.
- Robinson, S.M., Wilson, C.H., Burt, A.D., Manas, D.M., and White, S.A. (2012). Chemotherapy-Associated Liver Injury in Patients with Colorectal Liver Metastases: A Systematic Review and Meta-analysis. *Ann Surg Oncol* 19: 4287–4299.
- Robledinos-Antón, N., Fernández-Ginés, R., Manda, G., and Cuadrado, A. (2019). Activators and Inhibitors of NRF2: A Review of Their Potential for Clinical Development. *Oxid Med Cell Longev* 2019: 1–20.
- Rogers, H., Adeniyi, O., Ramamoorthy, A., Bailey, S., and Pacanowski, M. (2021). Clinical Pharmacology Studies Supporting Oligonucleotide Therapy Development: An Assessment of Therapies Approved and in Development Between 2012 and 2018. *Clin Transl Sci* 14: 468–475.



- Romualdo, G.R., Leroy, K., Costa, C.J.S., Prata, G.B., Vanderborght, B., Silva, T.C. da, et al. (2021). In Vivo and In Vitro Models of Hepatocellular Carcinoma: Current Strategies for Translational Modeling. *Cancers (Basel)* 13: 5583.
- Rui, L. (2014). Energy Metabolism in the Liver. In *Comprehensive Physiology*, (Wiley), pp 177–197.
- Russell, W.E., Coffey, R.J., Ouellette, A.J., and Moses, H.L. (1988). Type beta transforming growth factor reversibly inhibits the early proliferative response to partial hepatectomy in the rat. *Proceedings of the National Academy of Sciences* 85: 5126–5130.
- Russell, W.E., Kaufmann, W.K., Sitaric, S., Luetkeke, N.C., and Lee, D.C. (1996). Liver regeneration and hepatocarcinogenesis in transforming growth factor- $\alpha$ -targeted mice. *Mol Carcinog* 15: 183–189.
- Ryan, M.J. (2016). Ablation techniques for primary and metastatic liver tumors. *World J Hepatol* 8: 191.
- Sacco, R., Antonucci, M., Bresci, G., Corti, A., Giacomelli, L., Mismas, V., et al. (2016). Curative therapies for hepatocellular carcinoma: an update and perspectives. *Expert Rev Anticancer Ther* 16: 169–175.
- Sagaert, X., Vanstapel, A., and Verbeek, S. (2018). Tumor Heterogeneity in Colorectal Cancer: What Do We Know So Far? *Pathobiology* 85: 72–84.
- Sajadimajd, S., Aghaz, F., Khazaei, M., and Raygani, A.-V. (2023). The anti-cancer effect of resveratrol nano-encapsulated supplements against breast cancer via the regulation of oxidative stress. *J Microencapsul* 1–12.
- Sameer, A.S. (2013). Colorectal cancer: molecular mutations and polymorphisms. *Front Oncol* 3: 114.
- Schicht, G., Seidemann, L., Haensel, R., Seehofer, D., and Damm, G. (2022). Critical Investigation of the Usability of Hepatoma Cell Lines HepG2 and Huh7 as Models for the Metabolic Representation of Resectable Hepatocellular Carcinoma. *Cancers (Basel)* 14.
- Schindl, M.J. (2005). The value of residual liver volume as a predictor of hepatic dysfunction and infection after major liver resection. *Gut* 54: 289–296.
- Schneider, C.A., Rasband, W.S., and Eliceiri, K.W. (2012). NIH Image to ImageJ: 25 years of image analysis. *Nat Methods* 9: 671–675.
- Schurink, I.J., Willemse, J., Verstegen, M.M.A., Laan, L.J.W. van der, and Jonge, J. de (2020). Long-Term Perfusion of the Liver Outside the Body: Warming Up for Ex Vivo Therapies? *Hepatology* 72: 1485–1487.
- Sen, S., Williams, R., and Jalan, R. (2005). Emerging Indications for Albumin Dialysis. *Am J Gastroenterol* 100: 468–475.
- Shao, C., Zhang, Q., Kuang, G., Fan, Q., and Ye, F. (2022). Construction and application of liver cancer models in vitro. *Engineered Regeneration* 3: 310–322.
- Sharma, A., Houshyar, R., Bhosale, P., Choi, J.-I., Gulati, R., and Lall, C. (2014). Chemotherapy induced liver abnormalities: an imaging perspective. *Clin Mol Hepatol* 20: 317.
- Shen, C.-J., Lin, P.-L., Lin, H.-C., Cheng, Y.-W., Huang, H.-S., and Lee, H. (2019). RV-59 suppresses cytoplasmic Nrf2-mediated 5-fluorouracil resistance and tumor growth in colorectal cancer. *Am J Cancer Res* 9: 2789–2796.

- Shin, S., Wakabayashi, J., Yates, M.S., Wakabayashi, N., Dolan, P.M., Aja, S., et al. (2009). Role of Nrf2 in prevention of high-fat diet-induced obesity by synthetic triterpenoid CDDO-Imidazolide. *Eur J Pharmacol* 620: 138–144.
- Shoup, M. (2003). Volumetric Analysis Predicts Hepatic Dysfunction in Patients Undergoing Major Liver Resection. *Journal of Gastrointestinal Surgery* 7: 325–330.
- Siegel, R.L., Miller, K.D., Fuchs, H.E., and Jemal, A. (2021). Cancer Statistics, 2021. *CA Cancer J Clin* 71: 7–33.
- Singal, A.G., and El-Serag, H.B. (2015). Hepatocellular Carcinoma From Epidemiology to Prevention: Translating Knowledge into Practice. *Clinical Gastroenterology and Hepatology* 13: 2140–2151.
- Sinn, D.H., Cho, J.-Y., Gwak, G.-Y., Paik, Y.-H., Choi, M.S., Lee, J.H., et al. (2015). Different Survival of Barcelona Clinic Liver Cancer Stage C Hepatocellular Carcinoma Patients by the Extent of Portal Vein Invasion and the Type of Extrahepatic Spread. *PLoS One* 10: e0124434.
- Skonieczna, M., Adamić-Organisciok, M., Hudy, D., Dziedzic, A., Los, L., Składany, L., et al. (2022). Hepatocellular cancer cell lines, Hep-3B and Hep-G2 display the pleiotropic response to resveratrol and berberine. *Adv Med Sci* 67: 379–385.
- Smittenaar, C.R., Petersen, K.A., Stewart, K., and Moitt, N. (2016). Cancer incidence and mortality projections in the UK until 2035. *Br J Cancer* 115: 1147–1155.
- Song, T., Li, L., Wu, S., Liu, Y., Guo, C., Wang, W., et al. (2021). Peripheral Blood Genetic Biomarkers for the Early Diagnosis of Hepatocellular Carcinoma. *Front Oncol* 11.
- Sparrelid, E., Olthof, P.B., Dasari, B.V.M., Erdmann, J.I., Santol, J., Starlinger, P., et al. (2022). Current evidence on posthepatectomy liver failure: comprehensive review. *BJS Open* 6: zrac142.
- Staurengo-Ferrari, L., Badaro-Garcia, S., Hohmann, M.S.N., Manchope, M.F., Zaninelli, T.H., Casagrande, R., et al. (2019). Contribution of Nrf2 Modulation to the Mechanism of Action of Analgesic and Anti-inflammatory Drugs in Pre-clinical and Clinical Stages. *Front Pharmacol* 9.
- Stoffels, B., Enkirch, S., Websky, M., Vilz, T., Pantelis, D., Manekeller, S., et al. (2016). Postoperatives Leberversagen nach erweiterten Leberresektionen – eine Übersicht, gestützt durch eine retrospektive Single-Center-Analyse. *Zentralblatt Für Chirurgie - Zeitschrift Für Allgemeine, Viszeral-, Thorax- Und Gefäßchirurgie* 141: 405–414.
- Strober, W. (2015). Trypan Blue Exclusion Test of Cell Viability. *Curr Protoc Immunol* 111: A3.B.1-A3.B.3.
- Sun, H., Zhu, J., Lin, H., Gu, K., and Feng, F. (2017). Recent progress in the development of small molecule Nrf2 modulators: a patent review (2012-2016). *Expert Opin Ther Pat* 27: 763–785.
- Sung, H., Ferlay, J., Siegel, R.L., Laversanne, M., Soerjomataram, I., Jemal, A., et al. (2021). Global Cancer Statistics 2020: GLOBOCAN Estimates of Incidence and Mortality Worldwide for 36 Cancers in 185 Countries. *CA Cancer J Clin* 71: 209–249.
- Supek, F., Bošnjak, M., Škunca, N., and Šmuc, T. (2011). Revigo summarizes and visualizes long lists of gene ontology terms. *PLoS One* 6.
- Syed, A.J., and Anderson, J.C. (2021). Applications of bioluminescence in biotechnology and beyond. *Chem Soc Rev* 50: 5668–5705.

Tang, B., Zhu, J., Liu, F., Ding, J., Wang, Y., Fang, S., et al. (2022). xCT contributes to colorectal cancer tumorigenesis through upregulation of the MELK oncogene and activation of the AKT/mTOR cascade. *Cell Death Dis* 13: 373.

Tao, Y., Wang, M., Chen, E., and Tang, H. (2017). Liver Regeneration: Analysis of the Main Relevant Signaling Molecules. *Mediators Inflamm* 2017: 1–9.

Tebay, L.E., Robertson, H., Durant, S.T., Vitale, S.R., Penning, T.M., Dinkova-Kostova, A.T., et al. (2015). Mechanisms of activation of the transcription factor Nrf2 by redox stressors, nutrient cues, and energy status and the pathways through which it attenuates degenerative disease. *Free Radic Biol Med* 88: 108–146.

Tellapuri, S., Sutphin, P.D., Beg, M.S., Singal, A.G., and Kalva, S.P. (2018). Staging systems of hepatocellular carcinoma: A review. *Indian Journal of Gastroenterology* 37: 481–491.

Thoolen, B., Maronpot, R.R., Harada, T., Nyska, A., Rousseaux, C., Nolte, T., et al. (2010). Proliferative and Nonproliferative Lesions of the Rat and Mouse Hepatobiliary System. *Toxicol Pathol* 38: 5S-81S.

Torrente, L., Maan, G., Oumkaltoum Rezig, A., Quinn, J., Jackson, A., Grilli, A., et al. (2020). High NRF2 Levels Correlate with Poor Prognosis in Colorectal Cancer Patients and with Sensitivity to the Kinase Inhibitor AT9283 In Vitro. *Biomolecules* 10: 1365.

Trépo, C., Chan, H.L.Y., and Lok, A. (2014). Hepatitis B virus infection. *The Lancet* 384: 2053–2063.

Truant, S., Oberlin, O., Sergent, G., Lebuffe, G., Gambiez, L., Ernst, O., et al. (2007). Remnant Liver Volume to Body Weight Ratio  $\geq 0.5\%$ : A New Cut-Off to Estimate Postoperative Risks after Extended Resection in Noncirrhotic Liver. *J Am Coll Surg* 204: 22–33.

Tsim, N.C. (2010). Surgical treatment for liver cancer. *World J Gastroenterol* 16: 927.

Ueno, H., Mochizuki, H., Hatsuse, K., Hase, K., and Yamamoto, T. (2000). Indicators for Treatment Strategies of Colorectal Liver Metastases. *Ann Surg* 231: 59.

Uhlén, M., Fagerberg, L., Hallström, B.M., Lindskog, C., Oksvold, P., Mardinoglu, A., et al. (2015). Tissue-based map of the human proteome. *Science* (1979) 347.

Uriarte, I., Fernandez-Barrena, M.G., Monte, M.J., Latasa, M.U., Chang, H.C.Y., Carotti, S., et al. (2013). Identification of fibroblast growth factor 15 as a novel mediator of liver regeneration and its application in the prevention of post-resection liver failure in mice. *Gut* 62: 899–910.

Vandeputte, C., Guizon, I., Genestie-Denis, I., Vannier, B., and Lorenzon, G. (1994). A microtiter plate assay for total glutathione and glutathione disulfide contents in cultured/isolated cells: performance study of a new miniaturized protocol. *Cell Biol Toxicol* 10: 415–421.

Verma, S., Purohit, J.S., Arora, A., Sinha, S., and Chaturvedi, M.M. (2021). Liver regeneration: Metabolic and epigenetic regulation. *Hepatoma Res* 7.

Volk, M.L., and Marrero, J.A. (2008). Early detection of liver cancer: Diagnosis and management. *Curr Gastroenterol Rep* 10: 60–66.

Wahab, R., Gopalan, V., Islam, F., Smith, R.A., Qiao, B., and Lam, A.K. (2017). Cellular expression, in-vitro and in-vivo confirmation of GAEC1 oncogenic properties in colon cancer. *Eur J Cell Biol* 96: 487–495.

- Wakabayashi, H., Nishiyama, Y., Ushiyama, T., Maeba, T., and Maeta, H. (2002). Evaluation of the Effect of Age on Functioning Hepatocyte Mass and Liver Blood Flow Using Liver Scintigraphy in Preoperative Estimations for Surgical Patients: Comparison with CT Volumetry. *Journal of Surgical Research* 106: 246–253.
- Wakabayashi, N., Chartoumpekis, D. V., and Kensler, T.W. (2015). Crosstalk between Nrf2 and Notch signaling. *Free Radic Biol Med* 88: 158–167.
- Wakabayashi, N., Itoh, K., Wakabayashi, J., Motohashi, H., Noda, S., Takahashi, S., et al. (2003). Keap1-null mutation leads to postnatal lethality due to constitutive Nrf2 activation. *Nat Genet* 35: 238–245.
- Wakabayashi, N., Shin, S., Slocum, S.L., Agoston, E.S., Wakabayashi, J., Kwak, M.-K., et al. (2010). Regulation of Notch1 Signaling by Nrf2: Implications for Tissue Regeneration. *Sci Signal* 3: ra52–ra52.
- Wang, X., Xu, Y., Wang, R., Dai, N., Zhang, W., and Li, F. (2020). The significance of arginase-1 expression in the diagnosis of liver cancer. *Medicine* 99: e19159.
- Wang, Z.-G., He, Z.-Y., Chen, Y.-Y., Gao, H., and Du, X.-L. (2021). Incidence and survival outcomes of secondary liver cancer: a Surveillance Epidemiology and End Results database analysis. *Transl Cancer Res* 10: 1273–1283.
- Watson, J., Hydon, K., and Lodge, P. (2016). Primary and secondary liver tumours. *InnovAiT: Education and Inspiration for General Practice* 9: 477–482.
- Weis, S., Franke, A., Berg, T., Mössner, J., Fleig, W.E., and Schoppmeyer, K. (2015). Percutaneous ethanol injection or percutaneous acetic acid injection for early hepatocellular carcinoma. *Cochrane Database of Systematic Reviews* 2019.
- White, M.A., Fong, Y., and Singh, G. (2016). Chemotherapy-Associated Hepatotoxicities. *Surgical Clinics of North America* 96: 207–217.
- Woodfield, S.E., Shi, Y., Patel, R.H., Jin, J., Major, A., Sarabia, S.F., et al. (2017). A Novel Cell Line Based Orthotopic Xenograft Mouse Model That Recapitulates Human Hepatoblastoma. *Sci Rep* 7: 17751.
- Wu, K.C., Cui, J.Y., and Klaassen, C.D. (2011). Beneficial Role of Nrf2 in Regulating NADPH Generation and Consumption. *Toxicological Sciences* 123: 590–600.
- Wu, S., Lu, H., and Bai, Y. (2019). Nrf2 in cancers: A double-edged sword. *Cancer Med* 8: 2252–2267.
- Wu, T., Heuillard, E., Lindner, V., Bou About, G., Ignat, M., Dillenseger, J.-P., et al. (2016). Multimodal imaging of a humanized orthotopic model of hepatocellular carcinoma in immunodeficient mice. *Sci Rep* 6: 35230.
- Xiao, W., Wang, R.-S., Handy, D.E., and Loscalzo, J. (2018). NAD(H) and NADP(H) Redox Couples and Cellular Energy Metabolism. *Antioxid Redox Signal* 28: 251–272.
- Xiong, H., Veedu, R.N., and Diermeier, S.D. (2021). Recent Advances in Oligonucleotide Therapeutics in Oncology. *Int J Mol Sci* 22: 3295.
- Xu, D., Xu, M., Jeong, S., Qian, Y., Wu, H., Xia, Q., et al. (2018). The Role of Nrf2 in Liver Disease: Novel Molecular Mechanisms and Therapeutic Approaches. *Front Pharmacol* 9: 1428.

- Xu, D.G., Lv, W., Dai, C.Y., Zhu, F.F., Xu, G.H., Ma, Z.J., et al. (2015). 2-(Pro-1-ynyl)-5-(5,6-dihydroxypenta-1,3-diyanyl) Thiophene Induces Apoptosis Through Reactive Oxygen Species-Mediated JNK Activation in Human Colon Cancer SW620 Cells. *Anat Rec* 298: 376–385.
- Xu, W., Hellerbrand, C., Köhler, U.A., Bugnon, P., Kan, Y.-W., Werner, S., et al. (2008). The Nrf2 transcription factor protects from toxin-induced liver injury and fibrosis. *Laboratory Investigation* 88: 1068–1078.
- Xu, Z., Zhang, F., Sun, F., Gu, K., Dong, S., and He, D. (2015). Dimethyl fumarate for multiple sclerosis. *Cochrane Database of Systematic Reviews*.
- Yagishita, Y., Gatbonton-Schwager, T.N., McCallum, M.L., and Kensler, T.W. (2020). Current Landscape of NRF2 Biomarkers in Clinical Trials. *Antioxidants (Basel)* 9: 716.
- Yamada, Y., Webber, E.M., Kirillova, I., Peschon, J.J., and Fausto, N. (1998). Analysis of liver regeneration in mice lacking type 1 or type 2 tumor necrosis factor receptor: Requirement for type 1 but not type 2 receptor. *Hepatology* 28: 959–970.
- Yamamoto, M., Kensler, T.W., and Motohashi, H. (2018). The KEAP1-NRF2 System: a Thiol-Based Sensor-Effector Apparatus for Maintaining Redox Homeostasis. *Physiol Rev* 98: 1169–1203.
- Yang, J.D., Hainaut, P., Gores, G.J., Amadou, A., Plymoth, A., and Roberts, L.R. (2019). A global view of hepatocellular carcinoma: trends, risk, prevention and management. *Nat Rev Gastroenterol Hepatol* 16: 589–604.
- Yang, X.-Z., Dou, S., Sun, T.-M., Mao, C.-Q., Wang, H.-X., and Wang, J. (2011). Systemic delivery of siRNA with cationic lipid assisted PEG-PLA nanoparticles for cancer therapy. *Journal of Controlled Release* 156: 203–211.
- Yeh, H.-W., Karmach, O., Ji, A., Carter, D., Martins-Green, M.M., and Ai, H. (2017). Red-shifted luciferase–luciferin pairs for enhanced bioluminescence imaging. *Nat Methods* 14: 971–974.
- Yip, D., and Cho, C.H. (2013). A multicellular 3D heterospheroid model of liver tumor and stromal cells in collagen gel for anti-cancer drug testing. *Biochem Biophys Res Commun* 433: 327–332.
- Yu, G., Wang, L.-G., Han, Y., and He, Q.-Y. (2012). clusterProfiler: an R Package for Comparing Biological Themes Among Gene Clusters. *OMICS* 16: 284–287.
- Zavattari, P., Perra, A., Menegon, S., Kowalik, M.A., Petrelli, A., Angioni, M.M., et al. (2015). Nrf2, but not  $\beta$ -catenin, mutation represents an early event in rat hepatocarcinogenesis. *Hepatology* 62: 851–862.
- Zhang, C., Wang, H.-J., Bao, Q.-C., Wang, L., Guo, T.-K., Chen, W.-L., et al. (2016). NRF2 promotes breast cancer cell proliferation and metastasis by increasing RhoA/ROCK pathway signal transduction. *Oncotarget* 7: 73593–73606.
- Zhang, M., Zhang, C., Zhang, L., Yang, Q., Zhou, S., Wen, Q., et al. (2015). Nrf2 is a potential prognostic marker and promotes proliferation and invasion in human hepatocellular carcinoma. *BMC Cancer* 15: 531.
- Zhang, Q., Lou, Y., Bai, X.-L., and Liang, T.-B. (2020). Intratumoral heterogeneity of hepatocellular carcinoma: From single-cell to population-based studies. *World J Gastroenterol* 26: 3720–3736.

- Zhang, Y., Talalay, P., Cho, C.G., and Posner, G.H. (1992). A major inducer of anticarcinogenic protective enzymes from broccoli: isolation and elucidation of structure. *Proceedings of the National Academy of Sciences* 89: 2399–2403.
- Zhao, J., Yu, S.-Z., Cai, Q., Ma, D., Jiang, L., Yang, L.-P., et al. (2021). Identifying the Key Genes in Mouse Liver Regeneration After Partial Hepatectomy by Bioinformatics Analysis and in vitro/vivo Experiments. *Front Genet* 12.
- Zhao, X.-Q., Zhang, Y.-F., Xia, Y.-F., Zhou, Z.-M., and Cao, Y.-Q. (2015). Promoter demethylation of nuclear factor-erythroid 2-related factor 2 gene in drug-resistant colon cancer cells. *Oncol Lett* 10: 1287–1292.
- Zheng, Y., Yang, H., He, L., Mao, Y., Zhang, H., Zhao, H., et al. (2017). Reassessment of different criteria for diagnosing post-hepatectomy liver failure: a single-center study of 1683 hepatectomy.
- Zhou, F., Shang, W., Yu, X., and Tian, J. (2018). Glypican-3: A promising biomarker for hepatocellular carcinoma diagnosis and treatment. *Med Res Rev* 38: 741–767.
- Zimta, A.-A., Cenariu, D., Irimie, A., Magdo, L., Nabavi, S.M., Atanasov, A.G., et al. (2019). The Role of Nrf2 Activity in Cancer Development and Progression. *Cancers (Basel)* 11.
- Zipper, H., Brunner, H., Bernhagen, J., and Vitzthum, F. (2004). Investigations on DNA intercalation and surface binding by SYBR Green I, its structure determination and methodological implications. *Nucleic Acids Res* 32.
- Ziv, E., Zhang, Y., Kelly, L., Nikolovski, I., Boas, F.E., Erinjeri, J.P., et al. (2020). NRF2 Dysregulation in Hepatocellular Carcinoma and Ischemia: A Cohort Study and Laboratory Investigation. *Radiology* 297: 225–234.